SOLID AND SOLUBLE PRODUCTS OF ENGINEERED WATER/ROCK INTERACTIONS IN SHALE RESERVOIRS

A Dissertation

by

LIFU ZHANG

Submitted to the Office of Graduate and Professional Studies of
Texas A&M University
in partial fulfillment of the requirements for the degree of

DOCTOR OF PHILOSOPHY

Chair of Committee,	Franco Marcantonio
Co-Chair of Committee,	Berna Hascakir
Committee Members,	Michael Tice
	Michael Pope
Head of Department,	Julie Newman

December 2020

Major Subject: Geology

ABSTRACT

Hydraulic Fracturing (HF) is an effective technique for hydrocarbon extraction from low-permeability shale reservoirs. It involves injecting a mixture of pressurized water, sand, and small amounts of chemicals into wells to introduce fractures in rock formations, which allows hydrocarbons to flow. However, with significant increases in production of oil and natural gas, concerns about potential environmental impacts resulting from excessive freshwater usage and wastewater contamination were raised. The average water requirement for an unconventional well is 1-3 orders of magnitude greater than a conventional well. After hydraulic fracturing, 5–85% of the HF fluid returns to the surface and may cause groundwater and surface water contamination when improperly treated. To reduce consumption, transportation, and disposal cost of water, flowback water was commonly reinjected for subsequent hydraulic fracturing by industry. However, because of complex interactions between injected water and reservoir rocks, induced fractures may be blocked by impurities carried by flowback water and mineral precipitation by water-rock reaction. Therefore, knowledge of water-rock interactions during hydraulic fracturing provides important information about the changes within the formation and ways to effectively manage the flowback waters.

My research focuses on investigating water-rock interactions during hydraulic fracturing in the lower Eagle Ford Formation and the Marcellus Formation. Simple interactions between deionized water and reservoir rocks and complicated interactions between flowback water and reservoir rocks were studied under static and dynamic

conditions to understand basic interaction mechanisms and evaluate effects of reuse of flowback water on hydraulic fracturing performance. Moreover, interactions between pseudo Marcellus Formation rocks and water were conducted to simplify water-rock system and understand how water-rock interactions affect flowback water properties. Pertinent low-cost pre-treatment methods were investigated to better manage Marcellus Formation flowback water for reinjection purposes. The results of my PhD work have potential to be adapted to the field-scale application directly and will contribute to successful management of flowback waters.

DEDICATION

I dedicate my dissertation work to my parents, Yuliang and Ruirong, who have always loved me unconditionally and give me encouragement during the challenges. I am truly thankful for having you in my life. This work is also dedicated to my best friends, Ziye, Mike, and Tanwei who have supported me throughout the doctorate program. I give special thanks to research groups from Geology & Geophysics Department and Petroleum Engineering Department for helping me develop my technology skills.

ACKNOWLEDGEMENTS

I would like to thank my committee chair, Dr. Marcantonio, Co-chair, Dr. Hascakir and my committee members, Dr. Tice, and Dr. Pope for their guidance and support throughout the course of this research.

Thanks also go to members at Heavy Oil, Oil Shales, Oil Sand & Carbonate Analysis and Recovery Method Research Team and technicians at the Ramey Thermal Recovery Laboratory and the Radiogenic Isotope Geochemistry Laboratory for their support and for making their facility available for the experimental work.

Finally, thanks to the department faculty and staff for making my time at Texas A&M University a great experience.

CONTRIBUTORS AND FUNDING SOURCES

Contributors

This work was supervised by a dissertation committee consisting of Professors Franco Marcantonio, Mike Tice and Mike Pope of the Department of Geology & Geophysics and Professor Berna Hascakir of the Department of Petroleum Engineering.

All other work conducted for the dissertation was completed by the student independently.

Funding Sources

Graduate study was financially supported by Berg-Hughes Center for petroleum and sedimentary systems in Geology & Geophysics Department and Crisman Institute for petroleum research in Petroleum Engineering Department at Texas A&M University.

NOMENCLATURE

U.S.	United States
BTU	British Thermal Units
CH_4	Methane
C	Carbon
H	Hydrogen
O	Oxygen
HI	Hydrogen Index
OI	Oxygen Index
TOC	Total Organic Carbon
USGS	United States Geological Survey
tcf	Trillion Cubic Feet
bbl	Billion Barrels
HF	Hydraulic Fracturing
IEA	International Energy Agency
mD	MilliDarcy
TDS	Total Dissolved Solids
EPA	Environmental Protection Agency
NORM	Naturally occurring radioactive materials
pCi/g	picocuries/gram
pCi/L	picocuries/liter

TSS	Total Suspended Solids
CEC	cation exchange capacity
meq	millequivalents
T sheet	tetrahedral silica sheet
O sheet	octahedral alumina sheet
XRF	X-ray Fluorescence
XPS	X-ray Photoelectron Spectroscopy
XRD	X-ray Diffraction
TGA	Thermal Gravimetric Analysis
psig	pounds per square in gauge
ICP-MS	Inductively Coupled Plasma Mass Spectrometry
SEM	Scanning Electron Microscopy
EDS	Energy Dispersive X-Ray Spectroscopy
IC 900	Chromatography 900
EIA	U.S. Energy Information Administration
ANOVA	Single Factor Analysis of Variance
Tukey HSD	Tukey's Honestly Significant Difference
PCA	Principal Component Analysis
PC	Principal Component
ppm	Parts Per Million
wt.%	Weight Percent
CFS	Coagulation/Flocculation/Sedimentation

rpm	revolutions per minute

TABLE OF CONTENTS

Page

ABSTRACT ii

DEDICATION iv

ACKNOWLEDGEMENTS v

CONTRIBUTORS AND FUNDING SOURCES vi

NOMENCLATURE vii

TABLE OF CONTENTS x

LIST OF FIGURES xiii

LIST OF TABLES xvi

CHAPTER I INTRODUCTION 1

1.1 An Overview of Energy Resources: Renewable and Nonrenewable 1
1.2 Occurrence, Migration, and Accumulation of Petroleum 4
1.3 The Rise of Unconventional Resources 12
1.4 Challenges and Solutions to Recovery Hydrocarbons from Shale Formations 19
1.4.1 Technical Challenge 19
1.4.2 Economic Challenge 21
1.4.3 Environmental Challenge 23
1.5 Management of Hydraulic Fracturing Waters in the U.S. 27
1.5.1 Flowback Water and Produced Water Characteristics 27
1.5.2 Flowback Water Constituents 31
1.5.3 Management of the Flowback water 34
1.6 Water-Rock Interaction Occurring During Hydraulic Fracturing 38
1.7 Stability of Colloids in Water after Water-Rock Interaction 48
1.8 The Eagle Ford Formation 54
1.8.1 Geologic Overview of the Eagle Ford Formation 54
1.8.2 Heterogeneity of the Eagle Ford Formation 62
1.8.3 Production History of the Eagle Ford Formation 64
1.8.4 Water Use in the Eagle Ford Formation 68
1.9 The Marcellus Formation 70
1.9.1 Geologic Overview of the Marcellus Formation 70

1.9.2 Production History of the Marcellus Formation....76
1.9.3 Challenges Associated with the Development of the Marcellus Formation ...79
Summary 82
References 84

CHAPTER II THE IMPACT OF SPATIALLY VARYING RESERVOIR MINERALOGY ON HYDRAULIC FRACTURING PERFORMANCE. CASE STUDY: WATER-ROCK INTERACTION IN LOWER EAGLE FORD FORMATION CHEMOFACIES 118

2.1 Introduction 119
2.2 Materials and Methods 123
2.3 Results and Discussions 132
2.3.1 Rock Characterization 132
2.3.2 Water-Rock Interaction Results 137
Summary 149
References 152

CHAPTER III THE IMPACT OF RE-INJECTING FLOWBACK FLUIDS ON FORMATION DAMAGE. CASE STUDY: THE MARCELLUS SHALE 159

3.1 Introduction 160
3.2 Materials and Methods 165
3.3 Results and Discussions 171
3.3.1 Rock Characterization 171
3.3.2 Flowback Water Characterization 173
3.3.3 Water-Rock Interaction Results 178
Summary 189
References 191

CHAPTER IV A SYSTEMATIC STUDY OF WATER-ROCK REACTIONS TO UNDERSTAND FLOWBACK WATER FROM MARCELLUS FORMATION AND PERTINENT TREATMENT FOR REUSE 198

4.1 Introduction 199
4.2 Materials and Methods 204
4.2.1 Sample Preparation....204
4.2.2 Experimental Design 206
4.3 Results and Discussion....209
4.3.1 Control Experiments on Pseudo Rock Samples and Water 209
4.3.2 Experiments on Flowback Water Samples....221
Summary 228
References 230

CHAPTER V CONCLUSIONS....236

APPENDIX A 238
APPENDIX B 247
APPENDIX C 254

LIST OF FIGURES

Page

Figure 1 Energy consumption in the U.S. in 2019. 3

Figure 2 Van Krevelen diagrams is used to classify kerogen types 8

Figure 3 Structural and stratigraphic oil and gas traps illustration 12

Figure 4 Map indicating shale plays in U.S.. 14

Figure 5 For the seven major shale plays across the U.S., the location map on the left and proved oil and natural gas reserves on the right. 16

Figure 6 Permeability ranges of the largest U.S. Shale Plays. 19

Figure 7 Estimated water usage for per HF well in different shale reservoirs in U.S. 25

Figure 8 Three methods are commonly used to dispose of returned water: a) deep well injection, b) release of the water after treatment and c) reuse of the water. 35

Figure 9 A diagram for cation exchange processes on the rock surface. 44

Figure 10 The mechanism of redox reaction and an example of siderite oxidation. 46

Figure 11 The dimension of the particles in water bodies 49

Figure 12 Illustration of the double layer structure in a liquid at contact with a negatively charged particle. 51

Figure 13 Illustration of different potentials near particle surface. 53

Figure 14 Paleogeographic reconstruction of North America during the Late Cretaceous. 56

Figure 15 Location map for the Eagle Ford Formation, which extends from the Maverick Basin, across the San Marcos Arch, and ending in the East Texas Basin. 57

Figure 16 Stratigraphic column of the Eagle Ford Formation in Maverick Basin (study area), San Marcos Arch, and East Texas Basin 58

Figure 17 Eagle Ford hydrocarbon production map 61

Figure 18 Texas Eagle Ford Shale daily oil (A) and natural gas production (B) from 2008 through 2020 66

Figure 19 Eagle Ford Shale drilling permits issued from 2008 through 2020. 68

Figure 20 Location map for the Marcellus Formation. 71

Figure 21 Stratigraphic column for the Marcellus Formation that is bounded above by Mahantango Formation and below by Onondaga Limestone. 72

Figure 22 Paleogeographic reconstruction of Eastern North America during the Middle Devonian. 74

Figure 23 Marcellus Formation daily natural gas production from 2008 through 2019. . 77

Figure 24 In Pennsylvania, 90% of wastewater has been reused or recycled since 2013. 81

Figure 25 The location map for the study area 124

Figure 26 Five chemostratigraphic units were divided by vertical distribution of elements and TOC in the lower Eagle Ford. 125

Figure 27 Schematic illustration of core-flooding experimental set-up 128

Figure 28 TGA plot of all lower Eagle Ford samples from different chemofacies 137

Figure 29 Loading plot of enriched major elements in produced water after static experiments 143

Figure 30 Score plot of each produced water sample in static experiments 145

Figure 31 Loading plot of major elements in dynamic experiments shows the relationships between elements. 149

Figure 32 The location map for the Marcellus Formation.. 165

Figure 33 The untreated flowback water is colored orange with some suspended solids settled within the water 169

Figure 34 Characterization of Marcellus Formation rock sample 172

Figure 35 TGA plot of initial Marcellus Formation rock sample. 172

Figure 36 Flowback water characterization: initial flowback water was filtered and evaporated respectively and then analyzed. 174

Figure 37 Characterization of residue from evaporation of initial flowback water 176

Figure 38 SEM Images of (a) flowback residue and (b) initial Marcellus Formation rock sample at 2,500X magnification. 177

Figure 39 SEM Images of rock samples before and after static experiments and dynamic experiments at 2,500X magnification. 189

Figure 40 The change in TDS with pH for all experiments. 218

Figure 41 Relationships between particle size and pH (figure on the left) and absolute value of the zeta potential and pH (figure on the right) for all experiments. .219

Figure 42 Ion concentration, pH, TDS, particle size, and zeta potential values of the flowback water originated from the Marcellus Formation hydraulic fracturing activity.....222

Figure 43 The changes in water samples after adding chemicals and CFS treatment. ..225

Figure 44 The percentage removal TDS after each pretreatment. 226

Figure 45 The relation between absolute zeta potential and particle size for each sample after each pretreatment. 228

LIST OF TABLES

Page

Table 1 Classification and characteristics of Kerogen based on hydrogen index and oxygen index ratio 7

Table 2 Source rock quality in terms of hydrocarbon generation based on TOC content and Rock-Eval pyrolysis experimental results 9

Table 3 Top 10 countries with technically recoverable shale resources. 15

Table 4 Summary of mineralogy, kerogen type, and TOC content in the most productive U.S. shale reservoirs 17

Table 5 Percentage and volume of estimated water usage per day in the U.S. in 2015 by category 23

Table 6 The types and purposes of most common chemicals used in HF operation 26

Table 7 The average HF fluid recovery rates from major shale reservoirs 28

Table 8 Generalized compositions of flowback water and produced water 29

Table 9 The summary of average TDS in wastewater from the major U.S. shale reservoirs 30

Table 10 Summary of NORM concentrations in drink water, earth surface and produced water from shale reservoirs. 31

Table 11 Classification of formation water from the main U.S. shale reservoirs based on variation in salinity 33

Table 12 Summary of technologies for removing inorganic contents and organic contents in flowback water and produced water. 36

Table 13 Summary of the cost of main technologies for treating flowback water and produced water 37

Table 14 Relative stability of common minerals under chemical weathering 40

Table 15 Dissolution reactions and solubility constant (K_{sp}) of common minerals present in shale reservoirs 43

Table 16 Values of cation exchange capability for different minerals 45

Table 17 Rection examples of complete and partial dissolution of minerals in water.....47

Table 18 The classification and properties of mixtures based on particle size.....49

Table 19 Relationship between zeta potential and particle stability.....54

Table 20 Daily oil and gas production in July 2020 of the top 5 operators in the Eagle Ford Formation. 67

Table 21 Daily gas production in March 2019 of the top 5 operators in the Marcellus Formation.....78

Table 22 Summary of geochemical characteristic of each chemofacies.....126

Table 23 Mineralogy of each sample obtained through XRD analysis (wt. %).....133

Table 24 Elemental concentrations of each original sample obtained through XRF analysis 134

Table 25 Decomposition and dehydroxyliation temperature of minerals and organic matter in the lower Eagle Ford samples 135

Table 26 Mass loss at particular temperature during TGA test.....136

Table 27 Characterization of supernatant water samples from static experiments.....139

Table 28 Calculated p-values of enriched elements for different chemofacies. 141

Table 29 Mean enriched elemental concentrations (ppm) in static produced water for different chemofacies.....142

Table 30 Characterization of produced water samples after dynamic experiments.....146

Table 31 Calculated p-values of enriched elements for chemofacies after dynamic experiments.....148

Table 32 Penetration depth and detection limits for XPS, XRD, and SEM.....167

Table 33 Ions detected by ICP-MS and IC 900 169

Table 34 Characterization of deionized water and filtered flowback water.....175

Table 35 Ion contents in deionized water and filtered flowback water analyzed by ICP-MS and IC 900 176

Table 36 Characterization of produced water samples from static experiments.....179

Table 37: Ion contents in water before and after static experiments, ppm. 181

Table 38 Mineralogy and Possible Dissolution/Precipitation Reactions in Marcellus Formation Rock Sample 182

Table 39 Characterization of produced water samples from dynamic experiments 183

Table 40 The average ion contents in water before and after dynamic experiments analyzed by ICP-MS and IC 900 185

Table 41 Average elemental concentrations of rock samples before and after experiments. 186

Table 42 Mineralogy of samples before and after experiments 187

Table 43 Composition (wt. %) of four standard minerals analyzed by XRF 205

Table 44 Summary of water parameters in produced water after one-component mineral-water interactions at room temperature and reservoir temperature... 210

Table 45 Linear correlations between mineral concentration and water parameters at room and reservoir temperature. 216

Table 46 pH, TDS, particle size, and zeta potential results for the supernatant after pretreatment. 226

CHAPTER I

INTRODUCTION

The rapid and large-scale extraction of unconventional resources from shale reservoirs utilizing horizontal hydraulic fracturing has significantly improved economic development in the U.S. This chapter aims to review the two most prolific shale reservoirs in the U.S., the Eagle Ford Formation and the Marcellus Formation, which form the study units for my thesis. Recent energy types and their importance to economic development are first reviewed. Unconventional resources, particularly those extracted in shale reservoirs, have triggered an energy revolution in the world; these resources are reviewed with a focus on the development history of shale reservoirs, technology resolution, and potential economic and environmental impacts during energy production. Next, the importance of Eagle Ford Formation and Marcellus Formation is highlighted by reviewing their geologic background and production history separately. Finally, critical research problems existing in the two formations or recent studies are discussed. These specific problems are the focus of my research objectives, which are further discussed in the following chapters.

1.1 An Overview of Energy Resources: Renewable and Nonrenewable

Energy provides the material foundation for human civilization and is one of the most important components of economic infrastructure. It is stored and available in

different forms and sources. Based on how quickly energy can be replenished, energy sources are divided into two groups: renewable and nonrenewable (Weiss, 1962). Renewable energy can be replenished in a short time, and commonly includes hydropower, solar, wind, tidal, geothermal energy from inside the earth, and biomass from plants. These resources play an important role in the supply of energy today and will play an even more crucial role in the future of the energy sector. In 2019, renewable energy (**Figure 1**) contributed approximately 11% of total U.S. energy consumption (EIA, 2020). Moreover, it was projected that renewable energy will be the fastest-growing energy source in the future with the increase in the consumption by an average 2.3% per year between 2015 and 2040 (IEO, 2017). However, there are some technical challenges that renewable energy faces. For example, the unsteady supply of wind and solar power necessitates storage that does not yet exist on a sufficient scale; current power grid is not equipped to handle widespread use of these sources. Therefore, nonrenewable energy resources will continue to be necessary until these challenges are overcome. Nonrenewable energy resources cannot be replenished on a human time scale and are available in limited supplies. They mainly include oil, natural gas, coal, and nuclear power that together account for more than 80% of total U.S. energy consumption (EIA, 2020).

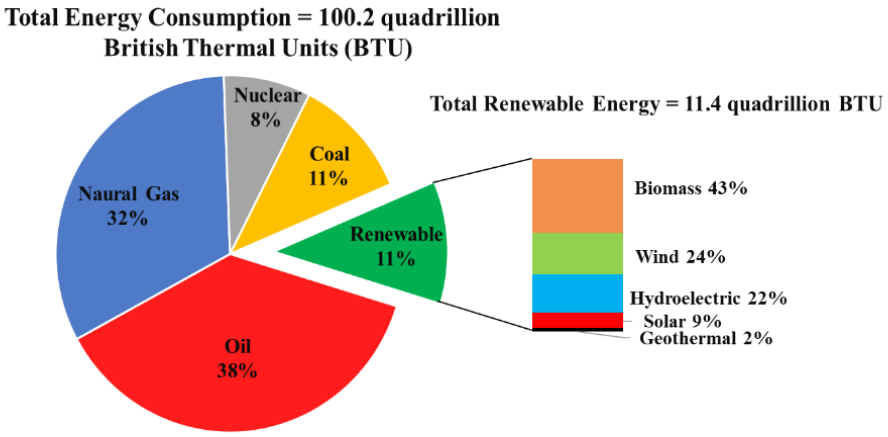

Figure 1 Energy consumption in the U.S. in 2019. Renewable energy and nonrenewable energy accounted for approximately 11% and 89% of total U.S. energy consumption. Image modified from U.S. Energy Information Administration (2020).

Nonrenewable energy resources derived from fossil sources, particularly oil and natural gas, are known as petroleum. Petroleum is a complex mixture of hydrocarbon molecules mainly composed of hydrogen and carbon as well as small amount of nitrogen, oxygen, sulfur, and heavy metals as impurities, and existing in liquid, gaseous, semi-solid, and solid forms (Tissot and Welte, 1984). In particular, crude oil is liquid phase petroleum both at underground and normal surface conditions and contains different amounts of dissolved gases, bitumen, and other impurities. Natural gas refers to petroleum gas and consists of lighter paraffin hydrocarbons, in which the most abundant is methane gas (CH_4) (Tissot and Welte, 1984). Semi-solid and solid forms of petroleum are made up of heavy hydrocarbons and bitumen. They comprise materials such as asphalt, tar, pitch, albertite, etc. (North, 1985).

1.2 Occurrence, Migration, and Accumulation of Petroleum

A petroleum system "encompasses a pod of active source rock and all related oil and gas and includes all the essential elements and processes needed for oil and gas accumulation to exist" (Magoon and Dow, 1994). Therefore, diagnosing its essential elements (source rock, reservoir rocks, and cap rock) and processes (generation, migration, and accumulation of petroleum) is critical to understand petroleum system (Magoon and Dow, 1994). In general, the history of a petroleum system begins with the deposition of organic matter, followed by conversion of organic matter into kerogen, transformation of kerogen into hydrocarbons, then migration of hydrocarbons from sources rocks to reservoir rocks, and finally accumulation of hydrocarbons in reservoir rocks (Tissot and Espitalie, 1974; Tissot and Welte, 1984).

The process of converting organic matter in sedimentary rocks into petroleum is called maturation. During the maturation process, petroleum is formed from productive source rocks which contain high organic carbon content. This organic content represents the fossilized remains of prehistoric plants and animals that were gradually buried in rock layers. Therefore, petroleum is also called a fossil fuel (Sato, 1990). These fossilized organisms undergo degradation and mature progressively to generate hydrocarbons within the several hundred meters and millions of years of burial (Tucker, 1988). Specifically, as burial of organic-rich sediments progresses, associated increases in temperature and pressure drive the processes of diagenesis (formation of kerogen), catagenesis (oil and wet gas window), and metagenesis (dry gas window), which together convert organic matter

into petroleum. About 10-20% of petroleum is generated during diagenesis, while more than 80% of petroleum is formed during catagenesis and metagenesis (Tissot and Welte, 1984; Libes, 2009).

Diagenesis takes place within the first few thousand years during shallow burial and at temperature <60°C (Tissot and Welte, 1984; Horsfield and Rullkötter, 1994). During early diagenesis, biogenic methane is first produced as the main hydrocarbon product by microbial activity. With increasing burial depth, water in the original organic materials is forced out, and other constituents such as proteins and carbohydrates break down to form new structures that comprise a waxy material known as kerogen (Dow, 1977; Durand, 1980; Tissot and Welte, 1984). Kerogen is defined as macromolecular organic matter disseminated within sedimentary rocks which is insoluble in common organic solvents (Forsman and Hunt, 1958).

Catagenesis is the second stage of maturation of organic matter and occurs under conditions of deeper burial and temperatures between 60-200°C (Tissot and Welte, 1984; Libes, 2009). During catagenesis, kerogen is thermally degraded and starts to form hydrocarbon chains, marking the conversion of kerogen into hydrocarbons (Durand, 1980). The formation of different petroleum products requires specific windows of conditions. Depending on the extent of thermal maturation and the original composition of deposited organic materials, kerogen breaks down to form lower-molecular-weight products including oil, bitumen, and natural gas over long geological time (Gizjel, 1980). Oil is mainly yielded during lower thermal maturities between 100-150°C while gas is

yielded during higher thermal maturities between 150-220°C (Jüntgen and Klein, 1975; Hunt, 1991).

Metagenesis is the last stage of maturation and conversion of organic matter to hydrocarbons. It takes place at temperatures >200°C (Hunt, 1996). During metagenesis, methane and hydrogen-depleted graphitic carbon residue are generated from the remaining kerogen and bitumen (Tissot and Welte, 1984).

In summary, the generation of petroleum is a result of the increase in temperature and pressure conditions during burial which causes progressive cracking of organic matter in sediments. During these processes, kerogen plays a central role in hydrocarbon production.

In kerogen, there are three main elements: carbon (C), hydrogen (H), and oxygen (O). Typically, the ratios of H and O contents to total organic carbon present in kerogen are used to assess origin of organic matter. These two parameters are called the hydrogen index (HI) and oxygen index (OI) (Van Krevelen, 1950; Tissot and Welte, 1984). For example, HI is relatively high in marine organisms and algae because they are commonly made up of lipid- and protein-rich organic matter. It is relatively low in land plants that are composed of carbohydrate-rich constituents (Emerson and Hedges, 1988). In contrast, OI is higher in land plants and inert organic material than marine organisms because it is rich in polysaccharides (Emerson and Hedges. 1988; Meyers, 1997).

The elemental composition of kerogen (**Table 1** and **Figure 2**), particularly HI and OI, is used for classification into four types indicating if the host rock will be oil or gas prone (Van Krevelen, 1950). Type I kerogen has high atomic H/C and low O/C ratios (HI

range >1.25; OI range < 0.15) and is most likely to produce oil. This type of kerogen is often composed of algal materials deposited in both marine and lacustrine environments (Tissot and Welte, 1984). Type II kerogen has intermediate atomic H/C and O/C ratios (HI <1.25; OI range: 0.03-0.18) and is capable of generating oil and little gas. It normally contains a mixture of terrestrial and marine organic materials commonly deposited in but not restricted to marine environments (Tissot and Welte, 1984; Durand, 1980). Type III kerogen is characterized by lower atomic H/C ratios and higher O/C ratios (HI <1; OI range: 0.03-0.3) than types I and type II and generally produces natural gas and little or no oil. It is mainly derived from wood-like material, algae, and plankton deposited mainly in terrestrial environments (Tissot and Welte, 1984). Type IV kerogen has the lowest atomic H/C ratios and highest O/C ratios (HI <0.5; OI range: 0.03-0.3) of any type of kerogen and comprises mostly inert organic matter, which has no potential to produce hydrocarbons (Weber and Green, 1981). Type IV kerogen's pathway lies below the type III and sometimes is not shown on Van Krevelen diagrams.

Table 1 Classification and characteristics of Kerogen based on hydrogen index and oxygen index ratio. Table modified from AAPG Wiki (2016).

Kerogen Type	HI	OI	Source Material	Depositional Environment	Hydrocarbon Generated
Type I	>1.25	<0.15	Mainly algae	Lacustrine	Mainly oil
Type II	<1.25	0.03 - 0.18	Mainly plankton, some contribution from algae	Marine	Mainly gas, little oil
Type III	< 1	0.03 - 0.3	Mainly plants	Terrestrial	Mainly gas, little oil
Type IV	< 0.5	0.03 - 0.3	Reworked and oxidized material	Varied settings	None

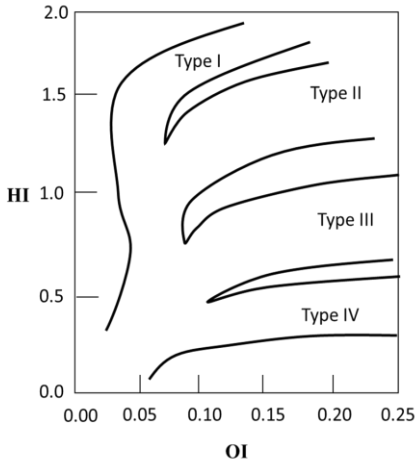

Figure 2 Van Krevelen diagram is used to classify kerogen types. Based on hydrogen index and oxygen index, kerogen is divided into 4 types. Image modified from Walters (2006) with permission from Springer.

However, not all rocks contain kerogen, and therefore do not have the potential to produce oil or gas. Moreover, rocks containing kerogen may also not form productive petroleum reservoirs. Generally, different necessary elements (source, reservoir, and cap rocks) and processes (generation, migration, accumulation, and trap formation) are required to occur in the correct time and space so that organic matter is able to be converted into a petroleum accumulation; these elements and processes form a complete petroleum system (Magoon and Dow, 1994).

Source rock, reservoir rock, and cap rock are three necessary elements in the generation and accumulation of hydrocarbon resources (Hyne, 2011). Typically, source rock refers to rocks with high concentration of organic material where kerogen is capable of being transformed into hydrocarbon resources under favorable subsurface temperature and pressure (Brooks et al., 1987). Source rocks were deposited in a variety of

environments, including deep water marine and lacustrine settings, and need millions of years to be buried deeply and generate sufficient volumes of oil and gas (Goodwin et al., 2014). To estimate petroleum generative potential, Peters and Cassa (1994) reported a scale to assess source rocks: rocks with total organic carbon (TOC) contents less than 0.5 wt. % are poor sources; 0.5-1.0 wt. % are fair sources; 1.0-2.0 wt. % are good sources; and more than 2.0 wt. % are very good or excellent source rocks. Another method, Rock-Eval pyrolysis, which is regarded as more accurate than the TOC scale, is widely used to evaluate petroleum generative potential (Espitalié et al., 1977; Peters, 1986). In this analysis (**Table 2**), two parameters, S_1 (free hydrocarbon already present in the rock sample before analysis) and S_2 (hydrocarbon compounds generated from kerogen cracking during pyrolysis) are recorded and used to determine the petroleum potential of a source rock (Tissot and Welte, 1984). Good generation potential of source rock typically is indicated by high TOC content and high (S_1+S_2) value (Gogoi et al., 2008).

Table 2 Source rock quality in terms of hydrocarbon generation based on TOC content and Rock-Eval pyrolysis experimental results. Reprinted in Peters (1986) with permission from AAPG Bulletin.

Quality	TOC (wt. %)	S_1 (mg HC/gm rock)	S_2 (mg HC/gm rock)
Poor	0.0–0.5	0.0–0.5	0.0–2.5
Fair	0.5–1.0	0.5–1.0	2.5–5.0
Good	1.0–2.0	1.0–2.0	5.0–10.0
Very good	> 2.0	> 2.0	>10.0

After hydrocarbons are generated in the source rocks, they flow vertically or laterally under the influence of pressure through cracks and pores within rocks and are

stored in porous and permeable rocks that are known as reservoir rocks (Dimri et al., 2012). Although igneous and metamorphic rocks can sometimes act as reservoir rocks if they accommodate hydrocarbons, reservoir rocks are dominated by sedimentary rocks, including mainly sandstones and carbonate rocks because they commonly have high porosity. Sandstone, a clastic sedimentary rock, is composed of sand-sized (0.0625-2 mm) grains with porosity generally varying from 10-40% and permeability ranging from less than 1 to over 50,000 milliDarcys (mD) (Dott, 1964; Coneybeare, 1967; Keelan, 1982). Sandstone reservoirs typically are porous and permeable enough to allow flow and storage of large quantities of hydrocarbons. Therefore, more than 60% of the world oil reserves occur in sandstone reservoirs (Goodwin et al., 2014). Carbonate rock is a sedimentary rock composed of more than 50% of carbonate minerals, primarily including calcite and dolomite, with porosity ranging from 5-25% and permeability varying from less than 5 to more than 10,000 mD (Enos and Sawatsky, 1981; Coneybeare, 1967; Keelan, 1982; Lucia, 1995). Because dolostone typically is much more porous than limestone, dolomite reservoirs have higher hydrocarbon production than limestone reservoirs. It was estimated that 80% of carbonate reservoirs in the U.S contain dolomite, whereas the rest contain calcite (Zenger et al., 1980).

The movement of newly generated hydrocarbons from source rocks to reservoir rocks is defined as migration. Migration comprises two stages: primary migration and secondary migration. Primary migration is the movement of hydrocarbons out of their source rock through fractures and pores created by increased pressure and is also called expulsion (Leythaeuser et al., 1984). It follows pressure gradients from the center of

source rocks to adjacent reservoir strata. Expulsion sometimes occurs in pulses because of pressure decline and fracture closure after the first expulsion. More expulsions continue to happen as long as petroleum creates enough pressure and fractures re-open. Primary migration can be both upward and downward in direction depending on pressure gradients (Chapman, 1983). Secondary migration refers to the further movement of hydrocarbons outside of the source rock towards carrier rocks and reservoir rocks (Tissot and Welte, 1984). Unlike primary migration during which hydrocarbons migrate mainly vertically and through less permeable and porous source rocks, secondary migration is lateral within porous and permeable rock strata (Tissot and Welte, 1984; Chapman, 1983). Sandstone and carbonate are the most common carrier rocks that allow secondary migration because of their high porosity and permeability. The primary mechanism for secondary migration is buoyancy. Because oil and gas have lower densities than the surrounding pore fluids, they generally move and accumulate in the structurally highest part within reservoir rocks (Tissot and Welte, 1984).

The upward migration of petroleum is stopped by a cap rock, which is an impermeable rock sealing above and around a reservoir rock. Cap rock should be large enough to prevent oil and gas from escaping to the earth's surface, considering the basin scale (Kearey, 2001). It commonly includes evaporites, chalks, shale, and cemented rocks. (Melvin, 1991; Huxley; 1986). The arrangement of the reservoir and cap rocks, called a trap, is where the migrated petroleum can be accumulated and preserved (Tissot and Welte, 1984). Depending on how it is formed, two types of traps are recognized: structural and stratigraphic (**Figure 3**) (Allen and Allen, 1990). Structural traps are formed when the

reservoir rock and cap rock have been deformed by tectonic activity like faulting and folding. Stratigraphic traps are formed when the reservoir rock is deposited as a discontinuous layer truncated by erosion.

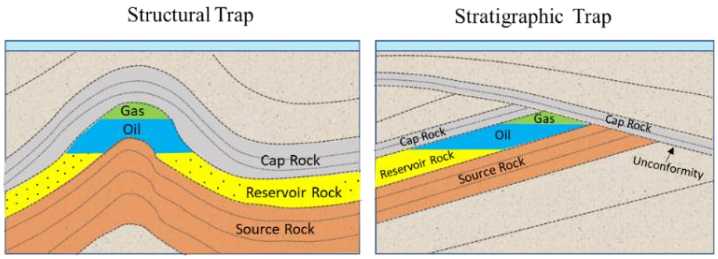

Figure 3 Structural and stratigraphic oil and gas traps illustration. Image modified from ManuRoquette (2019).

1.3 The Rise of Unconventional Resources

Petroleum reservoirs are broadly classified as conventional and unconventional reservoirs (EIA, 2013; Gordon 2012; Leimkuhler and Leveille, 2012). Conventional reservoir rocks mainly are sedimentary rocks with relatively high porosity and permeability, including sandstone and carbonate rock (Keelan, 1982; Enos and Sawatsky, 1981; Lucia, 1995). In conventional reservoirs, hydrocarbons are trapped by overlying cap rock layers with lower permeability. Because they are easier and less expensive to produce, conventional oil and gas were the first targets of industry. By contrast, unconventional reservoir rocks have low porosity and permeability compared to their conventional counterparts, and primarily include gas and oil shale, tight sands, coalbed methane, and methane hydrates (Baker, 1981; Pápay, 2013; EIA, 2013). The

unconventional reservoirs trap the hydrocarbons in place without a cap rock, but the hydrocarbon resources are difficult to produce commercially with traditional technology. Gas and oil shale is a shale reservoir predominantly composed of shale that is both source rock and reservoir rock (Aguilera, 1978). Tight sand is a sandstone reservoir with unusually low permeability (<0.1 mD) because of cementation, compaction, or poor sorting (Suárez, 2012). Coal-bed methane refers to natural gas that contains a high percentage of methane and is stored in deeply buried coal seams (Suárez, 2012). The permeability of coal seams lies in the range of 0-50 mD (McKee et al., 1988). Methane hydrate is methane that is trapped within the crystal structure of water, forming a solid similar to ice (USGS, 2009). The pore structure of methane hydrate can be on the order of angstroms in scale (Beaudoin et al., 2014). The development of these unconventional resources has led to a surprising increase in gas and oil production in the U.S since 2006 (Suárez, 2012).

The world's demand for energy is rising rapidly, whereas resources from conventional reservoirs are running out. The U.S. Energy Information Administration (EIA) estimated that world energy consumption will grow by 28% between 2015 and 2040 and fossil fuels will still account for more than 75% of world energy consumption through 2040 (IEO, 2017). Although at present, conventional sources provide the most oil and natural gas, conventional reservoirs will be unable to supply more than a fraction of energy demand by 2040 (IEO, 2013). Hence developing unconventional resources is increasingly important to meet the energy deficit. Among all unconventional resources, shale oil and gas resources are viewed as critical potential sources of hydrocarbon production because

oil and gas resources in shale formations represent 10% of and 32% of the world's oil and natural gas technically recoverable resources (IEO, 2013). This fraction continues to rise in 2020. In the United States, shale oil and natural gas resources also exist in large quantities (**Figure 4**). EIA reported that the United States has the second largest shale oil resources and fourth largest shale gas resources (**Table 3**), compared with the other 41 countries assessed (AEO, 2014). Moreover, due to the significant production of hydrocarbon resources from shale reservoirs, the United States currently is the largest oil and natural gas producer in the world (EIA, 2019).

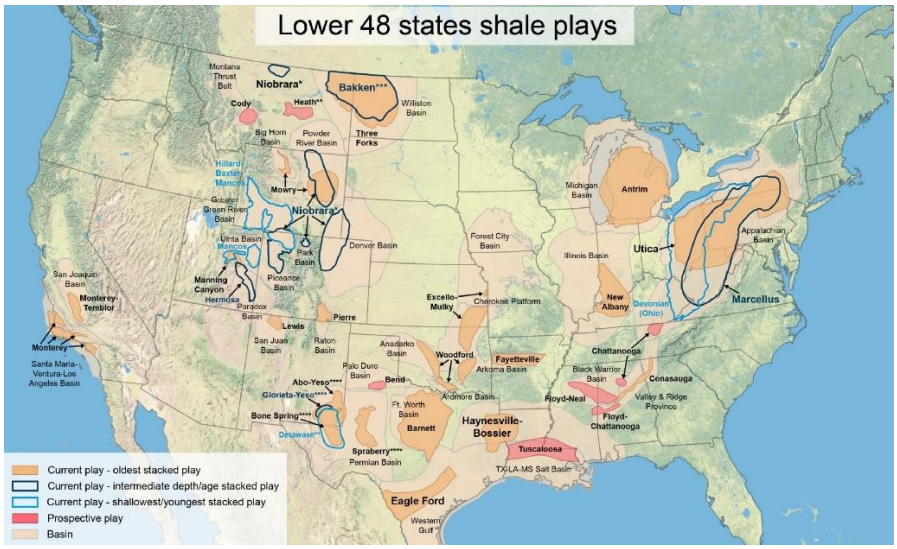

Figure 4 Map indicating shale plays in U.S. Reprinted in U.S. Energy Information Administration (2016).

Table 3 Top 10 countries with technically recoverable shale resources. Reprinted in U.S. Energy Information Administration (2013).

Shale oil			Shale gas		
Rank	**Country**	**billion barrels (bbl)**	**Rank**	**Country**	**trillion cubic feet (tcf)**
1	Russia	75	1	China	1115
2	U.S.	58	2	Argentina	802
3	China	32	3	Algeria	707
4	Argentina	27	4	U.S.	665
5	Libya	26	5	Canada	573
6	Australia	18	6	Mexico	545
7	Vebezuela	13	7	Australia	437
8	Mexico	13	8	South Africa	390
9	Pakistan	9	9	Russia	285
10	Canada	9	10	Brazil	245
World Total		**345**	**World Total**		**7299**

In the United States, the top 7 most prolific shale reservoirs (**Figure 5**) at present are the Bakken Formation (Montana and North Dakota), Eagle Ford Formation (Texas), Haynesville Formation (Louisiana and Texas), Appalachia Basin (containing Marcellus Formation and Utica Formation covering Pennsylvania, Ohio, West Virginia, and New York), Anadarko Basin (Oklahoma and Texas), Niobrara Formation (Colorado and Wyoming), and Permian Basin (Texas) (EIA, 2019). These reservoirs currently constitute a major portion of oil and gas production in U.S., and their contributions are expected to continue to increase over the next 30 years (EIA, 2019).

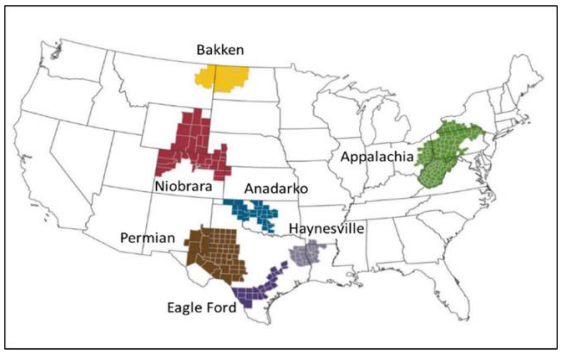

Shale Plays		Oil Reserves, million barrels	Natural Gas Reserves, trillion cubic feet
Bakken		5,862	12
Eagle Ford		4,734	30.8
Haynesville		not available	44.7
*Appalachia	Marcellus	345	135.1
	Utica	not available	23.9
Niobrara		317	not available
Permian		11,096	46.7
Anadarko		560	21.4
Sub-total		22,914	314.6
All U.S. Proved Reserves		47,053	504.5

Figure 5 For the seven major shale plays across the U.S., the location map on the left and proved oil and natural gas reserves on the right (*The Marcellus and the Utica Formation have been combined into one Appalachia region). Modified from U.S. Energy Information Administration (2019).

In these shale reservoirs, organic-rich shale (also called black shale) commonly is considered to be the major rock type (Vine and Tourtelot, 1970). Black shales consist of mixtures of fine grained quartz and clay minerals with different organic contents along with other minerals potentially including carbonate minerals, sulfide minerals, feldspars, and oxide minerals (O'Brien and Slatt, 1990; Slatt and Rodriguez, 2012; Vine and Tourtelot, 1970; Yaalon, 1962). Some shale formations are not composed of typical shales (>75% of clay minerals) (Chermak and Schreiber, 2014). For instance, the Eagle Ford Formation, Utica Formation, Anadarko Basin, and part of the Niobrara Formation are organic-rich calcareous-shales that are dominated by carbonate minerals instead of clay minerals. However, they are classified as oil and gas shale because they contain shale components which are mainly composed of clay-size minerals. The organic matter was preserved from decay in black shale because it was typically deposited under anoxic and reducing conditions (Blatt and Robert, 1996). High subsurface pressures and temperatures during burial convert the organic matter to hydrocarbons. However, the clay contents with

low permeability severely limit gas and oil flow, which leads to the hydrocarbons remaining within the shale rather than migrating into other reservoir rocks. Therefore, shale is both source rock and reservoir rock.

Although the seven most highly productive unconventional reservoirs are shale reservoirs, their geological characteristics (especially mineralogy, organic content, and kerogen type; **Table 4**) and hydrocarbon production potential vary considerably from play to play. The properties listed in Table 4 help engineers to evaluate production potential of shale reservoirs. For instance, Type I kerogen is oil prone; Type II kerogen is capable of generating oil and little gas; Type III kerogen is gas prone; and Type IV kerogen has no potential to produce hydrocarbons (refer to Table 1) (Tissot and Welte, 1984; Weber and Green, 1981).

Table 4 Summary of mineralogy, kerogen type, and TOC content in the most productive U.S. shale reservoirs (Bresch and Carpenter, 2009; Sorensen et al., 2010; Chalmers et al., 2012; Chermak and Schreiber, 2014; Bai et al., 2016; Cortez, 2012; Jiang et al., 2016).

Shale Plays	General Mineralogy	Kerogen Type	TOC Range %
Bakken	Illite, quartz, dolomite and minor amounts of pyrite, chlorite, calcite, and smectite	Type I and Type II	2-23%
Eagle Ford	Calcite, quartz, pyrite, illite, kaolinite and minor amounts of dolomite, plagioclase, feldspars, and apatite	Type I and Type II	2-12%
Haynesville	Illite, quartz, feldspar, calcite, and minor amount of pyrite, smectite, kaolinite, chlorite	Type II, III and IV	0.5-6%
Marcellus	Quartz, calcite, dolomite, illite, kaolinite smectite, feldspar, pyrite, and gypsum.	Type II and Type III	1-11%
Utica	Calcite, quartz, illite, chlorite and minor amount of dolomite	Type III	1-5%
Niobrara	Quartz, calcite, illite, and smectite	Type II and Type III	0.1-5%
Permian	Carbonate minerals, quartz, feldspar, pyrite, and apatite	Type II and Type III	1-8%
Anadarko	Calcite, dolomite, quartz, and clays	Type II and Type III	1.8-10%

In particular, the Bakken Formation is composed of organic-rich shale, siltstone, and sandstone, in which clay minerals and quartz are the dominant minerals (Kasper, 1992). Both oil and gas are produced primarily from shale and sandstone layers. The Eagle Ford Formation typically consists of organic-rich calcareous-shale with dominant carbonate minerals (mainly calcite) in which oil and gas are produced (Surles, 1987). The Haynesville Formation is lithologically heterogeneous, and is composed of argillaceous shale, calcareous shale, sandstone, and dolomite. Abundant gas is extracted from shale layers (Ewing, 2001). The Marcellus Formation lithology varies significantly across the Appalachian basin, comprising calcareous shale, sandstone, and limestone (Ettensohn and Barron, 1981; Harper, 1999). Gas is the main hydrocarbon produced in the Marcellus Formation. The Utica Formation is located a few thousand feet below the Marcellus Formation, which is widely known as a source of natural gas. It is described as carbonaceous black shale containing a high amount of carbonate minerals. The Niobrara Formation is composed of mixed lithologies of chalk (mainly calcite) and marl (mainly calcite and clay minerals), where both oil and gas are produced (Luneau et al., 2011). The Permian Basin, including several source rocks (Woodford, Barnett, and Wolfcamp), is categorized as either calcareous shale or non-calcareous shale, depending on the relative contribution of carbonate minerals versus clay (Engle et al., 2016). Both oil and gas are produced in these source rocks. The Permian Basin is currently the highest producing oilfield in the world, and its oil production accounts for more than one third of total U.S. oil production (EIA, 2019). The Anadarko Basin consists of organic-rich calcareous-shale and holds one of the most prolific natural gas reserves in U.S (Ball et al., 1991).

1.4 Challenges and Solutions to Recovery Hydrocarbons from Shale Formations

1.4.1 Technical Challenge

To recover hydrocarbons from shale formations, there are three main challenges the petroleum industry faces. The first challenge is the low permeability of shale. Shale was considered a source rock but not a good reservoir rock by industry until the 2000s, because extremely small grain and pore sizes made it relatively impermeable (typically <0.1 mD; **Figure 6**) (Law and Curtis, 2002; Cantisano et al., 2013). Therefore, hydrocarbons were thought to be locked in shale and uneconomical to produce.

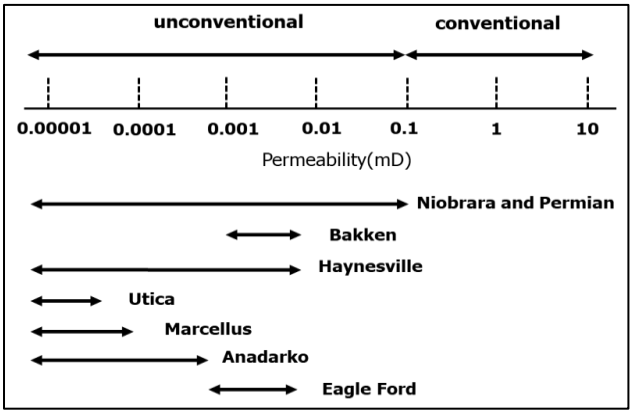

Figure 6 Permeability ranges of the largest U.S. Shale Plays. They are the targets for horizontal drilling and hydraulic fracturing. Some formations also contain conventional reservoirs, like Permian Basin and Bakken Formation, which means the permeability of these reservoirs is larger than 0.1 mD. But they are not shown in this figure because they do not use hydraulic fracturing (Faraj, 2012; Hughes, 2013; Jarvie, 2012; Law and Curtis, 2002; Cantisano et al., 2013).

However, the application of horizontal drilling and hydraulic fracturing (HF) artificially increases the permeability of shale and enhances hydrocarbon production. Therefore, at present, energy companies are able to directly tap source rock within shale reservoirs using these tools. Horizontal drilling is a drilling process starting with a vertical well that turns horizontal within the reservoir rock to access more hydrocarbon resources (Allouche et al., 2000; DC Solid Control, 2013). Thus, more oil and natural gas can be produced with fewer wells and less surface disturbance. The first recorded horizontal well was drilled near Texon, Texas in 1929 (Popular Horizontal, 1991). With advancements in drilling motors and steering, horizontal drilling became widespread in the 1980s (Helms, 2008).

The permeability of a shale formation can be enhanced due to hydraulic fracturing which is a technique that involves injection of millions of gallons of highly pressurized hydraulic fracturing fluid, typically consisting of 90% water, 9.5% sand, and 0.5% chemical additives, to create small fractures and increase permeability in shale reservoirs (Ground water Protection Council, 2009; Gandossi and Von Estorff, 2015). It was first successfully applied in 1950 but has been used extensively in the U.S. since 2008 (EIA, 2014). Natural gas production in the United States had declined from 24.2 trillion cubic feet (tcf) in 2000 to 23.5 tcf in 2005. The decline was reversed by 2008 when gas production rose to over 26 tcf and reached 90.6 tcf in 2019 (EIA, 2019). Thus, commercial shale gas production has increased greatly due to horizontal drilling and hydraulic fracturing. Currently, hydraulically fractured horizontal wells account for more than 69% of all oil and gas wells drilled in the United States (EIA, 2018). Moreover, produced shale

oil and natural gas in U.S. represent 60% of total U.S. oil production and 70% of total U.S. dry gas production, respectively (EIA, 2019).

As of 2020, the coronavirus pandemic has caused distortions across world oil markets. The price of U.S. oil turned negative for the first time in history in April 2020 (Watts, 2020). Moreover, the pandemic has slowed fracturing activities in the United States. Drilled wells awaiting fracturing services have exceeded 5,700 assets at the end of May 2020, which is the highest level since December 2017 (Woodroof, 2020)

1.4.2 Economic Challenge

Although advanced technologies allow energy companies to extract hydrocarbons from shale formations that were unworkable just a few years ago, new costs to the extraction process were introduced, which leads to the economic challenge. In addition to drilling toward the target formation, like vertical drilling used in conventional reservoirs, horizontal drilling also alters the direction of the drill bit from vertical to horizontal. Therefore, a horizontal well not only drills thousands of feet down to reach the deposit, but also extends thousands of feet horizontally from the well bore, which causes an increase in labor and basic input cost (Mitchell 1995; Beattie, 2019). Moreover, once the well is established, millions of gallons of water, sand, and chemicals are injected into the shale formation to create fractures. In general, vertical drilling uses about 80,000-600,000 gallons of water per well whereas hydraulic fracturing uses 2,000,000–5,000,000 gallons of water per well to develop fractures and carry sand to prevent fracture closure

(Hagemeier and Hutt, 2009; Gregory et al., 2011; Lippes 2015). Transporting millions of gallons of water by trucks and pipes to the well adds to the cost of each well. In addition, although chemicals added into HF fluid only account for less than 0.5% of the total HF fluid, the huge volumes of water mean that chemicals cannot be ignored and are still costly for operators. All of these contribute to the cost of a horizontal well. The cost of oil production per barrel from conventional reservoirs in the U.S. is approximately $30-$40 (Beattie, 2019). However, the oil cost-per-barrel from shale reservoirs varies from $40-$90 (Rosenberg, 2019). Therefore, the average horizontal well by hydraulic fracturing is more expensive than the average vertical well in shale formation. When oil prices are less than the cost of fracturing, it is less likely for energy companies to construct new wells through HF.

Besides excess freshwater usage, hydraulic fracturing operation generates huge volumes of wastewater during the hydrocarbon extraction process that must be disposed of after well production is complete. This wastewater with complicated composition cannot be handled by municipal water treatment facilities that are not designed to treat such high levels of contamination. Additional technologies were established for the treatment of wastewater. Therefore, treatment of wastewater hugely adds to the cost of hydraulic fracturing. Moreover, this problem is also closely related to the environmental challenge and will be introduced in the following section.

1.4.3 Environmental Challenge

The increased well production in shale formations was accompanied by rising concerns about potential environmental impact resulting from excessive use of water. Thus, the third challenge is environmental. In general, the water requirement for unconventional production is 1-3 orders of magnitude greater than conventional production (Hagemeier and Hutt, 2009; Gregory et al., 2011; Lippes, 2015). This increased water usage not only increases the cost of hydraulic fracturing and but also reduces access to fresh water for people. The United States Geological Survey (USGS) estimated total water usage in the United States in 2015 (the most recent year available) by category (**Table 5**).

Table 5 Percentage and volume of estimated water usage per day in the U.S. in 2015 by category. Total water usage was estimated to be 322,000 million gallons per day. Table modified from U.S. Geological Survey (2018).

Category	Percentage	Volume, million gallons
Thermoelectric	41.30%	132,986
Irrigation	36.60%	117,852
Public Supply	12.10%	38,962
Self-Supplied industrial	4.60%	14,812
Aquaculture	2.30%	7,406
Mining	1%	3,220
Self-Supply Domestic	1%	3,220
Livestock	<1%	<3,220

Hydrocarbon production is a part of the mining category in Table 5 which represented about 1% of the total water used in the U.S. in 2015. Because the water used for HF just accounted a small percentage of the industrial water at that time, it was

suggested that hydraulic fracture did not use significantly more water than other energy sources (Spang, et al., 2011; Jackson et al., 2014). However, the construction of horizontal wells with hydraulic fracturing has accelerated dramatically. According to the U.S. Department of Energy, more than two million hydraulic fracturing wells in the U.S. were established by 2013. Although the current total number of hydraulic fracture wells in the U.S. is not yet available, this number must be significantly greater because the dramatic increase in shale oil and gas production has meant that more than 95% of new wells drilled today are hydraulically fractured (EIA, 2018). The water use per HF well has increased dramatically since 2013 and projected that water use for HF could continue to increase more than 20-fold in some regions from 2018 to 2030 (Kondash et al., 2018). Moreover, several studies reported that average water consumption in U.S. shale plays was about 4 million barrels in 2014, up to 29 million barrels in 2016 and 70 million barrels in 2017 (Kondash et al, 2016; Marathon Oil, 2019).

Depending on the characteristics of shale reservoirs, the amount of water required to hydraulically fracture oil and gas wells varies widely (Gallegos et. al, 2015; ACS, 2015). The average hydraulic fracturing water usage in the U.S. strongly correlated with the area of shale reservoirs where hydraulically fractured horizontal wells accounted for the greatest proportion of wells (Gallegos et al., 2015). Therefore, most water consumption that was used to hydraulically fracture wells (**Figure 7**) coincided with the main U.S. shale formations: Eagle Ford, Haynesville, Permian, Barnett, Bakken, Fayetteville, Woodford, Marcellus, and Utica Formation (ACS, 2015). Currently, some U.S. states, such as New Mexico, California, Arizona, Colorado, and Nebraska have experienced significant strains

on their water supplies because of global heating (Holden, 2019). Moreover, 70 % of U.S. could face water shortages by 2050 due to climate change, population increases, and economic growth (Roy et al., 2010). Thus, water usage for HF could stress arid or semi-arid regions and states with limited groundwater supplies (Lancon and Hascakir, 2018).

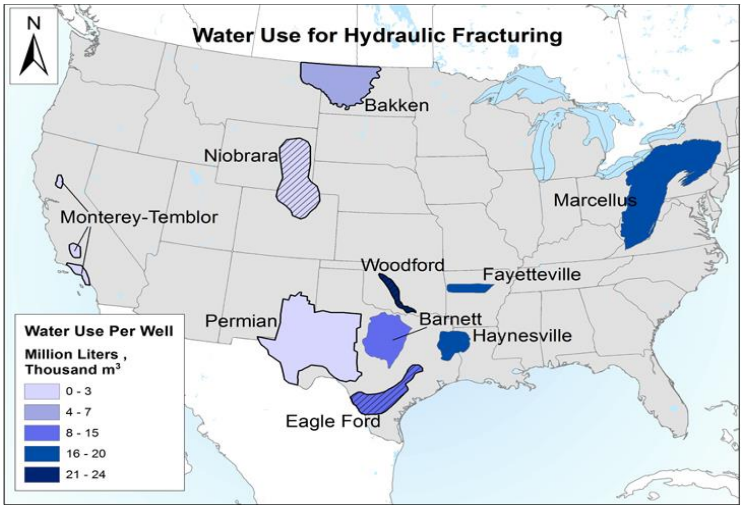

Figure 7 Estimated water usage for per HF well in different shale reservoirs in U.S. Reprinted in Kondash and Vengosh (2015).

Besides water, HF fluids also contain approximate 0.5% of chemicals. The purpose of adding chemicals is to initiate fractures and prevent blockage of cracks by dissolving minerals, and to maintain or increase fluid viscosity to suspend sands (Huang et al. 1995; EPA, 2004; 2011; Ground water Protection Council, 2009). According to a report from the U.S. Congress, more than 750 chemicals are listed as chemicals for hydraulic fracturing (Waxman et al., 2011). Moreover, based on energy company preference, water quality, and site-specific characteristics of the target formation, various chemicals are used in different shale reservoirs. Although less than 20 total chemicals generally are used in a

given fracturing operation, these chemicals would pose potential risks to human health and environment if the fluid was treated improperly and released accidentally (**Table 6**). 632 HF chemicals identified throughout the U.S were examined and it was demonstrated that 75% of the chemicals could affect skin, eye, and respiratory systems; 40% could affect the brain, immune, and cardiovascular system; 37% could affect the endocrine system; and 25% could cause cancer and mutations (Colborn et al., 2011). Recently, to protect public health, regulations requiring the disclosure of fracturing fluid composition were established by a few state government (McFeely, 2012; Wiseman, 2012).

Table 6 The types and purposes of most common chemicals used in HF operation. Table modified from Ground Water Protection Council (2009).

Additive Type	Main Compound	Chemical Formula	Purpose
Diluted Acid (15%)	Hydrochloric acid	HCl	Helps dissolve minerals and initiate cracks in the rock
Biocide	Glutaraldehyde	$C_5H_8O_2$	Eliminates bacteria in the water that produce corrosive byproducts
Breaker	Ammonium persulfate	$(NH_4)_2S_2O_8$	Delay breakdown of the gel polymer chains
Corrosion Inhibitor	N,n-dimethyl formamide	C_3H_7NO	Prevents the corrosion of the pipe
Crosslinker	Potassium hydroxide	NaOH	Maintains fluid viscosity as temperature increases
Friction Reducer	Polyacrylamide	$(C_3H_5NO)n$	Minimizes friction between the fluid and the pipe
Gel	Guar gum	$C_{10}H_{14}N_5Na_2O_{12}P_3$	Thickens water to suspend the sand
Iron Control	Citric acid	$C_6H_8O_7$	Prevents precipitation of metal oxides
Oxygen Scavenger	Ammonium bisulfite	$(NH_4)HSO_4$	Removes oxygen from the water to protect the pipe from corrosion
pH Adjusting Agent	Sodium carbonate	Na_2CO_3 or K_2CO_3	Maintains the effectiveness of other components

Besides water contamination, hydraulic fracturing process can lead to air pollution. The emitted air pollutants include volatile organic gases, sulfur dioxide, nitrogen oxides, and particulate matter from oil and gas itself, and radioactive materials from subsurface

geochemical species (Glass Geltman and LeClair 2018; Moore et al. 2014). These emissions have both acute and chronic health impacts and may cause cancer, which are categorized as hazardous air pollutants and have been regulated by U.S. Environmental Protection Agency (Cohen et al. 2017; EPA 2016b).

1.5 Management of Hydraulic Fracturing Waters in the U.S.

1.5.1 Flowback Water and Produced Water Characteristics

After hydraulic fracturing operation, 5–85% of the HF fluid returns to the surface and is referred to as flowback or produced water (Vidic et al., 2013). The difference between flowback and produced water is time spent in the well. Flowback water refers to the fluid returning to the surface within the first two weeks after stimulation by fracturing, which consists partially of the injected HF fluids and formation water that entrapped in the target formations (Gregory et al., 2011). Produced water is considered to be the remaining fluid that flows from the well after the initial two-week period during the lifetime of well production, which mainly contains formation water that is high in gas and oil (Ziemkiewicz and Thomas, 2015). Many operators define them by water quality. Compared to produced water, flowback water more closely represents the initial HF fluid. However, because the transition from flowback water to produced water is hard to discern and definitions can be subjective when reporting data, some studies do not distinguish flowback water from produced water and consider that they are all returned wastewater

through the production well and a by-product of well production (Marcon et al., 2017; Haluszczak et al., 2013). However, in general, flowback water is less saline than produced water and can be treated for reinjection purposes. In this dissertation, flowback water will be investigated to understand water-rock interaction and formation damage in terms of its reinjection potential.

Different shale reservoirs have various HF fluid recovery rates (**Table 7**). Even from the same shale reservoir, the fraction of HF fluid recovered varies widely. The various flowback rates indicate different amount of hydraulic fracturing fluid is retained in the reservoir. The more developed the fracture network, the more water that is absorbed in the fracture surfaces and then retained (Lu et al. 2017).

Table 7 The average HF fluid recovery rates from major shale reservoirs (Boschee, 2014; Township, 2013; Kondash et al., 2016; Clark et al., 2013)

Unconventional Development	HF Fluid Recovery Rates
Eagle Ford	<15%
Permian Basin	20%-40%
Marcellus	10%-40%
Utica	10%-20%
Bakken	15%-40%
Haynesville	~5%
Niobrara	~20%

The properties of flowback water and produced water also vary considerably depending on the geochemistry of formation, the quality of injected HF fluids, the type of hydrocarbons being produced, and even the lifetime of a reservoir. Although it is not possible to use a single set of chemical properties to describe them, several groups of

constituents are commonly detected in most types of the flowback water and produced water. The generalized compositions of returned water are summarized in **Table 8**.

Table 8 Generalized compositions of flowback water and produced water (Nesbitt, 2007; Graham et al., 2017; USGS, 1999; Hayes, 2009; Haluszczak et al., 2013; Ziemkiewicz and Thomas, 2015)

pH	3.5 to 8.0
TDS	12,000 to 300,000 ppm
Dissolved organic compounds	Carboxylic acid, xylene, acetone, benzene, toluene, ethylbenzene, bromoform, poly aromatic hydrocarbons
Dissolved inorganic solids	Sodium, calcium, magnesium, barium, strontium, iron, aluminum, carbonates, bicarbonates, sulfates, sulfides, bromides, silicates
Dissolved gases	Oxygen, carbon dioxide, hydrogen sulfide
Partially soluble organics	Aromatic hydrocarbons, phenols, aliphatic
Suspended solids, micro-organisms	Algae, bacteria, fungi, yeast
Suspended inorganic solids	Clay, sand, calcium carbonate, iron sulfides
Dispersed oil	Oil droplets
Radioactive materials	Uranium, radium, radon

The major constituents of flowback water are listed below.

1. Salt content: Flowback waters are mainly composed of inorganic materials and typically expressed as salinity or total dissolved solids (TDS). The TDS of most of flowback water and produced water are much higher than that of seawater (~35,000 mg/L) and can reach 300,000 mg/L (Graham et al., 2017). TDS in wastewater from the main U.S. shale reservoirs are given in **Table 9**. In general, salt contents or TDS are mainly dominated by Na, Cl, Mg, Ca, Fe, Ba, S, and Sr. Their concentrations show an increasing trend with time during hydraulic fracturing (Haluszczak et al, 2013; Ziemkiewicz and Thomas, 2015). The potential sources of these elements include dissolved minerals

determined by the geology of a basin (refer to minerology in Table 4), injected liquids, and formation water (Gregory et al., 2011).

Table 9 The summary of average TDS in wastewater from the major U.S. shale reservoirs (Slutz, et al., 2012; Zhou et al., 2014; Silva et al., 2012; Coday et al., 2015; McLaughlin et al., 2013; Hancock et al., 2013).

Unconventional Development	Average TDS, mg/L	Main Components	Potential Sources
Bakken	250,000	Na, Cl, Mg, Ca, Fe, Ba, S and Sr, carbonates, bicarbonates, sulfates, sulfides, bromides, silicates	Dissolution of carbonate, silicate, and sulfide minerals; HF fluids; Formation water
Eagle Ford	40,000		
Haynesville	120,000		
Permian Basin	140,000		
Marcellus	130,000		
Utica	130,000		
Anadarko	110,000		
Niobrara	25,000		

2. Oil and grease: This term refers not to a single chemical compound but rather to various organic compounds associated with hydrocarbons in the formation, including free oil, dispersed oil, and dissolved oil (Rhee et al., 1989). These constituents usually co-occur with methane in the shale reservoir and frequently occur in the formation brine (Butkovskyi et al., 2017). The quantities and properties of organic contaminants are mainly influenced by the type of hydrocarbon product that water is in contact with, volume of water production, and production duration (Guerra and Drewes, 2008). The oil and grease content in flowback water in the western United States ranges from 40 to 2,000 mg/L (Guerra and Drewes, 2008).

3. Inorganic and organic toxic compounds: These compounds are derived from chemicals added into HF fluid to improve drilling and production operations. More than 750 chemicals were used in hydraulic fracturing (GWPC & IOGCC, 2015). However, only

a few states have established laws that require operators to disclose HF fluid composition. In most states, chemicals are still trade secrets and not available to the public.

4. Naturally occurring radioactive materials (NORM): The NORM, such as uranium, radium, and radon, are in low concentrations in normal surface water but are in high concentrations in groundwater or formation water from shale reservoirs, and are brought to the surface by hydrocarbon production during hydraulic fracturing (USGS, 1999). The concentrations of radioactive elements generally are reported as picocuries/gram (pCi/g) of solid material or picocuries/liter (pCi/L) of water or air. NORM in produced water from shale reservoirs is 1-3 orders of magnitude higher than those in earth surface and allowed in drinking water (**Table 10**).

Table 10 Summary of NORM concentrations in drink water, earth surface and produced water from shale reservoirs. The concentrations of radioactive elements are generally reported as picocuries/gram (pCi/g) of solid material or picocuries/liter (pCi/L) of water or air (USGS, 1999; 2012; EPA, 1976; Gundersen and Szabo, 1995).

NORM	Maximum contaminant level in drinking water, pCi/L	Concentration range in earth surface, pCi/g	Concentration range in produced water from U.S. shale reservoirs, pCi/L
Uranium	30	0.1-32	0-10,000
Radium	5	0.1-16.0	0-40,000
Radon	300	0.1-2000	0-50,000

1.5.2 Flowback Water Constituents

Although flowback water is less saline than produced water, regulated metal elements, TDS, NORM, and some toxic organic compounds (benzene, toluene,

ethylbenzene and polycyclic aromatic hydrocarbons) in flowback water have high concentrations, some of which exceed the drink water maximum contaminant standards by many thousands of times (Hayes, 2009; Haluszczak et al., 2013; Lester et al., 2015; Ziemkiewicz and Thomas, 2015). The sources of these constituents are mainly due to the chemicals added into HF fluids as well as components mobilized from shale formation (Guerra and Drewes, 2008; Gregory et al., 2011).

Although various chemicals are added to HF fluids and some of those chemicals are confidential to the companies and not available to the public, several studies compared HF fluid and flowback water composition and reported that the primary composition of the water comes from materials in the shale itself as opposed to the additives in the drilling fluid (Ziemkiewicz and Thomas, 2015; Haluszczak et al., 2013).

Formation water also contributes a large portion of the TDS in the flowback water. It is the water that occurs naturally within the pores of rock, which generally has high salinity and is often called formation brine (Fanchi, 2002). Depending on enrichment of chlorine (Cl) and bromine (Br) in formation water from the Marcellus Formation, several studies concluded that formation water with high salinity was derived from highly evaporated seawater that had been diluted with fresh water or seawater (Dresel, 1985; Dresel and Rose, 2010; Haluszczak et al., 2013). The salinity of formation waters from the main U.S. shale reservoirs (**Table 11**) was classified as high (TDS>200,000 mg/L), medium (50,000-100,000 mg/L) and low (<50,000 mg/L) (Kondash et al., 2016). When hydraulic fractures are induced in shale reservoirs, HF fluid mixes with formation water. Near the production well, reservoir pressure drops significantly, and gas flow velocity

increases dramatically, which leads to evaporation of the mixed water and an increase in the concentration of salts in remaining water. This evaporation process can result in serious salt accumulation in the flowback water or even salt precipitation near production wells even if TDS in the initial formation water is not high (Van Dorp et al., 2009).

Table 11 Classification of formation water from the main U.S. shale reservoirs based on variation in salinity (Kondash et al., 2016).

Formation water salinity	TDS, mg/L	Unconventional Development
High	>200,000	Marcellus Formation and Bakken Formation
Medium	50,000-100,000	Haynesville Formation and Barnett Formation
Low	<50,000	Niobrara Formation and Eagle Ford Formation

Besides mixing with formation water, HF fluids also interact with formation rocks. Such water-rock interactions start as HF fluids are introduced into reservoir rocks through induced fractures. It can initially dissolve or transform minerals and ultimately re-precipitate new solids as interactions proceed. Although flowback fluids are contaminated by dissolved solids from reservoirs rock that have to be removed after well production, the chemical compositions of the fluids provide an unique opportunity to observe the chemical evolution of shale reservoir, which is mainly influenced by intrinsic rock properties, starting composition of HF fluids, and water-rock contact duration (Wang et al., 2015). Among these factors, rocks containing different minerals and elements determine the propensity of rock constituents to partition into fluids (Hayes, 2009; Wang et al., 2015; 2016; Ali and Hascakir, 2015b; 2017).

1.5.3 Management of the Flowback water

Considering the high concentrations of constituents in flowback water, improper disposal and release of flowback water to groundwater and surface water could pose risks to environment and human health. For example, from 2005 to 2015, flowback water components were frequently detected in drinking groundwater aquifers in Pennsylvania because of direct disposal or accidental leakage of flowback water associated with the Marcellus Formation (Warner, et al., 2013; Padep, 2015). Recently, federal regulations were established to regulate disposal of returned water and protect public drinking water sources by the Environmental Protection Agency (EPA) (40 CFR Part 435). Therefore, flowback water is no longer allowed to be released to the surface directly. However, flowback water is inevitable in oil and gas production. How to best manage this water economically and environmentally is critical to the operators' success. To minimize the environmental impact related to water contamination, three strategies (**Figure 8**) often are chosen to dispose of returned water by energy companies: 1) deep well injection, 2) release of the water after treatment and 3) reuse of the water.

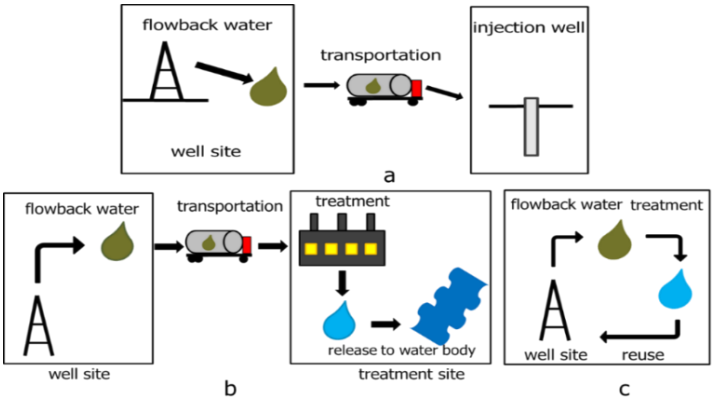

Figure 8 Three methods are commonly used to dispose of returned water: a) deep well injection, b) release of the water after treatment and c) reuse of the water.

Deep well injection entails powerfully forcing flowback fluid into deep wells beneath Earth's surface (Lustgarten, 2012). The aim of an injection well is to dispose of flowback water rather than to acquire gas. This method does not require much wastewater treatment cost. Thus, it is a relatively inexpensive method for dumping the hazardous wastewater because companies are no longer allowed to release it into surface water directly (EPA, 2012). Currently, shale reservoirs in Texas, including Barnett Shale, Eagle Ford Shale, and Haynesville Shale, have mainly used disposal wells to dispose of wastewater water because of cost considerations and availability of disposal wells (Ma et al., 2014).

Release of water after treatment means flowback water is handled through a wastewater treatment system and is going to be released back into surface waters under regulations by the Federal Clean Water Act and EPA. Currently, many different types of technology are tested and employed at specific locations for the treatment of flowback water. Common treatment involves the removal of solids and dissolved inorganic and

organic substances and any radioactive or carcinogenic materials (Hammer et al., 2012) (**Table 12**).

Table 12 Summary of technologies for removing inorganic contents and organic contents in flowback water and produced water. Table modified from Sun et al. (2019).

Technology		Subcategory	Purposes
Removal of Inorganic Contents	Media Filtration	N / A	Using media filter to remove total suspended solids (TSS) from water.
	Membrane Processes	Micro/ Ultra/ Nano-filtration	Using membrane filters, such as micro-and ultra-filtration, to reduce TSS down to very low levels.
		Reverse osmosis	Using a semipermeable membrane to remove dissolved salt from water (up to about 50,000 mg/L TDS).
	Thermal Treatment	Distillation/ Evaporation/ Crystallization	Purifying the water by heating and can treat high-saline waters to a zero liquid discharge standard.
	Ion Exchange	N / A	Resin is used to remove unwanted ions from solution.
	pH Adjustment	N / A	Removing metals rather than treating chlorides or TDS.
	Oxidation	N / A	Remove organic matter, bacteria, hydrogen sulfide, and precipitate metals.
	Chemical Treatment	Precipitation/ Coagulation/ Flocculation	Using chemical coagulants to keep solids forming larger masses and precipitating from the wastewater.
Removal of Organic Contents	Physical Separation	Hydrocyclone	Separating solids and oil particles from liquid based on the density of the materials.
		Filtration	Using filter media and filter operations to remove oil and grease.
		Centrifuge	Separating fluids of different specific gravity.
	Coalescence	N / A	Collecting small oil droplets that can be more removed by the other technologies.
	Flotation	N / A	Removing tiny oil bubbles by dissolving and releasing air under pressure in the water
	Adsorption	N / A	Removing oil and grease by absorbents.

Although there are many water management options available for shale operators, there is no one-size-fits-all solution. Understanding the costs and limitation for each technology is important for operators to balance costs and benefits and develop a blended

management system (**Table 13**). Overall, the treatment method remains a costly procedure due to huge volumes of flowback water produced during hydraulic fracturing along with stricter regulations and standards about the high quality of released wastewater.

Table 13 Summary of the cost of main technologies for treating flowback water and produced water. Modified in Okullo (2017) with permission from the National Academies Press.

Technology	Technologies Notes	Estimated Cost, $/bbl
Absorption and Ion Exchange	1. Used media cannot be re-used or regenerated, which could increase cost.	0.1-1.5
Membranes	1. Involves reverse osmosis and micro/ ultra/ nano-filtration. 2. The pre-treatment for reverse osmosis could increase the cost.	0.5-1.5
Dilution	1. Involves blending wastewater with freshwater to reduce TDS. 2. Can be used to dilute NORM in wastewater.	1.5-2.0
Setting	1. Must allow enough time for solids to settle. 2. After solids settle out of the water, other technologies could be used for further treatment.	2.0-2.5
Filtration	1.Involves media filtration to remove organic and inorganic contaminants in wastewater	2.0-3.0
Chemical Precipitation	1. Involves pH adjustment, oxidation, and addition of chemicals. 2. Less expensive method but still requires experienced operators	2.5-4.0
Clarification	1. Involves flotation to remove organic matter	3.5-4.5
Thermal Treatment	1. Involves distillation, evaporation, and crystallization 2. Require substantial amounts of energy to obtain high quality water	2.0-8.0

Although the above two methods control or minimize the risk of water contamination, the use of extremely large quantities of water is still an urgent problem, especially for arid areas that face water shortfalls. Another route is reuse of flowback water. The water after production is partially treated initially and re-injected for subsequent hydraulic fracturing operations. The reused water only has to meet the requirements of the fracking companies rather than federal regulations. Therefore, this new method is popular among the industry because of not only significantly reducing the

initial required quantity of fresh water but also reducing the volume of contaminated water that must be treated and disposed. About 1.4 million US dollars was saved if 50% of fresh water and 50% of flowback water was used rather than 100% of fresh water based on a Montney well located in northeastern British Columbia (Paktinat et al., 2011). However, using this method may cause another problem. The reuse of flowback water with little or no treatment could largely reduce treatment and disposal costs, but it may cause blockage of created fractures and lower the recovery efficiency due to complex water-rock interactions. Thus, this dissertation mainly focuses on interaction between injected fluids and reservoir rocks during hydraulic fracturing. The details on water-rock interaction processes are provided in the next section.

1.6 Water-Rock Interaction Occurring During Hydraulic Fracturing

Considering that millions of gallons of fresh water or flowback water are injected into reservoirs, it is critical to understand how water-rock interactions affect hydraulic fracturing performance. Water-rock interactions start by introducing HF fluids into the reservoir; these fluids have the potential to modify existing or induced pores and flow pathways, may alter the properties of the reservoir, and may contaminate production fluids with metals and other salts. To develop methods to reduce freshwater usage and better treat flowback water either for release or reinjection proposes, knowledge of water-rock interaction mechanisms between shale formations and HF fluids have been provided by several studies. Experiments on engineered fluids interacting with Marcellus Shale

samples at reservoir conditions shows evidence for mineral dissolution, secondary mineral precipitation, and enrichment of trace elements in produced water (Marcon et al., 2017). Two studies of water-rock interactions compared the impact of water chemistry on element mobilization from Eagle Ford and Bakken Shales. Their conclusions were that the rate and extent of elemental mobilization are strongly associated with the composition of formation and fracturing fluids, and with interaction duration (Wang et al., 2015; 2016). Interactions between shale samples from Longmaxi Formation in China and water led to a dramatic increase in TDS of the flowback fluid because of dissolution of formation minerals (Li et al., 2017). Different water-rock interactions occurred after experiments between samples from four shale reservoirs and water, which were identified by the change in water chemistry and mineralogy on the rock surface (Ali and Hascakir, 2017). In addition, a series of geochemical studies demonstrated that water contained various constituents after interacting with different shale reservoirs because of different water-rock interactions, and that its composition reflects characteristics of the zone of shale that was drilled (Hayes, 2009; Ziemkiewicz and Thomas, 2015). Overall, all above studies show the changes in flowback water compositions provide direct observations on the chemical evolution of shale reservoir and valuable information on the mobilization of elements due to water-rock interactions.

Water-rock interactions are weathering processes that physically or chemically change rocks into smaller pieces at or near earth's surface by the action of water (Goldich, 1938). In physical weathering, water breaks down rocks, but does not change the rocks' chemical compositions. For example, the action of a river pushing rocks against the

surrounding rocks can eventually break them apart. In contrast, chemical weathering occurs when there are changes in the chemical compositions of the rocks after exposure to the environment. Depending on their resistance to chemical weathering, minerals present in rocks will completely or partially dissolve in water (**Table 14**). Minerals like hematite, gibbsite, quartz, and clay minerals are the most stable minerals in rocks. Igneous minerals, carbonate minerals, and halite are the least stable at earth surface.

Table 14 Relative stability of common minerals under chemical weathering (Goldich, 1938).

Minerals	Chemical Formula	Stability of Minerals	Rate of Weathering
Hematite	Fe_2O_3	most stable	slowest
Gibbsite	$Al(OH)_3$	stability decreases	weathering rate increases
Quartz	SiO_2		
Clay minerals			
K-feldspar	$KAlSi_3O_8$		
Na-rich feldspar	$NaAlSi_3O_8$		
Ca-feldspar	$CaAl_2Si_2O_8$		
Olivine	$(Mg,Fe)_2SiO_4$		
Calcite	$CaCO_3$		
Halite	NaCl	least stable	fastest

The most common chemical processes during water-rock interactions are dissolution/precipitation, cation exchange, redox reactions, and mineral transformations (Elango and Kannan 2007). According to these chemical processes, the concentration of ions in water may increase or decrease; mobility of the dissolved constituents may be affected; and pH of water may change.

Dissolution and precipitation depend on if the water is saturated with reservoir minerals and if excess mineral components are present. Typically, as water contacts reservoir rock surface, dissolution and precipitation processes take place between water

and rocks in the following steps. First, water is unsaturated with reservoir minerals. Thus, elements released from minerals on rock surface begin to dissolve into the water, which creates small dissolution pits at the surface. Then, some dissolved ions move far away from rock surface into the water from high concentration regions to low concentration regions through diffusion (Kirkwood et al., 1960). As mineral dissolution proceeds, ions continue to dissolve into the water and eventually become supersaturated with minerals near the rock surface. Finally, nanoscale particles are created by precipitation which fill dissolution pits or accumulate on the rock surface. Some particles may leave the surface and precipitate to form larger particles on the rock surface (Shao et al., 2010). Therefore, dissolution of minerals increases the concentration of ions in water, while precipitation decreases the concentration of ions in water.

The mobilization of elements from rocks to water is a result of dissolution of minerals which is controlled by their solubility. Solubility is defined as the maximum amount of compounds (solid, liquid or gaseous substances) which will dissolve into the water at a specified temperature and pressure (Hodgman and Holmes, 1942). For gases, as the temperature increases, the solubility of a gas decreases because more molecular motion breaks weak intermolecular bonds and results in escape from solution. Gas solubility increases with increasing pressure (Henry, 1803). Henry's Law states that “the solubility of a gas in a liquid is directly proportional to the pressure of that gas above the surface of the solution” (Henry, 1803). In contrast, the solubility of liquid and solid substances exhibits complex behavior with temperature. In general, as temperature increases, the solubility of a solid or liquid can increase or decrease depending on whether

the dissolution reaction is endothermic (system absorbs energy from its surroundings) or exothermic (system releases energy to surroundings). In endothermic reactions, the system absorbs heat energy provided by increased temperature and adjusts to promote the dissolution reaction (Le Chatelier and Boudouard, 1898). In nature, most minerals dissolve more with increasing temperature. In exothermic reactions, increased temperature introduces more heat energy into the system, but it cannot be absorbed by the system and thus inhibits the dissolution reaction (Le Chatelier and Boudouard, 1898). A few minerals decrease solubility with increasing temperature. A common and important example is carbonate minerals, mainly including calcite, dolomite, and aragonite, which are less soluble in hot water (Larson and Buswall, 1942). Additionally, the solubility can be characterized by an equilibrium constant (K_{sp}) that is defined as the product of the activities of the solutes dissolved into solution (Rossotti and Rossotti, 1961). The dissolution reactions and K_{sp} of minerals commonly found in shale reservoirs are summarized in **Table 15**. In summary, for two minerals with same number of ions, the mineral with the higher K_{sp} value is more soluble. Increasing pressure also leads to an increase in solubility of minerals, but for condensed phases, the pressure effect on solubility is typically weaker than temperature and usually neglected in practice (Hildebrand, 1924; Gibson, 1938).

Table 15 Dissolution reactions and solubility constant (K_{sp}) of common minerals present in shale reservoirs (Reesman and Keller 1968; Reesman 1973; Wilkin et al. 1998; Ali and Hascakir, 2017).

Mineral	Mineral Dissolution Reaction in Water	Solubility Constant, moles/liter
Calcite	$CaCO_3 \rightleftharpoons Ca^{2+}+CO_3^{2-}$	$10^{-8.48}$
Quartz	$SiO_{2(s)}+2H_2O \rightleftharpoons H_4SiO_{4(aq)}$	$10^{-9.90}$ - $10^{-11.70}$
Illite	$K_{0.6}Mg_{0.25}Al_{2.3}Si_{3.5}O_{10}(OH)_2 \rightleftharpoons 0.25Mg^{2+}+0.6K^{+}+2.3Al^{3+}+3.5SiO_2+5H_2O-8H^{+}$	$10^{-45.80}$ - $10^{-73.00}$
Kaolinite	$Al_2Si_2O_5(OH)_4 \rightleftharpoons 2SiO_2+2Al^{3+}+5H_2O-6H^{+}$	$10^{-37.00}$ - $10^{-40.00}$
Pyrite	$FeS_2+2.5O_{2(aq)}+H_2O \rightleftharpoons Fe^{2+}+2SO_4^{2-}+2H^{+}$	$10^{-26.89}$
K-feldspar	$KAlSi_3O_8+4H_2O \rightleftharpoons K^{+}+Al^{3+}+3H_4SiO_{4(aq)}-4H^{+}$	$10^{-20.00}$
Plagioclase	$CaAl_2Si_2O_8 \rightleftharpoons Ca^{2+}+2Al^{3}+2H_4SiO_{4(aq)}-8H^{+}$	$10^{-13.97}$ - $10^{-14.60}$
Gypsum	$CaSO_4 \cdot 2H_2O \rightleftharpoons Ca^{2+}+SO_4^{2-}+2H_2O$	$10^{-4.58}$
Dolomite	$CaMg(CO_3)_2 \rightleftharpoons Ca^{2+}+2CO_3^{2-}+Mg^{2+}$	$10^{-17.09}$

Cation exchange describes the processes by which dissolved cations in solution are absorbed on negatively charged surfaces of particles or exchange with other cations that have already absorbed on the rock surfaces (Birkeland, 1999; Brady and Weil, 2008). In general, clay minerals are the most common cation exchangers because they have negatively charged surfaces. Clay minerals contain silicon (Si) and aluminum (Al). The substitution of Si^{4+} by Al^{3+} in the mineral structure results in the negatively charged surfaces of clays (Carroll, 1959). Organic matter also commonly has negatively charged surfaces because the dissociation of organic acid increases the surface negative charge of organic molecules (Wang et al., 1997). Some oxides also have cation exchange capability because oxygen ions are not able to fully coordinate with other exchangeable ions (Carroll, 1959). For example, goethite (FeOOH) and hematite (Fe_2O_3) are iron oxihydroxides. Negative charges are retained on their surfaces due to incoordination of oxygen with Fe^{3+}. For all cation exchangers, surface negative charges can be balanced by cations from rock particles or solution. The main exchangeable ions associated with cation exchange are

Al^{3+}, Ca^{2+}, Mg^{2+}, Na^{+}, K^{+}, and H^{+} (Rayment and Higginson 1992). Based on their electrical charge, ions in water have different tendencies to be adsorbed or desorbed. For instance, Al ions are much more likely to be adsorbed onto clay surfaces than Na ions due to higher electrical charge (**Figure 9**). Therefore, cation exchange is commonly used to remove hardness from water by exchanging Ca and Mg ions for Na ions (Ibrahim et al., 2019).

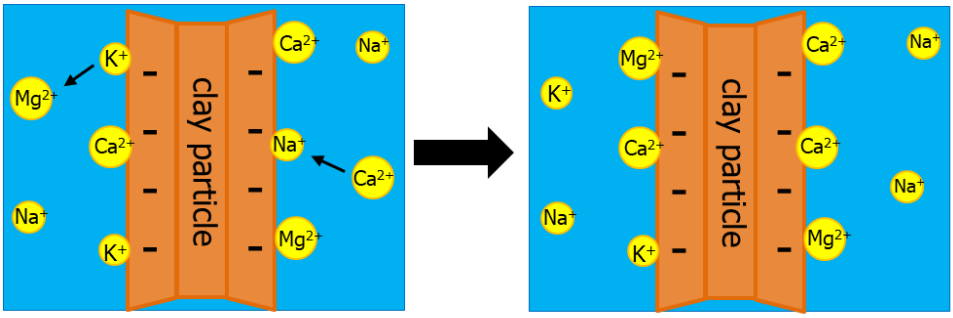

Figure 9 A diagram for cation exchange processes on the rock surface. Ions have different tendencies to be adsorbed or desorbed on mineral surface based on their electrical charge. Image modified from MoJo and Zamanian (2017).

Cation exchange is characterized by cation exchange capacity (CEC) which indicates the sum of exchangeable cation charge that a soil can adsorb (Carroll, 1959). It is expressed in units of millequivalents per 100 grams (meq/100g). Clay minerals and oxides that commonly have cation exchange capability are listed in **Table 16**. Besides cation exchange, anion exchange also occurs. However, in most cases, the cation exchange capacity is much greater than the anion exchange capacity, but the opposite can occur in highly weathered soils (Brady and Weil, 2008).

Table 16 Values of cation exchange capability for different minerals. Table modified from Gräfe et al. (2017).

Mineral	Formula	CEC (meq/100g)
Kaolinite	$Al_2Si_2O_5(OH)_4$	3-15
Montmorillonite	$(Na,Ca)_{0.3}(Al,Mg)2Si_4O_{10}(OH)_2•n(H_2O)$	80-120
Chlorite	ClO_2	10-40
Hematite	Fe_2O_3	4-100
Goethite	FeO(OH)	4-100
Illite	$(K,H_3O)(Al,Mg,Fe)_2(Si,Al)_4O_{10}[(OH)_2,(H_2O)]$	20-50
Smectite	$(Na,Ca)_{0.33}(Al,Mg)_2(Si_4O_{10})(OH)_2·nH_2O$	20-100

Redox reactions (also called oxidation-reduction reactions) are a type of chemical reaction that involve a transfer of electrons from one reactant to another (Gillespie, 1920). Redox reactions always include an oxidation and a reduction. The species that is oxidized loses electrons and its oxidation number increases, while the species that is reduced gains electrons and its oxidation number decreases; an example is shown in **Figure 10**. In natural surface environments, oxygen is the most common oxidizing agent. Water in equilibrium with the atmosphere will be oxidizing by virtue of the presence of oxygen. In contrast, water infiltrating into the ground will become more reduced as it reacts with reducing agents. For instance, organic matter, as a strong reducing agent, would be oxidized if it were not isolated from oxygen in water. Therefore, it cannot be preserved and accumulate in in large quantities in sedimentary rocks under oxidizing condition except under exceptional circumstances. In addition, many elements, like iron, sulfur, and manganese, exist in more than one oxidation state. Thus, redox reactions are more likely to take place between minerals containing these elements (Gillespie, 1920). Finally, elements could have different solubility under natural conditions when present in different oxidation

states. For example, Fe and Mn are more soluble under reducing condition and are more easily precipitated as oxyhydroxide minerals under oxidizing condition (Tribovillard et al., 2006). In contrast, many trace elements such as U, V, Ni, Mo, Cr, and Co (redox sensitive trace elements) are more soluble under oxidizing condition, and are useful indicators of reducing paleoenvironment conditions when identified in elevated concentrations in black shales (Tribovillard et al., 2006). Therefore, redox reactions affect water composition by modifying mobility of dissolved ions in the water.

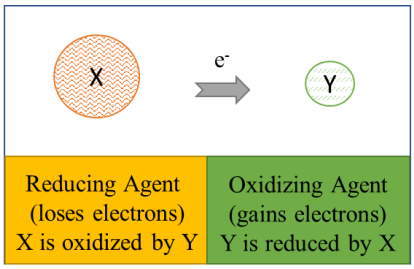

Redox Reaction Example of Siderite Oxidation

$4FeCO_3 + 6H_2O + O_{2(aq)} \rightarrow 4Fe(OH)_{3(s)} + 4CO_2$

Reducing Agent: $FeCO_3$ Oxidizing Agent: O_2

Figure 10 The mechanism of redox reaction and an example of siderite oxidation.

Mineral transformation refers to reactions in which minerals exposed to water are transformed into new chemical products (IUPAC, 1997). Two processes are important in mineral transformation. The first process is that unstable primary minerals are altered into stable secondary minerals. This process, also called hydrolysis, occurs when water molecules are dissociated into hydrogen and hydroxide ions that react with primary minerals to form new minerals (IUPAC, 1997; La Iglesia et al., 1976). The second process

is that secondary minerals are altered into other secondary minerals (Kerr, 1952; Eberl, 1984). Clay minerals play an important role in transformation of minerals because they are often either a product or a reactant in these processes. Some unstable minerals, like carbonate minerals and halite, will completely dissolve in water. Other minerals, including many silicate minerals like feldspars and micas, partially dissolve and form stable clay minerals through hydrolysis. Examples of mineral dissolution reactions are given in **Table 17**.

Table 17 Rection examples of complete and partial dissolution of minerals in water.

Complete Dissolution	**Calcite**	$CaCO_3 \rightarrow Ca^{2+} + CO_3^{2-}$
	Halite	$NaCl \rightarrow Na^{+} + Cl^{-}$
Partial Dissolution	**Feldspar**	$3KAlSi_3O_8 + 2H^{+} + 12H_2O \rightarrow 2K^{+} + KAl_3Si_3O_{10}(OH)_2 + 6H_4SiO_4$ (Feldspar→Illite)
	Mica	$2K(Mg_2Fe)(AlSi_3)O_{10}(OH)_2 + 10H^{+} + 0.5O^{2} + 7H_2O \rightarrow Al_2Si_2O_5(OH)_4 + 2K^{+} + 4Mg^{2+} + 2Fe(OH)_3 + 4H_4SiO_4$ (Mica→Kaolinite)

During hydrolysis, mineral cations are released into solution and replaced by hydrogen ion, producing a new mineral. This process is irreversible. Once secondary minerals are formed, further water-rock reaction (the second process) will convert them into other secondary minerals. For example, illite can convert into kaolinite by removing additional cations (Baes and Mesmer, 1976). Clay minerals usually contain tetrahedral (T) silica sheets and octahedral (O) alumina sheets. They can be classified as 1:1 or 2:1 clays (Grim, 1968). The structure of 1:1 clays consists of one T sheet and one O sheet, and examples are kaolinite and serpentine. The structure of 2:1 clays is made up of one O sheet

sandwiched between two T sheets, and examples are illite and smectite. Extreme water-rock interaction will remove one of the two T layers from a 2:1 clay and leave it with 1:1 structure (Karathanasis and Hajek, 1983). Eventually, after these two processes, the transformation of silicate minerals into clay minerals reduces the complexity of mineral structures, and the removed ions from minerals are released into water and change the water composition.

In summary, due to these chemical processes during water-rock interaction, the chemical compositions of both rock and fluid are modified as water passes through rock.

1.7 Stability of Colloids in Water after Water-Rock Interaction

After water-rock interaction, a mixture is generated that is made up of particles from reservoir rocks that dissolved or suspended in the water. In general, the property of a mixture is not only highly dependent on various water-rock interactions, but also affected by the size of particles. These particles are atoms and molecules that are very small in diameter, or colloids and suspended particles that are large in diameter (Graham, 1861) (**Figure 11**). Based on particle size (**Table 18**), mixtures are classified as solutions, colloidal suspensions, and suspensions (Graham, 1861; Selmi, 1845).

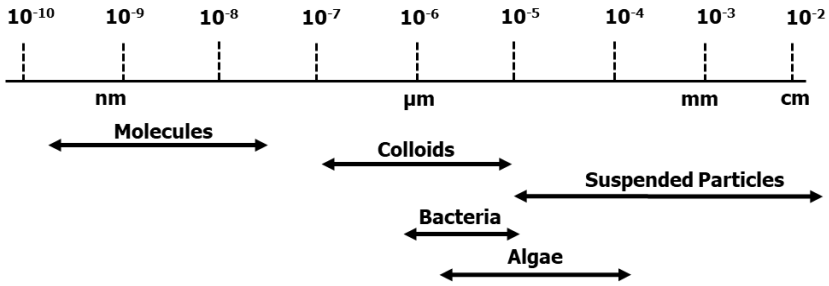

Figure 11 The dimension of the particles in water bodies (Graham, 1861; Selmi, 1845; Young, 2016).

Table 18 The classification and properties of mixtures based on particle size. Table modified from Young (2016).

Property	Solution	Colloidal Suspension	Suspension
Particle Size	$<10^{-7}$ m	10^{-7} to 10^{-5} m	$>10^{-5}$ m
Nature	Homogeneous	Heterogeneous	Heterogeneous
Sedimentation	Do not settle	Do not settle	Settle on standing
Visibility	Particles invisible	Particles can be observed under ultra-microscope	Particles may be visible by naked eye
Filterability	Can pass through filter papers	Can pass through filter papers	Cannot pass through filter papers

In chemistry, a solution is defined as a transparent and homogeneous mixture composed of two or more substances. It does not settle out and cannot be filtered but can be separated by distillation. Particles in solution are mainly composed of atoms, ions, and molecules (IUPAC, 1997). A suspension is a heterogeneous mixture that contains suspended particles in the solvent. The particles in suspensions contain clumps of particles or mineral grains, most of which are large enough to be observed by naked eyes and eventually settle or form sediment (Brady and Senese, 2004). A colloidal suspension is intermediate between a solution and a suspension. It is also a heterogeneous mixture but

the particles in colloidal suspension can pass through filter papers and do not settle. These particles include aggregates of atoms, molecules, and ions (Graham, 1861).

In the gas and oil industry, there are no typical profiles of HF fluids and flowback water because of their complex compositions. For HF fluids, hundreds of chemicals would be used to get the optimal fluids. These chemicals include various combinations of diluted acid, gels, cross-linkers, corrosion inhibitors, pH adjusters, clay stabilizers, and other ingredients, which are the main sources of particles in HF fluids (Stringfellow et al., 2014). Most of the inorganic chemicals can dissolve or ionize into water and commonly form a solution with water. Some of the organic chemicals, which are composed of aggregates of fine particles, like gels, instead generate colloidal suspensions (BOE, 2009). Therefore, HF fluid is typically a solution or colloidal suspension depending on the size of different chemicals. Flowback water is generally a colloidal suspension with average particle size varying from 1 to 10 μm (Ahuja, 2015). However, it contains much more colloids than HF fluids. Sometimes it can be a suspension with sufficient large particles (Stewart and Arnold, 2011). Concentrations of colloids in flowback water can reach 10^{11} particles/mL (Xiong et al. 2016). These colloids in flowback water were not ingredients from HF fluids but were mainly formed in shale formations during the fracturing process (Stringfellow et al. 2014; Ferrer et al., 2015). Thus, to ensure chemicals in HF fluids work well during fracturing operation or prevent pore blockage by contaminants from flowback water during reinjection process, understanding the stability of particles is important.

Particles in the water that do not come together are called stable. Typically, the life of a particle varies from fractions of a second to hundreds of years. The most important

factors influencing the stability of particles are particle size and concentration of surface charge (Peavy et al., 1985). Larger particles settle from water by gravity more rapidly than smaller particles, which lowers stability of the system (Losev et al., 1989). However, smaller particles are not necessarily stable because the surface charge also controls particle stability. In particular, when particles are placed in an electrolytic solution, ions in the water near the particles will be affected by the charged surface. The oppositely charged ions (**Figure 12**) will balance the surface charge and form an electrical double layer around particles (Grahame, 1947).

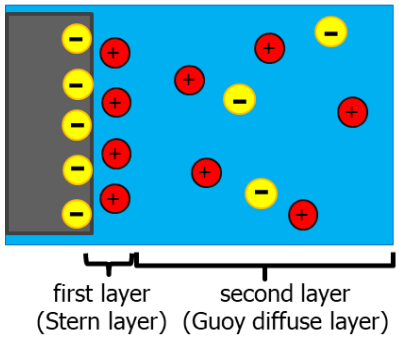

Figure 12 Illustration of the double layer structure in a liquid at contact with a negatively charged particle.

The first layer, also known as Stern layer, consists of ions that are strongly bound to the surface and will travel with it (Stern, 1924). The second layer, known as the Guoy diffuse layer, is made up of free ions attracted to the first layer electrostatically. Ions in the second layer are loosely associated with the particles. Therefore, they can move into the fluid under the influence of electrical attraction and thermal motion (Gouy, 1910). For two similarly charged particles, this double layer structure creates a repulsive electrostatic

potential which prevents them contacting each other (Israelachvili, 1992). Additionally, there is another intermolecular force called van der Waals force. It is a distance-dependent attractive force between atoms or molecules, which is strong at close distance but decreases more rapidly than the electrostatic force (van der Waals, 1873). When two particles in the water are close, the interaction between two objects is dominated by these two opposite forces. Thus, the stability of particles is governed by the balance of the attractive and repulsive interactions. In general, if the electrostatic force is greater than the van der Waals force, the particles will remain dispersed even at close distance. However, if the van der Waals force is stronger, the particles will agglomerate.

The quantity of ions in the solution also has great influence on the stability of particles (Peavy et al., 1985). A high ionic concentration in water can cause compression of the double layer, which pushes counter ions toward the surface of the particles. If the double layer is sufficiently compressed, the net force will be attractive because the van der Waals force dominates. Under these conditions, particles come together and settle even if their original size is small.

The stability of colloids can be characterized by zeta potential. This is a measure of the surface electrical charge of particles suspended in liquid (**Figure 13**) and is caused by the net electrical charge contained at the slipping plane in the double layer (Metcalf and Eddy, 1991).

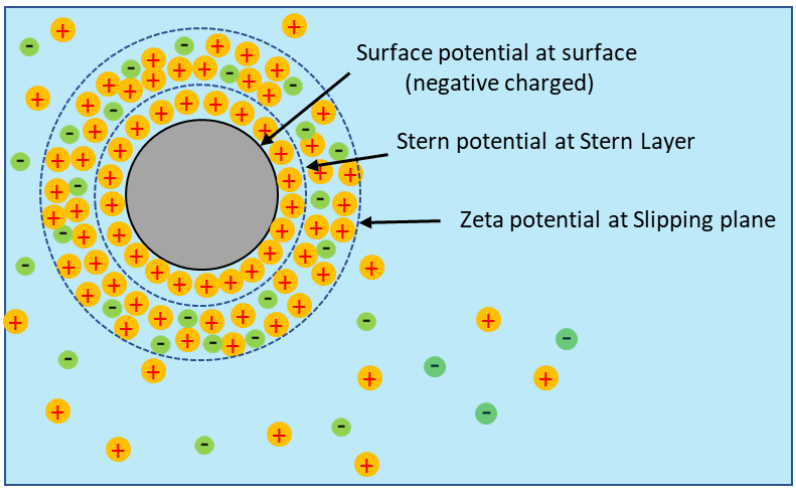

Figure 13 Illustration of different potentials near particle surface. Zeta potential is measured at the slipping plane, which is not equal to the particle surface potential or Stern potential. Image modified from Larryisgood (2011).

Within the second layer of the double layer, a slipping plane is conventionally introduced and separates mobile fluid from fluid attached to the surface. Electric potential at this plane is zeta potential (Morrison and Ross, 2002; Jiang et al., 2008). Zeta potential is not equal to the particle surface potential or Stern potential in the double layer, because they are defined at different locations (refer to Figure 13). Although the location of the slipping plane usually is unknown, zeta potential values have been useful for predicting whether particles are likely to coagulate. Generally, the magnitude of the zeta potential indicates the degree of electrostatic repulsion between particles (Greenwood and Kendall, 1999; Hanaor et al., 2012) (**Table 19**). When the absolute zeta potential (negative or positive) of particles is high, the repulsive forces exceed the attractive forces, which leads to a relatively stable condition. Thus, particles with high absolute zeta potential are stabilized while particles with low absolute zeta potentials tend to coagulate or flocculate.

Table 19 Relationship between zeta potential and particle stability. Reprinted in Kumar and Dixit (2017) with permission from Elsevie.

Absolute Zeta Potential [mV]	Stability Behavior of the Particle
0 - 5,	Rapid coagulation
10 - 30	Incipient instability
30 - 40	Moderate stability
40 - 60	Good stability
>61	Excellent stability

In summary, water-rock interactions occurring during hydraulic fracturing are complex because every shale formation has distinct characteristics and the created HF fluids are site-specific. Hence, my research only aims to investigate water-rock interaction in two productive shale reservoirs, including the Eagle Ford Formation and the Marcellus Formation. Simple interactions between deionized water and reservoir rocks and complicated interactions between flowback water and reservoir rocks have been studied to understand interaction mechanisms and evaluate the effect of reuse of flowback water on hydraulic fracturing performance. Therefore, the next two sections will review existing literature on the background of the Eagle Ford Formation and the Marcellus Formation separately.

1.8 The Eagle Ford Formation

1.8.1 Geologic Overview of the Eagle Ford Formation

The Eagle Ford Formation was named from exposures at the town of Eagle Ford near Dallas, Texas (Hill, 1887). It has been studied for over 120 years with most historical

studies primarily focused on outcroppings (Stephenson, 1929; Stephenson and Reeside, 1938; Adkins and Lozo, 1951; Lock et al., 2010). However, thanks to drilling activity, more recent studies were conducted on the subsurface using well logs and cores to further investigate the Eagle Ford Formation (Donovan and Staerker, 2010, Hentz and Ruppel, 2010, Dawson and Almon, 2010; Harbor, 2011; Hentz et al., 2014).

The Eagle Ford Formation is a carbonate mudstone formation deposited in the Late Cretaceous, from the Middle-Cenomanian to the end of the Turonian (Adkins and Lozo, 1951). It was deposited during the transgression of the Cretaceous Western Interior Seaway (KWIS) in North America (Robinson, 1997). During the time of Eagle Ford deposition, marine water covered most of the North American midcontinent and led to the formation of the KWIS, a shallow inland sea stretched from Gulf of Mexico to arctic regions and separated North America into two land masses, Laramidia and Appalachia (Stanley, 1999). **Figure 14** shows the KWIS and the approximate location of the Eagle Ford Formation in the Late Cretaceous.

Figure 14 Paleogeographic reconstruction of North America during the Late Cretaceous. Brown represents coastlines, light blue represents shelf margins, medium blue represents slopes and dark blue represents abyssal depths. The locations of Appalachia, Laramidia and Western Interior Seaway, and Eagle Ford deposition are shown. Image modified from Blakey (2013) with permission from Deep Time Maps™.

Widespread carbonate deposition during the Cretaceous suggests that warm marine water was present around ancient continents, which caused a decrease in ocean currents between poles and the equator, then formed anoxic zones, and finally created a favorable environment for organic shales to be deposited (Everhart, 2007). Under favorable conditions of carbonate accumulation and organic matter preservation, the deposition of Eagle Ford started on the stable shelf of the southern end of the KWIS as it merged into the Gulf of Mexico (Robinson, 1997; Workman, 2013). After the influence of several tectonic and structural events, the Eagle Ford Formation has become a complex petroleum reservoir that is different from other conventional reservoirs due to its significantly low permeability and carbonate-rich lithology.

The Eagle Ford Formation was deposited unconformably above the Cenomanian Buda Limestone and unconformably below the Coniancian to Campanian Austin Chalk at a depth of approximately 4,000 to 12,000 feet with average thickness of 250 feet (Parra et al., 2013). It is located in South-Central Texas extending about 400 miles from the Maverick Basin, through the Central Texas Platform, across the San Marcos Arch, and extending into the East Texas Basin (**Figure 15**). In the East Texas Basin, the Maness Shale was defined and inferred to be equivalent to the lower unit of the Eagle Ford Formation in the Maverick Basin and the San Marcos Arch. The Woodbine Group, Pepper Shale, and Eagle Ford Shale (Figure 15) were regarded as the equivalents of the upper unit of Eagle Ford Formation (Hentz et al., 2014).

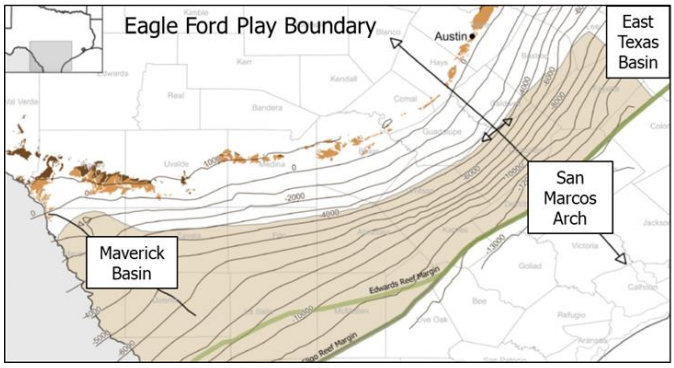

Figure 15 Location map for the Eagle Ford Formation, which extends from the Maverick Basin, across the San Marcos Arch, and ending in the East Texas Basin. Image modified from U.S. Energy Information Administration (2014).

In the East Texas Basin, the Maness Shale was defined and inferred to be equivalent to the lower unit of the Eagle Ford Formation in the Maverick Basin and the San Marcos Arch. The Woodbine Group, Pepper Shale, and Eagle Ford Shale (**Figure 16**)

were regarded as the equivalents of the upper unit of Eagle Ford Formation (Hentz et al., 2014).

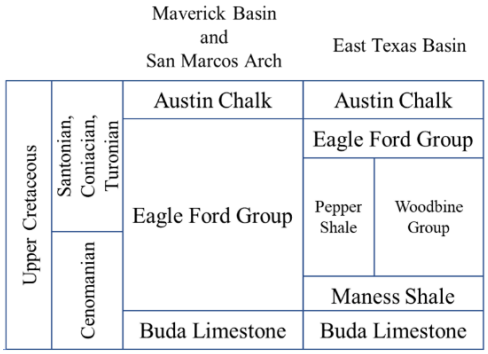

Figure 16 Stratigraphic column of the Eagle Ford Formation in Maverick Basin (study area), San Marcos Arch, and East Texas Basin. Image modified from Fairbanks et al. (2016).

Structural features strongly control the thickness of the Eagle Ford Formation (Dravis, 1980). It is thickest in the Maverick Basin, roughly 400 to 600 feet, and gradually thins by more than 95% northeastern from Maverick Basin towards the crest of San Marcos Arch where it is less than 50 feet, (Winter, 1961, Hentz and Ruppel, 2010). The significant regional thickness variations are generally explained by an unconformity at the base of the overlying Austin Chalk and were mainly controlled by tectonic and structural features (Winter, 1961; Treadgold, 2011; Ewing, 2003). For instance, the Maverick Basin originated as a fault-bounded rift valley that was filled with terrigenous siliciclastic rocks during the Triassic or Early Jurassic (Scott, 2004). Continued fault growth and salt withdrawal created additional accommodation within the Maverick Basin, which resulted in formation of a sediment depocenter during the beginning of the Late Cretaceous when

the Eagle Ford Formation started to deposit (Bennett, 2015). The San Marcos Arch is the southeastern extension of the Paleozoic Llano Uplift and its high paleotopography separated the Maverick Basin and East Texas Basin (Dravis, 1980). The development of fault systems also created Eagle Ford thickness variations, including the Luling Fault Zone, Fashing Fault Zone, Charlotte Fault Zone, and the Balcones Fault Zone, all of which were active during Eagle Ford deposition. After deposition of the Eagle Ford Formation, these tectonic and structural features continued to produce thickness variations in younger Cretaceous units (Donovan and Staerker, 2010).

There are four major margins in the Eagle Ford Formation: 1) the western margin of the Eagle Ford is the Burgos Basin, located in northeastern Mexico; 2) the northeastern margin is defined by the transition from the carbonate-rich lower Eagle Ford Formation to the silica-rich Pepper Formation in the East Texas Basin; 3) the southern boundary runs along the Sligo Reef Margin; 4) the northern boundary roughly corresponds with areas in Frio, Maverick and Zavala counties where oil starts to generate from the source rocks of Eagle Ford Formation (Hentz et al., 2014; EIA, 2014). Therefore, the extent of the Eagle Ford Formation also was largely constrained by regional tectonic features, including the Maverick Basin, the San Marcos Arch, Sligo Reef Margin, and the East Texas Basin (Hentz and Ruppel, 2010; Hentz et al., 2014).

Sedimentary rocks in the Eagle Ford Formation are described as alternating mudstone with limestone along with varying levels of organic content and occasional bentonites (Faust, 1990). Mudstone varies from massive to well-laminated with nonexistent to pervasive bioturbation that sometimes completely destroyed original

sedimentary fabrics (Dawson, 2000). Based on distinct changes in gamma-ray profiles responding to potassium, uranium, and thorium components in rock units, the Eagle Ford Group is generally divided into two members: the lower Eagle Ford Formation and the upper Eagle Ford Formation (Dawson 1997; 2000; Robinson, 1997; Donovan et al., 2015). The lower Eagle Ford Formation contains higher gamma-ray values than the upper Eagle Ford Formation because of relatively higher clay and organic contents which suggests the lower shale member was deposited in a more anoxic water column (Donovan and Staerker, 2010). The Lower Eagle Ford Formation is characterized by organic–rich mudrock deposited within a transgressive systems tract (Donovan and Staerker, 2010; Tian et al., 2012). The upper Eagle Ford Formation is characterized by calcareous-rich mudrock deposited within a highstand systems tract during regression. (Donovan and Staerker, 2010). Because the lower Eagle Ford Formation is associated with organic-rich mudstones, it is the primary target of the Eagle Ford play for industry. Moreover, the overall Eagle Ford Group is distinguished from other unconventional reservoirs in U.S. due to its high calcite content (Chermak and Schreiber, 2014), which improves its brittleness and makes this play easier to stimulate, hence increasing its attractiveness for oil companies for hydraulic fracturing. Other minerals commonly in the Eagle Ford are quartz, mixed layer clays including kaolinite and illite, and minor amounts of dolomite, ankerite, and pyrite (Elston 2014; Wang et al., 2015).

Besides minerals, total organic contents range from 2-12% of the Eagle Ford rocks (Za Za Energy, 2013). The source rock in Eagle Ford Group is dominated by Type I and Type II kerogen with the potential to produce both oil and natural gas (Jiang et al., 2016).

Because the thermal maturity of kerogen in the Eagle Ford Group is strongly geographically controlled (**Figure 17**), there are three main areas of production (EIA, 2011). The northern and shallowest part of the Eagle Ford reservoir is the up-dip oil window. This portion contains higher oil volumes, but lower pressure than its down-dip southern counterparts (Centurion et al., 2012). The middle part is the wet-gas or condensate window. The southern end of the reservoir is the deepest part of Eagle Ford Group and is the down-dip dry gas window. Unlike conventional reservoirs in which natural gas, oil, and water are layered by their respective densities, the Eagle Ford Group is an inverted petroleum system because the capillary pressure is too high for hydrocarbons to flow through the reservoir and stratify. Therefore, oil is on top of gas in the Eagle Ford Group.

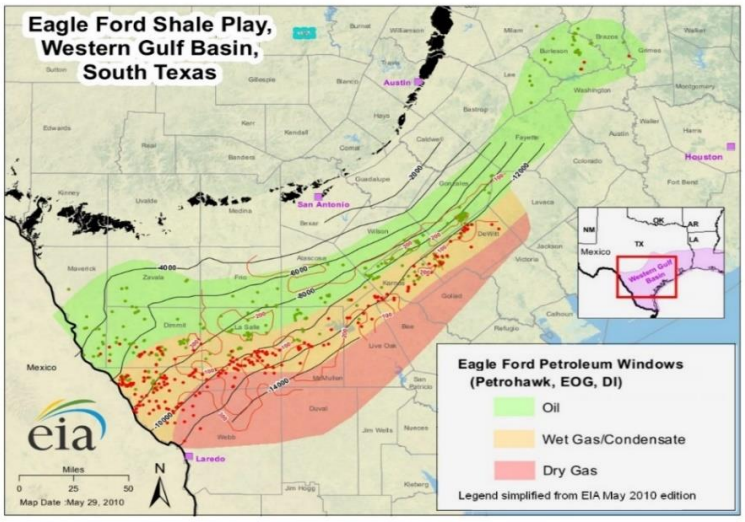

Figure 17 Eagle Ford hydrocarbon production map. Red and green points represent wells producing oil and gas. Eagle Ford shale comprises three "windows". Oil, wet gas/condensate, and gas show as green, orange, and red, respectively. Reprinted in U.S. Energy Information Administration (2011).

1.8.2 Heterogeneity of the Eagle Ford Formation

Eagle Ford Formation was historically considered a simple and homogenous rock unit which received little attention from geological survey. However, it aroused the geologists' interest when a wide range of well production rates were revealed, indicating significant geologic variability in Eagle Ford Formation (Donovan and Staerker, 2010). Recent studies have illustrated the dramatic vertical and subtle horizontal variability of strata within the Eagle Ford Formation. Based on lithologic observations in outcroppings, the vertical Eagle Ford Group section was sub-divided into 5 lithofacies and demonstrated that their divisions defined in exposures at the surface correlate with strata in the subsurface (Donovan and Staerker, 2010). Later the Eagle Ford Group 5 lithofacies were subdivided into 16 sub-facies based on petrophysical, biostratigraphic, and geochemical data, further indicating significantly vertical variation of the Eagle Ford Formation (Donovan et al., 2012). Correlation of individual beds in the Eagle Ford Group, demonstrated minor lateral variation of Eagle Ford Formation on the scale of a horizontal well, which suggests little lateral difference in depositional environment at scales up to 5km (Gardner et al., 2013). Integration of petrophysical, geochemical, and lithologic data from an oil well located in Maverick Basin, classified the lower Eagle Ford Formation into 5 petrophysical classes, 5 chemofacies, and 4 lithofacies (Amin et al., 2016). Their petrophysical classification was successfully applied to a nearby well with a different hydrocarbon production rate where core samples were not available for lithofacies and chemofacies characterization. Therefore, all studies indicate a pervasive heterogeneity

present in the Eagle Ford Group, which is a result of effect of paleoenvironment on dynamic sediment supply. In particular, the carbonate platform where Eagle Ford Formation was deposited had uneven paleotopography because of pre-existing carbonate platform deposition and subsequent erosion (Faust, 1990; Donovan and Staerker, 2010). As the platform was flooded from early to middle Cenomanian at the beginning of the Late Cretaceous, basin restriction and episodic anoxic conditions were created. Additionally, the occasional occurrence of storm deposits within Eagle Ford Formation also shows evidence that this basin experienced storm events (Donovan and Staerker, 2010; Donovan et al., 2012). Bentonite interbedded in mudrocks suggests regional volcanism (Hentz and Ruppel, 2010). Therefore, the Eagle Ford Formation was deposited in a restricted basin, influenced by storm events and episodic shallow-water anoxia (Donovan and Staerker, 2010; Donovan et al., 2012). These conditions not only contributed to deposition and preservation of organic matter but also made the Eagle Ford Formation highly vertically heterogeneous.

The significant geological variation of the Eagle Ford Formation provides an ideal opportunity to investigate the impact of the heterogeneity of shale formation on water-rock interactions. Although valuable information on interaction mechanisms between water and reservoir rocks was provided in the literature (Marcon et al., 2017; Wang et al., 2015; 2016; Li et al., 2017; Ali and Hascakir, 2017), all studies used one rock sample to represent the whole shale formation when conducting water-rock experiments. However, during the deposition of shale formations, complex depositional processes, like sea-level change, organic productivity, storm frequency, and diagenetic processes, result in shale

formations that are highly heterogeneous. Therefore, one rock sample may not be enough to interpret the entirety of geochemical processes occurring between shale and water. The question asked in my study is this: Does varying reservoir mineralogy within one shale formation cause different interactions and how do these affect hydraulic fracturing performance?

1.8.3 Production History of the Eagle Ford Formation

The Eagle Ford Formation is located in South Texas extending from the Maverick Basin, across the San Marcos Arch and ending in the East Texas Basin, approximately 50 miles wide, 400 miles long (Hentz and Ruppel, 2010; Guiltinan, 2015), which is one of the biggest North American unconventional reservoirs. EIA estimated that the proved reserves of tight oil and natural gas in Eagle Ford were 4,734 billion barrels and 30.8 trillion cubic feet respectively, which accounted for 20.6% and 9.0% of all U.S. shale oil and gas resources (EIA, 2019). Thus, the Eagle Ford Formation has become one of the major producers of oil and gas for southeast Texas and has contributed to the significant increase in production of hydrocarbon resources in U.S. from 2010 to the present. However, it received little attention from energy companies prior to 2008. Although it was known to contain significant amounts of hydrocarbons and was known as the source rock for the overlying Austin Chalk which has been an oil and gas producer since the 1920s, the Eagle Ford Formation itself had such a low permeability (<0.1 mD) that hydrocarbons could not flow through the rock into a production well (Childs et al., 1988; DrillingInfo,

2012). In 2007, Eagle Ford Group oil and liquid gas production was less than 57 barrels per day, none of which was from horizontal wells (EIA, 2011). The change occurred in 2008 when a horizontal well drilled in Eagle Ford Group located at LaSalle County by Petrohawk Energy Corporation that had an initial flow rate of 7.6 million cubic feet of natural gas per day, which demonstrated hydraulic fracturing and horizontal drilling were useful to produce hydrocarbons from the Eagle Ford Group and therefore unlocked its potential. To date, more than 21,000 horizontal wells in the Eagle Ford region were drilled (RRC, 2015). Texas Production Data Query System reported that oil production in Eagle Ford Group has increased exponentially from 352 barrels per day in 2008 to 867,783 barrels per day in 2020, and natural gas production increased from 2 million cubic feet per day in 2008 to 4,544 million cubic feet per day in 2020 (**Figure 18**).

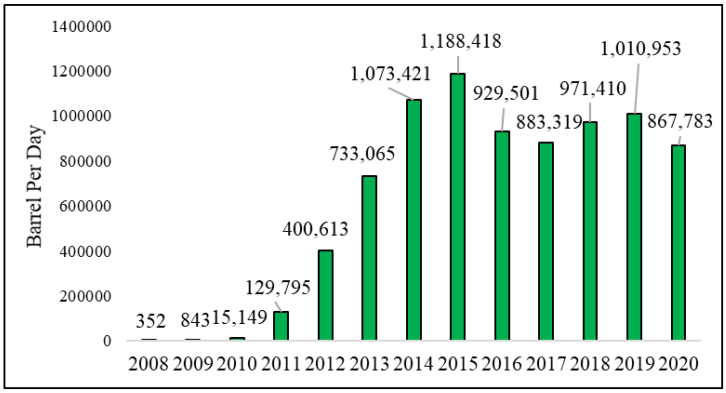

A-Eagle Ford Shale Daily Oil Production

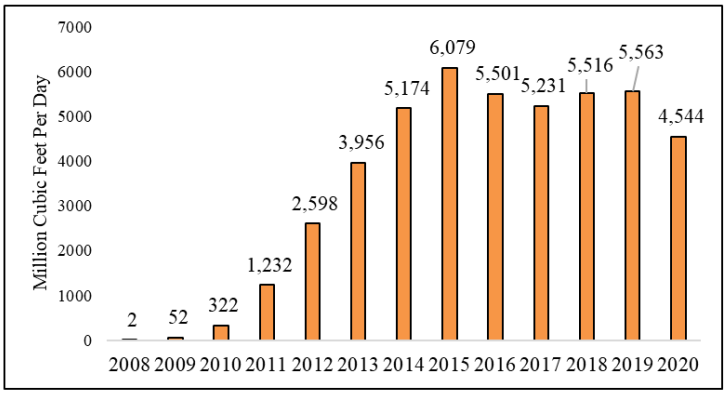

B-Eagle Ford Shale Daily Natural Gas Production

Figure 18 Texas Eagle Ford Shale daily oil (A) and natural gas production (B) from 2008 through 2020. Data obtained from Texas Railroad Commission.

As the application of horizontal drilling and hydraulic fracturing into the Eagle Ford Formation started from 2008, more source rock sections were exposed, and the permeability of the Eagle Ford Formation was dramatically increased, which now allows more than 200 operators to tap into previously inaccessible shale reserves (Arnett et al., 2014). Companies such as EOG Resources Inc., Lewis Petro Properties, Chesapeake Energy Corporation, Marathon Oil Corporation, ConocoPhillips, Devon Energy, and Sanchez Energy are the leading producers in the Eagle Ford Formation (**Table 20**). These

companies are working to unlock vast hydrocarbons saturating in the Eagle Ford Formation. At the same time, the increased drilling activity and production have had extraordinary economic impacts on south Texas.

Table 20 Daily oil and gas production in July 2020 of the top 5 operators in the Eagle Ford Formation. Data obtained from ShaleProfile.com.

Top 5 oil operators	Oil production, barrels per day	**Top 5 gas operators**	Natural gas production, million cubic feet per day
EOG Resources	189,106	Lewis Petro Properties	543,341
Chesapeake Energy	137,791	EOG Resources	468,828
Marathon Oil	92,674	Sanchez Energy	441,786
ConocoPhillips	78,567	Chesapeake Energy	432,886
Devon Energy	61,530	ConocoPhillips	288,176

According to a report from University of Texas at San Antonio, Eagle Ford Group oil and gas production contributed an estimated more than $50 billion in economic development and supported jobs reaching over 36,000 in 2016 in the region of 21 counties in southwest and south-central Texas (Oyakawa et al., 2017). Moreover, the University of Texas and San Antonio's Center for Community and Business Research projected that Eagle Ford Group will support almost 68,000 full-time jobs by 2020. However, since the outbreak of the coronavirus pandemic in the U.S., energy companies have cut jobs because of an unprecedented energy demand-supply imbalance. Texas, as the home to the Permian Basin and Eagle Ford Formation, has lost more than 45,000 jobs in its upstream energy sector since February 2020 (Takahashi, 2020). Moreover, the pandemic has slowed down fracturing activities in the Eagle Ford Group (**Figure 19**), leading to a drop in drilling

permits issued in the Eagle Ford Formation by more than 50% compared to 2019 (Hart Energy, 2020)

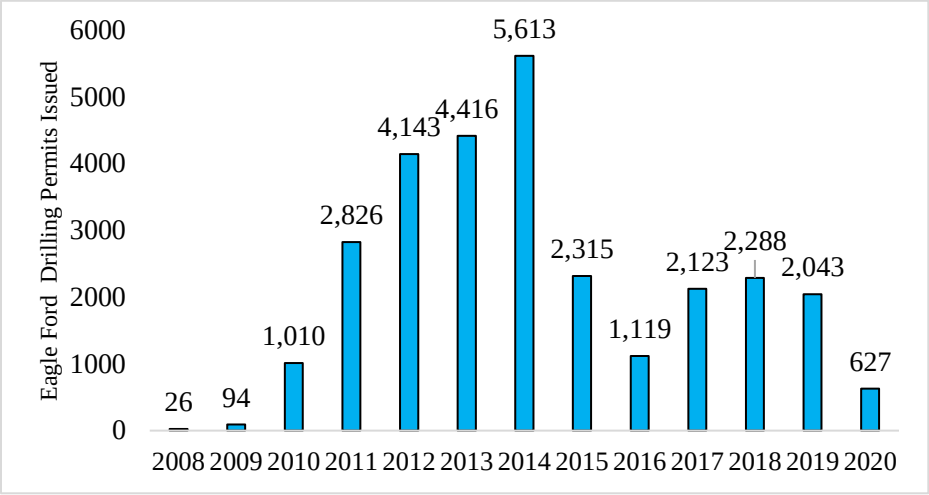

Figure 19 Eagle Ford Shale drilling permits issued from 2008 through 2020. Data obtained from Texas Railroad Commission.

1.8.4 Water Use in the Eagle Ford Formation

Although using hydraulic fracturing with horizontal wells in the Eagle Ford Group has greatly increased oil and gas production, its low permeability requires injection of large volumes of pressurized water to create fractures. In a typical HF well, the amount of water consumed by fracturing process is much larger than that required for other processes, such as well preparation, drilling, and production (Mohtar et al., 2018). In 2016, the average amount of water used in a HF well in South Texas' Eagle Ford Shale oil field was 9.7 million gallons, up from 4.5 million gallons in 2013 (Hiller, 2018). With more

than 21,000 horizontal wells established in the Eagle Ford Group, the unit was ranked top three in U.S. shale plays by water use (Ceres, 2016). In addition, 90% of water for Eagle Ford Group wells is fresh water sourced from groundwater aquifers and the remaining 10% comes from surface and brackish water with TDS of 1000 ppm or greater (Nicot et al., 2012; Arnett et al., 2014). Concerns over this freshwater use have grown in terms of high and increasing water stress, such as drought and declining groundwater supplies (Ceres, 2016).

Halliburton Company reports that in Eagle Ford Group horizontal wells, less than 15% of HF fluid returns to surface as flowback water. Therefore, most of HF fluid is consumed or lost during the fracturing process, likely to evaporation during production, absorption in underground fracture surfaces, or in hydrocarbon products (Mohtar et al., 2018). The average TDS in flowback water from the Eagle Formation ranges from 15,000-55,000 mg/L. This type of flowback water has relatively low salinity compared to flowback water with high salinity from other major U.S. shale plays like the Marcellus Formation and Bakken Formation (refer to Table 9). However, few studies reported the reuse or recycling of flowback water in the Eagle Ford Group, perhaps because of the low quantity of flowback water returned to surface. Currently, the most used practice to manage flowback water in the Eagle Ford Group is disposing it into injection wells underground, which leads to further concern about groundwater contamination and induced seismic activity (Ma et al., 2014).

1.9 The Marcellus Formation

1.9.1 Geologic Overview of the Marcellus Formation

The Marcellus Formation was deposited in the Appalachian Basin during the Middle Devonian, about 390 million years ago. It extends (**Figure 20**) across parts of New York, Pennsylvania, Ohio, West Virginia, and edges over the borders of Kentucky, Maryland, and Virginia (Clark, 1918). It appears in outcroppings along its northern margins in the Adirondack Mountains, and in the subsurface throughout the eastern United States (Colton, 1970). The Marcellus Formation encompasses approximately 95,000 square miles at a depth from 1,000 feet in outcrops to -8,000 feet subsea (EIA, 2017). Based on well log interpretation made by New York State geological survey agencies, the Marcellus Formation shows an increase in depth from northwest to southeast and a decrease in thickness from west to east due to the asymmetric structure of the Appalachian Basin (EIA, 2017). The Marcellus Formation is thickest in New York, being roughly 900 feet thick, becoming thinner in northeastern Pennsylvania, ranging from 200 feet to 600 feet, and finally pinches out in the subsurface along the eastern overthrust belt, which is the eastern boundary of the unit. Resource exploitation reveals most of the current production of Marcellus Formation is in areas with depth between 2,000 to 6,000 feet and with thickness more than 50 feet (EIA, 2017).

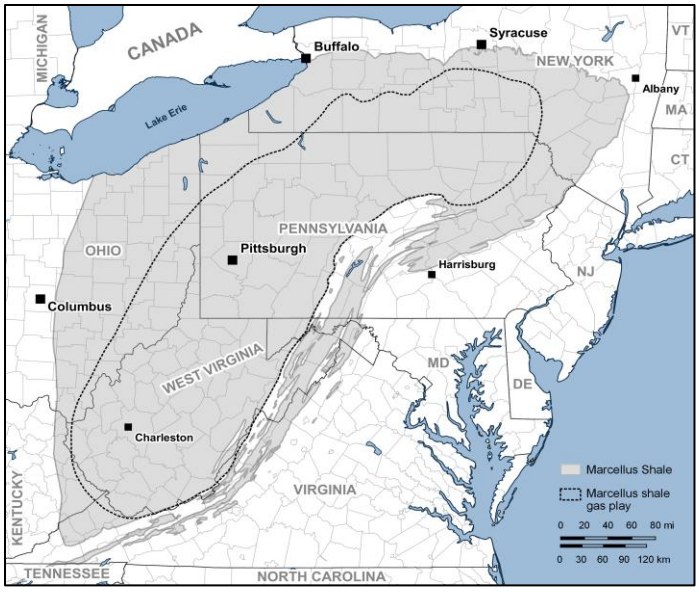

Figure 20 Location map for the Marcellus Formation. Reprinted in Gretarsson (2019).

The Marcellus Shale was first named in 1839 by James Hall, a geologist of the New York State Geological Society, after a distinctive outcrop was discovered near the village of Marcellus, Onondaga County, New York (Neal, 1979). This shale unit is bounded (**Figure 21**) above by the Middle Devonian Mahantango Formation and below by the Lower Devonian Onondaga Limestone (de Witt et al., 1993; Roen, 1983; Lash and Engelder, 2011).

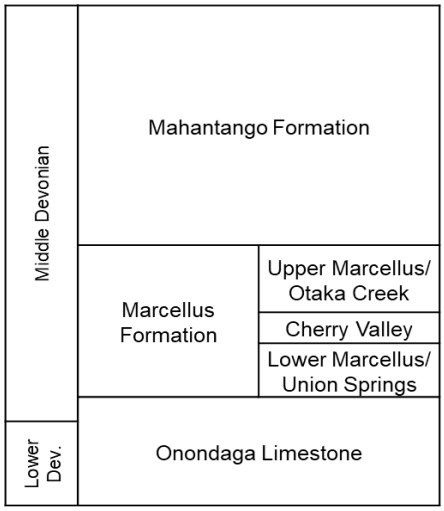

Figure 21 Stratigraphic column for the Marcellus Formation that is bounded above by Mahantango Formation and below by Onondaga Limestone. It is divided into Union Springs Shale, Cherry Valley Limestone and Oatka Creek Shale (Cooper, 1930; de Witt et al., 1993; Roen, 1983; Lash and Engelder, 2011).

The Marcellus Formation is sub-divided into the Union Springs Shale (lower Marcellus Formation) and the Oatka Creek Shale (upper Marcellus Formation), which are separated by the Cherry Valley Limestone (Cooper, 1930; Lash and Engelder, 2011). The Union Springs Shale, as the basal unit of Marcellus Formation, is an organic-rich shale, siltstone, and limestone with abundant pyrite laminations and framboids (Soeder et al., 2014). Because of its highest organic contents, the Union Springs Shale is the most gas productive part of the Marcellus Formation. Separating the Union Springs Shale from the overlying Oatka Creek Shale is the Cherry Valley Limestone which consists of a dark, organic-rich limestone with many voids filled with carbonate crystals (Cooper, 1930; Soeder et al., 2014). This member often is identified in northern West Virginia but is not continuous throughout the depositional area of Marcellus Formation (de Witt et al., 1993). In southern Pennsylvania and part of West Virginia, the Purcell Limestone occurs within

the Marcellus Formation. The stratigraphic relationship of these two units remains unresolved (Repetski et al., 2012; 2013). Above the Cherry Valley Limestone is the Oatka Creek Shale, which is described as soft, fissile shale with some concretions usually composed of siderite. Compared with the Union Springs Shale (the lower Marcellus Formation), the Oatka Creek Shale (the upper Marcellus Formation) contains lower organic matter, more clay content, and low gamma-ray log values (Popova et al., 2015). Sedimentary rocks in the overall Marcellus Formation are typically described as organic rich black shale interbedded with thin gray silty shale and limestone layers. Scattered pyrite, scarce fossils, and zones of carbonate concretions also occur in Marcellus strata (Ettensohn and Barron, 1981; Harper, 1999).

Marcellus Formation lithology varies significantly due to the complex depositional environments in which it formed. The Appalachian Basin formed as a classic foreland basin that began its development during the Taconic Orogeny in the Early-Middle Ordovician, around 472 million years ago (Ettensohn, 2008). Because discontinuous subsidence of the Appalachian Basin started in the late Precambrian, accommodation space was created for a series of Paleozoic seas to allow sediments to accumulate (Colton, 1970). During the Taconic Orogeny, the Taconic Mountains were formed and became an eastern barrier for the Appalachian Basin (Faill, 1997). Following the Taconic Orogeny was the Acadian Orogeny that began in the Middle Devonian (**Figure 22**).

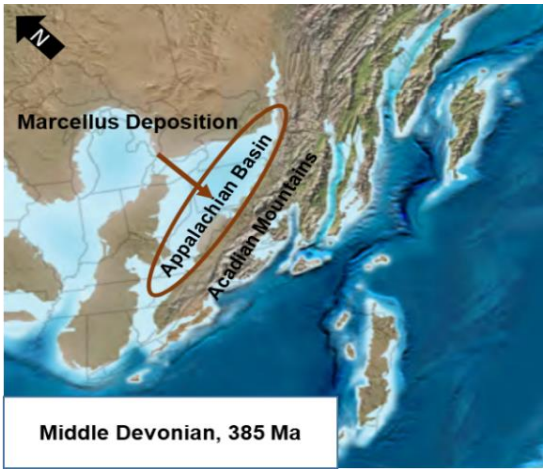

Figure 22 Paleogeographic reconstruction of Eastern North America during the Middle Devonian. Light blue represents shelf margins, medium blue represents slopes and dark blue represents abyssal depths. The approximate location of Appalachian Basin, Acadian Mountains and Marcellus deposition are shown. Modified from Blakey (2013) with permission from Deep Time Maps™.

Based on paleogeographic reconstructions of Eastern North America during the Middle Devonian, the Appalachian Basin was situated at approximately 25–35° south of the equator, which was rotated clockwise about 90° to the south from its present position (Ver Straeten, 2007). At this latitude, the Appalachian Basin had a tropical to subtropical climate (Ettensohn and Barron, 1981). As the first sediments deposited in the basin in the earliest phase of the Acadian Orogeny, the Marcellus Formation covered most of the northern Appalachian Basin (Martin, 2008). The tropical to subtropical climate at the near equatorial latitudes and the rain shadow effect of the Acadian Mountains on the seaway resulted in creation of trade winds and seasonal storm activity within the basin (Werne et al., 2002). Moreover, the erosion of the Acadian Mountains provided terrigenous sediments that formed the Marcellus Formation. Furthermore, eolian siliciclastic sediment was supplied by trade winds and arid conditions to the Marcellus depositional basin (Potter

et al., 1980). Because of the rise of the mountains and rapid subsidence of the basin floor, Marcellus deposition produced a transgressive sequence in deepening conditions (Ettensohn, 1998). The deepening sea along with the surrounding paleogeographic features also led to the formation of a restricted basin with anoxic conditions, which decreased in the supply of carbonates but thereby contributed to the preservation of the organic matter (Barrett, 2008).

The Marcellus Formation is primarily composed of quartz, calcite, dolomite, mixed-layer clays (illite, kaolinite and smectite), feldspar, pyrite, and gypsum. (Zielinski and McIver, 1982; Hosterman and Whitlow, 1983; Paronish et al., 2016). Clay minerals are more abundant in the upper Marcellus Formation and carbonate minerals are more common in the lower Marcellus Formation. Pyrite is typically toward the base of the Formation (Avary and Lewis, 2008; Boyce and Carr, 2009; Paronish et al., 2016). The high abundance of quartz and carbonate minerals increases the brittleness of Marcellus Formation shale, making Marcellus Formation shale plays easier to stimulate and hence attractive for fracking companies (Jarvie et al., 2007). The Marcellus Formation also includes high concentrations of organic matter. Total organic content of the Marcellus Formation ranges from <1% to >11% (Zielinski and Mciver, 1982; Nyahay et al., 2007; Reed and Dunbar, 2008). Kerogen in the source rocks is a mixture of Type II and Type III, which generally produces more natural gas and little oil (Chalmers et al., 2012). Thermal maturity in the Marcellus Formation generally increases to the southeast. In southeastern New York and Pennsylvania, shales are in the gas window. To the west, shales are more likely in the oil window (EIA, 2017).

1.9.2 Production History of the Marcellus Formation

Shale gas production in the U.S. accounted for 30% of U.S. natural gas production in 2015 and is projected to more than double to 70% of total U.S. natural gas in 2040 (AEO, 2016). Among all shale plays across the U.S., the Marcellus Formation is the largest identified North American shale gas play. EIA estimated that the Marcellus Formation, mainly in the most active areas in Pennsylvania and West Virginia, contains proved reserves of 135.1 trillion cubic feet natural gas and 345 million barrels oil that represent 39.5% and 1.5% of all the U.S. shale gas and crude oil, respectively (EIA, 2019). Therefore, the large volume of gas reserves in the Marcellus Formation not only makes it the largest active play, but also demonstrates the best potential to be a large gas supplier in the future.

However, like other unconventional reservoirs, the Marcellus Formation had a history of low gas production due to the extremely low porosity and permeability of shale units. In general, sandstone reservoir rocks can reach up to 30% porosity with permeability in the range of ten to several hundred milliDarcys (Bear, 1972; Ehrenberg and Nadeau, 2005). However, porosity in the Marcellus Formation ranges from 0.5-15%, and permeability is in the microDancy to nanoDarcy range (Van Tyne, 1993; Lee et al., 2011). Before 2000, shallow, organic-rich areas with pervasive development of natural fractures were popular targets for industry using conventional techniques (Perry and Wickstrom, 2010). However, gas production from wells drilled in the Marcellus Formation rarely reached commercial quantities and had relatively long capital recovery periods. Horizontal

drilling and hydraulic fracturing were successfully applied to the Marcellus Formation in 2003 by Range Resources Company, resulting in economic production of natural gas and turning the Marcellus Formation into a major natural gas field (EIA, 2019). Natural gas production in the Marcellus Formation has increased rapidly (**Figure 23**) from 1.2 billion cubic feet per day in 2008 to more than 20 billion cubic feet per day in 2019 (EIA, 2019).

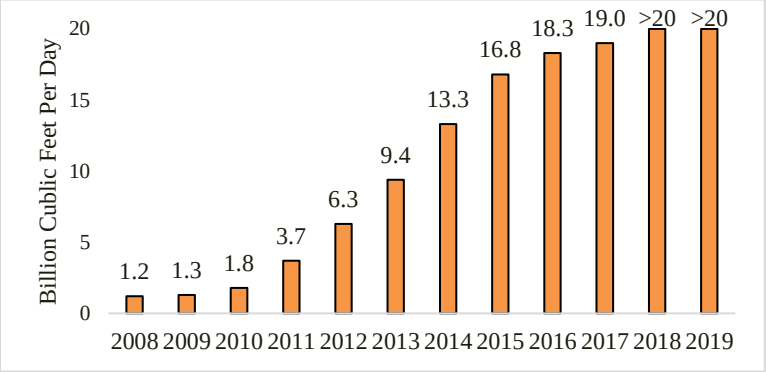

Figure 23 Marcellus Formation daily natural gas production from 2008 through 2019. After 2018, the Marcellus Formation and the Utica Formation have been combined into one Appalachia region by EIA. Data obtained from U.S. Energy Information Administration (2019).

As the largest natural gas field in the U.S., Marcellus Formation produces more than a fifth of the nation's gas output. Five dominant producers have driven this rapid expansion: Cabot, Chesapeake, Range Resources, EQT Corporation, and Rice Drilling (**Table 21**).

Table 21 Daily gas production in March 2019 of the top 5 operators in the Marcellus Formation. After 2019, Marcellus production data is not provided separately. Data obtained from ShaleProfile.com

Top 5 gas operators	Natural gas production, million cubic feet per day
Cabot	2,647,141
Chesapeake	2,329,789
Range Resources	2,002,125
EQT Corporation	1,840,076
Rice Drilling	1,605,202

The Marcellus Formation mainly produces in four states: Pennsylvania, West Virginia, Ohio, and New York (hydraulic fracturing has been banned in New York since 2015). In northeast Pennsylvania, dry gas is primarily produced (EIA, 2017). In southwestern Pennsylvania, West Virginia, and southeastern Ohio, gas becomes less thermally mature and more liquids-rich, making it more valuable (EIA, 2017). Among all active areas, the most development has occurred in Pennsylvania and West Virginia. Since 2008, about 11,000 wells were drilled in Pennsylvania and more than 2,000 wells in West Virginia (PA DEP, 2018; WV DEP, 2018). The development of the Marcellus Formation increases the overall economy of these states and brings significant employment and business opportunities that benefit their communities over the long term. Unlike the Eagle Ford Formation, the outbreak of the coronavirus has not caused widespread job losses in energy companies drilling in the Marcellus Formation. However, natural gas production in the Appalachian Basin, including the Marcellus Formation and the Utica Formation, has slowed by about 2% since February 2020 (Suttle, 2020). Moreover, to slow the spread of the coronavirus, several companies, including CNX Resources, EQT Corporation, and

Pittsburgh-based companies, have instituted mandatory work-from-home orders (Marcellus Drilling News, 2020).

1.9.3 Challenges Associated with the Development of the Marcellus Formation

Along with economic opportunities, development of the Marcellus Formation has also brought environmental challenges. In the Marcellus Formation, average water volumes for a vertical drilling are 85,000 gallons, whereas the water usage for hydraulic fracturing of a gas well ranges from 2.4-7.4 million gallons (Hurdle, 2018). Since 2008, more than 10,000 wells have been drilled in the Marcellus Formation. Thus, large quantities of freshwater usage in HF operations puts farming and drinking sources at risk. Moreover, flowback water recovered from Marcellus Formation gas wells ranges from 10-40% of the HF fluid (refer to Table 7). Ultimately, about 0.24-2.96 million gallons of wastewater are produced in a single well. Industry data showed that more than 242 million gallons of wastewater were produced in Pennsylvania gas and oil wells in 2017 alone (Kelso, 2019). Moreover, the composition of the wastewater is complex. The average TDS in Marcellus flowback water was 20,000-150,000 mg/L, mainly composed of Na, Cl, Mg, Ca, Ba, and Sr. (Gregory et al., 2011; Ziemkiewicz and Thomas, 2015). Other metal elements, like Pb, Se, Al, Mn, Fe, and Ra also exceeded the EPA's maximum contaminant levels (Gregory et al., 2011; Blauch, 2011; Ziemkiewicz and Thomas, 2015). Managing massive amounts of flowback water with complex compositions is a challenge for energy companies. Establishing disposal wells was the traditional way to treat Marcellus

Formation flowback water. However, the use of disposal wells was limited in many areas. For instance, new disposal wells are costly to permit and often face public opposition in terms of groundwater contamination (Groom, 2013). In addition, powerful earthquakes thousands of miles away may trigger swarms of minor quakes near injection wells. Thus, in Pennsylvania, injection wells have not been the primary disposal method, as the state's geology has been considered unsuitable (Arthur, et al., 2008). In New York, hydraulic fracturing was banned to protect public drinking water in the state by the New York Department of Environmental Conservation in 2015 (National Law Review, 2015). Therefore, in both Pennsylvania and New York, there are few disposal wells in the regions and Marcellus flowback water must be trucked to Ohio or West Virginia to be injected underground, leading to high transportation and disposal cost (Boschee, 2014; Davarpanah, 2018). Besides using disposal wells, release of the water to surface water after treatment also is expensive, because the cost of purifying flowback water to near potable quality is generally too great. To help reduce the total amount of fresh water used in operations and flowback water that has to be transported, treated, and disposed, operators have paid more attention to developing alternative water management methods, including reuse of flowback water to minimize the adverse environmental impact. At present, reuse of flowback water is prevalent in the Marcellus Formation (**Figure 24**), where about 90% of wastewater from wells was reused or recycled since 2013 in Pennsylvania respectively (Davarpanah, 2018).

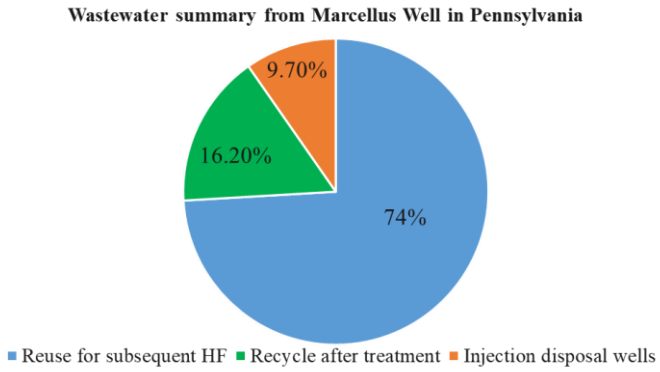

Figure 24 In Pennsylvania, 90% of wastewater has been reused or recycled since 2013. Wastewater sent to disposal wells has fallen to under 10%. Data obtained from Davarpanah (2018).

Although the general opinion is that flowback water is less saline than produced water and can be treated for reinjection, TDS in Marcellus Formation flowback water is extremely high (20,000-150,000 mg/L). Therefore, direct reuse of flowback water with little or no treatment could cause formation damage, which means the open fractures will be blocked by impurities carried by flowback water and mineral precipitation by flowback water-rock interaction. During flowback water-rock interaction, the high content of constituents in flowback and excess mineral components provided by shale formation may result in rapid mineral saturation and new mineral precipitation. Therefore, my second objective is to identify the impact of re-injecting flowback water on formation damage. The Marcellus Formation was chosen as my second study area due to prevalent reinjection of flowback water in this area.

Summary

The production of unconventional resources by advanced technology has changed the global perspective of dwindling hydrocarbon resources and met future demand for energy. However, development of unconventional resources also brings concern about impacts on freshwater demand and environmental pollution. Excessive freshwater usage and wastewater generation during hydraulic fracturing operation are pushing industry to develop new water management methods. Reuse of flowback water is an effective disposal strategy among energy companies because it reduces not only the initial required quantity of flesh water but also the volume of contaminated water that must be treated and disposed. However, reuse of flowback water may cause blockage of created fractures and lower the recovery efficiency due to complex water-rock interactions, which is a current consideration for industry.

Therefore, the aim of my research is to investigate water-rock interactions occurring during hydraulic fracturing to understand the basic interaction mechanisms and their impact on hydraulic fracturing performance. Two study areas were selected, the Eagle Ford Group and the Marcellus Formation, which are two of the most prolific shale reservoirs in the United States. The Eagle Ford Group was chosen because of its significantly vertical variability. Thus, my first research objective is to investigate the impact of the lithological heterogeneity on water-rock interactions. The Marcellus Formation was chosen because reuse of flowback water is prevalent in Marcellus Formation wells. Thus, my second and third research objectives are to investigate the

impact of reuse of flowback water on formation damage and the role of different minerals in flowback water properties.

References

40 CFR Part 435. 1979. Oil and Gas Extraction Point Source Category

AAPG Wiki. 2016. Kerogen. https://wiki.aapg.org/Kerogen. Accessed 1 August 2018.

Adkins, W. S., and Lozo, F. E. 1951. Stratigraphy of the Woodbine and Eagle Ford, Waco Area, Texas in the Woodbine and Adjacent Strata: Stratigraphy of the Woodbine and Eagle Ford, Waco Area, Texas Copyright 1951 by the Dallas Petroleum Geologists, p. 101-161.

Aguilera, R. 1978. Flow Units: From Conventional to Tight Gas to Shale Gas Reservoirs. The Trinidad and Tobago Energy Resources Conference, 27-30 June.

Ahuja, S. 2015. Food, Energy, and Water: The Chemistry Connection. ISBN 978-0-12-800211-7

Ali, M., and Hascakir, B. 2017. Water-Rock Interaction for Eagle Ford, Marcellus, Green River, and Barnett Shale Samples and Implications for Hydraulic Fracturing Fluid Engineering, SPE Journal, 22, 01, 162-171, SPE-177304-PA.

Ali, M., and Hascakir, B., 2015b. Water-Rock Interaction for Eagle Ford, Marcellus, Green River, and Barnett Shale Samples, SPE Eastern Regional Meeting, 13-15 October 2015, Morgantown, West Virginia, USA, SPE-177304-MS.

Allouche, E. N., Ariaratnam, S. T., and Lueke, J. S. 2000. Horizontal Directional Drilling: Profile of an Emerging Industry. J. Constr. Eng. and Manage, 126(1), 68-76.

Amin, S., Wehner, M., Heidari Z., and Tice, M. 2016. Rock Classification in the Eagle Ford Shale through Integration of Petrophysical, Geological, and Geochemical Characterization. SPWLA 57th Annual Logging Symposium, 25-29 June.

Arnett, B., Healy, K., Jiang, Z., LeClere, D., McLaughlin, L., Roberts, J., and Steadman, M. 2014. Water Use in the Eagle Ford Shale: An Economic and Policy Analysis of Water Supply and Demand

Arthur, J. D., Bohm, B., and Layne, M. 2008. Hydraulic Fracturing Considerations for Natural Gas Wells of the Marcellus Shale. Groundwater Protection Council Annual Forum. Cincinnati

Avary, K. L., and Lewis, J. E. 2008. New Interest in Cores Taken Thirty Years Ago: the Devonian Marcellus Shale in northern West Virginia

Baes, C. F., and Mesmer, R. S. 1976. The Hydrolysis of Cations. John Wiley & Sons, New York, London, Sydney, Toronto

Bai, B., Elgmati, M., Sun, Y., and Liu, L. 2016. Petrophysical Properties Characterization of Ordovician Utica Gas Shale in Quebec, Canada. Petrol. Explor. Develop. 2016, 43(1): 74–81.

Baker, O. 1981. Effect of Price and Technology on Tight Gas Resources of the United States. International Energy Conversion Engineering Conference (IECEC), Proceedings 16th Annual Meeting (Atlanta), v. 2, p. 1298-1303

Ball, M. M., Henry, M. E., and Frezon. S. E. 1991. Petroleum Geology of the Anadarko Basin Region, Province (115), Kansas, Oklahoma, and Texas

Barrett, R. 2008. The Depositional Setting of the Marcellus Black Shale. Appalachian Producers Issues Seminar. Independent Oil and Gas Association of West Virginia. Archived from the original (PDF) on July 15, 2008.

Bear, J. 1972. Dynamics of Fluids in Porous Media: New York, American Elsevier Publishing Company, Inc., 800 p.

Beattie, A. 2019. Shale Oil vs. Conventional Oil: What's the Difference? https://www.investopedia.com/articles/active-trading/051215/cost-shale-oil-versus-conventional-oil.asp

Beaudoin, Y. C., Waite, W., Boswell, R., and Dallimore, S. R. (eds). 2014. Frozen Heat: A UNEP Global Outlook on Methane Gas Hydrates. Volume 1. United Nations Environment Programme, GRID-Arendal.

Bennett, L. C. 2015. Interpretation of Late Cretaceous Volcanic Mounds and Surrounding Gulfian Series Formations Using 3D Seismic Data in Zavala County, Texas. Theses and Dissertations Retrieved from https://scholarworks.uark.edu/etd/1134

Birkeland, P. 1999. Soils and Geomorphology (3rd ed.). Oxford: Oxford University Press.

Blakey, R. 2013. NAU Geology, Early Cretaceous Paleogeographic Map: Retrieved 20 March 2013: www.cpgeosystems.com/paleomaps.html

Blatt, H., and Robert, J. T. 1996. Petrology: Igneous, Sedimentary and Metamorphic, 2nd ed., Freeman, pp. 281–292 ISBN 0-7167-2438-3

Blauch, M. 2011. Shale Frac Sequential Flowback Analyses and Reuse Implications, March 30, 2011. Environmental Protection Agency. Web. Accessed June 2015. PDF.

Boschee, P. 2014. Produced and Flowback Water Recycling and Reuse-Economics, Limitations, and Technology. https://spe.org/en/print-article/?art=231

Boyce, M., and Carr, T. 2009. Lithostratigraphy and Petrophysics of the Devonian Marcellus Interval in West Virginia and Southwestern Pennsylvania. DOI: https://doi.org/10.5724/gcs.09.29.0254

Brady, N. C., and Weil, R. R. 2008. The Nature and Properties of Soils (14th ed.). Upper Saddle River, USA: Pearson.

Brady. E. J., and Senese, F. 2004. Chemistry: Matter and its Changes, 4th Edition. Published by Wiley, ISBN: 0-471-21517-1.

Bresch, C., and Carpenter, J. 2009. Preliminary Analytical Results: Haynesville Shale in Northern Panola County, Texas. AAPG Search and Discover Article #90093 © 2009 GCAGS 59th Annual Meeting, Shreveport, Louisiana

Britannica Online Encyclopedia (BOE). 2009. Colloid. Retrieved 31 August 2009.

Brooks, J., Cornford, C., and Archer, R. 1987. Geological Society, London, Special Publications, 26, 17-46, 1, https://doi.org/10.1144/GSL.SP.1987.026.01.02

Butkovskyi, A., Bruning, H., Stefan A. E. Kools, Huub H. M. Rijnaarts, and Annemarie P. Van Wezel. 2017. Organic Pollutants in Shale Gas Flowback and Produced Waters: Identification, Potential Ecological Impact, and Implications for Treatment Strategies. Environmental Science & Technology 2017 51 (9), 4740-4754 DOI: 10.1021/acs.est.6b05640

Cantisano, M. T., Restrepo, D. P., and Cespedes, S. 2013. Relative Permeability in a Shale Formation in Colombia Using Digital Rock Physics. Presented at the Unconventional Resources Technology Conference, 12-14 August, Denver, Colorado, USA. SPE-168681-MS. http://dx.doi.org/10.1190/URTEC2013-092.

Carroll, D. 1959. Cation Exchange in Clays and Other Minerals. Bulletin of the Geological Society of America. 70 (6): 749–780.

Centurion, S. M., Cade, R., and Luo, X. L. 2012. Eagle Ford Shale: Hydraulic Fracturing, Completion and Production Trends, Part III: Paper SPE 166494 presented at SPE Annual Conference in New Orleans, Louisiana, USA, 30 September-2 October 2013.

Ceres. 2016. New Data: Water Use in Hydraulic Fracturing a Key Risk in Water-Stressed Regions in Texas and Colorado-Water Use per Well Doubles Even as Productio n Declines, Increasing Wastewater Disposal Risks. https://www.ceres.org/news-center/pr ess-releases/new-data-water-use-hydraulic-fracturing-key-risk-water-stressed-regions

Chalmers, G. R., Bustin, R. M., and Power, I. M. 2012. Characterization of Gas Shale Pore Systems by Porosimetry, Pycnometry, Surface Area, and Field Emission Scanning Electron Microscopy/Transmission Electron Microscopy Image Analyses: Examples from the Barnett, Woodford, Haynesville, Marcellus, and Doig Units. AAPG Bull. 96, 1099–1119.

Chapman, R. E. 1983. Chapter 9 Origin and Migration of Petroleum: Geological and Physical Aspects, Developments in Petroleum Science, Volume 16, Pages 179-207, ISSN 0376-7361

Chermak, J. A., and Schreiber, M. E. 2014. Mineralogy and Trace Element Geochemistry of Gas Shales in the United States: Environmental implications. International Journal of Coal Geology 126 (2014) 32–44

Childs, O., Steele, E. G., and Salvador, A. 1988. Correlation of Stratigraphic Units in North America (COSUNA) Project, Gulf Coast Region: American Association of Petroleum Geologists Bulletin, v. 93, p. 231-269.

Clark, C. E., Horner, R. M., and Harto, C. B. 2013. Life Cycle Water Consumption for Shale Gas and Conventional Natural Gas. Environ Sci Technol 47: 11829-11836. http://dx.doi.org/10.1021/es4013855

Clark, W. B. 1918. The Geography of Maryland. Maryland Geological Survey. vol. 10. Baltimore: Johns Hopkins Press

Coday, B. D., Almaraz, N., and Cath, T. Y. 2015. Forward Osmosis Desalination of Oil and Gas Wastewater: Impacts of Membrane Selection and Operating Conditions on Process Performance. J Membr Sci.

Cohen, A. J., Brauer, M., Burnett, R., Anderson, H. R., Frostad, J., and Estep, K. 2017. Estimates and 25-Year Trends of the Global Burden of Disease Attributable to Ambient Air Pollution: An Analysis of Data from the Global Burden of Diseases Study 2015. Lancet 389:1907–1918; doi:10.1016/S0140-6736(17)30505-6.

Colborn, T., Kwiatkowski, C., Schultz, K., and Bachran, M. 2011. Natural Gas Operations from a Public Health Perspective. Human and Ecological Risk Assessment: An International Journal. 17. 1039-1056. 10.1080/10807039.2011.605662.

Colton, G. W. 1970. The Appalachian Basin–Its Depositional Sequences and Their Geologic Relationships, in Fisher, G. W., Pettijohn, F. J., Reed Jr., J.C., and Weaver, K. N., eds., Studies on Appalachian Geology: Central and Southern, Interscience Publishers. 5-47.

Coneybeare, C. E. B. 1967. Influence of Compaction on Stratigraphic Analysis: Canadian Petroleum Geology Bulletin, v. 15, p. 331–345

Cooper, G. A. 1930. Stratigraphy of the Hamilton Group of New York: American Journal of Science, p. 116-134

Cortez, M. 2012. Chemostratigraphy, Paleoceanography, and Sequence Stratigraphy of the Pennsylvanian – Permian Section in The Midland Basin of West Texas, with Focus on the Wolfcamp Formation.

Davarpanah. A. 2018. The Integrated Feasibility Analysis of Water Reuse Management in the Petroleum Exploration Performances of Unconventional Shale Reservoirs. https://link.springer.com/article/10.1007/s13201-018-0717-7

Dawson, W. C. 1997. Limestone Microfacies and Sequence Stratigraphy: Eagle Ford Group (Cenomanian-Turonian) north-Central Texas outcrops: Gulf Coast Association Geological Societies Transactions, v. 47, p. 99-105.

Dawson, W. C. 2000. Shale Microfacies: Eagle Ford Group (Cenomanian-Turonian) North-Central Texas Outcrops and Subsurface Equivalents: Gulf Coast Association of Geological Societies Transactions, v. L, p. 607-622.

Dawson, W. C., and Almon, W. R. 2010. Eagle Ford Shale Variability: Sedimentologic Influences on Source and Reservoir Character in an Unconventional Resource Unit: Gulf Coast Association of Geological Societies Transactions, v. 60, p. 181-190.

DC Solid Control. 2013. Development Tendency of Horizontal Directional Drilling. Archived from the original on 8 July 2013

de Witt, Wallace, Jr., Roen, J. B., and Wallace, L. G. 1993. Stratigraphy of Devonian black shales and associated rocks in the Appalachian Basin, in Roen, J.B., and Kepferle, R.C., eds., Petroleum Geology of the Devonian and Mississippian Black Shale of Eastern North America: U.S. Geological Survey Bulletin, 1909-B, p. B1–B57.

Dimri, V. P., Srivastava, R. P., and Vedanti, N. 2012. Fractal Models in Exploration Geophysics: Application to Hydrocarbon Reservoirs, Elsevier, Amsterdam.

Donovan, A. D., and Staerker, T. S. 2010. Sequence stratigraphy of the Eagle Ford (Boquillas) Formation in the Subsurface of South Texas and outcrops of West Texas: Gulf Coast Association of Geological Societies Transactions, v. 60, p. 861-899.

Donovan, A. D., Pope, M. C., Gardner, R. M., Wehner, M. P., and Staerker, T. S. 2015. Making Outcrops Relevant to the Subsurface: Learnings from the Eagle Ford Group in West Texas: Unconventional Resources Technology Conference, San Antonio, Texas, 20–22 July, URTeC Paper 2154599, p. 558–573.

Donovan, A. D., Staerker, T. S., Pramudito, A., Li, G., Corbett, M. J., Lowery, C. M., Romero, A. M., and Gardner, R. D. 2012. The Eagle Ford Outcrops of West Texas: A Laboratory for Understanding Heterogeneities within Unconventional Mudstone Reservoirs. GCAGS Journal, v. 1 (2012), p. 162–185.

Dott, R. H. 1964. Wacke, Graywacke and Matrix – What Approach to Immature Sandstone Classification. Journal of Sedimentary Petrology. 34 (3): 625–632. doi:10.1306/74D71109-2B21-11D7-8648000102C1865D

Dow, W. G. 1977. Kerogen Studies and Geological Interpretations. Journal of Geochemical Exploration 7, 79-99.

Dravis, J. J. 1980. Sedimentology and diagenesis of the Upper Cretaceous Austin Chalk Formation, South Texas and northern Mexico: PhD Dissertation, Rice University, Houston, Texas, 532 p.

Dresel, P. E. 1985. The Geochemistry of Oilfield Brines from Western Pennsylvania. M.S. Thesis, Pennsylvania State Univ.

Dresel, P. E., and Rose, A. W. 2010. Chemistry and Origin of Oil and Gas well Brines in Western Pennsylvania. Pennsylvania Geol. Surv., 4th ser., Open-File Report OFOG 10–01.0, Portable Document Format (PDF).

DrillingInfo. 2012. Eagle Ford Shale Overview: Ramona Hovey, DrillingInfo, Inc.

Durand, B. 1980. Kerogen, Insoluble Organic Matter from Sedimentary Rocks, Éditions Technip, Paris, France, 525 p.

Durand, B. 1980. Sedimentary Organic Matter and Kerogen: Definition and Quantitative Importance of Kerogen, Kerogen: Techniq, p. 13–14

Eberl, D. D. 1984. Clay Mineral Formation and Transformation in Rocks and Soils. https://doi.org/10.1098/rsta.1984.0026

Ehrenberg, S. N., and Nadeau, P. H. 2005, Sandstone vs. Carbonate Petroleum Reservoirs: A Global Perspective on Porosity-Depth and Porosity-Permeability Relationships: American Association of Petroleum Geologists Bulletin. 89(4): 435-445.

Elango, L., and Kannan, R. 2007. Rock-Water Interaction and its Control on Chemical Composition of Groundwater. Chapter 11. Vol. 5. Developments in Environmental Science: Elsevier.

Elston, H. 2014. Mineralogical and Geochemical Assessment of the Eagle Ford Shale. Senior Thesis

Emerson, S., and Hedges, J. I. 1988. Processes Controlling the Organic Carbon Content of Open Ocean Sediments. Paleoceanography, 3:621-634.

Engle, M. A., Reyes, F. R., Varonka, M. S., Orem. W. H., Ma, L., Ianno, A. J., Schell, T. M., Xu, P., and Carroll, K. C. 2016. Geochemistry of Formation Waters from the Wolfcamp and "Cline" Shales: Insights into Brine Origin, Reservoir Connectivity, and Fluid Flow in the Permian Basin, USA, Chemical Geology, Volume 425, 2016, Pages 76-92, ISSN 0009-2541

Enos, P., and Sawatsky, L. H. 1981. Pore Networks in Holocene Carbonate Sedi ments. J. of Sedimentary Petrology. 51 (3): 961-985. http://dx.doi.org/10.1306/212F7DF 1-2B24-11D7-8648000102C1865D.

Espitalié, J., Madec, M., Tissot, B., Mennig, J., and Leplat, P. 1977. Source Rock Characterization Method for Petroleum Exploration, Offshore Technology Conference. Offshore Technology Conference (OTC) 2935, pp. 439-444.

Ettensohn, F. 1998. Compressional Tectonic Controls on Epicontinental Black-Shale Deposition; Devonian-Mississippian examples from North America in J. Schieber,

W. Zimmerle, and P. Sethi, eds., Shales and mudstones; I, Basin studies, sedimentology, and paleontology, p. 109- 128.

Ettensohn, F. 2008. Tectonism, Estimated Water Depths, and the Accumulation of Organic Matter in the Devonian-Mississippian black shales of the Northern Appalachian Basin, AAPG, Eastern Section Meeting Abstracts, Pittsburgh PA.

Ettensohn, F. R. and Barron, L. S. 1981. Depositional Model for the Devonian-Mississippian Black-Shale Sequence of North America: A tectono-climatic approach: U. S. Department of Energy Open-File Report 12040-2, 85 p

Ettensohn, F. R., and Barron, L. S. 1981. Tectono-climatic Model for Origin of Devonian- Mississippian Black Gas Shales of East-Central United States: AAPG Bulletin, v. 65, p. 1- 83.

Everhart, M. 2007. Oceans of Kansas Paleontology. Retrieved 2007-02-06.

Ewing, T. E. 2001. Review of Late Jurassic Depositional Systems and Potential Hydrocarbon Plays, Northern Gulf of Mexico Basin. Gulf Coast Association of Geological Societies Transactions. v. 51, pp. 85-96.

Ewing, T. E. 2003. Review of the Tectonic History of the Lower Rio Grande Border Region, South Texas and Mexico, and Implications for Hydrocarbon Exploration: SIPES Newsletter, v. 40, p. 16-21.

Faill, R. T. 1997. A Geologic History of the North-Central Appalachians; Part 1, Orogenesis from the Mesoproterozoic through the Taconic Orogeny: American Journal of Science, v. 297, p. 551-619.

Fairbanks, M. D., Ruppel, S. C., and Rowe, H. 2016. High-resolution Stratigraphy and Facies Architecture of the Upper Cretaceous (Cenomanian–Turonian) Eagle Ford Group, Central Texas. AAPG Bulletin (2016) 100 (3): 379–403.

Fanchi, R. J. 2002. Chapter 4 - Well Logging, Shared Earth Modeling, Butterworth-Heinemann, Pages 52-68, ISBN 9780750675222.

Faraj, B. 2012. Shale Gas Advancement Its Significance and Global Implications. Shale Gas World Europe 2012.

Faust, M. J. 1990. Seismic Stratigraphy of the Mid-Cretaceous Unconformity (MCU) in the Central Gulf of Mexico Basin, Geophysics, 55(7), 868-884

Ferrer, I., and Thurman, E. M. 2015. Chemical Constituents and Analytical Approaches for Hydraulic Fracturing Waters. Trends in Environmental Analytical Chemistry, 5, 18-25.

Forsman, J. P., and Hunt, J. M. 1958. Insoluble Organic Matter (Kerogen) in Sedimentary Rocks. Geochimica et Cosmochimica Acta 15, 170-182.

Gallegos, T. J., Varela, B. A., Haines, S. S., and Engle, M. A. 2015. Hydraulic Fracturing Water Use Variability in The United States and Potential Environmental Implications, Water Resour. Res., 51, 5839– 5845, doi:10.1002/2015WR017278.

Gandossi, L., and Von Estorff, U. 2015. An Overview of Hydraulic Fracturing and Other Formation Stimulation Technologies for Shale Gas Production – Update 2015 (PDF). Scientific and Technical Research Reports (Report). Joint Research Centre of the European Commission; Publications Office of the European Union.

Gardner, R., Pope M. C., Wehner M., and Donovan, A. D. 2013. Comparative Stratigraphy of the Eagle Ford Group Strata in Lozier Canyon and Antonio Creek, Terrell County, Texas.

Gibson, R. E. 1938. On the Effect of Pressure on the Solubility of Solids in Liquids. Am. Jour. Sci. Vol. 235-A, pp, 49-69.

Gillespie, L. J. 1920. Reduction Potential of Bacterial Cultures and of Waterlogged Soils, Soil Sci. 9:199-216

Gizjel, V. P. 1980. Characterization and Identification of Kerogen and Bitumen and Determination of Thermal Maturation by Means of Qualitative and Quantitative Microscopical Techniques, in How to Assess Maturation and Paleotemperatures: SEPM Short Course Notes, p. 1–56.

Glass Geltman, E. A., and LeClair N. 2018. Variance in State Protection from Exposure to NORM and TENORM Wastes Generated during Unconventional Oil and Gas Operations: Where We Are and Where We Need to Go. Solut J Environ Occup Health Policy 0:240–261; doi:10.1177/1048291118755387.

Gogoi, K., Dutta, M. N., Das, P. K.,and Curr, J. 2008. Source Rock Potential for Hydrocarbon Generation of Makum Coals, Upper Assam, India pp. 233-239

Goldich, S. S. 1938. A Study in Rock-weathering: Journal of Geology 46: 17-58.

Goodwin, A. R. H., Pirolli, L., May, E. F., and Marsh, K. N. 2014. Conventional Oil and Gas, Editor(s): Trevor M. Letcher, Future Energy (Second Edition), Elsevier, Pages 19-52, ISBN 9780080994246

Gordon, D. 2012. Understanding Unconventional Oil (PDF), Washington, DC: Carnegie Endowment for International Peace, retrieved 28 December 2013

Gouy, G. 1910. Sur la constitution de la charge electrique a la surface d'un electrolyte. Journal de Physique Theorique et Appliquee, Ser. 4, 9, 457-468 (in French).

Gräfe, M., Klauber, C., McFarlane, A., and Robinson, D. (Eds.). (2017). Clays in the Minerals Processing Value Chain. Cambridge: Cambridge University Press. doi:10.1017/9781316661888.

Graham, S., Joan, E., Dean, C. A., Yoshida, T. M., and Laur, P. M. 2017. Oil and Gas Produced Water as a Growth Medium for Microalgae Cultivation: A Review and Feasibility Analysis. LA-UR-16-22515

Graham, T. 1861. Graham Coined the Term "Colloid" in 1861.

Grahame, D. C. 1947. The Electrical Double Layer and the Theory of Electrocapillarity. Chemical Reviews. 41 (3): 441–501.

Greenwood, R., and Kendall, K. 1999. Electroacoustic Studies of Moderately Concentrated Colloidal Suspensions. Journal of the European Ceramic Society. 19 (4): 479–488. doi:10.1016/S0955-2219(98)00208-8.

Gregory, K. B., Vidic, R. D., and Dzombak, D. A. 2011. Water Management Challenges Associated with the Production of Shale Gas by Hydraulic Fracturing, Elements, 7(3), 181–186

Gretarsson. 2019. Marcellus Shale Revised Map 2019. https://commons.wikimedia.org/wiki/File:Marcellus_shale_revised_map_2019.png

Grim, R. 1968. Clay Mineralogy, 2nd Ed. McGraw-Hill Book Co.:New York

Groom, N. 2013. Fracking Water's Dirty Secret—Recycling. Sustainability. https://www.scientificamerican.com/article/analysis-fracking-waters-dirty-secret/

Ground Water Protection Council. 2009. Modern Shale Gas Development in the United States: A Primer (Report). DOE Office of Fossil Energy and National Energy Technology Laboratory. DE-FG26-04NT15455, pp. 56–66.

Guerra, K., and Drewes, J. E. 2008. Produced Water in the Western United States: Geographical Distribution, Occurrence, and Composition. Environ Eng Sci 25(2):239–246

Guiltinan, T. 2015. Assessing the Eagle Ford: Geology. DrillingInfo Energy. https://www.forbes.com/sites/drillinginfo/2015/08/31/assessing-the-eagle-ford-geology/#bde8e2a590c3

Gundersen, L. C. S., and Szabo, Z. 1995. Natural Radionuclides in Earth, Air, and Water, and The Effect on Human Health; in, Energy and The Environment—Application of Geosciences to Decision-making, L. M. H. Carter, ed.: U.S. Geological Survey, Circular 1108, p. 22-24.

GWPC & IOGCC. 2015. What Chemicals are Used in A Hydraulic Fracturing Job. Chemical Disclosure Registry. FracFocus. Retrieved 11 November 2015

Hagemeier, P., and Hutt, J. 2009. Hydraulic Fracturing, Water Use Issues Under Congressional, Public Scrutiny. Oil & Gas Journal, pp. 18–25

Haluszczak, L. O., Rose, A. W, and Kump, L. R. 2013. Geochemical Evaluation of Flowback Brine from Marcellus Gas Wells in Pennsylvania, USA. Applied Geochemistry 28: 55-61.

Hammer, R., Jeanne, V., and Larry. L. 2012. In Fracking's Wake: New Rules are needed to Protect Our Health and Environment from Contaminated Wastewater. Natural Resources Defense Council: D:12-05-A.

Hanaor, D. A. H., Michelazzi, M., Leonelli, C., and Sorrell, C. C. 2012. The Effects of Carboxylic Acids on the Aqueous Dispersion and Electrophoretic Deposition of ZrO_2. Journal of the European Ceramic Society. 32 (1): 235–244.

Hancock, N. 2013. High Salinity Produced Water Treatment Made Economically Viable, in Water Recycling and Desalination for the Oil and Gas Industry, Proceedings of International Desalination Association

Harbor, R. 2011. Facies Characterization and Stratigraphic Architecture of Organic-Rich Mudrocks, Upper Cretaceous Eagle Ford Formation, South Texas. Master's Thesis, University of Texas at Austin, Austin, TX. 195 pp.

Harper, J. A. 1999. Devonian, in Shultz, C.H., ed. The Geology of Pennsylvania: Pennsylvania Bureau of Topographic & Geologic Survey and Pittsburgh Geological Society, p. 108-127

Hart Energy. 2020. Drilling Permits Issued in Texas Fall by 50% for April. https://www.hartenergy.com/news/drilling-permits-issued-texas-fall-50-april-187575

Hayes, T. D. 2009. Sampling and Analysis of Water Streams Associated with the Development of Marcellus Shale Gas; Gas Technology Institute: December 2009.

Helms, L. 2008. Horizontal Drilling: North Dakota DMR Newsletter, v. 35, no. 1. https://www.dmr.nd.gov/ndgs/Newsletter/NL0308/pdfs/Horizontal.pdf

Henry, W. 1803. Experiments on the Quantity of Gases Absorbed by Water, at Different Temperatures, and under Different Pressures, Phil. Trans. R. Soc. Lond., 93, 29–274.

Hentz, T. F., Ambrose, W. A., and Smith, D. C. 2014. Eaglebine Play of the Southwestern East Texas Basin: Stratigraphic and Depositional Framework of the Upper Cretaceous (Cenomanian-Turonian) Woodbine and Eagle Ford Groups, (in press; preliminary version published online Ahead of Print 08 August 2014): AAPG Bulletin, doi: 10.1306/07071413232

Hentz, T. F., and Ruppel, S. C. 2010. Regional Lithostratigraphy of the Eagle Ford Shale: Maverick Basin to East Texas Basin. Gulf Coast Association of Geological Societies Transactions, v. 60, p. 325-337.

Hildebrand, J. H. 1924. Solubility. New York: Chemical Catalog Co.

Hill, R. T. 1887a. The Topography and Geology of the Cross Timbers and Surrounding Regions in Northern Texas: American Journal of Science, 3rd series, v. 33, p. 291-303.

Hiller, J. 2018. Bigger Wells, But More Water. https://www.expressnews.com/business/eagle-ford-energy/article/Bigger-wells-but-more-water-12512262.php

Hodgman, D. C., and Holmes, N. H. 1942. Handbook of Chemistry and Physics (26th edition). Chemical Rubber Publishing Co.

Holden, E. 2019. US States Face Water Crisis as Global Heating Increases Strain on Supplies. https://www.theguardian.com/global-development/2019/aug/06/us-states-water-stress-new-mexico-california-arizona-colorado

Horsfield, B., and Rullkötter, J. 1994. Diagenesis, Catagenesis, and Metagenesis of Organic Matter, In: Magoon, L.B., Dow, W.G. (Eds.), The petroleum system – from source to trap. AAPG Memoir, 60, pp. 189-189.

Hosterman, J. W., and Whitlow, S. I. 1983. Clay Mineralogy of Devonian Shales in the Appalachian Basin, USGS professional paper 1298

Huang, C. P., O'Melia, C. R., and Morgan, J. J. 1995. Aquatic Chemistry: Interfacial and Interspecies Processes. Washington, DC: American Chemical Society, Advances in Chemistry Series No. 244.

Hughes, D. 2013. Drill, Baby, Drill: Can Unconventional Fuels Usher in a New Era of Energy Abundance? Post Carbon Institute. Santa Rosa, California, USA.

Hunt, J. M. 1991. Generation of Gas and Oil from Coal and Other Terrestrial Organic Matter. Org. Geochem. 17, 673–680.

Hunt, J. M. 1996. Petroleum Geochemistry and Geology. 2nd Edition

Hurdle, J. 2018. Fracking Industry Water Use Rises as Drills Extend, Study Says.

Huxley, T. H. 1868. On a Piece of Chalk. Macmillan's Magazine "Archived copy". Archived from the original on 2011-07-18. Retrieved 2015-06-11

Hyne, N. J. 2011. Nontechnical Guide to Petroleum Geology, Exploration, Drilling, and Production, 2nd Ed.

Ibrahim, Y., Abdulkarem, E., Naddeo, V., Banat, F., and Hasan, S. W. 2019. Synthesis of Super Hydrophilic Cellulose-Alpha Zirconium Phosphate Ion Exchange Membrane via Surface Coating for the Removal of Heavy Metals from Wastewater. Science of the Total Environ. 690: 167-180.

Israelachvili, J. 1992. Intermolecular and Surface Forces. Academic Press: London.

IUPAC. 1997. Compendium of Chemical Terminology, 2nd ed. (the "Gold Book")

Jackson, R. B., Vengosh, A., Carey, J. W., Davies, R. J., Darrah, T. H., O'Sullivan, F., and Pétron, G. 2014. The Environmental Costs and Benefits of Fracking. Annu. Rev. Environ. Resour. 39, 327–362 (2014)

Jarvie, D. M. 2012. Shale Resource Systems for Oil and Gas: Part 1 – Shale-Gas Resource Systems, in Breyer J. A., ed., Shale reservoirs–Giant resources for the 21st century: AAPG Memoir, 97: 69–87.

Jarvie, D. M., R. J. Hill, T. R. Ruble, and R. M. Pollastro. 2007. Unconventional Shale-Gas Systems: The Mississippian Barnett Shale of North-Central Texas as One Model for Thermogenic Shale-Gas Assessment: AAPG Bulletin, v. 91, no. 4, p. 475–499, doi:10.1306

Jiang, J., Oberdörster, G., and Biswas, P. 2008. Characterization of Size, Surface Charge, and Agglomeration State of Nanoparticle Dispersions for Toxicological Studies. Journal of Nanoparticle Research. 11 (1): 77–89. Bibcode:2009JNR....11...77J. doi:10.1007/s11051-008-9446-4.

Jiang, Z., Zhang, W., Liang, C., Liang, W., Liu, Y., and Chen, X. 2016. Basic Characteristics and Evaluation of Shale Oil Reservoirs. Petroleum Research (2016) 2,149-163

Jüntgen, H., and Klein, J. 1975. Entstehung von Erdgas aus kohligen Sedimenten Erdöl Kohle, Erdgas, Petrochem. 28 (1975), pp. 65-73

Karathanasis, A. D., and Hajek, B. F. 1983. Transformation of Smectite to Kaolinite in Naturally Acid Soil Systems: Structural and Thermodynamic Considerations. Soil Science Society of America Journal.

Kasper, D. 1992. Stratigraphy and Sedimentology of the Bakken Formation of West-central Saskatchewan: A Preliminary Report. Energy and Resources.

Kearey, P. 2001. Dictionary of Geology, 2nd ed., Penguin Reference, London, New York, etc., p. 41. ISBN 978-0-14-051494-0.

Keelan, D. K. 1982. Core Analysis for Aid in Reservoir Description: Journal of Petroleum Technology, v. 34, p. 2483–2491, DOI: 10.2118/10011-PA

Kelso, M. 2019. Getting Rid of All of that Waste –Increasing Use of Oil and Gas Injection Wells in Pennsylvania. https://www.fractracker.org/2019/01/injection-wells-in-pennsylvania/

Kerr, P. F. 1952. Formation and Occurrence of Clay Minerals. Clays and Clay Minerals. 1 (1): 19–32. doi:10.1346/CCMN.1952.0010104

Kirkwood, J. G., Baldwin, R. L., Dunlop, P. J., Dunlop, L. J., and Kegeles, G. 1960. Flow Equations and Frames of Reference for Isothermal Diffusion in Liquids. The Journal of Chemical Physics 33(5):1505–13.

Kondash, A. J., Albright, E., and Vengosh, A. 2016. Quantity of Flowback and Produced Waters from Unconventional Oil and Gas Exploration, Science of The Total Environment

Kondash, A. J., Lauer, N. E., and Vengosh, A. 2018. The Intensification of the Water Footprint of Hydraulic Fracturing. Science Advances 15 Aug 2018:Vol. 4, no. 8, eaar5982 DOI: 10.1126/sciadv.aar5982

Kondash, A., and Vengosh A. 2015. Water Footprint of Hydraulic Fracturing. Environmental Science & Technology Letters Article. ASAP DOI: 10.1021/acs.estlett.5b00211.

Kumar, A., and Dixit, C. K. 2017. Advances in Nanomedicine for the Delivery of Therapeutic Nucleic Acids. pp. 43–58. doi:10.1016/B978-0-08-100557-6.00003-1. ISBN 9780081005576.

La Iglesia, Ángel, Martin-Vivaldi Jr, Juan Luis, and López Aguayo, Francisco. 1976. Kaolinite Crystallization at Room Temperature by Homogeneous Precipitation. III. Hydrolysis of Feldspars. Clays and Clay Minerals. 24 (6287): 36–42. Bibcode: 1990Natur.346.839J. doi:10.1038/346839a0.

Lancon, O., and Hascakir, B. 2018. Contribution of Oil and Gas Production in the US to the Climate Change, SPE Annual Technical Conference and Exhibition (ATCE 2018), 24-26 September 2018, Dallas, Texas, USA, SPE-191482-MS.

Larryisgood. 2011. Zeta Potential for A Particle in Dispersion Medium. https://en.wikipedia.org/wiki/File:Zeta_Potential_for_a_particle_in_dispersion_medium.png

Larson, T. E., and Buswell, A. M. 1942. Calcium Carbonate Saturation Index and Alkalinity Interpretations. Journal of the American Water Works Association 34: 1667–1684.

Lash, G. G., and Engelder, T. 2011. Thickness Trends and Sequence Stratigraphy of the Middle Devonian Marcellus Formation, Appalachian Basin: Implications for Acadian foreland basin evolution. AAPG Bulletin, v. 95, no. 1 (January 2011), pp. 61–103

Law, B. E., and Curtis, J. B. 2002. Introduction to Unconventional Petroleum Systems: AAPG Bulletin, v. 86, no. 11, p. 1851-1852

Le Chatelier, H, and Boudouard, O. 1898. Limits of Flammability of Gaseous Mixtures Bulletin de la Société Chimique de France (Paris), v. 19, pp. 483–488.

Lee, D. S., Hermann, J. D., Elsworth, D., Kim, H. T., and Lee, H. S. 2011. A Critical Evaluation of Unconventional Gas Recovery from the Marcellus Shale, Northeastern United States: Journal of Civil Engineering, Korean Society of Civil Engineers, 15(4): 697-687.

Leimkuhler, J., and Leveille, G. 2012. Unconventional Resources, 11 January Tech Leaders

Lester, Y., Ferrer, I., Thurman, E. M., Sitterley, K. A., Korak, J. A., Aiken, G., and Linden, K. G. 2015. Characterization of Hydraulic Fracturing Flowback Water in Colorado: Implications for Water Treatment. Science of the Total Environment 512: 637-44.

Leythaeuser, D., Radke, M., and Schaefer, R. 1984. Efficiency of Petroleum Expulsion from Shale Source Rocks. Nature 311, 745-748.

Li, Y., Huang, T., and Pang, Z. 2017. Geochemical Processes during Hydraulic Fracturing: A Water-Rock Interaction Experiment and Field Test Study Geosci J 21:753.

Libes, S. 2009. Introduction to Marine Biochemistry. 2C 2nd edition. United States: Elsevier Science Publishing Co Inc.-2

Lippes, J. R. 2015. Environmental Concerns Resulting from Horizontal Drilling. https://flimarcellusconference.files.wordpress.com/2011/07/environmental-concerns-resulting-from-horizontal-drilling1.pdf

Lock, B. E., Peschier, L., and Whitcomb, N. 2010. The Eagle Ford (Boquillas Formation) of Val Verde County, Texas—A window on the South Texas play: Gulf Coast Association of Geological Societies Transactions, v. 60 Stanley, Steven M. Earth System History. New York: W.H. Freeman and Company. pp. 487–489. ISBN 0-7167-2882-6.

Losev, E. S., Netrebko, N. V., and Orlova, I. V. 1989. Gravitational Sedimentation of Aggregating Particles in A Shear Flow. Fluid Dyn 24, 242–245 (1989). https://doi.org/10.1007/BF01075154

Lu, Y., Wang, H., Guan, B., Liu, P., Guo, L., Wu, J., and Yi, X. 2017. Reasons for the Low Fowback Rates of Fracturing Fluids in Marine Shale, Natural Gas Industry B, Volume 5, Issue 1,

Lucia, F. J. 1995. Rock-Fabric/Petrophysical Classification of Carbonate Pore Space for Reservoir Characterization. AAPG Bull. 79 (9): 1275-1300.

Luneau, B., Longman. M., Kaufman, P., and Landon, S. 2011. Stratigraphy and Petrophysical Characteristics of the Niobrara Formation in the Denver Basin, Colorado and Wyoming. Adapted from oral presentation at AAPG Rocky Mountain Section meeting.

Lustgarten, A. 2012. Injection Wells: The Poison beneath Us. ProPublica, www.propublica.org/article/injection-wells-the-poison-beneath-us.

Ma, G., Geza, M., and Xu, P. 2014. Review of Flowback and Produced Water Management, Treatment, and Beneficial Use for Major Shale Gas Development Basins. Shale Energy Engineering Conference

Magoon, L. B., and Dow, W. G. 1994. The Petroleum System, in L.B. Magoon and W.G. Dow, eds., The Petroleum System--From Source to Trap: AAPG Memoir 60, p. 3-24.

Mantell, E. M. 2011. Produced Water Reuse and Recycling Challenges and Opportunities across Major Shale Plays. EPA Hydraulic Fracturing Study Technical Workshop #4 Water Resources Management.

ManuRoquette. 2019. Stratigraphic Trap. Structural Traps. https://commons.wikimedia.org/wiki/File:StratigraphicTrap2.png. Accessed 20 August 2020

Marathon Oil. 2019. Water Management. https://www.marathonoil.com/lov2017/Environment/Water-Management/

Marcellus Drilling News. 2020. Marcellus/Utica Companies Switch to "Work from Home" Model. https://marcellusdrilling.com/2020/03/marcellus-utica-companies-switch-to-work-from-home-model/

Marcon, V., Joseph, C., Carter, K. E., Hedges, S. W., Lopano, C. L., Guthrie, G. D., and Hakala, J. A. 2017. Experimental Insights into Geochemical Changes in Hydraulically Fractured Marcellus Shale. Applied Geochemistry 2017 76, 36-50.

Martin, J. P. 2008. The Middle Devonian Hamilton Group Shales in the Northern Appalachian Basin: Production and Potential. New York State Energy Research and Development Authority. Archived from the original on 2008-08-08. Retrieved 2008-04-02.

McCarthy, K., Rojas, K., Niemann, M., Palmowski, D., Peters, K., and Stankiewicz, A. 2011. Basic Petroleum Geochemistry for Source Rock Evaluation. Oilfield Review 23, 32-43.

McFeely, M. 2012. State Hydraulic Fracturing Disclosure Rules and Enforcement: A Comparison. National Resource Defense Counsel.

McKee, C. R., Bumb, A. C., and Koenig, R. A. 1988. Stress-Dependent Permeability and Porosity of Coal and Other Geologic Formations. Society of Petroleum Engineers. doi:10.2118/12858-PA

McLaughlin J. B. 2013. Key Considerations for Frac Flowback/Produced Water Reuse and Treatment. Presented at NYWEA Spring Technical Conference, Syracuse, NY.

Melvin, J. L. 1991. Evaporites, Petroleum and Mineral Resources. Elsevier, Amsterdam

Metcalf, and Eddy. 1991. Wastewater Engineering: Treatment, Disposal, and Reuse, McGraw-Hill, New York, pp. 302-314; 470-472.

Meyers, P. A. 1997. Organic Geochemical Proxies of Paleoceanographic, Paleolimnologic, and Paleoclimatic Processes. Org. Geochem., 27:213-250.

Mitchell, B. 1995. Advanced Oil Well Drilling Engineering, 10th edn. Mitchell Engineering, San Francisco

Mohtar, R. H., Shafiezadeh, H., Blake, J., and Daher, B. 2018. Economic, Social, and Environmental Evaluation of Energy Development in the Eagle Ford Shale Play, Science of The Total Environment, Volume 646, 2019, Pages 1601-1614, ISSN 0048-9697

MoJo, K. and Zamanian, K. 2017. CEC pH. https://commons.wikimedia.org/wiki /File:CEC_pH.svg. Accessed 20 May 2018.

Moore, C. W., Zielinska, B., Pétron, G., and Jackson, R. B. 2014. Air Impacts of Increased Natural Gas Acquisition, Processing, and Use: A Critical Review. Env Sci Technol 48:8349–8359; doi:10.1021/es4053472

Morrison, I. D., and Ross, S. 2002. Colloidal Dispersions: Suspensions, Emulsions, and Foams (2nd ed.). New York, NY: Wiley. ISBN 978-0-471-17625-1.

National Law Review. 2015. New York State Formally Adopts Ban on Fracking: An Analysis of the New York State DEC's SEQRA Findings Supporting Its HVHF Ban.

Neal, D. W. 1979. Subsurface Stratigraphy of the Middle and Upper Devonian Clastic Sequence in Southern West Virginia and its Relation to Gas Production: West Virginia Geological and Economic Survey, United States Department of Energy Contract no. EY-76-C-05-5199, 152 p.

Nesbitt, B. 2007. Handbook of Valves and Actuators 1st Edition. ISBN: 9781856174947

Nicot, J. P., Reedy, R. C., Costley. R. A. and Huang, Y. 2012. Oil & Gas Water Use in Texas: Update to the 2011 Mining Water Use Report. Bureau of Economic Geology.

North, F. K. 1985. Petroleum Geology: Allen & Unwin, Inc., Winchester, MA

Nyahay, R., Leone, J., Smith, L. B., Martin, J. P., and Jarvie, D. J. 2007. Update on Regional Assessment of Gas Potential in the Devonian Marcellus and Ordovician Utica shales of New York: Search and Discovery Article 10136

O'Brien, N. R., and Slatt, R. M. 1990. Argillaceous Rock Atlas. Springer-Verlag, New York

Okullo, P. 2017. Frac Water: Recycling Objectives. https://www.nap.edu/read/24620/chapter/5#32

Oyakawa, J., Tunstall, T., Greszler, S., Stutts, K., Conti, G., Brennan, M., Juarez, K., Ramirez, J., Xie, Z., Long, M., Stone, E., and Martinez, A. 2017. Economic Impact of the Eagle Ford Shale. Business Opportunities and the New Normal.

Padep. 2015. DEP Office of Oil and Gas Management Compliance Report. http://www.depreportingservices.state.pa.us/ReportServer/Pages/ReportViewer.aspx?/Oil_Gas/OG_Compliance2005-2015. Accessed 15 Aug 2015

Paktinat, J., O'Neil, B. J., and Tulissi, M. G. 2011. Case Studies: Impact of High Salt Tolerant Friction Reducers on Freshwater Conversation in Canadian Shale Fracturing Treatments. Society of Petroleum Engineers. doi:10.2118/149272-MS

Pápay, J. 2013. Exploitation of Unconventional Petroleum Accumulations Theory and Practice. English edition 11-150.

Paronish, T. J., Shuvajit, B., and Timothy, C. 2016. Integrated Geologic Analysis from Two Marcellus Shale Science Wells in Northeastern West Virginia. Poster presentation given at AAPG 2016 Annual Convention and Exhibition, Calgary, Alberta, Canada, June 19-22, 2016.

Parra, P. A., Rubio, N., Ramirez, C., Guerra, V. A., Campos, I. R., Trejo, M. D., Olguin, J. Vargas, C. H., Valbuena, R., Soler, D. F., Weimann, M. I., Lujan, V., Bonningue, P., Reyes, P. G., Martinez, R., Munoz, R., Rodriquez, E., and Garcia, M. 2013. Unconventional Reservoir Development in Mexico: Lessons Learned from the Frist Exploratory Wells, Society of Petroleum Engineers, Unconventional Resources Conference- USA held in The Woodlands, Texas, USA, 10-12 April 2013, SPE 164545

Peavy, H. S., Rowe, D. R., and Tchobanoglous, G. 1985. Environmental Engineering McGraw Hill Publishing Company Ltd, pp11-46

Pennsylvania Department of Environmental Protection (PA DEP). 2018. Office of Oil and Gas. Retrieved from: on March 9, 2018.

Perry, C., and Wickstrom, L. 2010. The Marcellus Shale Play: Geology, History, and Oil and Gas Potential in Ohio [Presentation]: Ohio Division of Natural Resources and Ohio Geological Survey.

Peters, K. E. 1986. Guidelines for Evaluating Petroleum Source Rock Using Programmed Pyrolysis. AAPG Bulletin 70, 318-329.

Peters, K. E., and Cassa, M. R. 1994. Applied Source Rock Geochemistry, in: Magoon, The Petroleum System – From Source to Trap. American Association of Petroleum Geologists Memoir, 60, Tulsa, OK, pp. 93-117

Popova, O., Frye, E., and Panarelli, E. 2015. Updated Geologic Maps Provide Greater Detail for Marcellus Formation: U.S. Energy Information Administration, Today in Energy: http://www.eia.gov/todayinenergy/detail.cfm?id=20612.

Popular Horizontal. 1991. News Horizons. January/March

Potter, P. E., Maynard, J. B., and Pryor, W. A. 1980. Sedimentology of Shale: New York, Springer-Verlag, 303 p.

Rayment, G. E., and Higginson, F. R. 1992. Electrical Conductivity in 'Australian Laboratory Handbook of Soil and Water Chemical Methods' Inkata Press: Melbourne

Reed, J. R., and Dunbar, D. 2008. Using Arcgis to Estimate Thermogenic Gas Generation Volumes by Upper and Middle Devonian shales in the Appalachian Basin (abs.): AAPG Eastern Section meeting:

Reesman, A. L. 1973. Icicles: A Guide to the Quality and Movement of Groundwater. American Geological Society. Abstracts, 5(7), 777.

Reesman, A. L., and Keller, W. D. 1968. Aqueous Solubility Studies of High-Alumina and Clay Mineral Am. Mineral. 35, 929-941.

Repetski, J. E., Over, D. J., and Enomoto, C. B. 2013. Conodont-Based Correlation of the Marcellus/Millboro Formations in the Central Appalachian Basin: Geological Society of America Abstracts with Programs, v. 45, no. 7, p. 529.

Repetski, J. E., Over, D. J., and Rotter, D. L. 2012, Conodonts from the Marcellus Shale Interval in the Central Appalachians: Geological Society of America Abstracts with Programs, v. 44, no. 5, p. 2.

Rhee, C. E., Martyn, P. C., and Kremer, J. G. 1989. Sanitation District of Los Angeles County. Removal of Oil and Grease in Oil Processing Wastewaters.

Robinson, C. R. 1997. Hydrocarbon Source Rock Variability within the Austin Chalk and Eagle Ford Shale (Upper Cretaceous), East Texas, USA: International Journal of Coal Geology, v. 34, p. 287-305.

Roen, J. B. 1983. Geology of the Devonian Black Shales of the Appalachian Basin: Organic Geochemistry, 5(4): 241-254.

Rosenberg, E. 2019. Can Fracking Survive at $50 a Barrel? https://www.investopedia.com /articles/investing/072215/can-fracking-survive-60-barrel

Rossotti, J. C. F., and Rossotti, H. 1961. The Determination of Stability Constants and Other Equilibrium Constants in Solution. McGraw-Hill, New York.

Roy, S. B., Chen, L. Girvetz, E., Edwin, P., William, B. Mills, and Thomas, M. G. 2010. Evaluating Sustainability of Projected Water Demands Under Future Climate Change Scenarios.

Saltworks. 2018. Frac & Shale Produced Water Management, Treatment Costs & Options. https://www.saltworkstech.com/articles/frac-shale-produced-water-management-treatment-costs-and-options/

Sato, M. 1990. Thermochemistry of The Formation of Fossil Fuels. U.S. Geological Survey, MS 959, Reston, Virginia 22092, U.S.A.

Scott, R. W. 2004. The Maverick Basin: New technology—New Success, Gulf Coast Association of Geological Societies Transactions, v. 54, p. 603-620.

Selmi F. 1845. Studi sulla dimulsione di cloruro d'argento, Nuovi Annali delle Scienze Naturali di Bologna, fasc. di Agosto

ShaleProfile. 2019. Marcellus (PA) – Update through March 2019. https://shaleprofile.com/blog/appalachia/marcellus-pa-update-through-march-2019/. Accessed on 28 October 2020.

ShaleProfile. 2020. Eagle Ford – Update through July 2020. https://shaleprofile.com/blog/eagle-ford-monthly-update/eagle-ford-update-through-july-2020/. Accessed on 28 October 2020.

Shao, H. B., Ray, J. R., and Jun, Y. 2010. Dissolution and Precipitation of Clay Minerals under Geologic CO_2 Sequestration Conditions: CO_2-Brine-Phlogopite Interactions. Environmental Science and Technology 44(15): 5999–6005.

Silva, J. M., Matis, H., Kostedt, W. L., and Watkins, V. 2012. Produced Water Pretreatment for Water Recovery and Salt Production, Technical Report for RPSEA Contract 08122–36; Research partnership to secure energy for America: Niskayuna, NY

Slatt, R. M., and Rodriguez, N. D. 2012. Comparative Sequence Stratigraphy and Organic Geochemistry of Gas Shales: Commonality or Coincidence? J. Nat. Gas Sci. Eng. 8, 68–84

Slutz, J., Anderson, J., Broderick, R., and Horner, P. 2012. Key Shale Gas Water Management Strategies: An Economic Assessment Tool, Proceedings of the SPE/APPEA International Conference on Health, Safety, and Environment in Oil and Gas Exploration and Production, Perth, Australia

Soeder, D., Enomoto, C., and Chermak, J. 2014. The Devonian Marcellus Shale and Millboro Shale. 10.1130/2014.0035(05).

Sorensen, J. A., Schmidt, D. D., Smith, S. A., Bailey, T. P., Mibeck, B. A. F., and Harju, J. A. 2010. SUBTASK 1.2 – Evaluation of Key Factors Affecting Successful Oil Production in The Bakken Formation, North Dakota. Oil & Natural Gas Technology

Spang, E. S., Moomaw, W. R., Gallagher, K. S., Kirshen, P. H., and Marks, D. H. 2011. The Water Consumption of Energy Production: An International Comparison. Environ. Res. Lett. 9, 105002.

Stanley, S. M. 1999. Earth System History. New York: W.H. Freeman and Company. pp. 487–489. ISBN 0-7167-2882-6.

Stephenson, L. W. 1929. Unconformities in Upper Cretaceous Series of Texas: American Association of Petroleum Geologists Bulletin, v. 13, p. 1323-1334.

Stephenson, L. W., and Reeside, J. B. 1938. Comparison of Upper Cretaceous Deposits of Gulf Region and Western Interior Region: American Association of Petroleum Geologists Bulletin, v. 22, p. 1629-1638.

Stern, O. 1924. Zur Theorie der Elektrolytischen Doppelschicht. Zeitschrift für Elektrochemie. 30: 508. doi:10.1002/bbpc.192400182

Stewart, M., and Arnold, K. 2011. Produced Water Treatment Field Manual. 1st Edition. eBook ISBN: 9781856179850

Stringfellow, T. W, Domen, K. J., Camarillo. K. M., Sandelin, L.W., and Borglin, S. 2014. Physical, Chemical, and Biological Characteristics of Compounds Used in Hydraulic Fracturing, Journal of Hazardous Materials, Volume 275, Pages 37-54, ISSN 0304-3894,

Suárez, A. A. 2012. The Expansion of Unconventional Production of Natural Gas (Tight Gas, Gas Shale and Coal Bed Methane), Advances in Natural Gas Technology, Dr. Hamid Al-Megren (Ed.), ISBN: 978-953-51-0507-7

Sun, Y., Wang, D., Tsang, D. C. W., Wang, L., Ok, Y. S., and Feng, Y. 2019. A Critical Review of Risks, Characteristics, and Treatment Strategies for Potentially Toxic Elements in Wastewater from Shale Gas Extraction, Environment International, Volume 125, Pages 452-469, ISSN 0160-4120, https://doi.org/10.1016/j.envint.2019.02.019.

Surles, M. A. 1987. Stratigraphy of the Eagle Ford Group (Upper Cretaceous) and its Source-rock Potential in the East Texas Basin: Baylor Geological Studies Bulletin 45, Waco, Texas, 57 p.

Suttles, C. 2020. Oil, Gas and Plastics Hit by COVID-19; Producers Await Rebound. https://www.ellwoodcityledger.com/news/20200531/oil-gas-and-plastics-hit-by-covid-19-producers-await-rebound

Takahashi, P. 2020. U.S. Lost More Than 100,000 Oil and Gas Jobs in Coronavirus-Driven Bust. https://www.houstonchronicle.com/business/energy/article/U-S-lost-more-than-100-000-oil-and-gas-jobs-in-15336253.php

Technology Subgroup of the Operations & Environment Task Group. 2011. Man agement of Produced Water from Oil and Gas Wells. https://www.npc.org/Prudent_Deve lopment-Topic_Papers/2-17_Management_of_Produced_Water_Paper.pdf. Accessed on 17 August 2020.

Texas Railroad Commission (RRC). 2020. Drilling Permits Issued. Eagle Ford Sh ale Information. https://www.rrc.state.tx.us/oil-gas/major-oil-and-gas-formations/eagle-f ord-shale-information/

Texas Railroad Commission (RRC). 2020. Eagle Ford Shale Information. https:// www.rrc.state.tx.us/oil-gas/major-oil-and-gas-formations/eagle-ford-shale-information/

Tian, Y., Ayers, W. B., McCain, and W. D. 2012. Regional Analysis of Stratigraphy, Reservoir Characteristics, and Fluid Phases in the Eagle Ford Shale, South Texas: Gulf Coast Association of Geological Societies Transactions, v. 62, p. 471-483.

Tissot, B. P., and Welte, D. H. 1984. Petroleum Formation and Occurrence, 2nd edition. Springer-Verlag, Berlin, 699 p.

Tissot, B. P., Durand, B., Espitalie, J., and Combaz, A. 1974. Influence of Nature and Diagenesis of Organic Matter in Formation of Petroleum. AAPG Bulletin 58, 499-506.

Township, M. 2013. An Overview of Utica Shale Exploration and Associated Environmental Concerns. Geological and Environmental Sciences. Youngstown State University.

Treadgold, G. 2011. Sedimentology and diagenesis of the Upper Cretaceous Austin Chalk Formation, South Texas and northern Mexico: PhD Dissertation, Rice University, Houston, Texas, 532 p

Tribovillard, N., Thomas J. A., Timothy L., and Armelle R. 2006. Trace Metals as Paleoredox and Paleoproductivity Proxies: An Update. Chemical Geology 232 (1–2): 12–32. doi:10.1016/j.chemgeo.2006.02.012.

Tucker, M. E. 1988. Sedimentary Petrology, An Introduction, Blackwell, London. p197. ISBN 0-632-00074-0

U.S. Energy Information Administration (EIA). 2011. Trends in Eagle Ford Drilling Highlight the Search for Oil and Natural Gas Liquids. November 3. Available at: https://www.eia.gov/todayinenergy/detail.php?id=3770.

U.S. Energy Information Administration (EIA). 2013. About us. OECD, retrieved 28 December

U.S. Energy Information Administration (EIA). 2013. International Energy Outlook (IEO) https://www.eia.gov/outlooks/aeo/pdf/0383(2013).pdf

U.S. Energy Information Administration (EIA). 2013. Technically Recoverable Shale Oil and Shale Gas Resources: An Assessment of 137 Shale Formations in 41 Countries Outside the United States. https://www.eia.gov/analysis/studies/worldshalegas/

U.S. Energy Information Administration (EIA). 2014. Updates to the EIA Eagle Ford Play Maps. Washington, DC 20585

U.S. Energy Information Administration (EIA). 2016. Lower 48 States Shale Plays. https://www.eia.gov/maps/maps.htm

U.S. Energy Information Administration (EIA). 2016. U.S. Crude Oil and Natural Gas Proved Reserves 2016. https://www.eia.gov/naturalgas/crudeoilreserves/

U.S. Energy Information Administration (EIA). 2017. International Energy Outlook (IEO) https://www.eia.gov/outlooks/ieo/pdf/0484(2017).pdf

U.S. Energy Information Administration (EIA). 2017. Marcellus Shale Play Geology Review. https://www.eia.gov/maps/pdf/MarcellusPlayUpdate_Jan2017.pdf

U.S. Energy Information Administration (EIA). 2018. Annual Energy Outlook. https://www.eia.gov/outlooks/aeo/grt.php

U.S. Energy Information Administration (EIA). 2018. Form EIA-23L, Annual Report of Domestic Oil and Gas Reserves

U.S. Energy Information Administration (EIA). 2018. Hydraulically Fractured Horizontal Wells Account for Most New Oil and Natural Gas Wells. https://www.eia.gov/todayinenergy

U.S. Energy Information Administration (EIA). 2018. Monthly Energy Review, Table 1.3 and 10.1, April 2018, preliminary data.

U.S. Energy Information Administration (EIA). 2018. The United States Uses a Mix of Energy Sources. https://www.eia.gov/energyexplained/?page=us_energy_home

U.S. Energy Information Administration (EIA). 2019. EIA Adds New Play Production Data to Shale Gas and Tight Oil Reports. https://www.eia.gov/todayinenergy/detail.php?id=38372

U.S. Energy Information Administration (EIA). 2019. U.S. Crude Oil and Natural Gas Proved Reserves, Year-End 2018. U.S. Department of Energy. Washington, DC 20585

U.S. Energy Information Administration (EIA). 2020. Drilling Productivity Report. https://www.eia.gov/petroleum/drilling/

U.S. Energy Information Administration (EIA).2020. Monthly Energy Review-April Table 1.3 and 10.1. https://www.eia.gov/energyexplained/us-energy-facts/

U.S. Environmental Protection Agency (EPA). 1976. The Maximum Contaminant Level Established under the Safe Drinking Water Act, and Criteria.

U.S. Environmental Protection Agency (EPA). 2004. Evaluation of Impacts to Underground Sources of Drinking Water by Hydraulic Fracturing of Coalbed Methane Reservoirs.

U.S. Environmental Protection Agency (EPA). 2011. Proceedings of the Technic al Workshops for the Hydraulic Fracture Study: Chemical and Analytical Methods Wash ington DC. http://water.epa.gov/type/groundwater/uic/class2/hydraulicfracturing/hfwork shops.cfm

U.S. Environmental Protection Agency (EPA). 2012. Study of Potential Impacts of Hydraulic Fracturing on Drinking Water Resources: Progress Report

U.S. Environmental Protection Agency (EPA). 2016b. Integrated Science Assessment for Oxides of Nitrogen (Health Criteria). www.epa.gov/isa/integrated-science-assessment-isa-nitrogendioxide-health-criteria.

U.S. Geological Survey (USGS). 1999. Naturally Occurring Radioactive Minerals (NORM) in Produced Water and Oil-Field Equipment -- An Issue for the Energy Industry. https://pubs.usgs.gov/fs/fs-0142-99/fs-0142-99.pdf

U.S. Geological Survey (USGS). 2009. Gas Hydrate: What is it? Archived from the original on June 14, 2012, retrieved 28 December 2014

U.S. Geological Survey (USGS). 2012. Naturally Occurring Radionuclides in the Ground Water of Southeastern Pennsylvania

U.S. Geological Survey (USGS). 2018. Estimated Use of Water in the United States in 2015. ISBN 978-1-4113-4233-0

U.S. International Energy Agency (IEA). 2016. Annual Energy Outlook. https://www.eia.gov/outlooks/aeo/pdf/0383(2016).pdf

Van der Waals Johannes Diderik. 1873. Over de continuiteit van den gas- en vloeistoftoestand (On the Continuity of the Gaseous and Liquid States) (doctoral dissertation). Universiteit Leiden.

Van Dorp, Q. T., Slijkhuis, M., and Zitha, P. L. J. 2009. Salt Precipitation in Gas Reservoirs. Society of Petroleum Engineers. doi:10.2118/122140-MS

Van Krevelen, D. W. 1950. Graphical-Statistical Method for the Study of Structure and Reaction Processes of Coal, Fuel, 29, 269-84.

Van Tyne, A. M. 1993. Detailed Study of Devonian Black Shales Encountered in Nine Wells in Western New York State, in J. B. Roen and R. C. Kepferle, eds., 1993, Petroleum geology of the Devonian and Mississippian black shale of eastern North America: U.S. Geological Survey Bulletin, v. 1909, p. M1–M16.

Ver Straeten, C. 2007. Basinwide Stratigraphic Synthesis and Sequence Stratigraphy, Upper Pragian, Emsian and Eifelian Stages (Lower to Middle Devonian), Appalachian Basin, in Becker, R. T. and Kirchgasser, W. T., eds., Devonian Events and Correlations: Geological Society of London Special Publications, 278: 39-81.

Vidic R. D., Brantley S. L., Vandenbossche J. M., Yoxtheimer D., and Abad J. D. 2013. Impact of Shale Gas Development on Regional Water Quality, Science, 340(6134), 1235009.

Vine, J. D., and Tourtelot, E. B. 1970. Geochemistry of Black Shale Deposits – A Summary Report. Economic Geology. 65 (3): 253–273. doi:10.2113/gsecongeo.65.3.253.

Walters, C. C. 2006. The Origin of Petroleum. In: Hsu C.S., Robinson P.R. (eds) Practical Advances in Petroleum Processing. Springer, New York, NY. https://doi.org/10.1007/978-0-387-25789-1_2

Wang, L., Burns, S., Giammar, D. E., and Fortner, J. D. 2016. Element Mobilization from Bakken Shales as a Function of Water Chemistry. Chemosphere 149, 286-293.

Wang, L., Chin, Y. P., and Traina, S. J. 1997. Influence of Humic Substances on CO_2 Sorption by a Subsurface Mineral Separate and Its Mineralogical Components. Geochim. Cosmochim. Acta, 58, 553 – 566.

Wang, L., Fortner, J. D., and Giammar, D. E. 2015. Impact of Water Chemistry on Element Mobilization from Eagle Ford Shale. Environ. Eng. Sci. 32, 310-320

Warner, N. R., Christie C. A., Jackson, R. B., and Vengosh, A. 2013. Impacts of Shale Gas Wastewater Disposal on Water Quality in Western Pennsylvania. Environ Sci Technol 47(20):11849–11857. doi:10.1021/es402165b

Watts, W. 2020. Why Oil Prices Just Crashed into Negative Territory — 4 Things Investors Need to Know. https://www.marketwatch.com/story/why-the-oil-market-just-crashed-below-0-a-barrel-4-things-investors-need-to-know-2020-04-20

Waxman, H. A., Markey, E. J., and DeGette, D. 2011. Chemicals Used in Hydraulic Fracturing. United States House of Representatives, Committee on Energy and Commerce, Minority Staff

Weber G., and Green J. 1981. Guide to Oil Shale. National Conference of State Legislatures. Washington D.C. USA. p. 21

Weiss, P. 1962. Renewable Resources, a Report to the Committee on Natural Resources. National Academy of Science, National Research Council, Washington D.C., USA. Retrieved 2013-01-04

Werne, J. P., Sageman, B. B., Lyons, T. W., and Hollander, D. J. 2002. An Integrated Assessment of A “Type Euxinic” Deposit: Evidence for Multiple Controls on Black Shale Deposition in the Middle Devonian Oatka Creek Formation: American Journal of Science, 302(2): 110-145.

West Virginia Department of Environmental Protection (WV DEP). 2018. Office of Oil and Gas. Retreived from: on March 9, 2018. https://tagis.dep.wv.gov/oog/.

Wilkin, R., and Barnes, H. 1998. Solubility and Stability of Zeolites in Aqueous Solution: I. Analcime, Na-, and K-clinoptiloite. American Mineralogist 83(1): 746-761.

Winter, J. A. 1961. Stratigraphy of the Lower Cretaceous (Subsurface) of South Texas: Gulf Coast Association of Geological Societies Transactions, v. 11, p. 15-24.

Wiseman, H. 2012. Fracturing Regulation Applied, 22 Duke Envtl. L. & Pol'y F. 361, 367.

Wood, R., Gilbert, P., Sharmina, M., Anderson, K., Anthony Footitt, A., Steven Glynn, S., and Fiona, N. 2011. Shale Gas: A Provisional Assessment of Climate Change and Environmental Impacts. The Tyndall Centre, University of Manchester

Woodroof, N. 2020. Rystad Energy: US Fraccing Slowdown Creates DUC well Backlog https://www.oilfieldtechnology.com/special-reports/16062020/rystad-energy-us-fraccing-slowdown-creates-duc-well-backlog/

Workman, S. J. 2013. Integrating Depositional Facies and Sequence Stratigraphy in Characterizing Unconventional Reservoirs: Eagle Ford Shale, South Texas: Western Michigan University Master of Science Thesis defended in April 2013.

Xiong, B., Zydney, A. L., and Kumar, M. 2016. Fouling of Microfiltration Membranes by Flowback and Produced Waters from the Marcellus Shale Gas Play. Water research, 99, 162-170.

Yaalon, D. 1962. Mineral Composition of the Average Shale. Clay Miner. 5, 31–36

Young. R. O. 2016. Colloids and Colloidal Systems in Human Health and Nutrition. Int J Complement Alt Med 3(6): 00095. DOI: 10.15406/ijcam.2016.03.00095

Yoxtheimer, D. 2010. Water Management Options for Marcellus Natural Gas Development. Penn State College of Agricultural Sciences Cooperative Extension, Marcellus Shale Educational Webinar Series.

Za Za Energy Company Corporation, Presentation. 2013. Investor Presentation December 2014, p. 14., http://www.zazaenergy.com/

Zenger, D. H., Dunham, J. B., and Ethington, R. L. 1980. Concepts and Models of Dolomitization. Vol. 28, Society for Sedimentary Geology, Special Publications, 87-110. http://dx.doi.org/10.2110/pec.80.28.0087

Zhou, J., Baltazar, M., Sun, H., and Qu, Q. 2014. Water-Based Environmentally Preferred Friction Reducer in Ultrahigh-TDS Produced Water for Slickwater Fracturing in Shale Reservoirs, Proceedings of the SPE/EAGE European Unconventional Conference and Exhibition, Vienna, Austria

Zielinski, R. E., and McIver, R. D. 1982. Resource and Exploration Assessment of the Oil and Gas Potential in the Devonian Gas Shales of the Appalachian Basin: MLM-MU-82-61-0002, DOE/DP/0053-1125, 326 p.

Ziemkiewicz, P. F., and Thomas, H. Y. 2015. Evolution of Water Chemistry during Marcellus Shale Gas Development: A Case Study in West Virginia. Chemosphere 13

CHAPTER II

THE IMPACT OF SPATIALLY VARYING RESERVOIR MINERALOGY ON HYDRAULIC FRACTURING PERFORMANCE. CASE STUDY: WATER-ROCK INTERACTION IN LOWER EAGLE FORD FORMATION CHEMOFACIES*

Introduction of engineering fluids into reservoir rocks during hydraulic fracturing can initially dissolve or transform minerals and ultimately precipitate new solids as interactions proceed. These interactions may lead to modification of pores and flow pathways, alteration of properties of the reservoir, and contamination of production fluids. However, shale reservoirs are heterogeneous formations because of complex depositional environments. To understand water-rock interactions and how they affect hydraulic fracturing performance in terms of heterogeneity of shale, interactions between water and rocks from the lower Eagle Ford Formation were investigated.

Rock samples were collected from five chemofacies within the lower Eagle Ford Formation classified based on significant variations in geochemical properties and TOC. Water-rock experiments were conducted at static and dynamic conditions. In static experiments, crushed rock samples submerged into deionized water for three weeks at room conditions. In the dynamic experiments, deionized water flow passed crushed rock samples through a core-flooding experimental system for three hours at reservoir

* Reprinted with permission from "Solid and Soluble Products of Engineered Water/Rock Interactions in Eagle Ford Group Chemofacies" by Zhang et al., 2017. SPE Annual Technical Conference and Exhibition, San Antonio, Texas, USA, 9-11 October 2017, Copyright [2020] by Society of Petroleum Engineers.

conditions. Rock samples were characterized prior to interact with water, in terms of elemental concentrations, mineralogy, and organic contents. Produced water samples after interaction were analyzed to estimate the precipitation tendency of particles in water and the potential to modify flow pathway during hydraulic fracturing, with regards to ion contents, TDS, particle size, and zeta potential. Two statistical analyses, analysis of variance (ANOVA) and principal component analysis (PCA), were used to assess the similarity and difference in interactions between chemofacies.

This chapter provides information on interactions between water and the lower Eagle Ford Formation reservoir rocks, which improves understanding of interaction mechanisms.

2.1 Introduction

Oil and natural gas cannot be extracted through conventional technology effectively through shale reservoirs because of extremely low permeability (<0.1 mD) of the shale reservoirs, which does not allow hydrocarbon migration (Law and Spencer, 1993). Thus, hydraulic fracturing was used to induce more permeability into shale reservoirs by introducing small fractures into reservoirs.

As pressurized hydraulic fracturing fluids are injected into a shale reservoir through created fractures, equilibrium in the reservoir that was established for millions of years is broken and interactions between reservoir rocks and injected fluid occur. The fluids start to contact new rock surfaces created through fracturing process and mix certain

constituents from the pores containing highly saline formation brine (Balashov et al. 2015). As reactions proceed, original minerals present in the reservoir dissolve or transform and eventually re-precipitate as new solids. Such processes may result in modification of existing or induced pores and flow pathways, alteration of the properties of the reservoir, and contamination of production fluids with dissolved solids that must be removed after well production completion. Therefore, understanding water-rock interaction mechanisms and their effect on hydraulic fracturing performance is important (Abdulsattar et al., 2015; Ali and Hascakir, 2015b).

Flowback water is the water returned to the surface after hydraulic fracturing, which mainly includes injection fluids, formation water, and constituents released from reservoir rocks. It can contain significantly high concentrations of heavy elements, TDS, naturally occurring radioactive materials, and toxic organic compounds (Hayes et al., 2009; Haluszczak et al., 2013; Lester et al., 2015; Ziemkiewicz and Thomas, 2015). The primary constituents in flowback water are from materials in the shale formation rather than the additives in the HF fluids (Hayes, 2009; Ziemkiewicz and Thomas, 2015). Thus, the changes in water compositions provide direct observations on the mobilization of elements due to dissolution of reservoir minerals.

Generally, different chemical processes occur during water-rock interactions, mainly including dissolution/precipitation, cation exchange, mineral transformation, and redox reactions (refer to Section 1.6 Water-Rock Interaction Occurring During Hydraulic Fracturing in Chapter I). The chemical composition of water would be changed as it passes through rocks due to these chemical processes. However, it is not easy to understand these

chemical processes alone. If the complex systems, like HF water-rock interaction are considered, the problem becomes more complicated. Moreover, water-rock interactions will be site-specific, since every shale formation has unique characteristics. Hence, this chapter only focuses on such interactions for the lower Eagle Ford Formation.

The lower Eagle Ford Formation, as a typical unconventional reservoir in U.S., has been penetrated by more than 21,000 horizontal wells. Recent studies demonstrate that highly vertical variation occur within the Eagle Ford Formation, which leads to various well production rates (Donovan and Staerker, 2010; Donovan et al., 2012; Amin et al. 2016). Therefore, the Eagle Ford Formation is chosen as my study area to investigate the impact of vertical variation on water-rock interaction and hydraulic fracturing performance. In this chapter, the aim is to study possible interactions between rocks from different chemofacies within the lower Eagle Ford Formation and water. Thus, the next section briefly reviews existing literature on the Eagle Ford Formation. Details of geological background and production history of the Eagle Ford Formation are provided in Section 1.7 The Eagle Ford Formation in Chapter I.

The Eagle Ford Formation is a hydrocarbon-producing geological formation of significant importance owing to its capability of producing huge amounts of natural gas and oil. The proved reserves of nature gas and oil in the Eagle Ford Formation represent 6.1% and 10% of all U.S. gas and oil. Nowadays almost all hydrocarbons produced in the Eagle Ford Formation are from horizontal wells by hydraulic fracturing (EIA, 2019).

The Eagle Ford Formation is located in South Texas and was deposited during a worldwide second-order transgression in the Late Cretaceous, about 96 million years ago

(Dawson, 2000; Hentz and Ruppel 2011; Treadgold et al., 2011). Its lithologies are predominantly composed of organic-rich calcareous and fossiliferous marine shale interbedded thin limestone (Faust, 1990). Regionally within the Eagle Ford Group, two units were recognized: the lower Eagle Ford Formation and the upper Eagle Ford Formation (Dawson, 1997; 2000; Robinson, 1997; Donovan et al., 2015). The lower Eagle Ford Formation is described as organic–rich mudrock deposited during transgressive interval and the upper Eagle Ford Formation is calcareous-rich mudrock deposited during regressive interval. Because of relatively high organic contents, the lower Eagle Ford Formation is the primary target for industry. The chief Eagle Ford Group mineralogy is characterized by calcite, quartz, clays including kaolinite and illite, and minor amounts of dolomite, ankerite, and pyrite (Elston, 2014; Wang et al., 2015). Among them, calcite accounts for the largest weight percentage (40-90 wt. %) of the Eagle Ford Group (EIA, 2014). The high percentage of calcite along with quartz makes the Eagle Ford Formation more brittle and therefore more conducive to hydraulic fracturing. (Jarvie et al., 2007).

Geochemical processes that occur between the Eagle Ford Group and water were investigated by several lab studies. Interactions between lab generated fluid and rock samples from the Eagle Formation and the Bakken Formation were compared (Wang et al. 2015; 2016). They demonstrate that the rate and extent of water-rock interaction mainly depends on the geochemistry of the formation, composition of the fracturing fluid, and the contact time. In addition, due to high mass fraction of calcite with strong buffering capacity in the Eagle Ford Formation, they concluded initially acidic HF fluids could be neutralized after hydraulic fracturing and pH would back to neutral or higher values.

Experiments conducted between water and four shale samples from the Eagle Ford, Marcellus, Green River, and Barnett Formation show particles in the produced water after interacting with Eagle Ford sample were more likely to cause agglomeration of colloids and blockage of the fracturing openings (Ali and Hascakir, 2015).

These studies provide valuable information of water-rock interactions within the Eagle Ford Formation. However, when conducting water-rock experiments in their studies, only one rock sample was used to represent the whole shale formation, which may not be enough because shale formation is not a homogenous unit due to complex environmental conditions and depositional processes. Because the Eagle Ford Formation was deposited under conditions of basin restriction, storm events, and episodic anoxia, it shows highly heterogeneous in vertical variation and minor heterogeneous in lateral dimension. (Donovan and Staerker, 2010; Donovan et al., 2012; Amin et al., 2016). Thus, this chapter investigates water-rock interaction in the lower Eagle Ford Formation Chemofacies to understand the impact of vertical heterogeneity of the Eagle Ford Formations on hydraulic fracturing performance.

2.2 Materials and Methods

Rock samples were collected from Swenson core (140 feet long) in Well No.1 of the lower Eagle Ford Formation in the Maverick Basin (**Figure 25**). The lower Eagle Ford Formation was selected because it is associated with organic-rich rocks which contain the unconventional reservoir and are the primary target for industry. In addition, the Eagle

Ford Formation is thickest in the Maverick Basin and distinct heterogeneities are present vertically in Swenson well (Winter, 1961; Amin et al., 2016).

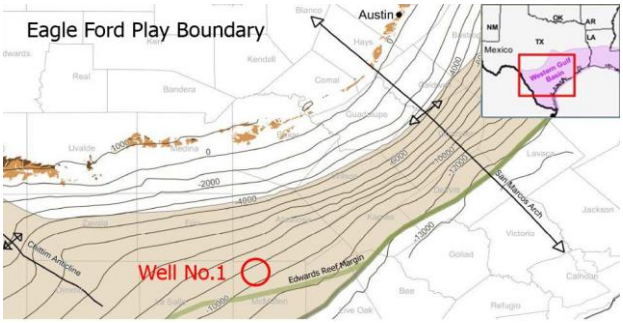

Figure 25 The location map for the study area (Well No.1 is located in the Maverick Basin at the Eagle Ford Shale play). Image modified from U.S. Energy Information Administration (2014).

The lower Eagle Ford of the Swenson core was classified into five chemofacies named LEF1 through LEF5 from top to bottom by Amin et al. (2016). Chemofacies were sub-divided based on stratigraphic variations in elemental concentrations (Ca, Si, Al, K, Fe, S, U, V, Ni, and Mo) and TOC (**Figure 26**). These elements were chosen either because they are major elements (Ca, Si, Al, K, Fe, and S) that compose of the bulk of the minerals in the lower Eagle Ford Formation, or because they are redox sensitive trace metals (U, V, Ni, and Mo) indicating paleoenvironmental conditions during the deposition of the lower Eagle Ford Formation (Tribovillard et al., 2006; Wright and Ratcliffe, 2010). Because of significantly vertical heterogeneity within the lower Eagle Ford Formation, chemofacies classification in their study based on geochemical properties correlated well with geological and petrophysical classifications based on texture and petrophysical

properties. Moreover, due to minor lateral variation within the lower Eagle Ford Formation relative to vertical variation, their petrophysical classification was successfully applied to a nearby well with different hydrocarbon production rate where core samples were not available for lithofacies and chemofacies characterization (Amin et al., 2016). Although geological and petrophysical classifications in the lower Eagle Ford Formation were also established, chemofacies classification depending on geochemical properties is more valuable for my objective about water-rock interactions upon element mobilization. The key geochemical characteristics of five chemofacies are summarized in **Table 22**. To compare interactions between chemofacies and within chemofacies, two samples per chemofacies were collected randomly.

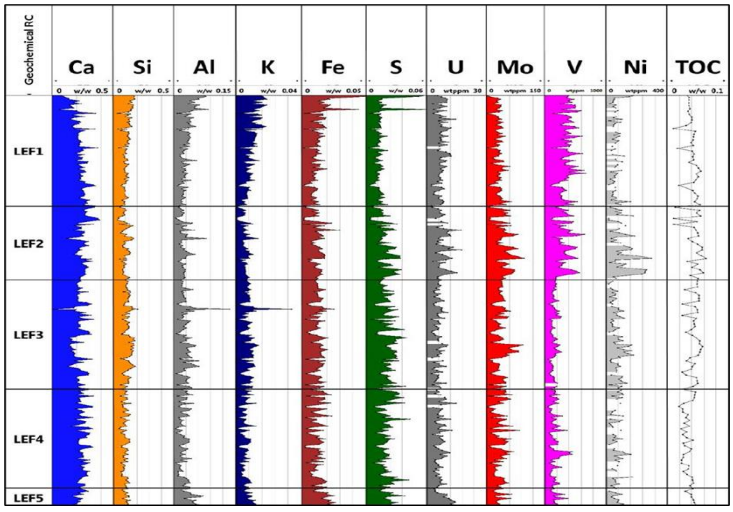

Figure 26 Five chemostratigraphic units were divided by vertical distribution of elements and TOC in the lower Eagle Ford. Image modified from Amin et al. (2016) with permission from SPWLA.

Table 22 Summary of geochemical characteristic of each chemofacies (Amin et al., 2016).

Sample	Chemofacies	Core Depth, feet	Geochemical Characteristics
1	LEF1	10,410.0-10,444.0	A continuous decrease in Ca content and increase in other major elements.
2			
3	LEF2	10,444.0-10,470.0	A significant increase in trace elements content such as V, Ni, Mo, and U.
4			
5	LEF3	10,470.0-10,508.5	Higher TOC (>4 wt %), and Ca content starts to decrease and then increase.
6			
7	LEF4	10,508.5-10,543.0	Distinguished by its low TOC (2-4 wt %).
8			
9	LEF5	10,543.0-10,550.0	U content is the highest in this interval. TOC is moderate to high (4-5 wt %).
10			

Prior to interacting with water, selected Eagle Ford Formation samples were crushed, mixed, and sieved into less than 1 mm to increase rock surface areas that were exposed to water, which aims to accelerate water-rock interaction. Then crushed samples were identified by a Tracer III-SD handheld X-ray Fluorescence (XRF) and a Powder X-ray Diffractometer (XRD) to determine elemental composition and mineralogy, respectively. In XRF analysis, major elements (Na, Mg, Al, Si, P, S, K, Ca, Ba, Ti, V, Cr, Mn, and Fe) were measured at an operating voltage of 15 kV and current of 27.3 µA with a vacuum pump and trace elements (Co, Ni, Cu, Zn, As, Pb, Th, Rb, U, Sr, Y, Zr, Nb, Mo, and Rh) were measured at 40 kV and 12.9 µA with a Ti and Al filter. Each sample was measured four times, and the final elemental concentrations were the average of induvial XRF data. The same crushed samples were analyzed by XRD for mineralogy. The continuous XRD scan range was set at scanning speed of 2 degrees per minute from 5-65 degrees (Jenkins and Snyder, 1996). Also, to determine the amount of organic contents and to verify the inorganic contents in rock samples, thermal gravimetric analysis (TGA) was conducted using the STA 449 Jupiter® at constant heating rates of 5 °C per minute

under 50 ml/min air and 20ml/min nitrogen gas injection from 25-900°C (Burger et al., 1985). Kerogen is a major part of organic matter in shale and is entirely consumed about 500-550 ºC (Abouzeid and Sinbawy, 1980; Kar and Hascakir, 2017). While calcite, which is the major carbonate minerals in the Eagle Ford Formation, starts to decompose at 600 ºC (Burger et al., 1985). Therefore, both kerogen and calcite decompose during combustion of shale samples, which can be identified by the weight loss of shale samples through TGA.

After completion of rock sample characterization, static and dynamic experiments on crushed rock samples and deionized water were conducted to better understand the water-rock interaction at stagnant water and during continuous water flow conditions. Deionized water was used in all experiments as injection fluid in this chapter, which was extended for flowback water in Chapter III.

In static experiments, 10 g crushed rock sample interacted with 50ml deionized water for three weeks at atmospheric temperature and pressure (71°F and 1 atm) to simulate stagnant conditions when water stays in the created fractures during hydraulic fracturing. In dynamic experiments, a core-flooding experimental set-up, containing a water pump, a core holder, a temperature and pressure controller, a separator, and a produced water container, was used to simulate continuous water injection at reservoir conditions (**Figure 27**). Deionized water was continuously injected at 18 ml/min rate into the core-holder containing about 280 g crushed rock sample for three hours and produced water was collected every half an hour. To avoid escape of rock particles from core-holder, a mesh and a filter paper were placed at the bottom of the core holder. Dynamic

experimental temperature was maintained between 242-244°F based on field well data provided by Core Laboratories Company and pressure was retained at 75 pounds per square in gauge (psig). Although experimental pressure was lower than the actual pressure at sample collection depth, it should be noted that minerals in water exhibit insignificant change of solubility with the changes in pressure (Hildebrand, 1924; Gibson, 1938). In addition, a control experiment was conducted before starting dynamic experiments to observe the reactivity of the core holder with deionized water. In the control experiment, deionized water was injected into the core-flooding experimental system without adding rock samples and collected water sample was subjected to same analyses that the produced water samples through core flood experiments were subjected.

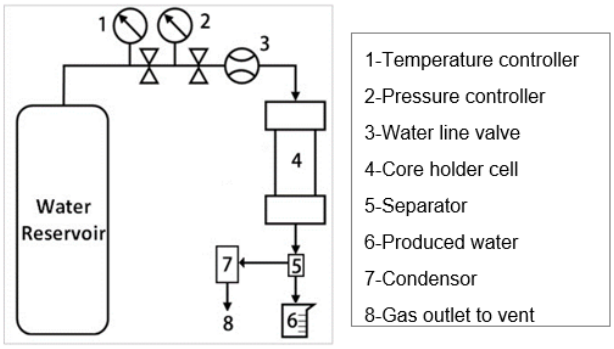

Figure 27 Schematic illustration of core-flooding experimental set-up

To assess if the experimental conditions are close to field HF case, the estimated rock surface area to water volume ratio in lab conditions is compared with field conditions, based on the calculation provided in Abdulsattar (2015). The calculation processes are in the following steps. First, approximate rock surface to water ratio in lab scale are derived

based on two assumptions. Assuming all crushed particles are spheres (radius is 0.05 cm) and bulk rock density is 2.5 g/cm^3 (Manger, 1963), the surface area for each particle is about 0.031 cm^2 and volume is 5.24*10^{-4} cm^3. Multiplying particle volume by rock density, the mass of individual particle is 1.31*10^{-3} g. Because 10 g and 280 g crushed samples are used in static and dynamic experiments, by dividing the total sample mass by the individual particle mass, the total number of particles in static and dynamic experiments is about 7633 and 21374, respectively. Then multiplying total number of particles by the surface area of individual particle, the total surface areas in each static and dynamic experiments are approximately 236.6 cm^2 and 6626.0 cm^2. Water used in static and dynamic experiments are 50 mL and 3240 mL (18mL/min *180 minutes). Therefore, the rock surface area to the water ratios in static and dynamic experiments are approximately 4.73 cm^2/mL and 2.04 cm^2/mL. Because there are variations in particle shape and size in real case, the actual ratio is probably higher than this due to non-sphericity and varying sizes of the real particles. In field scale, estimated rock surface area to water ratio ranges in hydraulic fracturing are 2-20 cm^2/mL, based on the assumption that the small fracture width ranges are from 0.1-1 cm (Ramurthy et al., 2011; Abdulsattar, 2015). Comparing the estimated lab and field rock surface to water volume ratios, the size of crushed rock samples and water volume used in static and dynamic experiments are reasonable. Although these calculations rely on assumptions that may be in error and there must be variation in fracture widths in the real case, attempt was made lab conditions close to field conditions in this study.

Water samples before and after static and dynamic tests were analyzed for TDS, zeta potential, and particle size. TDS was measured by an Oakton Conductivity Probe. The zeta potential was analyzed by a Nano ZetaPALS by Brookhaven Instruments Corporation. The particle size of suspensions in water samples was obtained by a particle size analyzer by Brookhaven Instruments Corporation. These water parameters aim to evaluate the particle precipitation tendency and infer the potential to modify flow pathway after water-rock interaction. In general, the supernatant samples with higher concentration of TDS increase the chance of particles to come together (WHO, 2011). The particles in the water with larger particle size will settle earlier and more rapidly due to higher settling velocity with the increasing particle size (Losev et al., 1989). The particles with smaller absolute zeta potential values have low stability and tend to come together and settle (refer to Table 19) (Greenwood and Kendall, 1999; Hanaor et al., 2012). Therefore, precipitation will more likely take place in water with high TDS, low absolute zeta potential, and large particle size (Weber, 1972).

In addition, all water samples including injected water and produced water were characterized by a high-resolution inductively coupled plasma mass spectrometry (ICP-MS) in Radiogenic Isotope Geochemistry Laboratory at Texas A&M University. To correspond to XRF analysis, 29 ions were analyzed by ICP-MS. Prior to water analysis, all water samples were acidified to 2% weight/volume nitric acid and indium was added as internal standard (Hall, 1992). According to statistics theory provided in Thompson and Nathanail (2003), if the concentration of one detected element in produced water after water-rock interactions was three times higher than that in blank solution, it was regarded

as an enriched element mobilizing from dissolution of minerals instead of water contamination from pipes and the core holder.

To determine whether identified enriched elements can reveal the different interactions between chemofacies, two statistical tests were used to assess the difference and similarity in these elements between chemofacies. The first one is single factor analysis of variance using Tukey's honest significance test (ANOVA using Tukey HSD), which was used to evaluate whether there are any statistically significant differences between the means of two or more groups within a single independent variable and identify where the differences occur between groups (Fisher, 1921; Tukey, 1949). In ANOVA, a calculated probability, known as p-value, is compared to a chosen significance level to determine if there is evidence to reject the null hypothesis (hypothesis of no difference) (Fisz, 1963; Everitt, 1988). The most common significance level is 0.05, indicating a 5% risk of concluding that a difference exists when there is no actual difference (Fisher, 1971). If the p-value is less than the significance level, the null hypothesis is rejected, indicating the differences between some of the means are statistically significant. If the p-value is greater than the significance level, the differences between the means are not statistically significant.

The second statistical test is principal component analysis (PCA) which is commonly used to condense the information of large datasets containing many variables into a smaller set of new composite dimensions, with a minimum loss of information (Pearson, 1901). By doing so, a set of new uncorrelated variables, called principal components (PC), are created and ordered to explain variability among the variables

included in the datasets. Typically, the first three principal components account for most of the variance in the original datasets and can access similarities and differences between variables and determine if variables can be grouped (Pearson, 1901). The difference between PCA and ANOVA is PCA can reveal the relationship between variables. For example, in nature, strontium (Sr) is strongly related to carbonate rock sources and prefers to substitute for calcium typically taking place in calcite (Salimen et al., 2006). Additionally, in sedimentary rocks, rubidium (Rb) commonly substitutes for potassium in minerals, like K-feldspar, mica, and clay minerals. (Salimen et al., 2006). These relationships between these elements can be revealed and grouped by PCA. Both loading plot and score plot are commonly used in PCA. In this study, loading plot is used for interpreting relations among individual elements in samples. Elements in the plot which are close have high correlation. Score plot is a three-dimensional plot used for interpreting relations among samples in chemofacies. In score plot, samples which are close are similar. In both plots, major and trace elements were separately analyzed because of different concentration ranges.

2.3 Results and Discussions

2.3.1 Rock Characterization

Prior to water-rock interactions, crushed rock samples from different chemofacies were identified by XRD and XRF to determine mineralogy and elemental concentrations.

XRD results shown in **Table 23** demonstrate all samples consisted of calcite and quartz with some clay minerals, including kaolinite and illite, and small amount of pyrite and dolomite. The excess calcite identified in lower Eagle Ford Group samples was supported by XRD analysis in previous studies (Chermak and Schreiber, 2014; Wang et al., 2015; Amin et al., 2016; Ali and Hascakir, 2017). The XRD results also indicate that the lower Eagle Ford Formation mineralogy varied with chemofacies, which is primarily controlled by various depositional processes and environments.

Table 23 Mineralogy of each sample obtained through XRD analysis (wt. %)

Sample		calcite	quartz	kaolinite	illite	pyrite	dolomite
LEF1	**1**	50.0	25.7	8.1	12.4	2.0	1.7
	2	66.0	16.5	5.3	11.5	0.7	0
LEF2	**3**	55.1	28.1	5.8	8.3	2.2	0.5
	4	51.7	24.1	8.2	9.6	2.7	3.7
LEF3	**5**	64.7	16.3	6.9	8.9	2.3	1.0
	6	54.1	18.5	11.8	13.4	2.1	0.1
LEF4	**7**	59.7	20.4	8.0	9.9	2.0	0
	8	55.0	20.4	9.7	12.6	2.3	0
LEF5	**9**	56.3	17.9	9.9	13.2	2.7	0
	10	66.5	14.8	10.1	6.8	1.8	0

In addition, 14 major elements (Na, Mg, Al, Si, P, S, K, Ca, Ba, Ti, V, Cr, Mn, and Fe) and 15 trace elements (Co, Ni, Cu, Zn, As, Pb, Th, Rb, U, Sr, Y, Zr, Nb, Mo, and Rh) were detected by XRF (**Table A-1**). The elemental composition in each sample associated with classification of chemofacies is shown in **Table 24**. Compared the XRF results obtained in this study with the key inorganic geochemical characteristics of related chemofacies in Amin et al. (2016), the abundance of these elements in each sample was consistent. Combined XRF with XRD results, Ca was mainly from calcite. Si came from

quartz and clay minerals. Al and K mainly made up of clay minerals. Fe and S were mainly in the form of pyrite. Although Mg (0.16-0.48wt. %) (refer to Table A-1) was detected by XRF in all samples, dolomite was not in all samples perhaps because Mg was from other minerals, like illite, rather than dolomite, or dolomite content was too low to be distinguished from the XRD background pattern.

Table 24 Elemental concentrations of each original sample obtained through XRF analysis. Major elemental concentrations were expressed in wt. % and trace elemental concentrations were expressed in ppm.

Chemofacies	Sample	Major Elements, average wt. %						Trace Elements, average ppm				
		Ca	Si	Al	K	Fe	S	Th	U	Mo	V	Ni
LEF1	1	16.0	13.0	4.2	1.3	1.6	1.1	6.7	14.6	25.1	275	61
	2	25.1	7.1	1.3	0.4	0.8	0.6	3.5	11.0	11.4	128	44
LEF2	3	19.7	11.0	1.5	0.3	1.0	1.1	3.4	8.5	24.4	170	54
	4	17.2	11.0	2.9	0.6	1.4	1.5	4.2	6.7	38.2	181	74
LEF3	5	24.2	8.4	1.5	0.4	0.9	0.8	3.5	4.9	11.8	76	37
	6	19.8	9.7	2.9	0.5	1.2	1.1	3.6	4.3	8.0	50	31
LEF4	7	22.7	8.5	1.4	0.4	1.0	1.0	3.3	5.5	17.2	93	45
	8	20.2	10.0	2.1	0.5	1.3	1.3	3.7	6.5	28.0	115	65
LEF5	9	20.5	8.9	2.8	0.7	1.5	1.3	4.7	6.7	16.2	61	50
	10	23.0	7.8	2.4	0.5	1.4	1.3	4.0	7.1	29.8	161	68

In addition, organic contents in each rock sample were determined by TGA (Burger et al., 1985; Kar et al., 2016). The decomposition or dihydroxyliation temperatures of the minerals and organic matter that can cause mass losses of the Eagle Ford Formation samples are summarized in **Table 25**. However, as shown in this table, temperature ranges for various reactions overlap. Therefore, it is difficult to obtain accurate quantitative analysis based on stoichiometric equations. However, qualitative analysis by TGA is still helpful to identify shale samples.

Table 25 Decomposition and dehydroxyliation temperature of minerals and organic matter in the lower Eagle Ford samples (Abouzeid and Sinbawy, 1980; Burger et al., 1985; Zhou et al., 2007; Foldvari, 2011)

Mineral / Matter	Temperature Range	Chemical Process
Kerogen	<550 °C	Decomposition of kerogen
Calcite	600–900 °C	Decomposition to form carbon dioxide
Quartz	900–1500 °C	Decomposition to form oxygen
Dolomite	500–700 °C	Decomposition of dolomite
Kaolinite	450-600 °C	Dehydroxylation of hydroxyl group
Illite	550–900 °C	Dehydroxylation of hydroxyl group

The weight loss data at particular temperatures of 10 initial samples is listed in **Table 26**. The mass losses of all samples were less than 5.5% even if the temperature reached 550 ºC. At 550 ºC, all organic matter was entirely consumed, and a part of clay minerals (kaolinite) released hydroxyl group (-OH) as water (Foldvari, 2011). Although it is difficult to distinguish multiple thermal processes, the results show organic matter just accounts for a very small proportion of the Eagle Ford Formation samples due to low weight losses of all samples. As the temperature increased to 700 ºC, clay minerals (kaolinite and illite) continued to release water and carbonate minerals (calcite and dolomite) started to decompose. However, mass losses of all samples were still low (<8%) even if the temperature reached 700 ºC.

Table 26 Mass loss at particular temperature during TGA test

Samples		Mass Loss at Certain Temperature °C				
Chemofacies		25°C	550°C	700°C	850°C	900°C
LEF1	Sample1	0%	3.16%	6.57%	23.89%	24.70%
	Sample2	0%	0.82%	3.54%	29.79%	34.60%
LEF2	Sample3	0%	3.42%	5.78%	29.60%	30.20%
	Sample4	0%	3.93%	6.98%	27.24%	28.00%
LEF3	Sample5	0%	3.50%	5.59%	32.04%	33.40%
	Sample6	0%	4.06%	6.82%	30.44%	30.80%
LEF4	Sample7	0%	5.23%	7.34%	34.33%	35.80%
	Sample8	0%	2.58%	5.41%	29.56%	30.20%
LEF5	Sample9	0%	3.17%	6.46%	30.16%	30.90%
	Sample10	0%	4.97%	7.73%	32.32%	36.10%

In addition, there were no significant transition points from organic matter decomposition to inorganic matter decomposition observed in all TGA plots **(Figure 28)**. However, the main mass loss of all Eagle Ford samples occurred between 700-850 °C, which was mainly caused by decomposition of carbonate minerals by release of CO_2 gas. In Eagle Ford samples, calcite is major carbonate mineral and is mainly consumed at this temperature interval. Therefore, according to TGA data, most of mass losses in the lower Eagle Ford samples were caused by decomposition of inorganic matter mainly from calcite.

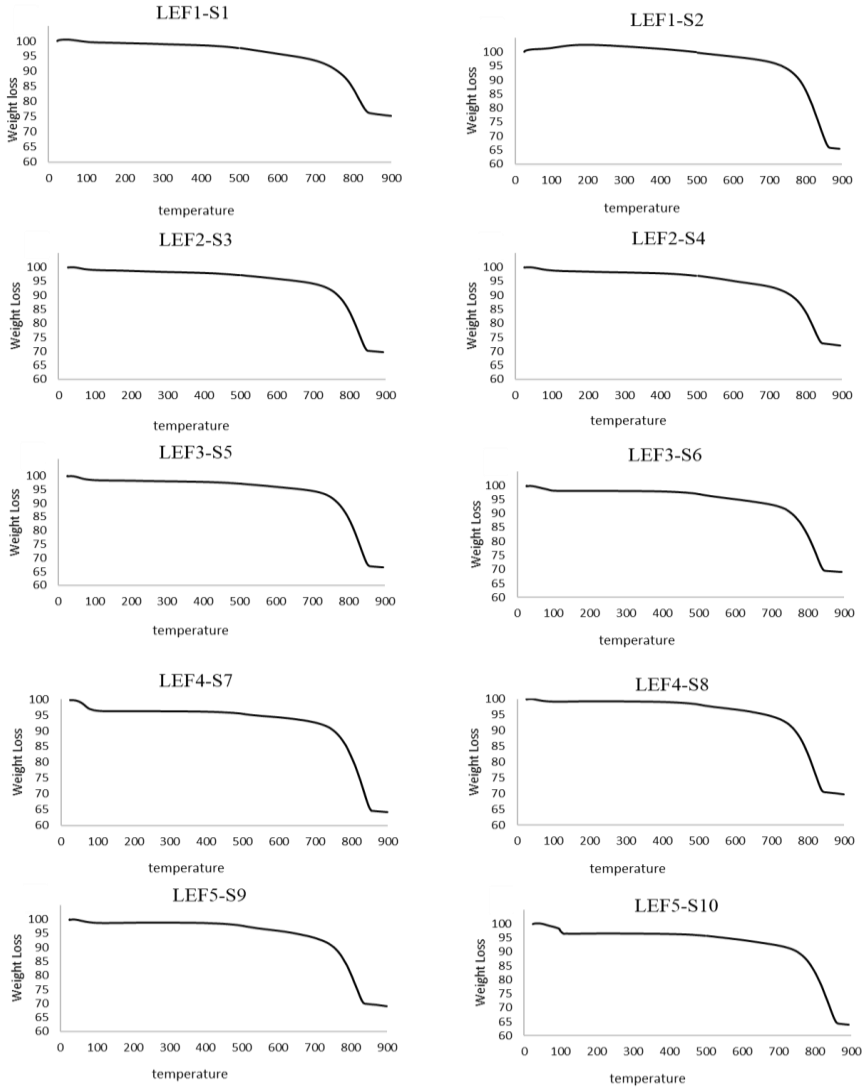

Figure 28 TGA plot of all lower Eagle Ford samples from different chemofacies

2.3.2 Water-Rock Interaction Results

Before water-rock experiments, blank tests were done to identify possible sources of artificially introduced contamination. In static experiments, deionized water was used as blank solution and first analyzed by ICP-MS. In dynamic experiments, deionized water

was injected into the core-flooding experimental system at reservoir conditions without adding rock samples and produced water was used as blank solution and analyzed. The compositions of blank solutions are given in the appendix section (**Table A-2**). In deionized water, 7.9 ppm of Na and 0.9 ppm of Si residual were detected, which are typically difficult to remove by deionization. But compared with the produced water samples after all water-rock experiments, they were insignificant and did not affect experimental results (shown in the following discussion). Other 27 elemental concentrations were less than 0.1 ppm or below the detection limit shown as negative value. In addition, after a dynamic experiment without any rock samples, small abundances of S, Ca, Al, Fe, K, Mo, Ni, V, P, Ba, Co, Cr, and Y were detected in produced water relative to the injected deionized water. Because no rock samples were added, these contaminants were mainly mobilized from the core holder and pipes. After determining possible contaminations from deionized water and from core-flooding instrument, static and dynamic water-rock experiments were investigated, respectively.

(a) Static Experimental Results

In static experiments, crushed rock samples from each chemofacies was submerged in deionized water for three weeks at room temperature and pressure. After experiments, TDS, zeta potential, and particle size in produced water samples were analyzed to estimate the precipitation tendency of particles in water.

The produced water analyses for static experiments are listed in **Table 27**. After 3 weeks' water-rock interaction, TDS and particle size in produced water samples from different chemofacies became 24-40 times and 1.2-4.0 times higher than these parameters in injected deionized water, respectively. Because of the slight decrease in absolute zeta potential, colloids in the produced water became less stable after experiments. Pores can be plugged by particles with size ranges between 1/3 and 1/7 the size of pore throat (Abrams, 1977). Therefore, according to particle sizes in produced water, it can be estimated that particles with size of about 0.6-2.4 μm in produced water can block pores with size range of 1.8-16.8 μm, if colloids continue to agglomerate and finally settle to the pore channels by gravity after water-rock interaction.

Table 27 Characterization of supernatant water samples from static experiments

Static Samples		TDS, ppm	Particle Size, nm	Zeta Potential, mV
Blank		22.1	596	10.78
LEF1	1	865	726	8.98
	2	445	1039	8.98
LEF2	3	563	1636	5.51
	4	837	1129	3.86
LEF3	5	534	1724	9.59
	6	749	948	6.09
LEF4	7	657	1404	4.11
	8	677	2391	4.29
LEF5	9	684	1182	7.55
	10	650	1643	7.31

Compared with water parameters of all samples from different chemofacies, particles in samples from LEF2 and LEF4 were more likely to come together and block

pores. In LEF2, sample 3 had relatively lower zeta potential and higher particle size relative to other samples, while sample 4 had lower zeta potential and higher TDS. In LEF4, both sample 7 and sample 8 had relatively lower zeta potential and larger particle size. Although particles in samples from other chemofacies were less likely to agglomerate relative to samples from LEF2 and LEF4, high TDS in all samples cannot be ignored in terms of the treatment of flowback water after hydraulic fracturing. In most static experiments, samples show a negative correlation between average particle sizes and absolute zeta potential. As particle size increased, absolute zeta potential value decreased perhaps because attraction and agglomeration of particles with low zeta potential led to the reduction in stability and growth of particles.

Produced water samples were further analyzed by the ICP-MS for ion contents. It was observed that 8 major elements (Na, Si, Ca, Al, S, K, Fe, and Mg) and 10 trace elements (Rb, Sr, Mo, Ni, V, Rh, Ba, Co, Y, and U) were enriched in produced water after water-rock interactions relative to deionized water (**Table A-3**). These elements were mobilized from rock dissolution. Compared with Na and Si residuals in deionized water, Na and Si concentrations in produced water were more than about ten times and three times higher, respectively. Therefore, they did not affect experimental results. In addition, although both S and Fe ions were enriched elements in produced water, S concentrations in each sample ranged over three orders of magnitude for Fe concentrations, which can be explained by the oxidation of pyrite. Dissolution of pyrite (FeS_2) released S and Fe ions, but ferrous iron (Fe^{2+}) was oxidized to ferric iron (Fe^{3+}) by dissolved oxygen and precipitated out of water through chemical reaction 1 (Moses et al., 1987).

$$FeS_2 + 3.75O_{2(aq)} + 3.5H_2O = Fe(OH)_{3(s)} + 2SO_4^{2-} + 4H^+ \ldots\ldots\ldots (1)$$

The enriched elements in produced water provide evidence for elemental mobilization from mineral dissolution. To further understand whether these elements after static experiment can reflect different interactions between chemofacies, two statistics tests, analysis of variance using Tukey's honestly significant difference test (ANOVA using Tukey HSD) and principal component analysis (PCA), were used to assess the difference in these elements. In ANOVA, each enriched element was considered as a single independent variable and each chemofacies was a group. Therefore, 18 variables and 5 groups were present in static experiments. Calculated p-values of each enriched elements are given in **Table 28**. Compared p-values with the common significance level of 0.05, the results show p-values of Ca, Al, Mg, Ni, and Ba were less than the chosen significance level, which indicates within each element, at least 2 chemofacies were different from each other. Other elements did not show significant differences between chemofacies, although they were enriched in produced water.

Table 28 Calculated p-values of enriched elements for different chemofacies. p-values of Ca, Al, Mg, Ni, and Ba were less than the chosen significance level (0.05). It indicates for these elements, at least 2 chemofacies are different from each other.

elements	**Na**	**Ca**	**Al**	**S**	**K**	**Mg**	**Sr**	**Mo**
p-value	0.36	0.01	0.02	0.39	0.38	0.01	0.07	0.31
elements	**Ni**	**V**	**Co**	**Ba**	**Rb**	**Fe**	**Y**	**U**
p-value	0.04	0.07	0.29	0.03	0.17	0.39	0.64	0.11

These elements representing significant differences between chemofacies were grouped by ANOVA using Tukey HSD procedure. They were arranged in alphabetical order from high to low concentration (**Table 29**). Within each element, chemofacies with different letter were significantly different. Between elements, chemofacies with same letter were unrelated because they are independent variables.

Table 29 Mean enriched elemental concentrations (ppm) in static produced water for different chemofacies. Elements were grouped in alphabetical order from high to low concentration by Tukey HSD procedure. Within each element, chemofacies with different letter are significantly different.

Chemofacies	Ca		Al		Mg		Ni		Ba	
	ppm	group	ppm	group	ppm	group	ppm	group	ppm	group
LEF1	15.24	C	0.048	B	1.70	C	0.003	C	0.024	B
LEF2	56.00	A	0.009	D	5.40	A	0.036	A	0.026	A; B
LEF3	40.80	B	0.019	C	5.06	A	0.006	C	0.034	A
LEF4	38.80	B	0.031	B; C	3.94	B	0.018	B	0.024	B
LEF5	17.34	C	0.085	A	2.07	C	0.007	B; C	0.043	C

In the table, no single element can be used to distinguish all five chemofacies. However, the combination of these five elements (Ca, Al, Mg, Ni, Ba) can be used to identify different chemofacies because of different abundance level of enriched elements. For example, LEF1 contained low Ca, Mg, and Ni and medium Al and Ba concentrations. LEF2 had high Ca, Mg, and Ni and medium-high Ba but lowest Al concentrations. LEF3 contained high Mg, Ba, medium Ca, and Al but low Ni concentrations. All elemental concentrations in LEF4 were medium. LEF5 contained low Ca, Mg, Ni, and Ba but high Al concentrations. Based on this data, except Al, concentrations of other four elements were high in LEF2, which indicates strong interactions occurred. In addition, these

elements are the key geochemical tracers measurable in production fluids to indicate the effective surface areas where water-rock interaction occurs and may infer fracture distributions induced by hydraulic fracturing.

The second statistic test is PCA that was used to reveal similarities and differences between samples and evaluate if samples can be grouped. Due to different concentration ranges between major and trace elements, they were separately analyzed in PCA. In addition, although Sr and Rb are trace elements, they are strongly associated with major elements, such as Ca and K in sedimentary rocks. Thus, they were analyzed with major elements in PCA (Salimen, et al., 2016). Loading plot for major elements after static experiments is shown in **Figure 29**. Elements which were close have high correlation.

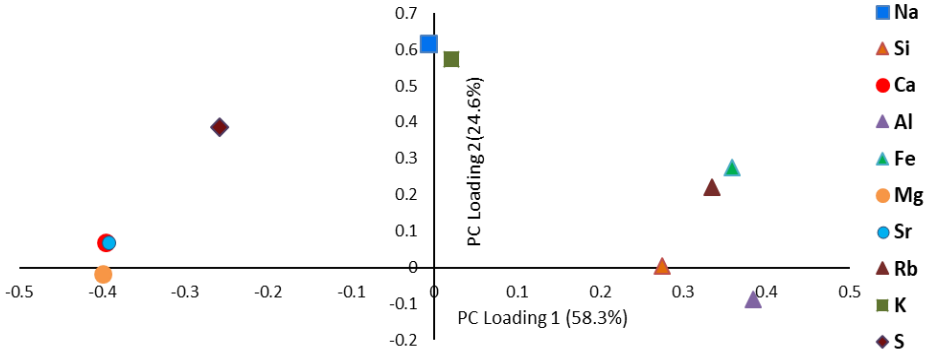

Figure 29 Loading plot of enriched major elements in produced water after static experiments. It shows the relationships between elements. Elements which are close have high correlation. The first and second principal components account for 58.3% and 24.6% of the variance in the original data, respectively.

According to the loading plot, the enriched major elements in produced water after static experiments were divided into three groups: 1) Ca, Mg and Sr were mobilized from the dissolution of carbonate minerals; 2) K and Na were associated with cation exchange from rock particles 3) Al, Si, Rb, and Fe were derived from dissolution of clay minerals. S was independent and may come from dissolution and oxidation of pyrite, but the released Fe ions were oxidized and precipitated out of water. For trace elements in static experiments, they were randomly distributed in loading plot and cannot be explained perhaps because of low concentrations in water and their small sample size (**Figure A-1**).

The 3-deminsion score plot was used to interpret relations among samples within chemofacies (**Figure 30**). Samples which were close are similar. For major elements, samples in LEF5 were close and distinguishable. Samples in LEF1 were not similar but distinguishable. Samples in LEF2, LEF3 and LEF4 were close and scattered in the middle of the plot. The distribution of samples in score plot can be interpreted by geochemical characteristics of chemofacies (refer to Table 22). Because of narrow stratigraphic interval of LEF5 (about 7 feet) relative to other chemofacies, produced water after interacting with rock samples from LEF5 had similar elemental concentrations and can be grouped. Unlike LEF1, rock samples in LEF2, LEF3, and LEF4 were mainly characterized by different TOC or trace elemental concentrations. Therefore, produced water samples after interacting with rock samples from these three chemofacies were relatively similar in terms of major elemental concentrations. Because LEF1 was characterized by continuous change in major elements, rock sample 1 and sample 2 collected from upper and lower LEF1 had significantly different major elemental compositions and caused the difference

in score plot. For trace elements, all samples scattered in the score plots and cannot be distinguished because of extremely low concentrations in produced water (**Figure A-2**).

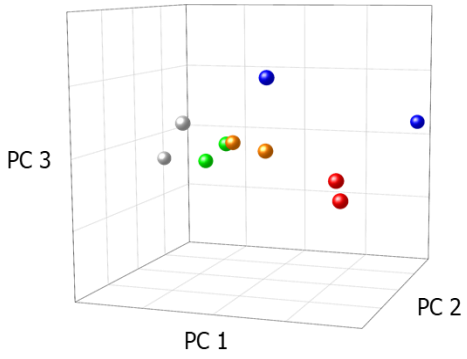

Principal Component	Fraction of Variance
PC1	58.28%
PC2	24.64%
PC3	8.92%

Figure 30 Score plot of each produced water sample in static experiments. Samples which are close are similar. The fraction of variance is the percentage of variance accounted for by each principal component.

(b) Dynamic Experimental Results

In dynamic experiments, deionized water was injected for three hours at 18 ml/min rate into the core-holder between 242-244 °F and 75 psig. The produced water samples were collected every half an hour and first characterized for water parameters, in terms of TDS, absolute zeta potential, and particle size. The average water parameters in the produced water from each chemofacies are listed in **Table 30**.

Table 30 Characterization of produced water samples after dynamic experiments

Dynamic Samples		TDS, ppm	Particle Size, nm	Zeta Potential, mV
Blank		35.4	387	28.41
LEF1	1	574	1680	19.2
	2	286	11340	9.8
LEF2	3	391	12655	8.21
	4	698	19275	6.24
LEF3	5	329	15563	11.99
	6	603	17404	15.56
LEF4	7	359	6232	10.49
	8	374	13219	13.27
LEF5	9	371	2211	13.03
	10	348	458	11.88

After 3 hours' dynamic water-rock interaction, TDS and particle size in produced water samples became 8-17 times and 1.2-50 times greater than these parameters in produced water after control experiment, respectively. Behavior of particles in the water became unstable due to decreased absolute zeta potential. In addition, because particle sizes in produced water after interacting with rock samples from LEF2, LEF3, and lower part of LEF4 were more than 10^{-5} m, these water samples became suspension from colloidal suspension. The reason that particles in water samples after dynamic experiments had bigger size than static experiments is because relatively fast water flow supported bigger suspended particles that were transported into the produced water container (Abbott and Francis, 1977). According to the relationship between particle size and plugged pore size, particles with size of about 0.5-19.3 μm in produced water can block pores with size range of 1.5-135.1 μm. Although at the beginning of hydraulic fracturing on field scale, injected fluid flow may be able to support suspended particles to travel across pores or

small fractures, but larger particles are likely to settle and plug the pores after the flow speed becomes slow.

Water parameter results also indicate produced water samples from LEF2, LEF3, LEF4, and lower part of LEF1 were more likely to agglomerate and block pores because of larger particle size, smaller absolute zeta potential, or higher TDS relative to other samples. Among them, samples from LEF2, especially sample 4 from lower part of LEF2, had greatest tendency to precipitate. In addition, the water parameters show a similar trend as static experiments that as particle sizes increased, the absolute zeta potential values decreased for the water samples produced through most of dynamic experiments.

The produced water samples from dynamic experiments were also analyzed for elemental concentrations by the ICP-MS (**Table A-4 to Table A-8**). Except Si and Al, other major elemental concentrations (Na, Ca, S, K, Fe, and Mg) show a decreasing trend with the increasing experimental time in produced water collected every half an hour because smaller crushed particles dissolved into water easily and rapidly at the beginning of experiments. The total mass of an element mobilized in dynamic produced water for 3 hours was estimated by equation 1.

$$\text{Total Mass of an element} = \int_0^t C(t) * Q * dt \ldots\ldots (1)$$

In this equation, C (t) is the intermediate concentrations of an element in produced water collected every half an hour and Q is the flow rate of core-flooding instrument. Compared with blank solution from the control experiment, 7 major elements (Na, S, Si,

Ca, Al, K, and Mg) and 2 trace elements (Sr and Rb) were enriched in all produced water. Due to short experimental duration, less enriched elements in produced water after dynamic experiment were detected than static experiments. Although ANOVA and PCA also were applied in dynamic experiments, shorter water-rock interaction in dynamic experiments led to statistics results were not as significant as these in static experiments. ANOVA results show p-values of all enriched elements were larger than the common significance level (0.05) (**Table 31**). Thus, there were no significant differences in these elements between chemofacies, although they were all enriched in produced water.

Table 31 Calculated p-values of enriched elements for chemofacies after dynamic experiments. Because of shorter interaction, no chemofacies are different from each other.

Enriched elements	**Na**	**Ca**	**Al**	**S**	**Si**	**Mg**	**Sr**	**Rb**	**K**
P-value	0.51	0.08	0.26	0.41	0.83	0.13	0.60	0.27	0.63

In PCA, loading plot obtained similar results as static experiments: Ca, Mg, and Sr were related to dissolution of carbonate minerals; K, Si, Na Al, and Rb were derived from dissolution of clay minerals or cation exchange; S was independent because of oxidation of pyrite (**Figure 31**). However, score plot cannot be obtained for dynamic experiments, because not enough enriched elements can be used.

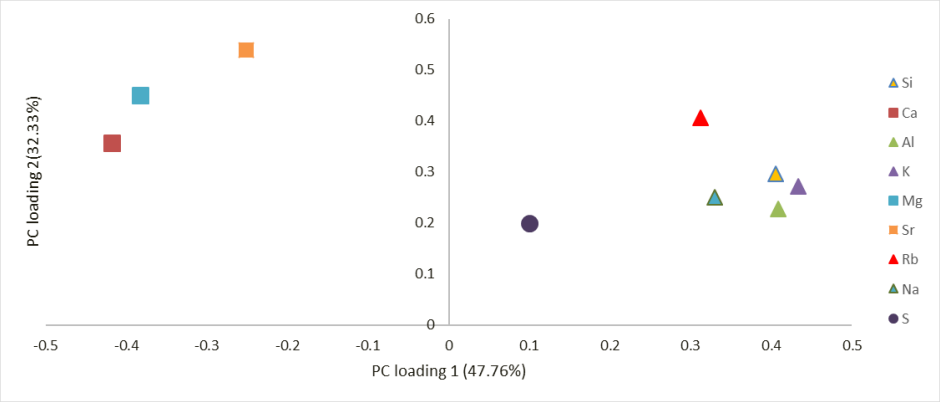

Figure 31 Loading plot of major elements in dynamic experiments shows the relationships between elements. Elements which are close have high correlation. The first and second principal components account for 47.76% and 32.33% of the variance in the original dataset, respectively.

Overall, based on water parameter and water composition analysis in both static and dynamic experiments, produced water after interacting with LEF2 had higher elemental concentrations and highest precipitation tendency relative to other chemofacies. It indicates strong water-rock interaction was observed in LEF2 of the lower Eagle Ford Formation. Thus, more attention should be paid to this chemofacies in terms of the hydraulic fracturing performance and treatment of flowback water after well completion.

Summary

To investigate impact of spatially varying reservoir mineralogy on hydraulic fracturing performance, static and dynamic water-rock experiments were conducted on deionized water and reservoir rocks from different chemofacies in the lower Eagle Ford

Formation. Rock samples were characterized for elemental concentrations and mineralogy first. Water samples were analyzed for ion contents, particle size, TDS, and zeta potential.

After water-rock interactions, 18 elements in static experiments and 9 elements in dynamic experiments were enriched in the produced water relative to blank solutions because of mineral dissolution. The sources of major elements were mainly from dissolution of carbonate and clay minerals, and cation exchange of rock particle. In static experiments, statistic test results indicate the combination of Ca, Al, Mg, Ni, and Ba concentrations in produced water was useful to distinguish different chemofacies and major elements divided chemofacies better than trace elements. Particles in produced water from LEF2 and LEF4 had higher precipitation tendency and were more likely to block small fracture openings during hydraulic fracturing according to analysis of particle size, TDS, and zeta potential. In dynamic experiments, because of short experimental duration and machine contamination, enriched elements were not helpful to identify chemofacies. However, water parameters measurements show particles in produced water from LEF2, LEF3, LEF4, and lower part of LEF1 were more likely to agglomerate because of high TDS, large particle size, or low absolute zeta potential. Thus, based on water analysis in both static and dynamic experiments, strong water-rock interaction was observed in LEF2 of the lower Eagle Ford Formation.

This chapter demonstrates that different interactions occurred at different depth within one shale formation because of vertical heterogeneity of the formation. These interactions had different effect on produced water properties. Thus, more attention should be paid to such heterogeneous shale reservoirs in terms of the hydraulic fracturing

performance and treatment of flowback water after well completion. In Chapter III, injected fluid was extended for flowback water and complicated flowback water-rock interactions were investigated to understand the effect of reinjection of flowback water on formation damage for the Marcellus Formation.

References

Abbott, J. E., and Francis, J. R. D. 1977. Saltation and Suspension Trajectories of Solid Grains in A Water Stream: Royal Society [London], Philosophical Transactions, v, 284, p. 225-254.

Abdulsattar, Z. R., Agim, K., Lane, R. H., and Hascakir, B. 2015. Physicochemical Interactions of Shale with Injected Water-Based Fluids, SPE International Symposium on Oil Field Chemistry, 13-15 April 2015, The Woodlands, Texas, USA, SPE-173727-MS. https://doi.org/10.2118/173727-MS

Abouzeid, A. Z. M., and Sinbawy, H. H. El. 1980. Calcination of Phosphates: Reactivity of Calcined Phosphate, Powder Technology, 26(1980)187-197.

Abrams, A. 1977. Mud Design to Minimize Rock Impairment Due to Particle Invasion. Society of Petroleum Engineers. doi:10.2118/5713-PA

Ali, M., and Hascakir, B. 2015b. Water-Rock Interaction for Eagle Ford, Marcellus, Green River, and Barnett Shale Samples, SPE Eastern Regional Meeting, 13-15 October, Morgantown, West Virginia, USA. https://doi.org/10.2118/177304-MS

Ali, M., and Hascakir, B. 2017. Water-Rock Interaction for Eagle Ford, Marcellus, Green River, and Barnett Shale Samples and Implications for Hydraulic Fracturing Fluid Engineering, SPE Journal, 22, 01, 162-171, SPE-177304-PA.

Allen, P. A., and Allen, J. R. 1990. Basin Analysis—Principles and Applications: Blackwell Sci. Pub., Oxford, 451 p.

Amin, S., Wehner, M., Heidari Z., and Tice, M. 2016. Rock Classification in the Eagle Ford Shale through Integration of Petrophysical, Geological, and Geochemical Characterization. SPWLA 57th Annual Logging Symposium, 25-29 June.

Balashov, V. N., Engelder, T., Gu, X., Fantle, M. S., and Brantley, S. L. 2015. A Model Describing Flowback Chemistry Changes with Time after Marcellus Shale Hydraulic Fracturing, AAPG Bulletin, V. 99, No. 1 (January 2015), pp. 143-154.

Burger, J., Sourieau, P., Combarnous, M., and Ramey, H. J. 1985. Thermal Methods of Oil Recovery. Gulf Publishing Company, Book Division. Technology & Engineering

Chermak, J. A., and Schreiber, M, E. 2013. Mineralogy and Trace Element Geochemistry of Gas Shales in the United States: Environmental implications. International Journal of Coal Geology 126 (2014) 32–44

Dawson, W. C. 1997. Limestone Microfacies and Sequence Stratigraphy: Eagle Ford Group (Cenomanian-Turonian) north-Central Texas outcrops: Gulf Coast Association Geological Societies Transactions, v. 47, p. 99-105.

Dawson, W. C. 2000. Shale Microfacies: Eagle Ford Group (Cenomanian-Turonian) North-Central Texas Outcrops and Subsurface Equivalents: Gulf Coast Association of Geological Societies Transactions, v. L, p. 607-622.

Dawson, W. C., and Almon, W. R. 2010. Eagle Ford Shale variability: Sedimentologic influences on source and reservoir character in an unconventional resource unit: Gulf Coast Association of Geological Societies Transactions, v. 60, p. 181-190.

Donovan, A. D., and Staerker, T. S. 2010. Sequence stratigraphy of the Eagle Ford (Boquillas) Formation in the subsurface of South Texas and outcrops of West Texas: Gulf Coast Association of Geological Societies Transactions, v. 60, p. 861-899.

Donovan, A. D., Pope, M. C., Gardner, R. M., Wehner, M. P., and Staerker, T. S. 2015. Making Outcrops Relevant to the Subsurface: Learnings from the Eagle Ford Group in West Texas: Unconventional Resources Technology Conference, San Antonio, Texas, 20–22 July, URTeC Paper 2154599, p. 558–573.

Donovan, A. D., Staerker, T. S., Pramudito, A., Li, G., Corbett, M. J., Lowery, C. M., Romero, A. M., and Gardner, R. D. 2012. The Eagle Ford Outcrops of West Texas: A Laboratory for Understanding Heterogeneities within Unconventional Mudstone Reservoirs. GCAGS Journal, v. 1 (2012), p. 162–185.

Elston, H. 2014. Mineralogical and Geochemical Assessment of the Eagle Ford Shale. The Ohio State University. School of Earth Sciences. Senior Thesis.

Everitt, B. 1998. The Cambridge Dictionary of Statistics. Cambridge, UK New York: Cambridge University Press. ISBN 978-0521593465.

Faust, M. J. 1990. Seismic Stratigraphy of the Mid-Cretaceous Unconformity (MCU) in the Central Gulf of Mexico Basin, Geophysics, 55(7), 868-884

Fisher, 1971. Section 7. The Test of Significance.

Fisher. R. A. 1921. On the "Probable Error" of a Coefficient of Correlation Deduced from a Small Sample. Metron 1, 3-32

Fisz, M. 1963. Significance Testing. Probability Theory and Mathematical Statistics (3 ed.). New York: John Wiley and Sons, Inc. p. 425.

Foldvari, M. 2011, Handbook of Thermogravimetric System of Minerals and Its Use in Geological Practice. Budapest, Hungary. Geological Institute of Hungary

Gibson, R. E. 1938. On the Effect of Pressure on the Solubility of Solids in Liquids. Am. Jour. Sci. Vol. 235-A, pp, 49-69.

Greenwood, R., and Kendall, K. 1999. Electroacoustic Studies of Moderately Concentrated Colloidal Suspensions. Journal of the European Ceramic Society. 19 (4): 479–488.

Hall, G. E. M. 1992. Inductively Coupled Plasma Mass Spectrometry in Geoanalysis: Journal of Geochemical Exploration, vol. 44, pp. 201-249. ev/1

Haluszczak, L. O., Rose, A. W., and Kump, L. R. 2013. Geochemical Evaluation of Flowback Brine from Marcellus Gas Wells in Pennsylvania, USA. Applied Geochemistry 28: 55-61.

Hanaor, D. A. H., Michelazzi, M., Leonelli, C., and Sorrell, C. C. 2012. The Effects of Carboxylic Acids on the Aqueous Dispersion and Electrophoretic Deposition of ZrO_2. Journal of the European Ceramic Society. 32 (1): 235–244.

Hayes, T. D. 2009. Sampling and Analysis of Water Streams Associated with the Development of Marcellus Shale Gas; Gas Technology Institute: December 2009.

Hentz, T. F., and Ruppel, S. C. 2011. Regional Stratigraphic and Rock Characteristics of Eagle Ford Shale in Its Play Area: Maverick Basin to East Texas Basin, Search and Discovery Article #10325, based on oral presentation at AAPG Annual Convention and Exhibition, Houston, Texas, USA, April 10-13, 2011.

Hildebrand, J. H. 1924. Solubility. New York: Chemical Catalog Co.

Jarvie, D. M., Hill, R. J., Ruble, T. R., and Pollastro, R. M. 2007. Unconventional Shale-Gas Systems: The Mississippian Barnett Shale of North-Central Texas as One Model for Thermogenic Shale-Gas Assessment: AAPG Bulletin, v. 91, no. 4, p. 475–499, doi:10.1306

Jenkins, R., and Snyder, R. L. 1996. Introduction to X-ray Powder Diffractometry, John Wiley, 403 p.

Kar, T., and Hascakir, B. 2017. In-situ Kerogen Extraction via Combustion and Pyrolysis. Journal of Petroleum Science and Engineering, Volume 154, 2017, Pages 502-512, ISSN 0920-4105, https://doi.org/10.1016/j.petrol.2017.01.051.

Kar, T., Ovalles C., Rogel, E., Vien, J., and Hascakir, B. 2016. The Residual Oil Saturation Determination for Steam Assisted Gravity Drainage (SAGD) and Solvent-SAGD. Fuel. 172. 10.1016/j.fuel.2016.01.029.

Law, B. E., and Spencer, C. W. 1993. Gas in Tight Reservoirs-An Emerging Major Source of Energy. in David G. Howell (ed.), The Future of Energy Gasses, US Geological Survey, Professional

Lester, Y., Ferrer, I., Thurman, E. M., Sitterley, K. A., Korak, J. A., Aiken, G., and Linden K. G. 2015. Characterization of Hydraulic Fracturing Flowback Water in Colorado: Implications for Water Treatment. Science of the Total Environment 512: 637-44.

Losev, E. S., Netrebko, N. V., and Orlova, I. V. 1989. Gravitational Sedimentation of Aggregating Particles in A Shear Flow. Fluid Dyn 24, 242–245 (1989). https://doi.org/10.1007/BF01075154

Moses, C. O., Nordstrom, D. K., Herman, J. S., and Mills, A. L. 1987. Aqueous Pyrite Oxidation by Dissolved Oxygen and by Ferric Iron. Geochim Cosmochim Acta 51:1561–1571

Pearson, K. 1901. On Lines and Planes of Closest Fit to Systems of Points in Space. Philosophical Magazine. 2 (11): 559–572.

Ramurthy, M., Barree, R. D., and Kundert, D. P. 2011. Surface-Area vs. Conductivity-Type Fracture Treatments in Shale Reservoirs. SPE Production & Operations 24 (04): 357-367

Robinson, C. R. 1997. Hydrocarbon Source Rock Variability within the Austin Chalk and Eagle Ford Shale (Upper Cretaceous), East Texas, USA: International Journal of Coal Geology, v. 34, p. 287-305.

Salimen, R., Plant, J., and Reeder, S., eds. 2006. Geochemical Atlas of Europe. Part 1, Background Information, Methodology and Maps. Espoo, Finland, Geological Survey of Finland, 526pp

Thompson, K. C., and Nathanail, P. 2003. Chemical Analysis of Contaminated Land (Sheffield Analytical Chemistry. 1st Edition, ISBN-13: 978-0849328107 Hall, G. E. M. 1992. Inductively Coupled Plasma Mass Spectrometry in Geoanalysis: Journal of Geochemical Exploration, vol. 44, pp. 201-249.

Treadgold, G. 2011. Sedimentology and Diagenesis of the Upper Cretaceous Austin Chalk Formation, South Texas and Northern Mexico: PhD Dissertation, Rice University, Houston, Texas, 532 p

Tribovillard, N., Thomas, J. A., Timothy, L., and Armelle, R. 2006. Trace Metals as Paleoredox and Paleoproductivity Proxies: An Update. Chemical Geology 232 (1–2): 12–32. doi:10.1016/j.chemgeo.2006.02.012.

Tukey, J. 1949. Comparing Individual Means in the Analysis of Variance. Biometrics. 5 (2): 99–114. JSTOR 3001913

U.S. Energy Information Administration (EIA). 2014. Updates to the EIA Eagle Ford Play Maps. U.S. Department of Energy Washington, DC 20585.

U.S. Energy Information Administration (EIA). 2019. U.S. Crude Oil and Natural Gas Proved Reserves, Year-End 2018. U.S. Department of Energy. Washington, DC 20585

Wang, L., Burns, S., Giammar, D. E., and Fortner, J. D. 2016. Element Mobilization from Bakken Shales as a Function of Water Chemistry. Chemosphere 149, 286-293.

Wang, L., Fortner, J. D., and Giammar, D. E. 2015. Impact of Water Chemistry on Element Mobilization from Eagle Ford Shale. Environ. Eng. Sci. 32, 310-320

Weber, W. J. 1972. Physicochemical Processes for Water Quality Control, Wiley Interscience, ISBN 0-471-92435-0.

Winter, J. A. 1961. Stratigraphy of the Lower Cretaceous (Subsurface) of South Texas: Gulf Coast Association of Geological Societies Transactions, v. 11, p. 15-24.

World Health Organization (WTO). 2011. Hardness in Drinking-water. Background Document for Development of WHO Guidelines for Drinking-water Quality. WHO/HSE/WSH/10.01/10/R

Wright, A. M., and Ratcliffe, K. 2010. Application of Inorganic Whole Rock Geochemistry to Shale Resource Plays. Canadian Unconventional Resources and International Petroleum Conference, Calgary, Alberta, Ca

Zhou, B., Han, S., Raja, R., and Somorjai, G. 2007. Nanotechnology in Catalysis 3. New York, New York. Springer Science & Business Media

Ziemkiewicz, P. F., and Thomas, H. Y. 2015. Evolution of Water Chemistry during Marcellus Shale Gas Development: A Case Study in West Virginia. Chemosphere 134:224-31.

CHAPTER III

THE IMPACT OF RE-INJECTING FLOWBACK FLUIDS ON FORMATION DAMAGE. CASE STUDY: THE MARCELLUS SHALE*

The Petroleum Industry commonly reuses flowback water in hydraulic fracturing to reduce consumption, transportation, and treatment cost of water. However, due to complex flowback water-reservoir rock interactions, impurities carried by flowback water and mineral precipitation may plug pores and fractures, which leads to formation damage and lowers recovery efficiency. Thus, it is critical to investigate flowback water-rock interactions for understanding the changes within the reservoir and minimizing formation damage.

Interactions between reservoir rocks and flowback water from the Marcellus Formation were investigated in this chapter. Simple deionized water-rock experiments and complicated flowback water-rock experiments were conducted under static and dynamic conditions. Before and after interacting with water, rock samples were analyzed to determine the changes on the rock surfaces, in terms of elemental concentrations, mineralogy, and surface morphology. Produced water samples were characterized to evaluate particle precipitation tendency and effects on hydraulic fracturing performance, in respect of ion contents, particle size, TDS, and zeta potential.

---

* Reprinted with permission from "A Laboratory Study of the Impact of Reinjecting Flowback Fluids on Formation Damage in the Marcellus Shale" by Zhang et al., 2020. SPE Journal, pages 788-799, in April 2020, Copyright [2020] by Society of Petroleum Engineers.

Compared with deionized water-rock interaction with flowback water-rock interaction, rock surfaces after flowback water-rock interaction demonstrate elemental composition change, more fine particles attachment, and new mineral accumulation because of flowback water contamination. In produced water, elemental concentrations, especially for Na and Cl ions, were abundant after flowback water-rock interactions, which were mainly mobilized from flowback water. Water parameter analysis indicates that particles in produced water after interacting with flowback water had highest precipitation tendency due to the highest TDS, largest particle size, and lowest absolute zeta potential. Thus, based on rock and water analysis, if flowback water without any pre-treatment would be reused in the subsequent hydraulic fracturing, blockage of created pores and flow pathways are more likely to occur. However, after filtration applied on flowback water, reinjection of flowback water does not complicate further the water-rock interaction and does not cause significant formation damage in the fractures.

This chapter aims to make a comparison between deionized water-rock interaction and flowback water-rock interaction to further understand the basic water-rock interaction mechanisms and evaluate formation damage caused by reuse of flowback water. The results improve our understanding on better management of flowback water.

3.1 Introduction

U.S. Energy Information Agency reported that the United States has the second largest technically recoverable shale oil resources and fourth largest technically

recoverable shale gas resources (EIA, 2013). Therefore, shale resources exist in large quantities in the United States. To extract oil and gas from shale formations effectively, hydraulic fracturing was applied extensively. It is a hydrocarbon well development process in which millions of gallons of pressurized water, sand, and, small volumes of chemical additives are injected into low-permeability shale reservoirs to create small fractures and enhance gas and fluid flow (Gandossi and Von Estorff, 2015). It has been used for over 60 years in the U.S. but has been widespread since 2008, which leads to the significantly increase in production of oil and natural gas in the U.S. and creates "shale revolution" (Brown and Yucel, 2013; EIA, 2014).

Among all the shale formations, the Marcellus Formation is the most popular target for gas exploration because it contains the estimated proved reserves of natural gas representing 39.6% of all the U.S. shale gas (EIA, 2019). It is also one of the first shale formations to be tapped, after the Barnett Formation in Texas. However, although the Marcellus Formation has long been known as an organic-rich shale in the Appalachian Basin, gas production using traditional vertical drillings was too low to be economical for the energy companies involved due to the extremely low permeability of shale units. However, the application of horizontal drilling and hydraulic fracturing enables greater access to natural gas from the Marcellus Formation. According to the latest EIA report, the Marcellus Formation daily natural gas production was only 1.2 billion cubic feet in 2008, while reached more than 20 billion cubic feet in 2019 (EIA, 2019).

The Marcellus Formation is an extensive black shale unit deposited in the Appalachian Basin during the Middle Devonian, about 390 million years ago, which

extends from New York State in the north to northeastern Kentucky and Tennessee in the south (Clark, 1981). It was first named as “Marcellus Shale” for exposures of organic-rich black shales at the town of Marcellus, Onondaga County, New York by James Hall (1839) and has been known as the Marcellus Formation recently which is subdivided into the Union Springs Shale, Cherry Valley Limestone, and the overlying Oatka Creek Shale from bottom to top (Cooper, 1930; Lash and Engelder, 2011). Compared with the Oatka Creek Shale, the Union Springs Shale has a significantly higher organic matter concentration, which is the most gas productive part of the Marcellus Formation (Popova et al., 2015). Sedimentary rocks present in the Marcellus Formation are described as organic-rich black shale interbedded with thin dark-gray silty shale and limestone layers (Ettensohn and Barron, 1981; Harper, 1999). The minerals in the Marcellus Formation are made up of quartz, mixed-layer clays (illite, kaolinite, and smectite), calcite, dolomite, feldspar, pyrite, and gypsum (Zielinski and McIver, 1982; Hosterman and Whitlow, 1983; Avary and Lewis, 2008; Boyce and Carr, 2009; Paronish et al., 2016). Among them, quartz, carbonate minerals, and illite are reported to account for the largest weight percentage. The high percentage of quartz and carbonate minerals improves brittleness of the shale unit and leads to hydraulic fracturing easier to create fractures in the Marcellus Formation.

Although the combination of hydraulic fracturing with horizontal drilling causes a huge boom in the extraction of natural gas in the Marcellus Formation, public concerns about potential impacts on drinking water and other environmental damage have significantly grown. Recent studies working on flowback water from Marcellus Formation gas wells reported that the average injection water volumes for hydraulic fracturing are

5.6 million gallons and 10-40% of wastewater returns to the surface as flowback water (Hurdle, 2018; Gregory et al., 2011). Moreover, the TDS found in Marcellus Formation flowback water range from 20,000-150,000 mg/L and is mainly made up of Na, Cl, Mg, Ca, Ba, Sr, Fe, Mn, K, and Br ions. (Gregory et al., 2011; Haluszczak et al., 2013; Ziemkiewicz and Thomas, 2015). The regulated metals along with some toxic organic components in Marcellus Formation flowback water exceed the drink water maximum contaminant standards level up to thousands of times (Hayes, 2009; Haluszczak et al., 2013; Ziemkiewicz and Thomas, 2015). Therefore, the high-volume wastewater produced during hydraulic fracturing with complicated chemical composition poses a great challenge for flowback water management. In Pennsylvania, the U.S. Environmental Protection Agency's has banned the disposal of hydraulic fracturing wastewater at public sewage plants to prevent untreatable contaminants entering public water systems since 2011. In New York, hydraulic fracturing was banned by the New York Department of Environmental Conservation in 2015 to protect public drinking water (National Law Review, 2015). Currently, except Ohio, there are limited underground injection wells that are used to dispose of flowback water from Pennsylvania and West Virginia. Thus, to reduce the amount of fresh water needed for well development and minimize the costs associated with disposal of flowback water in the Marcellus Formation, reuse of flowback water has been highly emphasized and commonly chosen by industry. By 2013, 90% of Marcellus flowback water has been reused or recycled in Pennsylvania and this trend has continued to the present (Davarpanah, 2018).

However, injecting flowback water may cause formation damage and deteriorate HF because of extremely high TDS levels in flowback water. The reuse of untreated or little treated flowback water could largely reduce treatment and disposal costs, but it may lower the recovery efficiency because of reduced fracture and/ or matrix permeability caused by impurities from flowback water and mineral precipitation from flowback water-rock interaction. Thus, it is important to understand the flowback water-rock interactions on formation damage during hydraulic fracturing.

Formation damage mechanisms, including physical and chemical damage, have been well studied. Physical formation damage refers to the reduction of formation permeability by nonchemical water-rock interaction. Fine particle migration and blockage is the main physical damage mechanism (Holditch, 1979; Gabriel and Inamdar, 1983; Civan, 2015). Chemical formation damage is caused by incompatibility between formation rock and fluids. Clay minerals, especially for smectites, tend to swell and cause the blockage of pore throats when being exposed to foreign fluids (Jones, 1964; Eslinger and Pevear, 1988). In shale formations, several studies demonstrate that clay minerals are the main source of formation damage (Yue, 2012; Zhang, 2017). However, besides clays, other minerals present in the reservoir rocks and components from injected fluids also contribute to water-rock interaction and their mutual effect will result in differences.

As more energy companies prefer to re-inject flowback water, formation damage possibly caused by flowback water has been paid more attention. However, the flowback water-rock interactions are not very well understood because components of this interaction require to develop understanding on different interactions occurring when

flowback water and reservoir rock come in touch. Therefore, this chapter investigates flowback water rock interaction to understand impact of re-injecting flowback water on the formation damage in the Marcellus Formation.

3.2 Materials and Methods

Marcellus Formation rock and flowback water samples were collected at depth of 6493.7 feet from a horizontal well of the Marcellus Formation by Southwestern Energy Company in the Appalachian Basin (**Figure 32**).

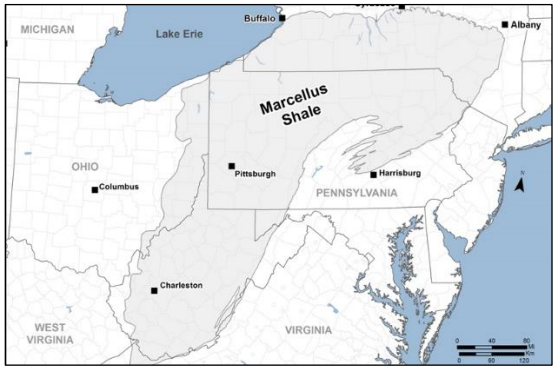

Figure 32 The location map for the Marcellus Formation. Reprinted in Drexel University (2017).

Before conducting water-rock experiments, rock sample was crushed and sieved into about 250 μm to increase rock surface areas to water ratio, which accelerates interaction rate. The detailed comparison of estimated lab and field conditions about rock surfaces to water volume ratios is provided in the Appendix B. After similar calculation

as Chapter II, the Marcellus Formation rock surface area to the water volume ratios in static and dynamic experiments are approximately 19.96 cm^2/mL and 8.28 cm^2/mL. In field scale, estimated rock surface area to water ratio ranges in hydraulic fracturing are 2-20 cm^2/mL, based on the assumption the small fracture width ranges are from 0.1-1 cm (Ramurthy et al., 2011; Abdulsattar et al., 2015). Compared the estimated lab and field rock surface to water volume ratios, the size of crushed rock samples and water volume used in static and dynamic experiments are reasonable.

Crushed rock sample was characterized by X-ray Photoelectron Spectroscopy (XPS), powder X-ray Diffraction (XRD), and high-resolution field emission Scanning Electron Microscope (SEM) for elemental concentrations, mineralogy, and morphology of the rock surfaces, respectively. The measurement depth and detection limits of these instruments are listed in **Table 32.** Compared with the size of crushed Eagle Ford Formation samples in Chapter II, the Marcellus Formation sample was crushed smaller because better measurement results can be obtained from XPS and SEM by analyzing relatively homogeneous sample surfaces with smaller particle size (Moulder et al., 1995). Moreover, XPS was used to determine the elemental concentrations of Marcellus Formation rock surfaces rather than XRF used in Chapter II for Eagle Ford Formation samples because XPS was more sensitive to detect some elements mobilized from flowback water, such as Na, Cl, C, and O (Moulder et al., 1995).

Table 32 Penetration depth and detection limits for XPS, XRD, and SEM (Moulder et al., 1995; Goldstein et al., 2003).

Equipment	Application	Penetration Depth	Detection Limit
XPS	Surface Elemental Composition	1~2 nm	0.1%~1%
XRD	Crystallized Compounds	on the order of μm	1%~2%
SEM	Surface morphology	on the order of μm	20X to 30000X

XPS is used for qualitative analysis of elements on a surface and can detect all elements except hydrogen and helium (Hercules and Hercules, 2008). In XPS analysis, a low-resolution scan survey spectrum was conducted first to identify elements present in rock samples. Then high-resolution scans were repeated three times to combine spectra and determine percentage atomic concentration of each element (Moulder et al., 1995). Atomic percent of elements obtained from XPS was converted to weight percent for data comparison and analysis. The same crushed samples were analyzed by XRD which is primarily used for phase identification of a crystalline material. The scan range was set at scanning speed of 2 degrees per minute from 5-65 degrees (Jenkins and Snyder, 1996). In addition, SEM provides images of the surface of a sample at high magnifications (Stokes, 2008). In this chapter, the morphology of rock surface was observed by SEM at 2500 magnification. Besides inorganic constituents in rock sample, organic matter was estimated by thermal gravimetric analysis (TGA) at constant heating rates of 5 ℃/min under 50 ml/min air and 20ml/min nitrogen gas injection from 25-900℃ (Burger et al., 1985). In shale, major part of organic matter is kerogen which is entirely consumed approximately 500-550 ºC and releases CO_2 and H_2O gases through reaction 1 (Abouzeid and Sinbawy, 1980). While calcite, the major carbonate minerals in the Marcellus

Formation sample, begins to decompose around 600 ºC and release CO_2 gas through reaction 2 (Burger et al., 1985). Therefore, kerogen and calcite decompose at different temperature intervals during combustion of shale samples, which can be identified by the weight loss of shale samples through TGA.

$$\text{Kerogen} \rightarrow H_2O_{(g)} + CO_{2(g)} \ldots\ldots\ldots (1)$$

$$CaCO_{3(s)} \rightarrow CaO_{(s)} + CO_{2(g)} \ldots\ldots\ldots (2)$$

To understand the constituents of flowback water, it was analyzed before water-rock experiments. Firstly, 200 ml untreated flowback water was evaporated in oven for one week and dried residue was analyzed for surface elemental composition with Energy Dispersive X-Ray Spectroscopy (EDS) and for mineralogy with XRD. EDS was used rather than XPS because flowback residue was continuously outgassing which made XPS instrument unstable. In addition, considering extremely high salinity levels of flowback water, to protect equipment, initial flowback water sample was filtered through a 2.5 µm filter paper. Filtered flowback water was further analyzed and used as injected water in the following experiments (**Figure 33**).

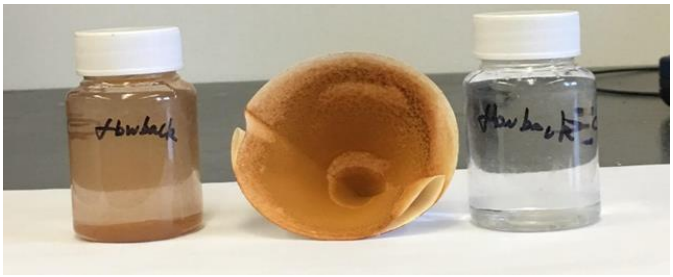

(a) (b) (c)

Figure 33 The untreated flowback water is colored orange with some suspended solids settled within the water. (a) Initial flowback water without any treatment (b) used 2.5 µm filter paper (To protect equipment, filter paper was used), and (c) filtered flowback water

In filtered flowback water, ion contents were analyzed by ICP-MS and Ion Chromatography 900 (IC 900). ICP-MS was primally used to detect cations and IC 900 was used for anions. Elements that can be analyzed and detection limits of ICP-MS and IC 900 are listed in **Table 33**. Because of the detection limit of each equipment, a 1:50 dilution of filtered flowback water sample was made for ICP-MS analysis and a 1:10 dilution was made for IC 900 analysis (Sugiyama and Tanoshima, 2007; Gros, 2013).

Table 33 Ions detected by ICP-MS and IC 900

Equipment	Detected Elements/ Ions	Detection Limit
ICP-MS	Na, Si, Ca, Al, S, K, Fe, Ti, Mg, Sr, Mo, Zn, Ni, Cu, V, Rh, Sn, P, Mn, As, Co, Pb, Th, Rb, Y, U, Cr, Zr and Nb	ppb range
IC 900	Cl, Br, F, SO_4^{2-} and NO_2^-	ppm range

To assess the precipitation tendency of particles in filtered flowback water, TDS, zeta potential, and particle size were analyzed. In general, water with higher TDS contains more particles and increases the chance of particles to form precipitates due to interaction between ionized substances. Particles in water with larger size tend to precipitate because

the increase in particle diameter results in the increase in settling velocity. Particles with smaller absolute zeta potential values have low stability and are more likely to coagulate or flocculate because attractive forces between particles exceed repulsive force (Kaya et al., 2003; Greenwood and Kendall, 1999). Therefore, particles in water with high TDS, low absolute zeta potential, and large particle size have high precipitation tendency (Weber, 1972; Ali et al., 2016). Because TDS of filtered flowback were still too high to be measured by TDS probe, according to procedure provided in USEPA (1999), it was estimated by measuring weight of residue after evaporating 20 ml filtered flowback water in a pre-weighed container in an oven. Zeta potential was analyzed by a Nano ZetaPALS instrument by Brookhaven Instruments Corporation. Particle size was obtained by a 90Plus Particle Size analyzer. In addition, pH of water samples was analyzed by a pH probe.

After completion of rock and flowback water characterization, static and dynamic water-rock experiments were conducted under different conditions. Rock sample was exposed to both deionized water and Marcellus Formation flowback water to better visualize the interaction between rock and flowback water. In static experiments, 10 g crushed rock sample interacted with 50 ml water for three weeks at room conditions (71°F and 1 atm) to simulate the stagnant water conditions. In dynamic experiments, the same core-flooding experimental set-up was used to simulate continuous water injection at reservoir conditions (refer to Figure 27). Water was continually injected at 18 ml/min rate into the core-holder containing about 280 g crushed rock sample for three hours at reservoir conditions and produced water was collected every half an hour. To avoid escape

of rock particles from core-holder in produced water container, a mesh and a filter paper were placed at the bottom of the core holder. Dynamic experimental temperature was maintained between 155-165 °F based on reservoir temperature at collection depth and pressure was retained at 75 psig. In addition, to trace possible artificially introduced contamination, a dynamic experiment without any rock samples was conducted through the core-flooding experimental system and collected water sample was subjected to same analyses that the produced water samples through core flood experiments were subjected.

After static and dynamic experiments, rock and water analyses were repeated to investigate the change on the rock surface and in water properties.

3.3 Results and Discussions

3.3.1 Rock Characterization

Prior to water-rock experiments, Marcellus Formation rock sample was characterized by XPS and XRD to estimate surface elemental concentrations and mineralogy (**Figure 34**).

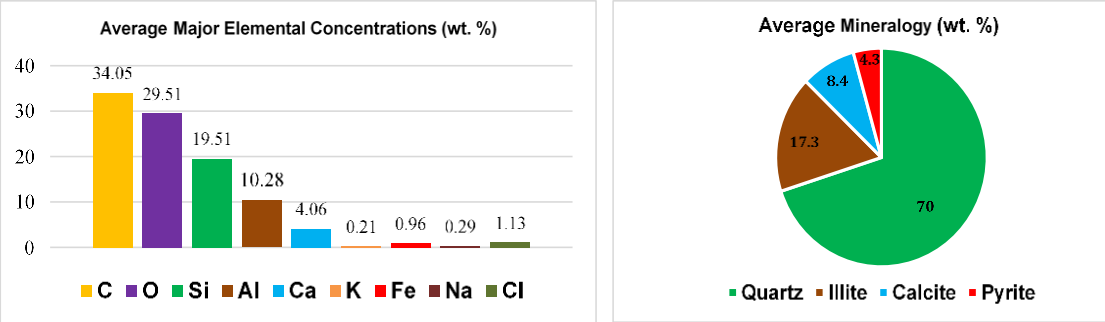

Figure 34 Characterization of Marcellus Formation rock sample. Elemental compositions were obtained by XPS on the left and mineralogy were obtained by XRD on the right.

In XPS result, 9 elements (C, O, Si, Al, Ca, K, Fe, Na, and Cl) represented more than 0.1% of the initial rock sample. The XRD measurement shows minerals in the Marcellus Formation rock sample mainly consist of quartz, illite, calcite, and pyrite. The major elements detected by XPS can be used to verify minerals identified by XRD. In addition, the carbon source derived from organic and inorganic contents in the rock was further analyzed by TGA. The TGA plot indicating the weight remaining of initial sample is given in **Figure 35**.

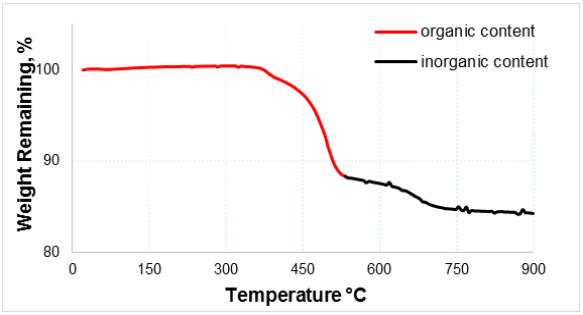

Figure 35 TGA plot of initial Marcellus Formation rock sample. The red curve indicates the decomposition of organic matter and black curve indicates the decomposition of inorganic matter. The weight loss reached 11.70% at 532°C and 15.76% at 900°C.

In general, during combustion of a shale sample, organic matter decomposition and inorganic matter decomposition occur sample during different temperature intervals and cause weight loss in TGA curve (Burger et al., 1985). Kerogen, major part of organic matter in shale, is entirely consumed approximately 500-550 ºC (Abouzeid and Sinbawy, 1980). Calcite, the major inorganic mineral containing carbon in Marcellus Formation sample, starts decomposing at around 600 ºC (Burger et al., 1985). Illite begins to release its hydroxyl group as water at around 550 ° C (Foldvari, 2011). In the TGA plot, the curve slope started to decrease at around 532°C, which indicates the end of organic matter decomposition and the beginning of inorganic matter decomposition. The weight loss reached 11.70% at 532 °C and became 15.76% at 900 °C. Therefore, the weight loss at 532°C is mainly associated with decomposition of kerogen and the weight loss between 532°C and 900°C is 4.10% caused by calcite decomposition and illite dehydroxylation.

3.3.2 Flowback Water Characterization

The quality of flowback water was determined before interacting with rock sample (**Figure 36**).

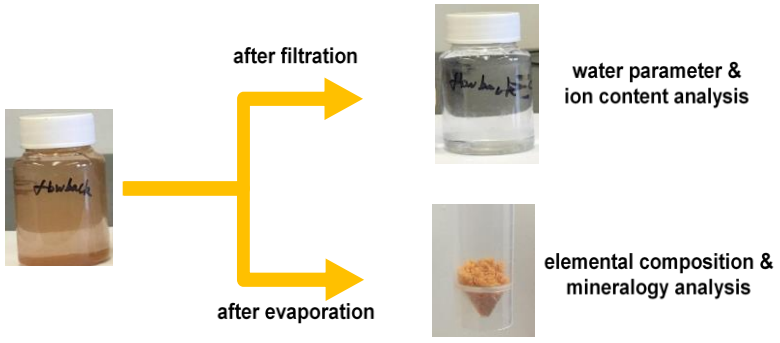

Figure 36 Flowback water characterization: initial flowback water was filtered and evaporated respectively and then analyzed.

Water parameters, including particle size, TDS, and zeta potential, were analyzed to evaluate particle precipitation tendency in filtered flowback water. Deionized water was used as blank solution and injected water in the experiments. Compared to deionized water, water parameters listed in **Table 34** show flowback water had much higher TDS, larger particle size, and lower absolute zeta potential, indicating a much higher precipitation tendency. Moreover, even if initial flowback water was filtered through a 2.5 μm sized filter paper, the size of particles in filtered flowback water was still much larger than the pores of the filter paper perhaps because of inevitable and continuous agglomeration of constituents in filtered flowback water. In addition, deionized water had a neutral pH of 7.4, while filtered flowback water was acidic with pH of 3.7. The possible sources of acidity came from HF chemicals or constituents in shale reservoir.

Table 34 Characterization of deionized water and filtered flowback water. Deionized water was used as blank solution and injected water in our experiments.

Water Samples	TDS, ppm	Particle Size, nm	Absolute Zeta Potential, mV	pH
Deionized water	85.9	502	31.27	7.4
Filtered Flowback Water	116,070	17,039	1.05	3.7

To understand the constituents in flowback water, filtered flowback water was characterized by ICP-MS and IC 900 for ion contents. Ions more than 0.1 ppm are listed in **Table 35**. The rest ions with lower concentrations are given in **Table B-1**. In deionized water (blank solution), small abundances of Na, Si, Cl, and S residual were detected. These elements are the difficult part to be removed by deionization. The rest elements were not detected or below the detection limit. In filtered flowback water, 18 elements (Cr, Rb, Ni, Cu, Na, Al, Mg, Si, S, Ca, Ti, Mn, Fe, As, Sr, K, Cl, and Br) were detected. The sources of these elements were derived from salts from formation water and minerals in the reservoir rocks (Haluszczak et al., 2013; Ziemkiewicz and Thomas, 2015). Among them, Na, Cl, Sr, Ca, K, Br, Mg, Fe, and K are ions typically reported in high concentrations in Marcellus Formation flowback water and represent a large fraction of the TDS (Haluszczak et al., 2013; Ziemkiewicz and Thomas, 2015; Hayes, 2009).

Table 35 Ion contents in deionized water and filtered flowback water analyzed by ICP-MS and IC 900. Listed ions were more than 0.1 ppm in the water samples. Deionized water was used as blank solution.

Ions in samples, ppm	Deionized water	Filtered flowback water
Cr	0	1.5
Rb	0	0.4
Ni	0	0.2
Cu	0	3.5
Na	47	84449
Al	0	0.5
Mg	0	674
Si	2	4.1
S	0.1	1.5
Ca	0	3904
Ti	0	0.51
Mn	0	2.4
Fe	0	46.3
As	0	0.3
Sr	0	7894
K	0	114
Cl	5.5	27868
Br	0	716

Meanwhile, surface elemental concentrations and mineralogy of the evaporation residue of initial flowback water were analyzed by EDS and XRD. The EDS result shows flowback residue was comprised of 9 elements (C, O, Na, Cl, Ca, Mg, Fe, K, and Sr) (**Figure 37**).

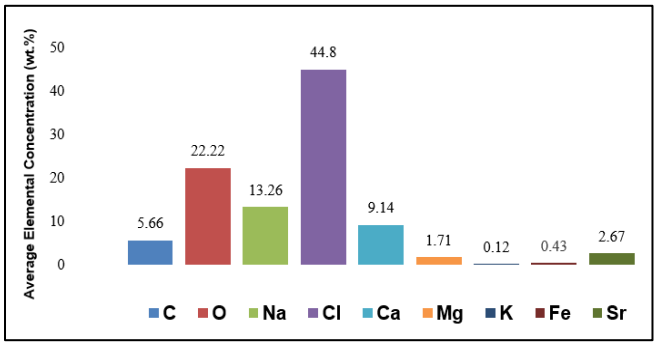

Figure 37 Characterization of residue from evaporation of initial flowback water

EDS is useful to analyze elemental concentrations of homogeneous samples with measurement depth at the level of micron scale (Goldstein et al., 2003). SEM images show surface of flowback residue was relatively flat and homogeneous, while surface of rock sample was rough and heterogeneous. Thus, EDS was more suitable for analyzing flowback residue rather than heterogeneous rock samples (**Figure 38**). According to EDS and other rock analysis results, the sources of C and O in flowback water were organic materials or inorganic materials. Other elements (Na, Cl, Ca, K, Mg, Fe, and Sr) had the same sources as flowback water because they were also detected in high concentrations in filtered flowback water (refer to Table 35). In XRD analysis, halite (NaCl) was the only mineral identified in flowback residue probably because NaCl was a highly ordered crystal while other constituents were in amorphous and poorly crystalline forms which were difficult to be detected by XRD (Klug and Alexander, 1974).

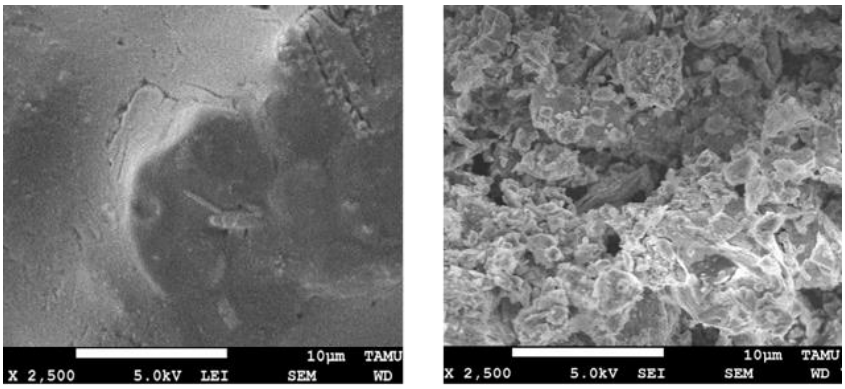

Figure 38 SEM Images of (a) flowback residue and (b) initial Marcellus Formation rock sample at 2,500X magnification. Surface of flowback residue is homogeneous relative to rock sample. Therefore, EDS is more suitable for analyzing it rather than heterogeneous rock sample.

3.3.3 Water-Rock Interaction Results

To better understand the influence of re-injection of flowback water on water-rock interaction, static and dynamic experiments were conducted both with deionized water and flowback water. Prior to water-rock experiments, deionized water was injected into an empty core holder at dynamic experimental settings as a control experiment to determine possible contaminations from core-holder and pipes. The produced water sample was collected and analyzed as blank solution for dynamic experiments. After control experiments, deionized water-rock and flowback water-rock tests at static and dynamic conditions were investigated experimentally, respectively.

3.3.3.1 Produced Water Characterization

In static experiments, rock sample interacted with deionized water and filtered flowback water for three weeks at room temperature and pressure (71°F and 1 atm). After experiments, TDS, zeta potential, particle size, and pH in produced water samples were analyzed to estimate the precipitation tendency of particles in water (**Table 36**).

Table 36 Characterization of produced water samples from static experiments

Samples	Static Experiments	Average TDS, ppm	Average Particle Size, nm	Average Absolute Zeta Potential, mV	pH
Water Samples	DI Water	85.9	502	31.27	7.4
	Filtered Flowback Water	116,070	17,039	1.05	3.7
Water-Rock Interaction	With DI Water	2770	1,245	4.38	7.5
	With Filtered Flowback Water	117,800	26,021	0.25	6.2

After deionized water-rock interaction, produced water became colloidal suspension from solution, according the change in the particle sizes. TDS and particle size in produced water became 32 times and 2.5 times higher than these parameters in deionized water, respectively. Stability behavior of particles after experiment was changed from moderate stability to rapid coagulation due to the decrease in absolute zeta potential. The pH value of produced water increased slightly due to dissolution of calcite. After flowback water-rock interaction, produced water shows the increases in TDS by 1.5% and particle size by 50% as well as lower absolute zeta potential indicating rapid coagulation behavior relative to injected filtered flowback water. The pH value of produced water increased from 3.7 to 6.2, which indicates hydrogen ions were neutralized by calcite through reaction 3.

$$CaCO_3(s) + 2H^+_{(aq)} \rightarrow Ca^{2+}_{(aq)} + CO_{2(g)} + H_2O_{(l)} \text{ …….. (3)}$$

Although water parameters in produced water after being exposed to deionized water and flowback water both indicate higher precipitation tendency relative to injected

water, particles in produced water after flowback water-rock interactions were more likely to block pores due to the extremely largest TDS, biggest particle size, and smallest absolute zeta potential among all water samples. If flowback water was injected and stayed in created fractures, small suspended particles in water would continue to grow and agglomerate because of water-rock interaction. According to Abrams' theory, particles with size ranges between 1/3 and 1/7 the size of pore throat can plug pores (Abrams, 1977). Thus, after deionized water-rock interaction, particles with average size of 1.25 μm can block pores with size range of 3.7-8.7 μm. After flowback water-rock interaction, particles with average size of 26 μm can block pores with size range of 78-182 μm. Therefore, if flowback water was reused in field HF operation, bigger pores would be blocked due to flowback water-rock interaction.

All produced water samples in static experiments were measured by ICP-MS and IC 900 for ion contents. If the concentration of one element in produced water after experiment was three times higher than that in blank solution (DI water or initial filtered flowback water), it was assumed to be mobilized from rock sample rather than water contamination (Thompson and Nathanail, 2003). Ion content results are summarized in **Table 37**.

Table 37: Ion contents in water before and after static experiments, ppm.

Static Experiments	Water Samples		Water-Rock Interaction	
	DI Water	Filtered Flowback	With DI Water	With Filtered Flowback
U	0	1.5	0.3	0
Cr	0	1.5	0	1.6
Co	0	0	0.2	0.5
Mo	0	0	67	12
Ni	0	0.2	3.1	8.2
Cu	0	3.5	0	0.9
Na	47	84449	308	82031
Al	0	0.4	0.3	0.8
Mg	0	674	5.5	657
Si	2.1	4.1	9.3	13.4
S	0.1	1.5	539	6.6
Ca	0.1	3904	277	4225
Ti	0	0.5	1.1	0.7
Mn	0	2.4	0	3.8
Fe	0	46.3	0	1.9
As	0	0.3	0	0.1
Sr	0	7894	64	8027
K	0	114	117	151
Cl	5.5	27868	432	23884
Br	0	716	3.6	466

After deionized water-rock interaction, 15 elements (U, Co, Mo, Na, Al, Ni, Mg, Si, S, Ti, Ca, Sr, K, Cl, and Br) were enriched in the produced water relative to injected water. Based on the mineralogy of Marcellus Formation sample and possible water and mineral reactions (**Table 38)**, Ca was released by dissolution of calcite because it was soluble in water with dissolved CO_2 (Benjamin, 2002). Sr was strongly associated with Ca by substitution for Ca in calcite (Salimen, et al., 2016). Si, K, Mg, and Al were a result of dissolution of small amount of illite or cation exchange between water and rock particles (Carroll, 1959). S was enriched in produced water but Fe was not because Fe^{2+} in pyrite was oxidized to form ferrihydrite ($Fe(OH)_3$), which was insoluble in water and precipitated out of water (Moses et al., 1987). Trace elements (U, Co, Mo, Na, Ni, Ti, and

Br) that were substituted for major elements in mineral structures or absorbed on surfaces of clay mineral and organic matter were released to water as mineral dissolution and cation exchange processes (Long and Angino, 1982).

Table 38 Mineralogy and Possible Dissolution/Precipitation Reactions in Marcellus Formation Rock Sample

Quartz	$SiO_{2(s)}+2H_2O=H_4SiO_{4(aq)}$
Illite	$K_{0.6}Mg_{0.25}Al_{2.3}Si_{3.5}O_{10}(OH)_2+11.2H_2O=0.25Mg^{2+}+0.6K^{+}+2.3Al(OH)_4^{-}+3.5H_4SiO_{4(aq)}+1.2H^{+}$
Calcite	$CaCO_3=Ca^{2+}+CO_3^{2-}$
Pyrite	$4FeS_2+15O_2+14H_2O=4Fe(OH)_3+8SO_4^{2-}+16H^{+}$

After flowback water-rock interaction, 5 elements (Si, Co, Mo, S, and Ni) were enriched in the produced water relative to filtered flowback water. Although less enriched elements were detected in produced water after flowback water-rock interaction relative to deionized water-rock interaction, it should be noted that Na, Sr, Cl, Mg, Ca, Br, and K were in high concentrations in produced water but mainly mobilized from flowback water rather than from rock sample. In addition, the decreases in Na, Cl, and Br concentrations in produced water after flowback water-rock interaction were mainly caused by related constituents precipitated on rock surfaces, which will be discussed in the rock characterization section.

In dynamic experiments, water was continuously injected for three hours at reservoir conditions. Produced water samples were collected every half an hour and characterized for TDS, zeta potential, and particle size. The average water parameters are listed in **Table 39** and water parameters for each water sample are given in **Table B-4**.

Table 39 Characterization of produced water samples from dynamic experiments

Samples	Dynamic Experiments	TDS, ppm	Particle Size, nm	Absolute Value of Zeta Potential, mV	pH
Water Samples	DI Water	87.3	418	34.08	7.4
	Filtered Flowback Water	116,070	17,039	1.05	3.7
Water-Rock Interaction	With DI Water	533	13,860	8.40	7.8
	With Filtered Flowback Water	124,300	16,950	1.24	7.1

After deionized water-rock interaction, TDS and particle size in produced water became 6.1 times and 33.2 times greater than these parameters in produced water after control experiment, respectively. Behavior of colloids in the water was changed from moderate stability to instability because of the decrease in zeta potential. In addition, because of the increase in particle size, the produced became suspension from solution. Like static experiment, pH value of produced water increased slightly. After flowback water-rock interaction, produced water had the similar precipitation tendency as the injected filtered flowback water. In the produced water, TDS increased by 7.1%; particle size decreased by 0.5%; and absolute zeta potential was slightly larger but indicates the same rapid coagulation behavior as filtered flowback water. The pH value of produced water was neutralized from 3.7 to 7.1 by calcite dissolution.

Compared dynamic results with static results, most of water parameters after dynamic experiments did not change significantly relative to static experiment due to short water-rock interaction. However, the reason about the big increase in particle size after dynamic deionized water-rock experiment is because bigger suspended particles were supported and transported by fast water flow through experimental system into produced water container (Abbott and Francis, 1977). According to the relationship between

particles and plugged pore size, after deionized water rock interaction, particles in produced water with average size of 13.9 μm can block pores with size range of 41.6-97.0 μm. After flowback water-rock interaction, particles with average size of 17.0 μm can block pores with size range of 51.0-119.0 μm. Thus, at the beginning of hydraulic fracturing by re-injecting flowback water, small particles are able to travel across pores supported by HF fluid flow, but larger particles in flowback water may settle down and accumulate to block pore channels after the flow speed become slow.

Ion contents in each produced water sample after dynamic experiments are shown in **Table B-2** and **Table B-3**. The average concentrations for enriched elements are listed in **Table 40**. After deionized water-rock interaction, 10 elements (Mo, Ni, Mg, Si, S, Ca, Sr, K, Cl, and Br) were enriched in the produced water relative to produced water after control experiment. They were primarily released by mineral dissolution. After flowback water-rock interaction, 4 elements (S, Co, Mo, and Ni) were enriched in the produced water relative to filtered flowback water. Like static experiment, Na, Sr, Cl, Mg, Ca, K, and Br contents were abundant in produced water but they were not enriched elements due to flowback water contamination. Among these elements, more Na ion was detected in produced water which led to the increase in TDS. Because only small amount of Na was released from rock sample based on deionized water-rock experimental result, the increase in Na ion in produced water was caused by the composition variation of flowback water. In addition, produced water after dynamic experiments had less enriched elements relative to static experiments due to shorter water-rock interaction.

Table 40 The average ion contents in water before and after dynamic experiments analyzed by ICP-MS and IC 900. Listed ions are more than 0.1 ppm in the produced water samples.

Samples	Water Samples		Water-Rock Interaction	
Dynamic Experiments	**DI Water**	**Filtered Flowback**	**With DI Water**	**With Filtered Flowback**
Cr	0	1.5	0	1.4
Co	0	0	0	0.2
Mo	0	0	20.6	2.4
Ni	0	0.2	0.4	5.2
Cu	0	3.5	0	1.9
Na	42	84449	58.5	88027
Al	0	0.4	0	0.5
Mg	0	674	1.1	657.2
Si	2.1	4.1	6.7	6.8
S	0.2	1.5	76.8	6.8
Ca	0.1	3904	33	3680
Ti	0	0.5	0	0.3
Mn	0	2.4	0	2.7
Fe	0	46.3	0	1.5
As	0	0.3	0	0.3
Sr	0	7894	9.7	7891
K	0	114	16.8	117
Cl	5.5	27868	33.6	27614
Br	0	716	0.2	794

3.3.3.2 Rock Characterization

Besides characterization of properties and compositions of water samples, evaluation of the change on rock samples is also important to understand the water-rock interactions. Therefore, rock analysis after static and dynamic experiments were repeated by XPS, XRD, and SEM to investigate the influence of water-rock interaction on rock surface.

First, after deionized water-rock and flowback water-rock experiments, 9 elements (C, O, Si, Al, Ca, K, Fe, Cl, and Fe) were detected by XPS on rock surface (**Table 41**). Compared samples after deionized water-rock interaction with samples after flowback

water-rock interaction, Ca, Na, and Cl slightly increased on the sample surface after being exposed to flowback water. The increases in these elemental concentrations were caused by flowback water contamination according to the composition of flowback residue consisting of high Ca, Na, and Cl concentrations. Meanwhile, the decreases in O or C after flowback water-rock interaction were observed perhaps because the constituents from flowback water accumulated on the rock surface, which resulted in initial materials containing O and C were buried deeper and were difficult to be detected (Ali and Hascakir, 2017). Based on ion content analysis above, major elements, like Si, Al, K, and Fe in produced water after deionized water-rock interactions were less than 100 ppm, which indicates only small amount of minerals dissolved into water. Thus, the difference in these elements on rock samples are explained by the influence of water-rock interaction or heterogeneities of rock surfaces.

Table 41 Average elemental concentrations of rock samples before and after experiments.

Rock Sample		**Average Elemental Concentration (wt. %)**										
		C	**O**	**Si**	**Al**	**Ca**	**K**	**Fe**	**Na**	**Cl**	**Mg**	**Sr**
Initial Rock Sample		34.05	29.51	19.51	10.28	4.06	0.21	0.96	0.29	1.13	0	0
Flowback Residue		5.31	20.83	0	0	8.57	0.11	0.40	12.43	42.0	1.60	2.50
Static Experiment	with DI Water	37.04	28.24	20.11	7.86	4.27	0.07	0.74	0.07	0.47	0	0
	with Flowback	32.29	27.66	21.03	9.49	4.62	0.07	0.40	0.36	3.74	0	0
Dynamic Experiment	with DI Water	32.18	32.02	18.41	8.50	6.21	0.09	1.34	0.05	1.19	0	0
	with Flowback	31.35	29.84	17.99	9.03	6.49	0.22	2.28	0.36	2.44	0	0

Mineralogy results of rock samples after experiments are given in **Table 42**. After deionized water-rock interaction in static and dynamic experiments, no new minerals or peaks were detected on rock surface in XRD patterns. But after flowback water-rock interaction, new peaks were found in XRD patterns which were identified as NaCl (halite) (**Figure B-1**). Because NaCl was the only mineral detected in flowback residue, impurities from flowback water accumulated on the rock surface after flowback water-rock interaction and less quartz was identified on rock surface.

Table 42 Mineralogy of samples before and after experiments

Rock Sample		**Average Mineralogy Concentration (wt. %)**				
		Quartz	**Illite**	**Calcite**	**Pyrite**	**Halite**
Initial Rock Sample		70	17.3	8.4	4.3	0
Flowback Residue		0	0	0	0	100
Static Experiment	with DI Water	67.5	17.9	8.1	6.5	0
	With Flowback Water	65.8	17.4	7.4	5.8	3.6
Dynamic Experiment	with DI Water	68.6	18.9	6.7	5.7	0
	With Flowback Water	63.6	19.0	7.7	4.2	5.6

Further, the changes on the rock surface morphology was visualized with SEM analysis (**Figure 39**). The SEM image shows rock surface of initial Marcellus Formation sample was relative flat. After deionized water-rock interaction in both static and dynamic experiments, rock surfaces became rough and a few clay-size particles were observed to attach to the rock surfaces. After flowback water-rock interaction, more small particles were visualized on rock surfaces. According to rock and produced water analysis above, new particles on rock surfaces after being exposed to flowback water were a result of physical attachment of clay-size materials from initial rock samples or new precipitates

accumulation, like NaCl, from flowback water. The size of these particles was about 1 μm. According to relationship between particle size and plugged pore size, in the experimental scale, only micrometer-scale pores are likely to be blocked. A preferred practice provided by Chesapeake Energy Corporation in EPA's Hydraulic Fracturing Study suggests that Marcellus Formation produced water should be treated through 20 μm filter to remove suspended solids, and blend with fresh water to decrease dissolved solids prior to reinjection of flowback water (Mantell, 2011). Therefore, after pre-filtration, it was acceptable to reuse the filtered flowback water, which did not cause significant formation damage in the fractures. However, it should be noted that bigger suspended impurities have already been removed by a 2.5 μm filter paper prior to water-rock experiments. If flowback water without treatment was reused in field hydraulic fracturing operation, larger pores and flow pathway would be blocked and formation damage would be caused. Thus, in the field scale, to minimize formation damage, we also suggest the removal of bigger particles before reinjection.

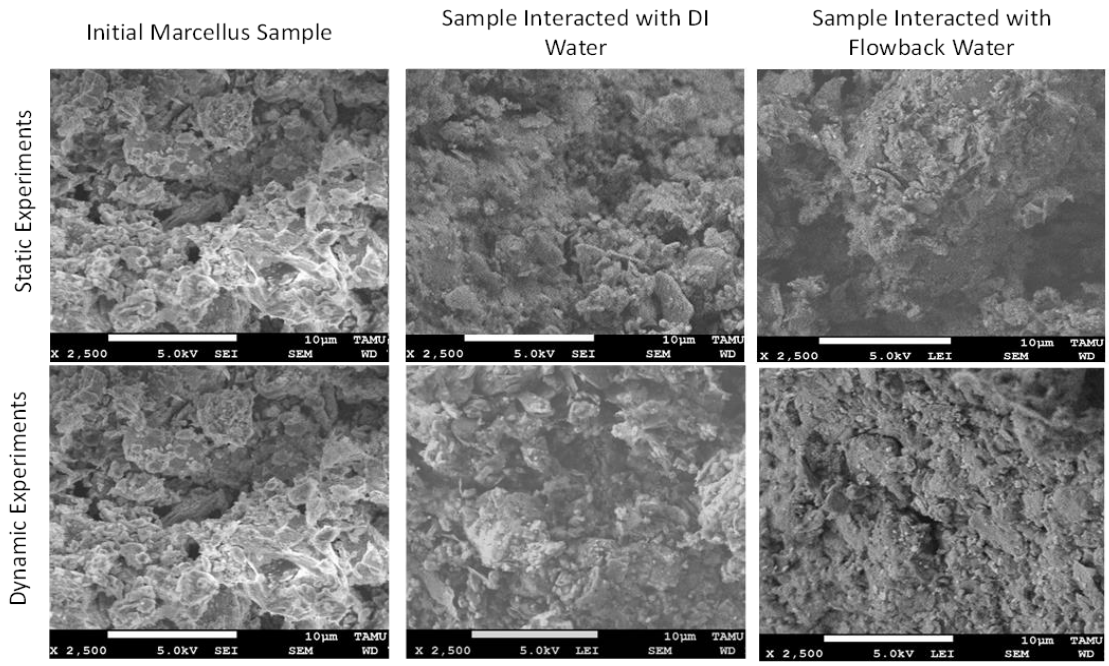

Figure 39 SEM Images of rock samples before and after static experiments and dynamic experiments at 2,500X magnification. After being exposed to flowback water, more small particles were observed on the rock surface.

Summary

Deionized water-rock interaction and flowback water-rock interaction were investigated on Marcellus Formation rock in static and dynamic conditions to evaluate the formation damage caused by re-injection of flowback water. Elemental concentrations, mineralogy, and morphology of the rock surfaces were identified. Ion contents, particle size, TDS, zeta potential, and pH of the water samples were characterized.

After flowback water-rock interaction in static and dynamic experiments, Na and Cl contents were in high concentrations in produced water and mainly mobilized from flowback water. However, most of those impurities remained in moveable water, instead

of precipitating on rock surface. Water parameter analysis indicates produced water after being exposed to flowback water had highest precipitation tendency leading to extremely highest TDS, largest particle size, and lowest absolute zeta potential relative to all water samples. Rock analysis indicates show rock surface elemental composition and mineralogy changed and more fine particles accumulated on rock surface because of flowback water contamination. Based on rock and water analysis, NaCl is the main problem in flowback water. In the experimental scale, only micrometer-scale pores tend to be blocked due to removal of impurities from flowback water by filtration before experiments. Thus, little formation damage was caused. However, if flowback water without treatment was reused in field hydraulic fracturing operation, larger pores and flow pathway would be blocked and formation damage would be caused.

In this chapter, experimental results evaluate the impact of reinjection of flowback water on formation damage. After pre-treatment applied on flowback water, it did not complicate further the water-rock interaction and did not cause significant formation damage in the fractures. However, water-rock interactions are still difficult to understand because multiple reactions and processes take place and control flowback water properties. Thus, next chapter aims to simplify the water-rock system and further investigate the effect of induvial minerals on flowback water properties by preparing different component pseudo rock samples based on mineralogy of Marcellus Formation.

References

Abbott, J. E., and Francis, J. R. D. 1977. Saltation and Suspension Trajectories of Solid Grains in A Water Stream: Royal Society [London], Philosophical Transactions, v, 284, p. 225-254.

Abdulsattar, Z. R., Agim, K., Lane, R. H., and Hascakir, B. 2015. Physicochemical Interactions of Shale with Injected Water-Based Fluids, SPE International Symposium on Oil Field Chemistry, 13-15 April 2015, The Woodlands, Texas, USA, SPE-173727-MS.

Abouzeid, A. Z. M., and Sinbawy, H. H. El. 1980. Calcination of Phosphates: Reactivity of Calcined Phosphate, Powder Technology, 26(1980)187-197.

Abrams, A. 1977. Mud Design to Minimize Rock Impairment Due to Particle Invasion. Society of Petroleum Engineers. doi:10.2118/5713-PA

Ali, M., and Hascakir, B. 2017. Water-Rock Interaction for Eagle Ford, Marcellus, Green River, and Barnett Shale Samples and Implications for Hydraulic Fracturing Fluid Engineering, SPE Journal, 22, 01, 162-171, SPE-177304-PA.

Avary, K. L., and Lewis, J. E. 2008. New Interest in Cores Taken Thirty Years Ago: the Devonian Marcellus Shale in northern West Virginia

Benjamin, M. M. 2002. Water Chemistry. McGraw-Hill. ISBN 978-0-07-238390-4.

Bish, D. L., and Post, J. E. 1989. Modern Powder Diffraction. Mineralogical Society of America, Washington, ISBN 0-939950-24-3

Boyce, M., and Carr, T. 2009. Lithostratigraphy and Petrophysics of the Devonian Marcellus Interval in West Virginia and Southwestern Pennsylvania

Brown, S., and Yucel, M. 2013. The Shale Gas and Tight Oil Boom: U.S. States' Economic Gains and Vulnerabilities. Council on Foreign Relations.

Burger, J., Sourieau, P., Combarnous, M., and Ramey, H. J. 1985. Thermal Methods of Oil Recovery. Gulf Publishing Company, Book Division. Technology & Engineering

Carroll, D. 1959. Cation Exchange in Clays and Other Minerals. Bulletin of the Geological Society of America. 70: 749–780.

Civan, F. 2015. Reservoir Formation Damage. 3rd Edition. ISBN 978-0-12-801898-9

Clark, W. B. 1918. The Geography of Maryland. Maryland Geological Survey. vol. 10. Baltimore: Johns Hopkins Press

Cooper, G. A. 1930. Stratigraphy of the Hamilton Group of New York: American Journal of Science, p. 116-134.

Davarpanah. A. 2018. The Integrated Feasibility Analysis of Water Reuse Management in the Petroleum Exploration Performances of Unconventional Shale Reservoirs. https://link.springer.com/article/10.1007/s13201-018-0717-7

Drexel University. 2017. Methane Levels Have Increased in Marcellus Shale Region Despite Dip in Well Installation. https://phys.org/news/2017-02-methane-marcellus-shale-region-dip.html/. Accessed 28 Oct 2020.

Eslinger, E., and Pevear, D. 1988. Clay Minerals for Petroleum Geologists and Engineers: Society of Economic Paleontologists and Mineralogists, Short Course Notes No. 22.

Ettensohn, F. R., and Barron, L. S. 1981. Depositional Model for the Devonian-Mississippian Black-Shale Sequence of North America: A Tectono-Climatic Approach: U.S. Department of Energy Open-File Report 12040-2, 85 p

Foldvari, M. 2011, Handbook of Thermogravimetric System of Minerals and Its Use in Geological Practice. Budapest, Hungary. Geological Institute of Hungary

Gabriel, G. A., and Inamdar, G. R. 1983. An Experimental Investigation of Fines Migration in Porous Media: Society of Petroleum Engineers Paper No. 12168.

Gandossi, L., and Von Estorff, U. 2015. An Overview of Hydraulic Fracturing and Other Formation Stimulation Technologies for Shale Gas Production – Update 2015 (PDF). Scientific and Technical Research Reports (Report). Joint Research Centre of the European Commission; Publications Office of the European Union.

Goldstein, J., Newbury, D. E., Joy, D. C., Lyman, C. E., Echlin, P., Lifshin, E., Sawyer, L., and Michael, J. R. 2003. Scanning Electron Microscopy and X-Ray Microanalysis. ISBN 978-1-4615-0215-9

Greenwood, R., and Kendall, K. 1999. Electroacoustic Studies of Moderately Concentrated Colloidal Suspensions. Journal of the European Ceramic Society. 19 (4): 479–488.

Gregory K. B., Vidic R. D., and Dzombak D. A. 2011. Water Management Challenges Associated with the Production of Shale Gas by Hydraulic Fracturing, Elements, 7(3), 181–186

Gros, N. 2003. Ion Chromatographic Analyses of Sea Waters, Brines and Related Samples. Water 2013, 5, 659-676; doi:10.3390/w5020659

Hall, J. 1839. Third Annual Report of the Fourth Geological District of the State of New York. New York Geological Survey, Annual Report.

Haluszczak, L. O., Rose, A. W., and Kump, L. R. 2013. Geochemical Evaluation of Flowback Brine from Marcellus Gas Wells in Pennsylvania, USA. Applied Geochemistry 28: 55-61.

Harper, J. A. 1999. Devonian, in Shultz, C. H., ed. The Geology of Pennsylvania: Pennsylvania Bureau of Topographic & Geologic Survey and Pittsburgh Geological Society, p. 108-127

Hayes, T. D. 2009. Sampling and Analysis of Water Streams Associated with the Development of Marcellus Shale Gas; Gas Technology Institute: December 2009.

Hercules, D., and Hercules, S. 2008. Surface Analysis. Encyclopedia Britannica. https://www.britannica.com/science/surface-analysis

Holditch, S. A. 1979. Factors Affecting Water Blocking and Gas Flow from Hydraulically Fractured Gas Wells. J Pet Technol 31 (12): 1515–1524. SPE-7561-PA.

Hosterman, J. W., and Whitlow, S. I. 1983. Clay Mineralogy of Devonian Shales in the Appalachian Basin, USGS professional paper 1298

Hurdle, J. 2018. Fracking Industry Water Use Rises as Drills Extend, Study Says.

Jenkins, R., and Snyder, R. L. 1996. Introduction to X-ray Powder Diffractometry, John Wiley, 403 p.

Jones, F. O., Jr. 1964. Influence of Chemical Composition of Water on Clay Blocking of Permeability: Petroleum Transactions, AIME, v. 231, p. 441–446, 10., 2118/631-PA

Kaya, A., Oren, A. H., and Yukselen, Y. 2003. Settling Behavior and Zeta Potential of Kaolinite in Aqueous Media. International Society of Offshore and Polar Engineers.

Klug, H. P., and Alexander, L. E. 1974. X-ray Diffraction Procedures for Polycrystalline and Amorphous Materials. 2nd ed. Wiley, New York.

Lash, G. G., and Engelder, T. 2011. Thickness Trends and Sequence Stratigraphy of the Middle Devonian Marcellus Formation, Appalachian Basin: Implications for Acadian foreland basin evolution. AAPG Bulletin, v. 95, no. 1 (January 2011), pp. 61–103

Long, D. T., and Angino, E. E. 1982. The Mobilization of Selected Trace Metals from Shales by Aqueous Solutions; Effects of Temperature and Ionic Strength. Economic Geology and the Bulletin of the Society of Economic Geologists, 77(3), 646-652.

Mantell, E. M. 2011. Produced Water Reuse and Recycling Challenges and Opportunities across Major Shale Plays. EPA Hydraulic Fracturing Study Technical Workshop #4 Water Resources Management

Moses, C. O., Nordstrom, D. K., Herman, J. S., and Mills, A. L. 1987. Aqueous Pyrite Oxidation by Dissolved Oxygen and by Ferric Iron. Geochim Cosmochim Acta 51:1561–1571

Moulder, J. F., Stickle, W. F., Sobol, P. E., and Bomben, K. D. 1995. Handbook of X-Ray Photoelectron Spectroscopy, Physical Electronics Division, Perkin-Elmer Corp., Norwalk

National Law Review. 2015. New York State Formally Adopts Ban on Fracking: An Analysis of the New York State DEC's SEQRA Findings Supporting Its HVHF Ban. July 7, 2015

Omelia, C. 1998. Coagulation and Sedimentation in Lakes, Reservoirs and Water Treatment Plants. Water Science and Technology. 37 (2): 129.

Paronish, T. J., Shuvajit B., and Timothy C. 2016. Integrated Geologic Analysis from Two Marcellus Shale Science Wells in Northeastern West Virginia. Poster presentation given at AAPG 2016 Annual Convention and Exhibition, Calgary, Alberta, Canada, June 19-22, 2016.

Popova, O., Frye, E., and Panarelli, E. 2015. Updated Geologic Maps Provide Greater Detail for Marcellus Formation: U.S. Energy Information Administration, Today in Energy: http://www.eia.gov/todayinenergy/detail.cfm?id=20612.

Pyrolysis. Journal of Petroleum Science and Engineering, Volume 154, 2017, Pages 502-512, ISSN 0920-4105, https://doi.org/10.1016/j.petrol.2017.01.051.

Ramurthy, M., Barree, R. D., and Kundert, D. P. 2011. Surface-Area vs. Conductivity-Type Fracture Treatments in Shale Reservoirs. SPE Production & Operations 24 (04): 357-367

Salimen, R., Plant, J., and Reeder, S., eds. 2006. Geochemical Atlas of Europe. Part 1, Background Information, Methodology and Maps. Espoo, Finland, Geological Survey of Finland, 526pp

Stokes, D. J. 2008. Principles and Practice of Variable Pressure Environmental Scanning Electron Microscopy (VP-ESEM). Chichester: John Wiley & Sons. ISBN 978-0470758748.

Sugiyama N., and Tanoshima, M. 2007. New! Agilent High Matrix Introduction Accessory Expands the Capabilities of ICP-MS. Agilent ICP-MS Journal, Issue 32

Thompson, K. C., and Nathanail, P. 2003. Chemical Analysis of Contaminated Land (Sheffield Analytical Chemistry. 1st Edition, ISBN-13: 978-0849328107 Hall, G. E. M. 1992. Inductively Coupled Plasma Mass Spectrometry in Geoanalysis: Journal of Geochemical Exploration, vol. 44, pp. 201-249.

U.S. Energy Information Administration (EIA). 2013. Annual Energy Outlook 2013 – EIA. https://www.eia.gov/outlooks/aeo/pdf/0383(2013).pdf

U.S. Energy Information Administration (EIA). 2014. Annual Energy Outlook. https://www.eia.gov/outlooks/aeo/pdf/0383(2014).pdf

U.S. Energy Information Administration (EIA). 2019. EIA Adds New Play Produ ction Data to Shale Gas and Tight Oil Reports. https://www.eia.gov/todayinenergy/detail. php?id=38372

U.S. Energy Information Administration (EIA). 2019. U.S. Crude Oil and Natural Gas Proved Reserves, Year-End 2018. U.S. Department of Energy. Washington, DC 20585

U.S. Geological Survey Information (USGS). 2011. Relevant to the U.S. Geological Survey Assessment of the Middle Devonian Marcellus Shale of the Appalachian Basin Province

United State Environmental Protection Agency [USEPA]. 1999. Total Dissolved Solids (TDS): EPA Method 160.1 (Gravimetric, Dried at 180 deg. C). Washington, DC: USEPA.

Weber, W. J. 1972. Physicochemical Processes for Water Quality Control, Wiley Interscience, ISBN 0-471-92435-0.

Yue, X. 2012. Interaction of Fracture Fluid with Formation Rock and Proppant on Fracture Fluid Clean-up and Long-Term Gas Recovery in Marcellus Shale Reservoirs. Petroleum and Natural Gas Engineering. Master Thesis.

Zielinski, R. E., and McIver, R. D. 1982. Resource and Exploration Assessment of the Oil and Gas Potential in the Devonian Gas Shales of the Appalachian Basin: MLM-MU-82-61-0002, DOE/DP/0053-1125, 326 p.

Ziemkiewicz, P. F., and Thomas, H. Y. 2015. Evolution of Water Chemistry during Marcellus Shale Gas Development: A Case Study in West Virginia. Chemosphere 134:224-31.

CHAPTER IV

A SYSTEMATIC STUDY OF WATER-ROCK REACTIONS TO UNDERSTAND FLOWBACK WATER FROM MARCELLUS FORMATION AND PERTINENT TREATMENT FOR REUSE

The significant production of hydrocarbon resources from shale reservoirs makes the United States the largest oil producer in the world. However, the production has been accompanied by rising concerns about excessive use of water and flowback water contamination. To manage flowback water and meet future water demand, the reuse of flowback water has been commonly chosen by industry.

Flowback water is a valuable representative indicator of water-rock interactions occurring during hydraulic fracturing. However, because rocks contain different minerals, various interactions take place during hydraulic fracturing which complicate the water-rock system and make the treatment of flowback water a difficult task. Hence, this chapter aims to investigate two types of water-rock systems for the Marcellus Formation: first, pseudo reservoir rock-water systems which serve as control experiments to simplify water-rock interactions; and second, flowback water from the Marcellus Formation hydraulic fracturing activity which represents the complicated water-rock system.

For simple water-rock systems, based on a representative mineralogy of Marcellus Formation rock sample, pseudo rock samples were prepared and one-, two-, three-, and four-component mineral-deionized water systems were created at room and reservoir temperatures to better understand the relationship between minerals and flowback water

properties. For complicated flowback water systems, different chemicals were tested to handle Marcellus Formation flowback water through a low-cost treatment method including coagulation, flocculation, and sedimentation (CFS).

Pseudo rock-water experimental results show that the characteristics of minerals mainly control flowback water properties. Both major minerals (primarily calcite, illite, and pyrite) and a minor mineral (halite) contaminate flowback water by increasing TDS contents and lowering the stability of the water system. In addition, pretreatment experimental results show that the integrated CFS process can destabilize Marcellus Formation flowback water but is less effective to remove TDS from flowback water than sedimentation alone. Simple sedimentation is sufficient to separate the impurities from Marcellus Formation flowback water.

The results in this chapter have the potential to be adapted to field-scale application directly and will contribute to the better management of flowback waters from the Marcellus Formation.

4.1 Introduction

With improvements in hydraulic fracturing and horizontal drilling, energy companies have been able to tap previously inaccessible source rock within shale reservoirs. Due to these advances, shale oil and gas production represents more than 60% and 70% of total U.S. oil and gas production (EIA, 2019). Moreover, because of the significant increase in oil production from shale reservoirs, the United States has been the

largest oil producer in the world since 2018. However, the increase in extraction of shale resources has been accompanied by rising concerns over potential environmental impact resulting from water that flows back up the wells.

In general, a fracturing job injects and pressurizes 2-7 million gallons of HF fluids into an individual well to develop fractures and release hydrocarbons from shales (Ground Water Protection Council, 2009; Hagemeier and Hutt, 2009; Gregory et al., 2011). Once hydraulic fracturing is finished, 5-85% of the HF fluids are recovered and considered as flowback water (mainly containing injected fluids) or produced water (mainly containing formation water). Flowback water is typically less saline than produced water and commonly reused as makeup water for subsequent hydraulic fracturing. However, both wastewaters consist of high concentrations of heavy metals, dissolved organics, and hydrocarbons (Gregory et al., 2011; Vidic et al., 2013; Ziemkiewicz and Thomas, 2015). Moreover, flowback water can have TDS reaching 6 orders of magnitude greater than the injected water (Blauch et al., 2009; Cluff et al., 2014). At present, hydraulically fractured horizontal wells account for more than 69% of all wells drilled in the United States and produce large quantities of flowback water, which brings public concerns about water contamination (EIA, 2018).

Although flowback water must be treated before reinjection, it provides the opportunity for indirect observation of water-rock interactions during hydraulic fracturing. Therefore, management of flowback water requires knowledge of the water-rock reactions that control water properties. Generally, a variety of chemical reactions and geochemical processes occur as water moves through shale formations. Processes such as

dissolution/precipitation, cation exchange, and redox reaction are generally responsible for geochemical variations of water (refer to Section 1.6 Water-Rock Interaction Occurring During Hydraulic Fracturing in Chapter I). Mineral dissolution and precipitation cause mass transfer between rock and water. They take place or not depend on whether the solution is saturated with respect to the solid phase. In natural aquifer system, dissolution and precipitation of carbonate and silicate minerals are common (Hogan, 2010). Cation exchange, a type of adsorption/desorption phenomenon, is also an important process during water-rock interaction. Clay minerals and organic matter commonly adsorb heavy-metal cations from water because cations are attracted by their negatively charged surfaces (Birkeland, 1999; Brady and Weil, 2008). Redox reactions, involving transfer of electrons from one ion to another, modify the mobility and concentrations of dissolved ions by changing their redox states (Gillespie, 1920). In sum, the mutual interactions of rock and water affected by various processes control the water properties and complicate the water-rock system.

It has been known that flowback water composition varies significantly since every shale formation differs considerably in rock composition (Wang et al. 2015; 2016; Ali and Hascakir, 2015b; 2017; Zhang et al., 2017; 2020). However, distinguishing between reactions or geochemical processes in flowback fluids is difficult because of their mutual interactions. Therefore, the need to simplify water-rock system is become necessary.

In addition, flowback water with high salinity cannot be handled by simple treatment technologies alone. In general, membrane separation technologies are an effective way to remove TDS and have been widely applied in desalination of mining

wastewater and seawater since 1966 (Riedinger and Schultz, 1966). However, due to high contaminant concentrations, membrane techniques have not found wide application for the desalination of flowback water. Pretreatment methods are typically required before application of membrane technologies to avoid deteriorating desalination performance (Chang et al., 2019). Coagulation, flocculation, and sedimentation (CFS) are the most common pretreatment methods to destabilize suspended solids and remove contaminants (Edzwald and Haarhoff, 2011). In flowback water, stability of impurities is mainly controlled by electrostatic forces around the particles and by gravitational forces (Israelachvili, 1992). Although removal of large suspended solids can be achieved by sedimentation, small particles cannot be effectively removed because electrostatic forces are stronger than gravitational forces (Edzwald and Haarhoff, 2011). To remove small particles in wastewater, weakening electrostatic forces and strengthening gravitational forces are necessary (Crittenden and Harza, 2005). Coagulation is designed to neutralize charges and weaken electrostatic forces around the particles; Flocculation is used to aggregate particles and strengthen gravitational forces; sedimentation can then remove aggregated particles by gravity (Crittenden and Harza, 2005). Thus, CSF treatment technologies are typically integrated to treat wastewaters but have limited application for the flowback water treatment.

In this chapter, the Marcellus Formation was selected as my study area. To simplify water rock interactions and better understand flowback water, pseudo reservoir rocks were prepared based on the mineral composition of the Marcellus Formation. Moreover, to investigate the efficiency of integrated CFS treatment method in removal of

contaminants in flowback water, Marcellus Formation flowback water obtained from hydraulic fracturing activities was experimentally manipulated. Hence, a brief introduction to the Marcellus Formation is provided. A detailed description of the Marcellus Formation is provided in Section 1.9: Marcellus Formation in Chapter I.

The Marcellus Formation extends across New York, Pennsylvania, Ohio, and West Virginia (Clark, 1981). It is the largest identified North American shale gas play. EIA estimated that the natural gas reserve in the Marcellus Formation represents 39.6% of all U.S. shale gas (EIA, 2019). The shale unit in the Marcellus Formation comprises Devonian age black shale deposited about 390 million years ago in the Appalachian Basin. The main minerals in the Marcellus Formation are quartz, clay minerals (illite or smectite–illite mixed clays), calcite, pyrite, dolomite, feldspar, and gypsum (Roen, 1984; Engle and Rowan, 2014). Halite is sometimes present in the bulk matrix and is a possible source of saline brine within the Marcellus Formation (Blauch et al. 2009). Although the Marcellus Formation contains significant amounts of natural gas, gas production through vertical wells rarely reached commercial quantities before 2008 because of low permeability (EIA, 2019). Subsequent advances in horizontal drilling and hydraulic fracturing have resulted in economic production of natural gas from the Marcellus Formation. However, development of the Marcellus Formation has also brought some environmental challenges. The average water volumes for hydraulic fracturing of Marcellus Formation Gas Wells are 5.6 million gallons and the average TDS found in Marcellus Formation flowback water are 20,000-100,000 mg/L (Gregory et al., 2011). At present, how to manage Marcellus Formation flowback water with high salinity is critical to the operators' success.

4.2 Materials and Methods

4.2.1 Sample Preparation

The Marcellus Formation is a main hydrocarbon gas producer in the United States. The gas is produced through hydraulic fracturing. The hydraulic fracturing activity in this formation results in high volume of flowback water with high contaminant concentration primarily due to interactions between hydraulic fracturing water and rocks. However, these interactions are complicated and make the treatment of flowback water a difficult task. Hence, throughout the scope of this chapter, two types of water-rock systems were examined for Marcellus Formation: first, pseudo reservoir rock-water systems which serve as control experiments to simplify water-rock interactions; and second, flowback water from Marcellus Formation hydraulic fracturing activity which represents complicated water-rock interactions. To reach these goals, both reservoir rock and flowback water from Marcellus Formation that were used in Chapter III were also used in this Chapter.

In chapter III, XRD analysis of the Marcellus Formation rock sample shows it contains 70% quartz, 17.3% illite, 8.4% calcite, and 4.3% pyrite (refer to Figure 34). To simplify the water-rock system, the mineralogy analysis was used to prepare, one-, two-, three, and four-component pseudo rock systems. First, high purity quartz, illite, calcite, and pyrite minerals were purchased separately from external chemical companies. To identify impurities, mineral standards were characterized by XRF for elemental composition and XRD for mineralogy. The XRF and XRD measurement were conducted

in the same setting as Chapter II and III. The main composition of the standard minerals was listed in **Table 43**.

Table 43 Composition (wt. %) of four standard minerals analyzed by XRF

	Ca	Si	Al	Fe	K	Mg	S	Ti	Ba
Calcite	38.00	0	0.11	0.03	0	0.62	0	0	0
Quartz	0	36.41	0	0	0	0.28	0	0	0
Illite	0.64	14.45	5.14	3.57	3.24	0.75	0.08	0.38	0
Pyrite	0.12	0	0.20	41.98	0	0	51.46	0.06	0.17

Calcite powder (calcium carbonate) was purchased from Sigma®. XRD analysis shows that calcite was the only mineralogical phase present in the sample. Minor elements, such as Mg, Al, and Fe were detected by XRF and with elemental abundances to less than 0.8 wt.%. The quartz powder (silicon dioxide) was purchased from Sigma®. Only quartz phase was identified by XRD. The only elemental impurity detected in this quartz was Mg at 0.28 wt.%. Illite standard was ordered as rock fragments from Ward's Geological Supply. It was crushed and then analyzed. XRD analysis indicates that this standard was composed of illite (70.4 wt.%) and quartz (29.6 wt.%). Besides major elements in illite (Si, K, Mg, Al, and Fe), small amounts of Ca, S, and Ti were detected. Although illite was not the only mineralogical phase, this standard was still used because quartz is also one of minerals present in the Marcellus Formation sample, and quartz has little effect on water properties due to its low solubility (discussed in the result section). Pyrite powder (iron disulfide) was obtained from Aldrich®. Pyrite was the only mineral identified by XRD.

XRF analysis indicated that Ca, Al, Ti, and Ba are also present with total abundance less than 0.6 wt.%.

4.2.2 Experimental Design

After identifying impurities in standard minerals, pseudo rock samples were prepared by mixing standard minerals at four concentrations (1, 2, 3, and 4 mg). These pseudo rock samples were then mixed with 40 mL of deionized water either at room temperature (23°C) or at reservoir temperature (75°C) for 24 hours to obtain one-component mineral systems in deionized water (calcite only, quartz only, illite only, and pyrite only), two-component mineral systems in deionized water (calcite + quartz, calite + illite, calcite + pyrite, quartz + illite, quartz + pyrite, and illite + pyrite), three-component mineral systems in deionized water (calcite + quartz + illite, calcite + quartz + pyrite, calcite + illite + pyrite, and quartz + illite +pyrite), and a four-component mineral system in deionized system (calcite + quartz + illite + pyrite). All mineral concentrations and combinations are provided in the appendix (**Table C-1**, **C-2**, **C-3,** and **C-4**). These pseudo rock-water experiments are control experiments in which one mineral concentration was changed, while other mineral concentrations are constant. The purpose of these experiments is to understand how water properties change when there is more than one mineral existing in water. To avoid artificial contamination, plastic tubes were used to collect produced water in room temperature experiments and glass tubes were used in

reservoir temperature experiments. All tubes were sealed during water-rock experiments. In all experiments, deionized water was used as injected water and blank solution.

After experiments, supernatant (about 2 mL) collected from each produced water sample was analyzed for zeta potential and particle size. The zeta potential (indicating the stability of particles) was measured by a nano ZetaPALS by Brookhaven Instruments Corporation. The particle size was obtained by a 90Plus Particle Size analyzer by Brookhaven Instruments Corporation. Then, each water sample was filtered through a 2-μm filter paper and analyzed for TDS and pH. TDS (evaluating the amounts of contaminants partitioned into the water) was measured by an Oakton Conductivity Probe. pH was measured by a pH probe. The combination of TDS, particle size, and zeta potential provides information on the stability of a colloid system (Weber, 1972). After water parameter analysis, a linear regression ($y=ax+b$) was applied to find the relationship between each parameter (y is pH, TDS, particle size, or zeta potential) and the mineral concentrations (x) in supernatant solution.

After understanding the effect of minerals on flowback water properties by analysis of pseudo rock-water systems, Marcellus Formation flowback water was investigated. The Marcellus Formation flowback water used in Chapter III was collected from the same well as the rock sample. Detailed characterization of this flowback water is provided in Section 3.32: Flowback Water Characterization. Based on experimental results on Marcellus Formation flowback water-rock interactions in Chapter III, we concluded reinjection of Marcellus Formation flowback water without pre-treatment in hydraulic fracturing would block flow pathways and cause formation damage. Thus, in

this chapter, to treat flowback water for reuse, the CFS method was tested as a pretreatment method to eliminate suspended solids from flowback water that would otherwise complicate the use of membrane technologies for desalination.

First, to evaluate efficiency in removing impurities by the integrated CFS method, 1g of chemicals including asphaltenes, sodium sulfate ($NaSO_4$), and ferric chloride ($FeCl_3$) were added separately into 20 ml initial flowback water to destabilize suspended solids. Mixtures were then immediately subjected to CFS tests in the following steps. 1. Coagulation step. Each sample was placed in a mixer for 1 minute of constant mixing at a rate of 200 revolutions per minute (rpm). 2. Flocculation step. Just after the first step, samples were mixed for 30 minutes at a constant rate of 30 rpm (Edzwald and Haarhoff, 2011). 3. In the final sedimentation step, the mixtures were allowed to settle for 90 minutes. The total CFS treatment duration for each sample was about 2 hours. In addition, a flowback water sample was allowed to settle for 2 hours without adding chemicals as an experimental control. After treatment, the supernatant was collected and analyzed for pH, TDS, particle size, and zeta potential. To test if pH affects the stability of these mixtures, all experiments were repeated by adding 5 mg sodium hydroxide (NaOH).

4.3 Results and Discussion

4.3.1 Control Experiments on Pseudo Rock Samples and Water

4.3.1.1 One-component Mineral-Water Interaction

Produced water parameters after one-component mineral-water interaction are listed in **Table 44**. Mineral types, mineral concentrations, and temperature influenced water parameters. When different minerals were mixed with water, water parameters changed obviously because different water-rock interaction took place. When the same minerals at different doses were blended with water, water parameters were similar because same water-rock interaction occurred. At different temperature, water parameters also changed because temperature influenced reaction rate and solubility of minerals (Laidler, 1987).

Table 44 Summary of water parameters in produced water after one-component mineral-water interactions at room temperature and reservoir temperature.

Mineral concentration, mg/mL		Experiments at room temperature (23°C)					Experiments at reservoir temperature (75°C)			
		pH	TDS, ppm	Particle Size, nm	Zeta Potential, mV		pH	TDS, ppm	Particle Size, nm	Zeta Potential, mV
Calcite 1	1	8.99	21.4	568	-12.25		8.73	28.0	890	-13.35
Calcite 2	2	9.04	26.8	648	-12.71		8.77	28.3	971	-14.53
Calcite 3	3	9.09	29.2	717	-12.40		8.77	29.7	1200	-14.12
Calcite 4	4	9.13	31.4	862	-12.54		8.81	30.2	989	-13.57
Quartz 1	1	7.50	6.3	523	-20.91		7.36	7.9	433	-19.82
Quartz 2	2	7.11	10.0	514	-18.81		7.10	11.6	463	-18.58
Quartz 3	3	6.74	10.1	509	-19.10		7.06	11.9	467	-18.15
Quartz 4	4	6.69	10.3	523	-18.98		6.91	12.2	488	-18.48
Illite 1	1	7.56	10.1	549	-14.33		8.64	26.7	554	-13.63
Illite 2	2	7.53	10.5	522	-14.11		8.63	32.1	587	-13.17
Illite 3	3	7.51	12.2	553	-15.34		8.66	35.6	601	-13.21
Illite 4	4	7.50	17.7	575	-14.27		8.64	38.5	623	-13.12
Pyrite 1	1	6.55	7.2	143	-4.38		3.7	65.6	1242	+6.19
Pyrite 2	2	5.53	11.2	224	-5.11		3.55	79.2	8210	+6.31
Pyrite 3	3	4.93	13.3	318	-4.30		3.51	81.1	>20000	+6.56
Pyrite 4	4	4.91	14.4	331	-5.44		3.42	86.9	>20000	+6.48

*Particle sizes of two pyrite samples (pyrite 3 and pyrite 4) at reservoir temperature are above detection limit (20000 nm).

* DI water as blank solution: pH: 7.59; TDS:1.67 ppm; particle size: 108 mv; absolute zeta potential: 24.5 mV

At room temperature, TDS and particle size were greatest in calcite solutions, increasing the likelihood of particle aggregation. This is consistent with the high solubility of calcite at room temperature compared with the other experimental minerals. Particles in quartz or illite solutions had lower precipitation tendency due to lower TDS, larger absolute zeta potential, and smaller particle size. Although little pyrite dissolved into water, its absolute zeta potential was the smallest among other minerals, which lowered the stability of particles in the solutions. At reservoir temperature, illite and pyrite solutions had higher TDS and particle size relative to their counterpart at room

temperature. Among all minerals, pyrite solutions at reservoir temperature had the lowest stability due to extremely large particle size, high TDS, and low absolute zeta potential.

The changes in pH, TDS, particle size, and zeta potential were governed by characteristics of each mineral. In particular, when calcite was introduced into water, pH in all samples increased because of calcite dissolution and carbonate acid/base equilibrium (reaction 1 and 2) (Plummer and Wigtey, 1976).

$$CaCO_3 \rightleftharpoons Ca^{2+} + CO_3^{2-} \quad \text{……..(1)}$$

$$CO_3^{2-} + H_2O \rightleftharpoons HCO_3^- + OH^-; \quad HCO_3^- + H_2O \rightleftharpoons H_2CO_3 + OH^- \text{…….(2)}$$

Generally, high temperature increases initial calcite dissolution rates, but the solubility of calcite decreases as temperature increases (Plummer et al., 1978a; Plummer and Busenberg, 1982). Thus, it was observed that in the solutions with lower calcite concentrations (Calcite 1, 2, and 3), TDS at reservoir temperature were slightly higher than their counterparts at room temperature because calcite dissolved faster at high temperature. However, in the solution with high calcite concentration (Calcite 4), TDS was lower at reservoir temperature because of the decrease in calcite solubility.

With increasing calcite concentration added into water, more calcite dissolved into water, which caused the increase in TDS, particle size, and pH. However, it was observed that zeta potential values were almost constant in all calcite solutions. Zeta potential of calcite indicates net charge (negative) present on the calcite particle surface. Although the zeta potential and surface species of calcite continue to be debated in the literature, the

general consensus is that different dissolved ions (H^+, OH^-, HCO_3^- , CO_3^{2-}, and Ca_2^+) and lattice ions (>$CO3^-$, >CaO^-, >$CaCO_3^-$, >$CaOH^{2+}$) are active in calcite solutions (Fuerstenau et al., 1968 ; Yarar and Kitchener, 1970; Moulin and Roques, 2003; Rodríguez and Araujo, 2006). Our results show that the zeta potential of calcite, which is the combination of the behavior of all of surface ions, does not change significantly with different mineral concentrations.

During quartz dissolution at circumneutral pH, quartz reacts with water to form a very weak acid (silicic acid, H_4SiO_4) as given below (Rimstidt and Barnes, 1980; Aagaard and Helgeson, 1982).

$$SiO_2 + 2H_2O \rightleftharpoons H_4SiO_{4(aq)} \text{ ……..(3)}$$

Generally, the solubility of quartz in deionized water is very low at room temperature and neutral pH. Therefore, similar TDS and particle size were observed as more quartz was added. The pH of quartz solutions decreased slightly with the increasing quartz concentrations. One possible reason for the acidity of quartz solutions is that dissociation of silica acid released H^+ (reaction 4) (Rimstidt and Barnes, 1980). However, because the silicic acid is a very weak acid with dissociation constant of $10^{-9.83}$, its behavior could not attribute to acidity in terms of low dissociation constants. Another possible reason could that be carbon dioxide adsorbed on the quartz powder dissolved, forming carbonic acid and increasing the H^+ concentration (reaction 5) (Van Praagh, 1939).

$$H_4SiO_{4(aq)} \rightleftharpoons H_3SiO_4^- + H^+ \text{……..(4)}$$

$$CO_2 + H_2O \rightleftharpoons H_2CO_{3(aq)} \rightleftharpoons HCO_3^- + H^+ \text{……..(5)}$$

The solubility of quartz increased with increasing temperature. Thus, TDS of quartz solutions were slightly higher at reservoir temperature. Zeta potential of quartz solutions is mainly influenced by charged unit ($Si\text{-}O^-$) on quartz particle surfaces (Antonio and Baptista, 2014). Like calcite solutions, zeta potential changed slightly with different quartz concentrations.

As a clay mineral, illite is stable at room temperature (Routson and Kittrick, 1971). Its dissolution reaction can be expressed as:

$$K_{0.6}Mg_{0.25}Al_{2.3}Si_{3.5}O_{10}(OH)_2 + 8H^+ \rightleftharpoons 0.25Mg^{2+} + 0.6K^+ + 2.3Al^{3+} + 3.5SiO_2 + 5H_2O \text{…..(6)}$$

As in quartz solutions, changes in all produced water parameters at different illite concentrations at room temperature were small. However, the solubility of illite increases with increasing temperature. Thus, TDS of illite solutions increased significantly at reservoir temperature. In addition, pH in illite solutions decreased slightly at room temperate but increased to around 8.6 at reservoir temperature. In addition to consuming H^+ during illite dissolution , the adsorption of metal cations or H^+ on illite particle surfaces or the release of other impurity ions from illite molecules during illite dissolution may influence the pH of illite solutions (Keller and Matlack, 1990). Illite solutions had similar zeta potential at different concentrations.

Pyrite is almost insoluble at ambient temperature. Therefore, TDS and particle size were very small. However, the exposure of pyrite to water and oxygen can cause oxidation of pyrite. This redox reaction is promoted with increasing temperature and can produce sulfate (SO_4^{2-}), H^+, and iron hydroxide ($Fe(OH)_3$) (reaction 7) (Singer and Stumm, 1968).

$$FeS_2 + 3.75O_{2(aq)} + 3.5H_2O \rightarrow Fe(OH)_{3(s)} + 2SO_4^{2-} + 4H^+ \text{.....(7)}$$

Because the Marcellus Formation reservoir temperature (75°C) was not enough to remove oxygen from water, increasing temperature in our experiments likely accelerated pyrite oxidation (Singer and Stumm, 1968). Therefore, the particle size of pyrite solutions increased dramatically perhaps because of formation of ferrihydrite ($Fe(OH)_3$) that is insoluble in water and tends to precipitate out of water (Moses et al., 1987). The pH of pyrite solutions decreased because of the release of H^+ during ferrihydrite precipitation. In addition, in the event of oxygen depletion, as in a closed system, the oxidation of sulfide can still continue using Fe^{3+} already present in the water as the oxidant (reaction 8) (Singer and Stumm, 1968).

$$FeS_2 + 14Fe^{3+} + 8H_2O \rightarrow 15Fe^{2+} + 2SO_4^{2-} + 16H^+ \text{.....(8)}$$

The zeta potential values of pyrite solutions were constant at different mineral concentrations but became positive at reservoir temperature from negative at room temperature. The reversal of zeta potential values is due to the specific adsorption of more

hydrolysed ferric ions onto the pyrite surface that formed through pyrite oxidization (Fornasiero et al., 1991).

Overall, although the solubility of minerals changed as the temperature rose, we observed that the effect of temperature on the solubilities of illite and pyrite was larger than its effect on the solubilities of calcite and quartz. In addition, even if the mineral concentrations and temperature affect water-rock interactions, the changes in water parameters were still controlled by each mineral's characteristics.

4.3.1.2 Multiple-Component Mineral-Water Interaction

pH, TDS, particle size, and zeta potential results of each supernatant for the two-, three-, and four-component mineral-water interaction are provided in the appendix (**Table C-5, C-6,** and **C-7**). Generally, because different mineral combinations interacted with water, different interactions occurred and led to variations in water parameters. However, the change in water parameters was still controlled by characteristics of minerals.

A linear regression (y=ax+b) was applied to find the relationship between every parameter (y is pH, TDS, particle size, or zeta potential) and the concentration of each mineral (x) in supernatant solution. Linear relations are defined based on R-Squared (R^2) values and given in **Table 45 (**Devore, 2011**)**. For R^2 between 0.8-1.0, the linear relation is named very good and given within a green cell in Table 45. For R^2 between 0.6-0.79, the linear relation is named moderately good and given within a yellow cell. For R^2 less

than 0.59, the linear relation is named bad and given within a red cell. White cells mean the measured parameters are above the detection limit of each measurement method.

Table 45 Linear correlations between mineral concentration and water parameters at room and reservoir temperature. Note: All values are R^2 values. Green cells show very good linear relations, yellow cells show moderately good linear relations, red cells show bad linear relations, and white cells mean the measured parameters are above equipment detection limit and cannot be analyzed.

Minerals concentration varies		linear relation coefficient	Parameters in supernatant (y)							
			room temperature (23°C)				reservoir temperature (75°C)			
			pH	TDS	Particle Size	Zeta Potential	pH	TDS	Particle Size	Zeta Potential
Calcite (C)		R^2	1.00	0.95	0.97	0.14	0.90	0.94	0.26	0.00
Quartz (Q)			0.92	0.61	0.01	0.52	0.92	0.72	0.93	0.62
Illite (I)			0.95	0.81	0.42	0.06	0.10	0.98	0.97	0.67
Pyrite (P)			0.86	0.93	0.93	0.30	0.95	0.89		0.75
C+I	I		0.85	0.99	0.17	0.18	0.58	0.91	0.42	0.69
	C		0.61	0.59	0.61	0.03	0.79	0.58	0.57	0.13
C+P	P		0.98	0.99		0.61	0.70	0.79		0.98
	C		0.66	0.57	0.48	0.77	0.53	0.72		0.61
C+Q	Q		0.98	0.92	0.11	0.07	0.79	0.53	0.17	0.00
	C		0.57	0.53	0.02	0.46	0.55	0.52	0.12	0.12
Q+I	I		0.91	0.96	0.21	0.69	0.67	0.92	0.05	0.39
	Q		0.84	0.06	0.02	0.18	0.79	0.86	0.70	0.03
Q+P	P		0.96	0.96	0.52	0.85	0.55	0.77	0.58	0.83
	Q		0.80	0.67	0.75	0.88	0.96	0.87	0.35	0.54
I+P	I		0.89	0.95	0.84	0.76	0.66	0.71	0.97	0.84
	P		0.86	0.94	0.00	0.77	0.84	0.09	0.96	0.67
C+Q+I	I		0.43	0.88	0.62	0.52	0.61	0.97	0.77	0.95
	Q		0.91	0.95	0.02	0.31	0.16	0.85	0.80	0.02
	C		0.52	0.54	0.33	0.02	0.51	0.74	0.53	0.95
C+Q+P	P		0.97	0.97	0.34	0.90	0.66	0.96	0.28	0.08
	Q		0.92	0.93	0.51	0.01	0.53	0.94	0.92	0.88
	C		0..52	0.63	0.09	0.08	0.52	0.88	0.63	0.88
C+I+P	P		0.88	0.99		0.90	0.81	0.95		0.89
	I		0.97	0.84	0.80	0.77	0.94	0.51	0.01	0.46
	C		0.56	0.87		0.92	0.53	0.68	0.01	0.95
Q+I+P	P		0.96	0.98	0.75	0.99	0.92	0.97		0.49
	I		0.96	0.96	0.94	0.88	0.88	0.00	0.51	0.07
	Q		0.67	0.78	0.71	0.90	0.98	0.84	0.52	0.93
C+Q+I+P	P		0.98	0.99	0.35	0.43	0.74	0.94	0.48	0.86
	I		0.70	0.80	0.06	1.00	0.50	0.93	0.73	0.96
	Q		0.84	0.96	0.47	0.56	0.43	0.86	0.51	0.84
	C		0.56	0.65	0.36	0.55	0.52	0.71	0.68	0.81

According to the results given in Table 45, at room temperature, very good correlations are mainly obtained for pH and TDS with mineral concentrations, which

indicates these parameters are sensitive to the change in mineral concentrations. **Figure 40** shows the relationship between pH and TDS of each solution at both temperatures (values at room temperature given with circles and values at reservoir temperature given with triangles). In the figure, the general trend for TDS is TDS become greater at reservoir temperature relative to room temperature, because more minerals dissolved at higher temperatures. For pH, like one-component experiments, adding calcite still increased pH and adding pyrite decreased pH. The decrease in pH caused by pyrite dissolution or oxidation was prevented because calcite has high buffering capacity (Bache, 1984). Dissolution of quartz slightly lowered pH of the mixtures. Illite solutions had different pH ranges at room and reservoir temperature (refer to Table 44). Thus, adding illite adjusted the pH of mixtures depending on the interaction temperature.

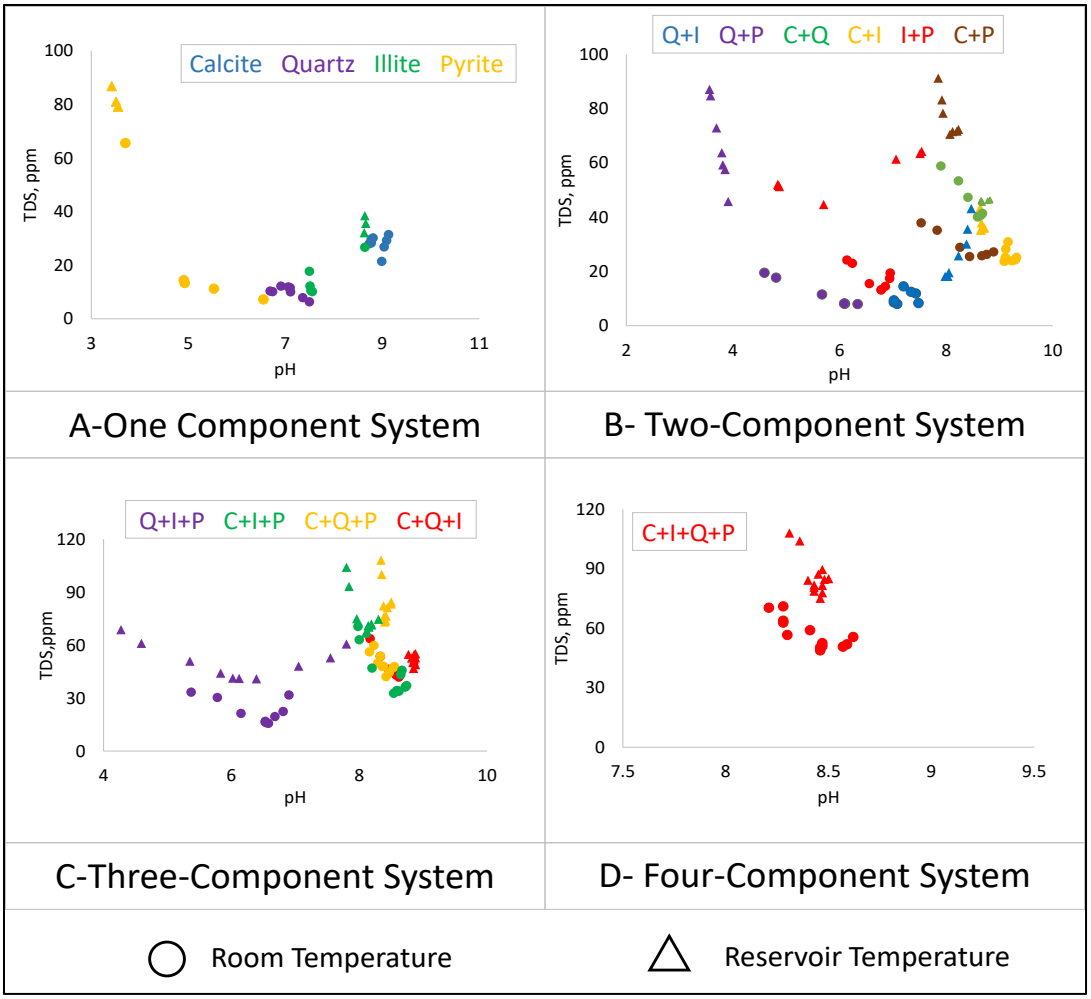

Figure 40 The change in TDS with pH for all experiments. Note: C represents calcite; Q represents quartz; I represents illite; and P represents pyrite. Circle represents experiments conducted at room temperature and triangle represents experiments conducted at reservoir temperature.

The relationship between particle size and pH for all experiments is shown in **Figure 41-A**. At room temperature, large particles (>10,000 nm) were produced mainly at high pH (pH around 8). In these experiments, both calcite and pyrite were added. Their interaction increased particle size and buffered pH in a high range. At reservoir temperature, large particle size also was observed at low pH (pH below 5). This is because

high temperature promoted oxidization of pyrite (Singer and Stumm, 1968), which led to agglomeration of particles and lowered the pH. Therefore, interactions with calcite and pyrite were main reasons for changing pH and increasing particle size in the supernatant solution, especially at reservoir temperature.

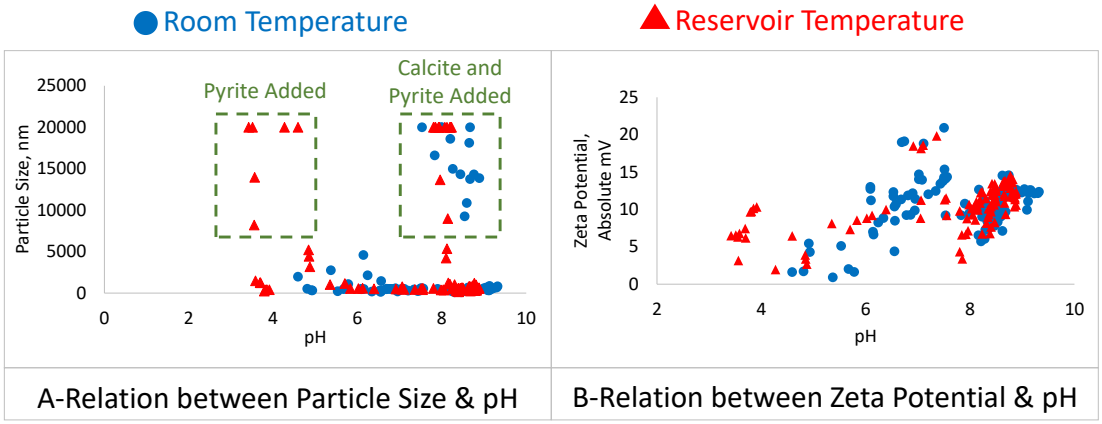

Figure 41 Relationships between particle size and pH (figure on the left) and absolute value of the zeta potential and pH (figure on the right) for all experiments. Note: Circle represents experiments at room temperature and triangle represents experiments at reservoir temperature.

The relationship between zeta potential and pH for all experiments is shown in **Figure 41-B**. In one-component experiments, the absolute zeta potential values of quartz were observed around 18-21 mV and pyrite around 4-6 mV (refer to Table 44). In multiple-component experiments, the absolute zeta potential values of mixtures mainly also fall in these ranges (4-21 mV). Based on all zeta potential data in our experiments (refer to zeta potential in Table C-5, C-6, and C-7), a trend was found that with an increase in one mineral concentration, the zeta potential of the mixtures commonly tends to

approach to the zeta potential value of the added minerals. For example, because pyrite had the lowest absolute zeta potential among all minerals, the absolute zeta potential of the mixtures continued to decrease as more pyrite was added, which reduced the stability of the system. This trend is useful to explain the extremely low zeta potential value of Marcellus Formation flowback water, which will be discussed in the following section.

Overall, the characteristics of minerals play major roles in the supernatant solutions. Because calcite is soluble in water with dissolved CO_2, calcite dissolution increases the particle precipitation tendency at both room and reservoir temperatures (Plummer, 1982). Quartz is stable at room and reservoir temperatures and its dissolution had little effect on water quality (Gunter et al., 1997). In contrast, illite contaminates water by changing pH and releasing dissolved solids. The effect of illite dissolution on water quality becomes stronger with increased temperature. Pyrite solubility is low at room temperature, but it is oxidized rapidly at reservoir temperatures, which is the main reason for low observed pH and a high tendency for particle precipitation in water. Particle precipitation in pyrite experiments was especially promoted because these experiments had the highest observed TDS, largest observed particle size, and lowest observed absolute zeta potential. Thus, compared with all major minerals in Marcellus Formation rock sample, calcite, illite, and pyrite primarily controlled experimental water quality, especially at reservoir temperature, by changing pH, increasing TDS and particle size, and decreasing zeta potential of the water system.

At reservoir temperature, correlations between the mineral concentrations and supernatant parameters became weaker (refer to Table 45). The possible reason is that the

chemical reactions occur more rapidly at higher temperature, but the rapid dissolution might bring water near saturation with respect to these minerals (Laidler, 1987). Thus, the differences between water parameters caused by various mineral concentrations became smaller and correlations between water parameters at reservoir temperature became weak. However, the relationship between zeta potential and mineral concentrations becomes stronger in three- and four-component mineral-water systems. In these experiments, more ions should be released by different minerals and might be adsorbed on the particle surfaces. Thus, the behavior of all of surface ions may strengthen the relationship between the zeta potential and mineral concentrations.

4.3.2 Experiments on Flowback Water Samples

4.3.2.1 Interpretation of Marcellus Formation Flowback Water Properties

Marcellus Formation flowback water was collected from the same well as a rock sample and was analyzed for ion concentration, pH, TDS, particle size, and zeta potential in Chapter III. A brief characterization of the flowback water is shown in **Figure 42**. Detailed ion contents are provided in Section 3.32: Flowback Water Characterization in Chapter III. Because the zeta potential value of the flowback water samples is close to zero, particles in the flowback water had an extremely high tendency to precipitate.

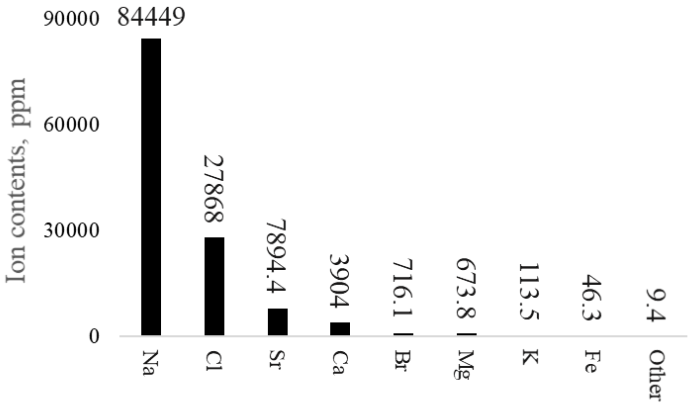

pH	TDS, ppm	Particle size, nm	Zeta Potential, absolute mV
3.7	116,070	17,039	1.05

Figure 42 Ion concentration, pH, TDS, particle size, and zeta potential values of the flowback water originated from the Marcellus Formation hydraulic fracturing activity (refer to Section 3.32 in Chapter III).

The combination of results from control experiments (refer to Figure 40 and 41) and Marcellus Formation flowback water parameters provides information to understand how flowback water quality changes after hydraulic fracturing. In control experiments, calcite and pyrite were main reason for changing Ph and particle size in water, especially at reservoir temperature. This interaction likely led to the large particle size and low Ph in Marcellus Formation flowback water. In the corresponding Marcellus Formation rock sample, calcite and pyrite account for 8.4% and 4.3% of the rock, or a mole ratio of calcite to pyrite of 2.3:1. However, according to reaction 9, the mole ratio of calcite to pyrite to completely neutralize Ph is 4:1 (Chermak and Schreiber, 2013). Thus, there was likely not enough available calcite to completely neutralize Ph during pyrite oxidation. Moreover, acids such as HCl are common chemical additives used in hydraulic fracturing (Ground Water Protection Council, 2009). Thus, after longer interactions at reservoir

conditions during hydraulic fracturing, added acid and excess pyrite oxidation likely resulted in the low Ph of Marcellus Formation flowback water.

$$FeS_2+4CaCO_3+3.75O_2+3.5\ H_2O \rightarrow Fe(OH)_{3(s)}+2SO_4^{2-}+4Ca^{2+}+4HCO_3^{-} \text{……..(9)}$$

In control experiments, a trend was observed that zeta potential of the mixtures tends to move to the zeta potential of the mineral with highest concentrations. This trend can be used to interpret the zeta potential of flowback water. In Marcellus Formation flowback water, sodium and chloride ions were the two highest among any other ions (refer to Figure 42). Although sodium chloride (NaCl) is not a major mineral in Marcellus Formation, it was mainly released from formation water (Blauch et al. 2009). NaCl is a highly soluble mineral with 357 mg dissolving in 1mL of water at 25 °C, and its solubility is not appreciably affected by temperature (384 mg/mL at 100 °C) (Smith, 1882). The zeta potential value of NaCl is around 0 because the net charge on NaCl particles is 0 (Oja et al., 1985; Haynes, 2013). Thus, large amounts of sodium and chloride ions not only provided the TDS in flowback water, but also were adsorbed on particle surfaces and led to the extremely low zeta potential of flowback water.

4.3.2.2 Pretreatment of Flowback Water for Reuse

Currently, to maintain the sustainability of the freshwater resources and reduce cost of hydraulic fracturing, more attention has been paid to high TDS in terms of the treatment of flowback water for reuse. Membrane technologies are effective to remove TDS but should be applied after pretreatment (Chang et al., 2019). The most common pretreatment method to remove suspended solids is coagulation, flocculation, sedimentation, and/or filtration. Large suspended solids can be removed from flowback water by sedimentation and filtration and small dissolved solids can be removed by combining the CFS method (Edzwald and Haarhoff, 2011; Rodriguez, et al., 2020). The results in Chapter III show that NaCl is the main problem in Marcellus Formation flowback water, but after a simple filtration process was applied on flowback water, reinjection of flowback water did not cause significant formation damage in the fractures. In this chapter, the CFS method was investigated to eliminate the impurities in flowback water prior to application of membrane technologies.

To remove suspended solids in flowback water, three different chemicals, including asphaltenes, $NaSO_4$, $FeCl_3$ and NaOH, were added separately in initial flowback water through integrated CFS method. Asphaltenes, as an organic compound, were used to evaluate whether it is effective to destabilize impurities in flowback water. $FeCl_3$ and $NaSO_4$ were used to aggregate particles and promote NaCl precipitation through coagulation and flocculation because Cl and Na are the main components in flowback water. To test if pH affects the stability of these mixtures, all experiments were repeated

after adding NaOH (a strong base). All samples with chemicals were prepared for 2 hours through an integrated CFS process. A flowback water sample without adding chemicals was settled for 2 hours as a control experiment. The image of each sample before and after pretreatment is provided in **Figure 43**.

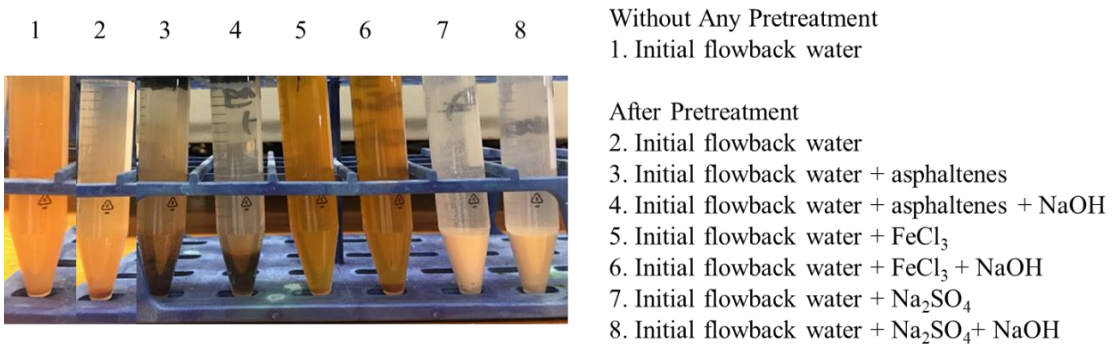

Figure 43 The changes in water samples after adding chemicals and CFS treatment. Note: Sample 1 is initial flowback water without any treatment. Sample 2 is initial flowback water after 2 hours sedimentation. Other samples were treated by adding chemicals and CFS process.

After simple sedimentation, flowback water became clear and small amounts of solids settled out of the water. After CFS treatment, flowback water also became clear and more solids were observed to settle out of flowback water in samples with asphaltenes and $NaSO_4$. Adding $FeCl_3$ or NaOH did not cause obvious changes in removal of solids in flowback water.

Each supernatant (2 mL) was analyzed after the system became stable. All water parameters are listed in **Table 46** and the efficiency of each chemical in removal of TDS are shown in **Figure 44.** After the CFS process, asphaltenes reduced TDS by 9.9% and $NaSO_4$ reduced TDS by 17.7%. $FeCl_3$ did not remove impurities but increased TDS by

29.4% perhaps because it decreased the pH of water system, causing more solids to dissolve back into the flowback water. NaOH increased the pH and only slightly improved TDS removal performance because the change in pH had little effect on the solubility of impurities (mainly NaCl) (Smith, 1882). However, sedimentation alone removed more than 81% of TDS from flowback water and is the most effective way to handle Marcellus Formation flowback water.

Table 46 pH, TDS, particle size, and zeta potential results for the supernatant after pretreatment.

Water used	Chemical used	TDS, ppm	Particle size, nm	Zeta Potential, absolute mV	pH
20ml flowback water without pretreatment	None	177,000	above equipment detection limit		
20ml flowback water after pretreatment	None	32,500	6,514	2.18	5.75
	1g Asphaltenes	159,480	16,437	1.38	4.92
	1g Asphaltenes + 5mg NaOH	154,960	10,768	1.61	9.61
	1g $FeCl_3$	229,080	8,259	2.61	1.45
	1g $FeCl_3$+ 5mg NaOH	184,040	4,743	3.13	1.46
	1g Na_2SO_4	145,640	2,079	8.72	4.48
	1g Na_2SO_4+5mg NaOH	143,500	6,554	2.46	9.82

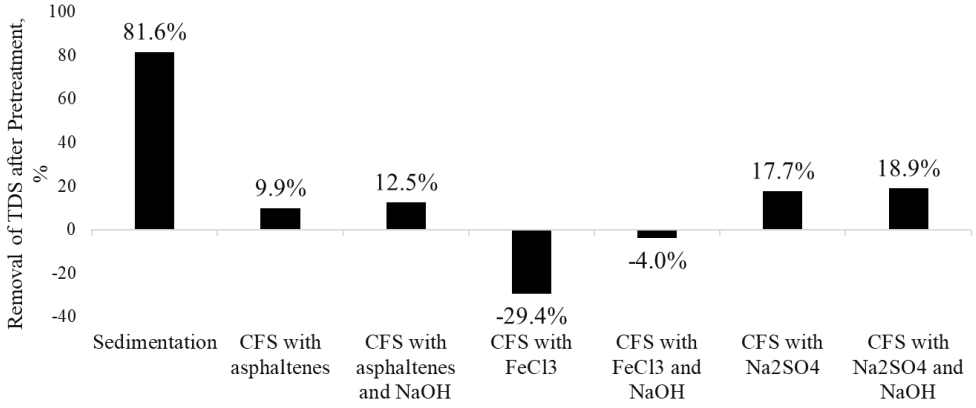

Figure 44 The percentage removal TDS after each pretreatment.

The relation between absolute zeta potential and particle size for each treated sample are provided in **Figure 45**. Absolute zeta potential and particle size were negatively correlated because particles with smaller zeta potential are unstable and tend to aggregate, which leads to the increase in particle size. Asphaltenes increased particle size and lowered zeta potential of the flowback water. Colloids had a high coagulation and flocculation tendency but most of them still suspended in water (Hunter, 1988). On the other hand, $NaSO_4$ largely decreased colloidal particle size and increased zeta potential of flowback water. This indicates that small particles remained suspended in the water and large particles settled out because coagulation and flocculation occurred in the flowback (Hunter, 1988). $FeCl_3$ only slightly changed zeta potential and particle size relative to the control experiment. Thus, based on water parameter data, $NaSO_4$ is more helpful to pre-treat flowback water through the CFS process than other chemicals. Compared with sedimentation, adding chemicals by CFS process can destabilize particles but was overall less effective at removing TDS from Marcellus Formation flowback water. To handle untreated flowback water with near 0 mV zeta potential, simple sedimentation is sufficient to separate the impurities from water because such flowback water already has high particle precipitation tendency. To further improve flowback water quality after sedimentation, membrane technologies would be applied to remove TDS from water.

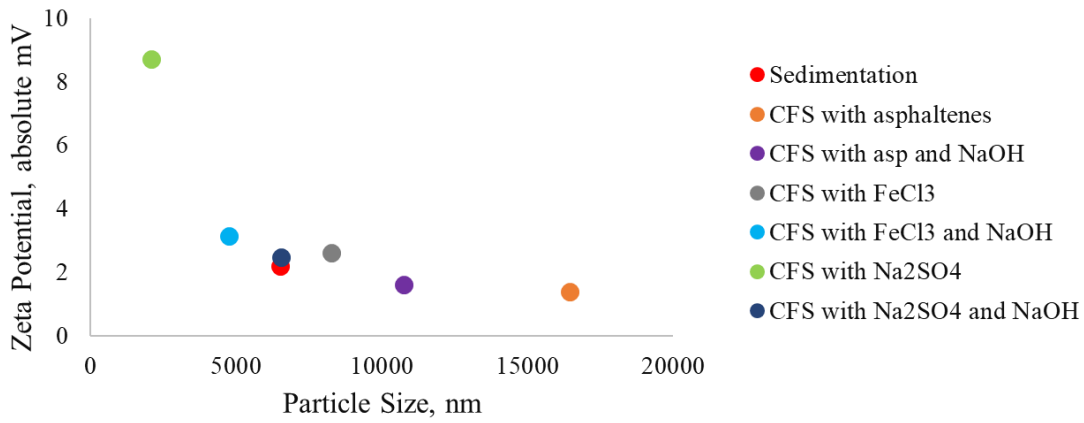

Figure 45 The relation between absolute zeta potential and particle size for each sample after each pretreatment.

Summary

Understanding the complicated interactions between water and rock is important to better engineer hydraulic fracturing fluids and to manage flowback water. In this chapter, two types of water-rock systems for Marcellus Formation were investigated. To better understand flowback water, pseudo reservoir rock-water systems were created as control experiments. To better manage flowback water, the CFS method was tested as a pretreatment to lower TDS in Marcellus Formation flowback water from hydraulic fracturing activities.

Control experimental results show that intrinsic characteristics of minerals mainly control water parameters. Moreover, relationships between water parameters provide important information between rock mineral composition and flowback water quality. In addition, pretreatment results show that by adding different chemicals, the effectiveness

of CFS on pretreatment of Marcellus Formation flowback waters can vary. However, for Marcellus Formation flowback water with high contaminant concentrations, simple sedimentation is sufficient (and may perform best) to separate impurities from flowback water.

Our results provide a quick methodology to investigate water-rock interactions and evaluate a low-cost treatment method to treat flowback water, which has potential to be adapted to the field-scale application.

References

Aagaard, P., and Helgeson, H. C. 1982. Thermodynamic and Kinetic Constraints on Reaction Rates among Minerals and Aqueous Solutions, 1. Theoretical considerations Amer. J. Sci., 282, pp. 237-285

Ali, M., and Hascakir, B. 2015b. Water-Rock Interaction for Eagle Ford, Marcellus, Green River, and Barnett Shale Samples, SPE Eastern Regional Meeting, 13-15 October, Morgantown, West Virginia, USA. https://doi.org/10.2118/177304-MS

Ali, M., and Hascakir, B. 2017. Water-Rock Interaction for Eagle Ford, Marcellu s, Green River, and Barnett Shale Samples and Implications for Hydraulic Fracturing Flu id Engineering, SPE Journal, 22, 01, 162-171, SPE-177304-PA. https://doi.org/10.2118/1 77304-PA

Antonio Alves Júnior, J., and Baptista Baldo, J. 2014. The Behavior of Zeta Potential of Silica Suspensions. New Journal of Glass and Ceramics, 4, 29-37. doi: 10.4236/njgc.2014.42004.

Bache, B. W. 1984.The Role of Calcium in Buffering Soils, Plant, Cell Environ., 7 (6) (1984), pp. 391-395

Birkeland, P. W.1999. Soils and Geomorphology (3rd ed.). Oxford: Oxford University Press.

Blauch, M. E., Myers, R. R., Moore, T., Lipinski, B. A., and Houston, N. A. 2009. Marcellus Shale Post-Frac Flowback Waters-Where is All the Salt Coming from and What are the Implications? In SPE Eastern Regional Meeting. Society of Petroleum Engineers.

Brady, N. C., and Weil, R. R. 2008. The Nature and Properties of Soils (14th ed.). Upper Saddle River, USA: Pearson.

Chang, H., Li, T., Liu, B., Vidic, R. D., Elimelech, M., and Crittenden, J. C. 2019. Potential and Implemented Membrane-Based Technologies for the Treatment and Reuse of Flowback and Produced Water from Shale Gas and Oil Plays: A Review. Desalination, 455, 2019, 34-57.

Chermak, J. A., and Schreiber, M, E. 2013. Mineralogy and Trace Element Geochemistry of Gas Shales in the United States: Environmental implications. International Journal of Coal Geology 126 (2014) 32–44

Clark, W. B. 1918. The Geography of Maryland. Maryland Geological Survey. vol. 10. Baltimore: Johns Hopkins Press

Cluff, M. A., Hartsock, A., MacRae, J. D., Carter, K., and Mouser, P. J. 2014. Temporal Changes in Microbial Ecology and Geochemistry in Produced Water from Hydraulically Fractured Marcellus shale Gas Wells. Environ. Sci. Technol. 48, 6508e6517.

Crittenden, J. C., Harza, M. W. 2015. Water Treatment: Principles and Design. 2nd Edition. Hoboken, NJ:Wiley. ISBN 0-471-11018-3

Devore, J. L. 2011. Probability and Statistics for Engineering and the Sciences (8th ed.). Boston, MA: Cengage Learning. pp. 508–510. ISBN 978-0-538-73352-6.

Edzwald, J. K., and Haarhoff, J. 2011. Seawater Pretreatment for Reverse Osmosis: Chemistry, Contaminant, and Coagulation, Water Research, 45, 5428-5440

Engle, M. A., and Rowan, E. L. 2014. Geochemical Evolution of Produced Waters from Hydraulic Fracturing of the Marcellus Shale, Morthern Appalachian Basin: A Multivariate Compositional Data Analysis Approach. International Journal of Coal Geology, 126, 45-56.

Fornasiero, D., Eijt, V., and Ralston, J. 1991. An Electrokinetic Study of Pyrite Oxidation. Colloids and Surfaces, 62 (1992) 63-73 63. Elsevier Science Publishers B.V., Amsterdam

Fuerstenau, M.C., Gutierrez, G., and Elgillani, D. A.1968. Trans. AIME 241 (1968) 319.

Gillespie, L. J. 1920. Reduction Potential of Bacterial Cultures and of Waterlogged Soils, Soil Sci. 9:199-216

Gregory K. B., Vidic R. D., and Dzombak D. A. 2011. Water Management Challenges Associated with the Production of Shale Gas by Hydraulic Fracturing, Elements, 7(3), 181–186

Ground Water Protection Council. 2009. Modern Shale Gas Development in the United States: A Primer (Report). DOE Office of Fossil Energy and National Energy Technology Laboratory. DE-FG26-04NT15455, pp. 56–66.

Gunter, W. D., Wiwchar, B., and Perkins, E. H. 1997. Aquifer Disposal of CO_2-rich Greenhouse Gases: Extension of the Time Scale of Experiment for CO2-sequestering Reactions by Geochemical Modeling. Mineral. and Petrol. 59, 121-140.

Hagemeier, P., and Hutt, J. 2009. Hydraulic Fracturing, Water Use Issues Under Congressional, Public Scrutiny. Oil & Gas Journal, pp. 18–25

Haynes, W. M. (ed.). 2013. CRC Handbook of Chemistry and Physics. 94th Edition. CRC Press LLC, Boca Raton: FL 2013-2014, p. 4-89

Hogan, C. M. 2010. Calcium. in A. Jorgenson and C. Cleveland (eds.) Encyclopedia of Earth, National Council for Science and the Environment, Washington DC

Hunter, R. J. 1988. Zeta Potential in Colloidal Science, Principles and Applications, Academic Press, p 220.

Israelachvili, J. 1992. Intermolecular and Surface Forces. Academic Press: London.

Keller, W. D., and Matlack, K. 1990. The pH of Clay Suspensions in the Field and Laboratory, and Methods of Measurement of their pH. Applied Clay Science, 5 (1990) 123-133. Elsevier Science Publishers B.V., Amsterdam

Laidler, K. J. 1987. Chemical Kinetics (3rd ed.). Harper & Row. p. 277. ISBN 0060438622.

Moses, C. O., Nordstrom, D. K., Herman, J. S., and Mills, A. L. 1987. Aqueous Pyrite Oxidation by Dissolved Oxygen and by Ferric Iron. Geochim Cosmochim Acta 51:1561–1571

Moulin, P., and Roques, H. J. 2003.Colloid Interface Sci. 261. 2003. 115.

Oja, T., Perterson, G. L., and Cannon, D. W. 1985. A Method for Measuring the Electrokinetic Properties of a Solution. U. S. Patent 4, 497, 207.

Plummer L. N., and Busenberg E. 1982. The Solubility of Calcite, Aragonite and Vaterite in CO_2-H_2O Solutions between 0 and 90 °C, and An Evaluation of the Aqueous Model for the System $CaCO_3$-CO_2-H_2O, Geochim. Cosmochim. Acta 46, t011-1040.

Plummer, L. N., and Wigtey, T. M. L. 1976. The Dissolution of Calcite in CO_2-Saturated Solutions at 25 °C and at Atmospheric Total Pressure, Geochim. Cosmochim. Acta 40, 191-202.

Plummer, L. N., Wigley, T. M. L., and Parkhurst, D. L. 1978a. The Kinetics of Calcite Dissolution in CO_2-Water Systems at 5 ° to 60 °C and 0.0 to 1.0 arm CO_2, Am. J. ScL 278, 179-216.

Riedinger, A. and Schultz, J. 1966. Acid Mine Water Reverse Osmosis Test at Kittanning, Pennsylvania. Office of Saline Waters Research and Development Report 217.

Rimstidt, J. D., and Barnes, H.L. 1980. The Kinetics of Silica-Water Reactions Geochim. Cosmochim. Acta, 44, pp. 1683-1699

Rodriguez, A. Z., Wang, H., Hu, L., Zhang, Y., and Xu, P. 2020. Treatment of Produced Water in the Permian Basin for Hydraulic Fracturing: Comparison of Different Coagulation Processes and Innovative Filter Media. Water, 12, 770.

Rodríguez, K., and Araujo, M. 2006. Temperature and Pressure Effects on Zeta Potential Values of Reservoir Minerals. Journal of Colloid and Interface Science 300 (2006) 788–794

Roen, J. B. 1984. Geology of the Devonian Black Shales of the Appalachian Basin. Organic Geochemistry, 5(4), 241-254.

Routson, R.C., and Kittrick, J. A.1971. Ilite Solubility. Soil Sci. Soc. Amer. J. 44, 139-142.

Singer, P. C., and Stumm, W. 1968. Kinetics of the Oxidation of Ferrous Iron. Proc. 2nd Symp. Coal Mine Drainage Res., pp. 12-34

Smith, W. 1882. Journal of the Society of Chemical Industry. Volume 1, Issue 3.

U.S. Energy Information Administration (EIA). 2018. Hydraulically Fractured H orizontal Wells Account for Most New Oil and Natural Gas Wells. https://www.eia.gov/t odayinenergy

U.S. Energy Information Administration (EIA). 2019. EIA Adds New Play Produ ction Data to Shale Gas and Tight Oil Reports. https://www.eia.gov/todayinenergy/detail. php?id=38372

U.S. Energy Information Administration (EIA). 2019. U.S. Crude Oil and Natural Gas Proved Reserves, Year-End 2018. U.S. Department of Energy. Washington, DC 20585

Van Praagh, G. 1939. 'Acidity' of Quartz. Nature 143, 1068 (1939). https://doi.org/10.1038/1431068a0

Vidic, R. D., Brantley S. L., Vandenbossche, J. M., Yoxtheimer, D., and Abad J. D. 2013. Impact of Shale Gas Development on Regional Water Quality, Science, 340(6134), 1235009.

Wang, L., Burns, S., Giammar, D. E., and Fortner, J. D. 2016. Element Mobilization from Bakken Shales as a Function of Water Chemistry. Chemosphere 149, 286-293.

Wang, L., Fortner, J. D., and Giammar, D. E. 2015. Impact of Water Chemistry on Element Mobilization from Eagle Ford Shale. Environ. Eng. Sci. 32, 310-320

Weber, W. J. 1972. Physicochemical Processes for Water Quality Control, Wiley Interscience, ISBN 0-471-92435-0.

Yarar, B., and Kitchener, J. A. 1970. Trans. Inst. Min. Metall. Sect. C, Min. Process. Extr. Metall. 79 (1970)23.

Zhang, L., Tice, M., and Hascakir, B., 2020. A Laboratory Study of the Impact of Re-Injecting Flowback Fluids on Formation Damage in the Marcellus Shale, SPE Journal, in-print, SPE-195336-PA.

Zhang, L., Tice, M., Marcantonio, F., and Hascakir, B. 2017. Solid and Soluble Products of Engineered Water/Rock Interactions in Eagle Ford Group Chemofacies, SPE Annual Technical Conference and Exhibition (ATCE 2017), 9-11 October 2017, San Antonio, Texas, USA, SPE-187296-MS.

Ziemkiewicz, P. F., and Thomas, H. Y. 2015. Evolution of Water Chemistry during Marcellus Shale Gas Development: A Case Study in West Virginia. Chemosphere 134:224-31

CHAPTER V

CONCLUSIONS

Considering the shortage of freshwater resources and environmental impacts resulting from flowback fluids originated from hydraulic fracturing activities, treatment and reuse of flowback water are generating more attention. However, because of complicated water-rock interactions, these waters are high in contaminants and the contamination concentrations are site specific, which makes the treatment of flowback water a very difficult task. Thus, understanding water-rock interactions are critical to better engineer hydraulic fluids and manage flowback water.

In my PhD study, three projects were finished to investigate water-rock interaction occurring during hydraulic fracturing in the Eagle Ford Formation and the Marcellus Formation. Firstly, experiments between water and rocks from five chemofacies in the lower Eagle Ford Formation demonstrates that various interactions took place within the same reservoir because of heterogeneity of the formation, which have different effect on hydraulic fracturing performance. Therefore, more attention should be paid to the heterogenous shale reservoirs in terms of hydraulic fracturing operation and flowback water treatment. Secondly, experiments between flowback water and reservoir rocks from the Marcellus Formation show evidence that reinjection of flowback water changed both rock surface and produced water properties, which more likely lead to formation damage if no treatment was made. But after proper treatment, reinjection of flowback water does not complicate the water-rock interaction and does not cause significant formation damage

in the fractures. Thirdly, pseudo rock-water systems were created for the Marcellus Formation and pretreatment methods were tested to remove contaminants from Marcellus flowback water. Results show minerals in reservoir rocks and in formation water change flowback water properties. The effect of water-rock interactions on flowback water quality is controlled by characteristics of minerals. Moreover, simple sedimentation is effective to remove the impurities from for flowback water with high contaminant concentrations.

The results in this dissertation provide quick methodologies to investigate water-rock interactions and manage flowback water, which improve our understand on water-rock interaction mechanism and treatment of flowback water, and have potential to be adapted to the field-scale application.

APPENDIX A

Table A-1: The XRF results of element concentrations (wt. %) of rock samples from different chemofacies in the lower Eagle Ford. The negative values are below the detection limit of XRF

Element	LEF1		LEF2		LEF3		LEF4		LEF5	
	1	2	3	4	5	6	7	8	9	10
Na	0.572	0.570	0.570	0.585	0.553	0.581	0.568	0.574	0.588	0.568
Mg	0.482	0.167	0.381	0.452	0.215	0.330	0.254	0.325	0.289	0.197
Al	4.240	1.340	1.510	2.930	1.540	2.940	1.430	2.140	2.840	2.420
Si	12.655	7.089	10.898	10.769	8.348	9.700	8.511	10.001	8.940	7.838
P	-0.020	-0.091	-0.007	0.014	0.056	0.063	-0.002	0.042	0.036	-0.005
S	1.130	0.630	1.111	1.519	0.840	1.098	0.991	1.340	1.351	1.342
K	1.311	0.395	0.340	0.640	0.440	0.466	0.368	0.496	0.686	0.532
Ca	16.071	25.100	19.686	17.240	24.190	19.840	22.740	20.230	20.540	23.118
Ba	0.253	0.066	0.090	0.150	0.082	0.172	0.076	0.119	0.159	0.154
Ti	0.165	0.072	0.086	0.118	0.083	0.113	0.086	0.116	0.132	0.125
V	0.030	0.011	0.015	0.015	0.006	0.010	0.007	0.009	0.003	0.013
Cr	0.007	0.005	0.020	0.020	0.005	0.006	0.005	0.007	0.006	0.005
Mn	0.020	0.020	0.020	0.020	0.020	0.021	0.020	0.020	0.020	0.020
Fe	1.640	0.820	1.030	1.420	0.910	1.210	0.930	1.330	1.520	1.310
Co	0.004	0.002	0.003	0.003	0.002	0.003	0.002	0.003	0.003	0.003
Ni	0.006	0.004	0.006	0.008	0.004	0.003	0.005	0.007	0.005	0.007
Cu	0.003	0.002	0.002	0.004	0.001	0.001	0.002	0.003	0.003	0.003
Zn	0.012	0.005	0.008	0.012	0.004	0.004	0.005	0.008	0.007	0.009
As	0.001	0.000	0.000	0.001	0.000	0.000	0.000	0.000	0.000	0.001
Pb	0.001	0.001	0.001	0.001	0.001	0.001	0.001	0.001	0.001	0.001
Th	0.001	0.000	0.000	0.000	0.000	0.000	0.000	0.000	0.000	0.000
Rb	0.007	0.003	0.002	0.003	0.002	0.002	0.002	0.003	0.004	0.003
U	0.001	0.001	0.001	0.000	0.000	0.000	0.001	0.001	0.001	0.001
Sr	0.072	0.076	0.065	0.058	0.056	0.046	0.048	0.053	0.048	0.046
Y	0.002	0.001	0.002	0.002	0.002	0.002	0.002	0.002	0.002	0.002
Zr	0.008	0.005	0.006	0.007	0.007	0.006	0.004	0.005	0.008	0.007
Nb	0.001	0.000	0.000	0.000	0.000	0.000	0.000	0.000	0.000	0.000
Mo	0.003	0.002	0.003	0.004	0.001	0.001	0.002	0.003	0.002	0.003
Rh	0.000	0.000	0.000	0.000	0.000	0.000	0.000	0.000	0.000	0.000

Table A-2: The ICP-MS results of the control experiments on deionized water composition and water-core holder interaction during dynamic experiments. The negative values are below the detection limit of ICP-MS

Elements	Deionized water, ppb	Water after water-core holder interaction, ppb
Na	7384.5	6082.3
Si	995.5	1060.7
Ca	26.7	300.6
Al	10.7	60.12
S	35.32	810.9
K	29.35	111.6
Fe	0.56	55.77
Ti	0.70	3.94
Mg	7.60	18.79
Sr	14.85	9.67
Mo	0.75	320.97
Zn	11.76	22.68
Ni	0.77	32.44
Cu	4.78	14.75
V	0.12	29.20
Rh	0.00068	0.0019
P	0.800	8.46
Mn	0.69	4.30
As	2.623	3.16
Ba	0.24	2.86
Co	-0.046	10.14
Pb	0.33	0.57
Th	0.07	0.10
Rb	-0.38	-0.035
Y	-0.0012	0.017
U	0.12	0.11
Cr	0.39	13.34
Zr	0.075	0.085
Nb	0.020	0.028

Table A-3: The ICP-MS results of static experiments. The negative values are below the detection limit of ICP-MS

Elements	Element concentrations of supernatant samples after static experiments, ppb									
	LEF1		LEF2		LEF3		LEF4		LEF5	
	1	2	3	4	5	6	7	8	9	10
Na	563680	237529	238247	398707	294828	299481	200430	245524	158690	132369
Si	3481	2709	2846	2839	3326	3352	3174	3098	3631	3597
Ca	11793	18698	46321	65483	36922	44672	42400	35308	16715	17966
Al	66.9	29.8	14.2	3.2	20.5	17.0	23.0	39.1	91.4	78.0
S	128452	64917	113601	271433	113086	137918	101820	104233	88911	78935
K	4529	3248	2943	3557	3398	3453	3449	2709	2521	2963
Fe	18.4	1.1	0.4	0.1	0.9	0.9	2.8	5.3	7.9	10.1
Ti	2.57	1.82	1.89	1.87	2.18	2.16	2.09	2.10	8.53	7.70
Mg	1029	2365	4806	5979	4654	5482	4198	3679	2045	2110
Sr	921	1403	2121	3293	2060	2580	2164	1773	1398	1241
Mo	1368	767	648	1593	592	287	1296	4109	1655	3435
Zn	12.4	25.5	31.8	45.3	18.7	23.5	11.0	8.8	17.3	18.5
Ni	1.3	4.7	23.8	47.5	6.5	6.1	18.9	17.3	6.4	7.8
Cu	3.5	18.2	9.7	6.4	5.9	3.2	3.7	2.1	5.5	6.6
V	48.7	25.8	13.8	5.0	4.5	1.6	5.8	6.5	6.4	21.7
Rh	0.03	0.04	0.06	0.09	0.06	0.08	0.07	0.06	0.05	0.05
P	1.9	1.3	1.9	1.9	1.2	1.4	1.3	1.8	2.9	3.7
Mn	1.3	1.3	3.0	3.9	1.9	2.9	2.0	2.0	6.5	7.4
As	7.4	6.2	5.9	6.0	5.9	5.4	5.9	6.1	7.5	7.7
Ba	21.6	27.4	24.8	26.8	25.3	42.4	26.2	22.5	4.7	3.9
Co	0.13	0.46	1.97	4.86	0.73	2.97	2.13	1.54	4.13	13.51
Pb	0.12	0.64	0.25	0.17	0.33	0.23	0.15	0.06	0.12	0.19
Th	0.08	0.07	0.07	0.07	0.07	0.07	0.07	0.07	0.59	0.70
Rb	2.5	1.7	1.1	1.6	1.4	1.4	1.7	2.1	2.2	1.9
Y	0.12	0.02	0.04	0.05	0.02	0.04	0.03	0.03	0.08	0.05
U	1.15	0.70	1.04	1.69	0.70	0.80	0.67	0.64	0.58	0.18
Cr	2.56	1.77	1.36	1.32	1.41	1.16	1.12	1.22	3.31	10.81
Zr	0.14	0.14	0.13	0.13	0.14	0.14	0.14	0.13	0.14	0.14
Nb	0.02	0.01	0.01	0.01	0.01	0.01	0.01	0.01	0.08	0.09

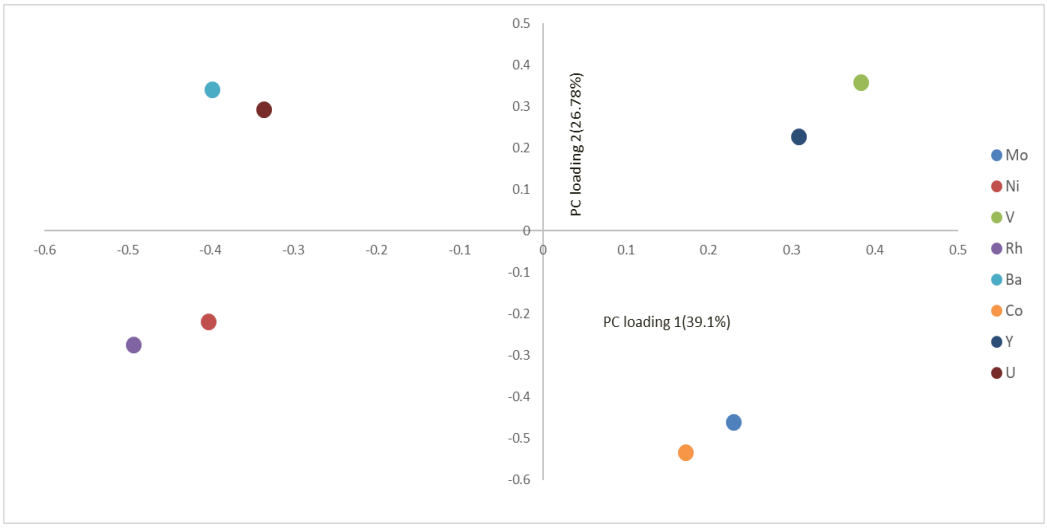

Figure A-1: Loading plot of trace elements in static experiments. Because of low concentrations in water samples and small sample size, trace elements in static experiments were randomly distributed.

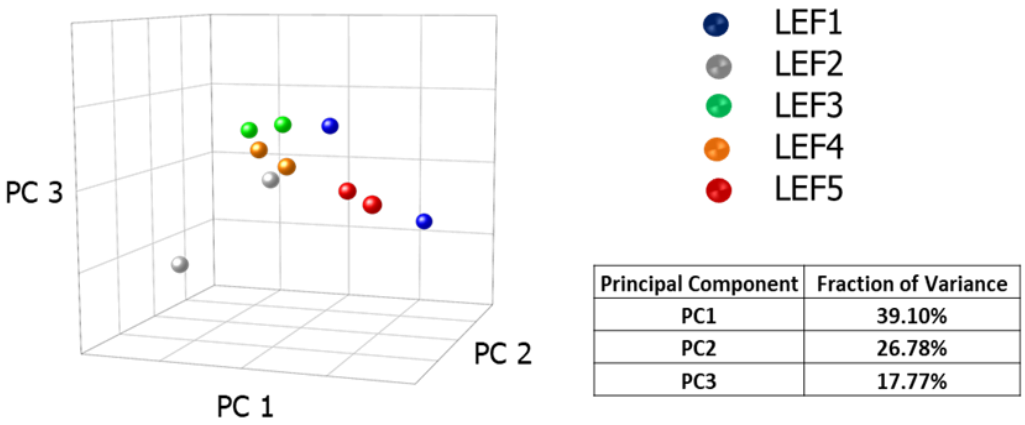

Principal Component	Fraction of Variance
PC1	39.10%
PC2	26.78%
PC3	17.77%

Figure A-2: Score plot of samples for trace elements in static experiments. The fraction of variance the percentage of variance is accounted for by a principal component. For trace elements, all samples scattered in the score plot and cannot be distinguished because of low concentrations in produced water.

Table A-4: The ICP-MS results of dynamic experiments on LEF1. The negative values are below the detection limit of ICP-MS

Element	Element concentrations of produced water after dynamic experiments, ppb											
	Sample 1						Sample 2					
	1	2	3	4	5	6	1	2	3	4	5	6
Na	347007	148095	57767	52548	34710	29744	204924	31857	17631	20300	9918	9165
Si	21327	11432	9206	19466	11588	15592	12171	4519	6272	8373	8666	3649
Ca	9585	3185	1647	3115	2814	1319	8656	4594	5888	5328	4806	3402
Al	103	717	1103	2737	1130	802	642	718	183	603	651	412
S	151445	67776	14433	11208	3167	5401	99645	15837	9434	12017	4277	3702
K	10414	4985	2386	3326	2974	2918	7594	2881	2308	2287	1729	1056
Fe	3.43	25.70	14.54	186.55	38.21	7.37	1.08	0.71	0.68	1.86	1.23	3.17
Ti	4.457	7.853	4.283	32.327	10.792	4.585	2.973	1.364	1.750	2.091	2.180	1.141
Mg	557	327	70	389	155	61	1148	433	344	321	178	178
Sr	795	226	56	96	116	92	675	248	287	310	247	237
Mo	3345	1472	613	522	181	266	1678	458	414	395	131	80
Zn	30.1	20.5	15.6	27.0	14.7	21.5	27.7	11.6	15.4	13.2	8.0	17.0
Ni	2.95	1.36	1.07	2.49	1.31	0.96	12.21	2.96	2.78	1.93	1.61	1.46
Cu	18.49	7.59	3.22	6.47	4.43	5.59	9.17	2.75	1.25	1.24	0.87	0.79
V	429.0	226.1	134.2	239.1	97.9	134.7	315.1	55.8	66.0	88.0	64.2	30.2
Rh	0.035	1.202	0.002	0.004	0.004	0.004	0.029	0.011	0.013	0.014	0.011	0.010
P	2.176	1.318	0.967	1.993	2.058	1.280	1.678	0.646	1.089	1.234	1.192	1.863
Mn	1.329	0.827	0.384	1.382	0.944	0.400	1.601	0.547	1.491	0.586	1.672	0.166
As	7.981	7.502	6.272	6.391	4.253	3.952	2.807	1.111	2.035	2.618	2.260	1.296
Ba	20.49	3.56	1.18	8.41	2.74	1.83	36.04	7.83	8.94	9.09	5.92	5.01
Co	0.067	-0.021	-0.065	0.307	0.016	-0.059	1.156	0.130	0.013	-0.022	-0.056	-0.077
Pb	0.073	-0.009	0.004	0.145	0.042	0.030	0.048	-0.019	-0.031	0.005	-0.004	0.081
Th	0.085	0.097	0.079	0.120	0.092	0.072	0.070	0.070	0.066	0.066	0.066	0.065
Rb	16.00	9.32	3.39	7.95	5.27	4.49	11.87	5.42	5.26	5.48	3.95	1.84
Y	0.0000	0.0389	0.0336	0.1886	0.0873	0.0058	0.0054	-0.0067	-0.0071	-0.0055	-0.0046	-0.0068
U	0.635	0.254	0.177	0.303	0.213	0.110	0.818	0.237	0.131	0.117	0.102	0.084
Cr	4.670	1.920	1.697	7.077	1.700	1.320	14.549	2.037	0.359	0.399	0.955	0.332
Zr	0.026	0.160	0.151	1.226	0.388	0.548	0.041	0.025	0.013	0.058	0.017	0.007
Nb	0.050	0.107	0.057	0.240	0.115	0.057	0.056	0.042	0.037	0.038	0.039	0.042

Table A-5: The ICP-MS results of dynamic experiments on LEF2. The negative values are below the detection limit of ICP-MS

Element	Element concentrations of produced water after dynamic experiments, ppb											
	Sample 3						Sample 4					
	1	2	3	4	5	6	1	2	3	4	5	6
Na	107650	43434	27522	10124	6176	6493	70361	292643	26021	14922	16851	9085
Si	7791	7159	14662	4663	6025	14336	1806	17307	5423	3243	10878	3817
Ca	23631	9735	11455	6368	5270	7059	8528	45299	10510	6720	11422	6707
Al	397	648	490	530	474	602	186	512	216	352	457	368
S	104081	35602	24724	9776	5966	5330	53370	248131	26441	16430	24060	12002
K	4762	3014	3635	1557	1327	2101	1495	11720	3022	1673	3387	1381
Fe	1.240	2.190	0.930	1.034	1.156	0.827	0.982	3.082	0.430	0.777	1.565	0.558
Ti	2.575	2.079	3.526	1.575	1.758	3.639	0.901	4.531	1.691	1.482	3.097	1.525
Mg	2068	866	836	521	379	427	925	3641	665	407	623	391
Sr	927	403	498	334	292	340	515	1909	473	343	550	368
Mo	957	593	782	179	139	180	441	4044	814	416	636	259
Zn	49.4	21.9	21.1	11.2	10.7	11.5	28.7	55.7	19.1	15.5	19.1	18.6
Ni	215.28	78.39	17.28	3.32	1.98	5.38	8.19	108.70	8.46	1.98	7.27	1.97
Cu	37.93	8.24	5.99	1.07	0.52	1.47	2.47	27.77	2.17	0.45	5.36	0.62
V	59.3	35.6	113.7	39.0	39.1	100.1	16.9	67.6	24.7	15.0	54.3	15.4
Rh	0.032	0.019	0.022	0.016	0.013	0.017	0.026	0.082	0.017	0.012	0.019	0.013
P	3.313	2.887	2.835	1.387	1.133	1.578	0.743	2.903	0.723	0.589	1.083	0.419
Mn	7.106	2.276	1.941	0.405	0.168	1.117	0.546	8.329	1.848	0.378	2.111	0.482
As	2.950	2.681	7.901	2.566	2.215	5.861	1.114	15.409	4.940	2.391	7.382	3.270
Ba	36.34	15.93	21.74	12.67	11.20	18.07	12.45	79.27	10.51	5.35	11.37	5.36
Co	2.686	0.723	0.188	-0.026	-0.056	-0.008	0.525	4.077	0.135	-0.037	0.134	-0.040
Pb	-0.017	0.011	0.061	0.003	-0.021	0.029	0.091	0.116	-0.015	-0.033	0.011	-0.030
Th	0.065	0.066	0.066	0.065	0.065	0.065	0.066	0.066	0.067	0.065	0.065	0.065
Rb	7.04	5.44	8.43	2.81	2.37	5.60	1.57	21.69	5.94	2.53	7.32	2.08
Y	0.0298	0.0009	-0.0031	-0.0072	-0.0071	-0.0061	0.0015	0.0373	-0.0064	-0.0077	-0.0057	-0.0074
U	0.870	0.200	0.189	0.124	0.100	0.105	0.476	0.707	0.161	0.111	0.116	0.089
Cr	1.538	1.017	0.248	0.276	0.280	0.120	11.013	2.424	0.295	2.473	0.322	0.239
Zr	0.047	0.015	0.021	0.011	0.009	0.016	0.012	0.039	0.050	0.015	0.678	0.030
Nb	0.039	0.037	0.040	0.036	0.035	0.036	0.040	0.045	0.038	0.035	0.037	0.035

Table A-6: The ICP-MS results of dynamic experiments on LEF3. The negative values are below the detection limit of ICP-MS

Element	Element concentrations of produced water after dynamic experiments, ppb											
	Sample 5						Sample 6					
	1	2	3	4	5	6	1	2	3	4	5	6
Na	32610	128356	14508	8864	8824	5766	249834	26757	22958	19935	11579	5478
Si	3095	15999	6587	10722	13950	12279	22319	4255	8247	3637	10404	9800
Ca	3047	15106	5476	4808	7334	4670	36281	8172	9607	5838	6636	6203
Al	381	709	560	741	398	649	560	277	463	427	595	532
S	19467	103874	11470	5297	7572	3456	191272	26683	24036	17675	9252	7097
K	1352	7213	2230	1912	2409	1534	10380	2600	2502	1411	2369	1903
Fe	1.797	2.115	0.901	1.283	1.297	1.113	2.653	0.722	1.781	1.126	2.744	0.776
Ti	1.437	4.306	2.200	3.027	4.122	3.320	5.447	1.688	2.569	1.501	3.697	2.804
Mg	314	1620	422	290	461	289	3665	713	508	430	285	313
Sr	174	721	271	228	345	241	1783	358	396	313	284	308
Mo	187	1136	351	198	210	91	822	204	247	131	119	112
Zn	20.1	21.8	14.7	13.6	12.6	9.2	63.6	15.9	16.8	13.9	13.1	8.8
Ni	2.26	16.75	1.87	1.96	2.42	1.46	30.25	4.42	3.29	1.72	1.36	1.84
Cu	2.41	12.54	0.81	1.30	0.84	0.84	19.44	2.18	1.84	0.66	1.42	1.55
V	14.7	43.3	15.3	24.4	30.9	22.2	45.4	6.7	14.0	5.7	17.1	15.8
Rh	0.006	0.023	0.008	0.007	0.011	0.007	0.049	0.011	0.012	0.011	0.009	0.010
P	0.751	2.547	0.772	1.224	1.078	1.427	2.099	0.663	0.903	0.431	1.271	0.542
Mn	0.275	2.740	0.461	0.807	1.235	0.613	7.813	1.662	3.037	0.543	1.964	1.537
As	0.667	4.569	2.346	3.735	6.181	3.975	8.120	2.964	6.705	2.980	8.392	7.098
Ba	5.37	23.00	5.13	4.95	6.08	5.11	85.57	29.70	47.36	29.73	40.62	57.89
Co	0.029	1.220	-0.043	-0.043	-0.043	-0.052	10.283	0.292	0.119	-0.019	-0.049	-0.021
Pb	-0.005	-0.005	-0.020	0.038	-0.026	-0.001	0.326	-0.019	0.000	0.012	0.054	0.065
Th	0.064	0.066	0.065	0.065	0.065	0.065	0.067	0.065	0.065	0.066	0.070	0.066
Rb	1.55	13.09	3.53	3.77	5.32	3.32	15.72	4.00	4.32	2.08	4.21	3.26
Y	-0.006	0.0088	-0.0069	-0.0064	0.0166	-0.0059	0.1656	-0.0040	0.0017	-0.0050	0.0094	-0.0043
U	0.139	0.336	0.103	0.090	0.095	0.083	0.636	0.125	0.101	0.076	0.092	0.075
Cr	2.503	1.830	0.276	0.241	0.173	0.114	7.976	0.972	0.440	0.182	0.159	0.109
Zr	0.022	0.066	0.015	0.017	0.042	0.035	0.054	0.013	0.020	0.014	0.030	0.014
Nb	0.037	0.039	0.037	0.036	0.043	0.037	0.055	0.039	0.036	0.035	0.036	0.036

Table A-7: The ICP-MS results of dynamic experiments on LEF4. The negative values are below the detection limit of ICP-MS

Element	Element concentrations of produced water after dynamic experiments, ppb											
	Sample 7						Sample 8					
	1	2	3	4	5	6	1	2	3	4	5	6
Na	58259	43258	34474	25057	23884	12887	43852	36614	27175	21567	19352	17212
Si	2260	5146	6906	6428	6626	4713	3048	5498	4567	3902	3553	3371
Ca	14595	12204	12196	9162	8604	6348	11489	12640	9095	6982	5911	5470
Al	86	406	408	437	527	323	118	375	404	381	342	318
S	58731	44245	34159	21535	17290	10126	30277	28262	18572	13484	10278	8610
K	1595	2825	3324	2714	2621	1664	1719	2800	2148	1625	1304	1138
Fe	1.829	6.867	4.038	3.223	2.705	1.481	3.139	9.162	8.061	8.668	5.041	5.285
Ti	1.174	1.866	2.297	2.162	2.072	1.678	1.415	2.042	1.820	1.632	1.507	1.418
Mg	1451	1218	1036	701	546	407	855	881	612	457	371	321
Sr	835	716	617	445	409	294	572	496	337	252	226	197
Mo	700	953	1247	992	745	503	840	1059	860	707	600	500
Zn	14.7	16.6	15.3	13.1	-0.3	10.8	107.4	40.4	21.0	16.5	14.9	11.7
Ni	75.58	71.61	80.13	72.24	67.78	46.38	16.12	14.26	9.39	5.57	4.30	3.83
Cu	7.59	16.96	21.65	23.58	25.74	21.32	12.47	21.40	4.81	2.33	1.70	1.46
V	22.3	38.3	24.3	22.9	20.5	18.1	19.2	25.1	12.6	11.7	12.0	11.9
Rh	0.028	0.025	0.021	0.016	0.013	0.010	0.020	0.017	0.011	0.009	0.007	0.006
P	0.863	1.173	1.261	1.317	2.199	0.930	1.077	1.320	1.119	0.933	0.897	1.001
Mn	6.768	4.986	10.347	12.744	13.881	11.089	2.107	2.640	1.891	1.510	1.263	1.232
As	0.993	1.860	3.213	3.766	4.066	2.979	1.237	3.102	2.967	2.656	2.339	2.137
Ba	11.75	12.58	12.06	9.62	9.51	7.11	12.51	14.13	9.03	6.49	5.40	4.60
Co	1.479	1.742	2.630	2.062	1.694	1.207	0.635	0.737	0.341	0.145	0.063	0.041
Pb	-0.030	0.006	0.004	0.004	0.024	0.001	3.863	1.767	1.000	0.785	0.687	0.706
Th	0.065	0.064	0.064	0.064	0.064	0.064	0.064	0.064	0.064	0.064	0.064	0.064
Rb	1.32	3.61	5.64	5.11	4.38	3.06	3.38	8.37	6.70	5.16	4.24	3.61
Y	0.0058	0.0023	0.0010	-0.0026	-0.0062	-0.0075	-0.0001	-0.0029	-0.0068	-0.0081	-0.0079	-0.0083
U	0.366	0.379	0.240	0.124	0.106	0.089	0.308	0.294	0.145	0.103	0.094	0.087
Cr	12.156	4.585	0.578	0.319	0.594	3.193	8.429	7.691	8.076	13.887	20.626	25.009
Zr	0.018	0.013	0.013	0.013	0.013	0.013	0.017	0.013	0.011	0.008	0.009	0.009
Nb	0.036	0.038	0.037	0.036	0.036	0.035	0.042	0.038	0.037	0.036	0.037	0.036

Table A-8: The ICP-MS results of dynamic experiments on LEF5. The negative values are below the detection limit of ICP-MS

Element	Element concentrations of produced water after dynamic experiments, ppb											
	Sample 9						Sample 10					
	1	2	3	4	5	6	1	2	3	4	5	6
Na	103255	56574	27139	16176	10522	8865	68986	42338	28610	14881	14447	8014
Si	4501	9080	5458	4465	5565	4715	6371	7896	6095	4294	3787	4074
Ca	5913	7225	4283	3724	3487	3452	8690	7140	5369	3597	4789	3152
Al	639	906	790	613	814	585	724	914	778	642	577	556
S	73387	38942	13552	8184	4954	4576	51003	31305	18919	6534	6846	3516
K	2670	4385	2725	1995	1959	1682	3551	3828	2889	1951	1548	1356
Fe	1.455	2.986	2.036	1.392	1.230	1.721	2.090	1.043	1.231	1.419	1.876	1.405
Ti	1.959	2.852	1.925	1.782	2.707	1.748	2.378	2.608	2.141	1.674	1.595	2.078
Mg	823	674	305	211	173	151	782	500	335	171	205	116
Sr	538	423	243	194	172	171	502	367	276	184	247	148
Mo	1144	1101	642	443	298	256	1712	1551	1045	539	428	259
Zn	16.4	5.0	6.8	18.8	11.5	8.4	21.3	15.5	17.2	19.0	12.0	6.6
Ni	13.21	16.25	2.82	1.53	1.32	1.13	88.56	14.66	8.09	1.53	1.76	1.09
Cu	2.77	6.51	1.73	0.75	0.77	0.60	21.29	7.01	3.79	0.57	0.91	0.37
V	22.3	19.9	13.2	13.6	17.0	15.6	39.1	48.2	48.3	48.5	40.8	46.3
Rh	0.019	0.014	0.008	0.006	0.006	0.005	0.017	0.011	0.008	0.006	0.008	0.005
P	0.653	0.345	0.755	0.733	1.155	0.699	0.604	0.694	0.748	0.802	0.823	0.794
Mn	0.957	2.100	0.693	0.307	0.315	0.261	2.622	1.698	1.017	0.336	0.478	0.115
As	2.619	5.826	3.607	2.971	3.413	3.264	4.711	5.810	4.634	3.457	3.543	2.784
Ba	15.05	10.47	4.47	3.05	2.57	2.24	11.88	10.04	7.19	4.35	7.20	3.77
Co	1.042	0.793	0.019	-0.054	-0.067	-0.070	0.583	0.127	0.028	-0.071	-0.064	-0.080
Pb	-0.025	0.029	0.004	-0.015	-0.003	-0.001	-0.006	0.009	0.003	-0.002	-0.005	0.004
Th	0.065	0.064	0.065	0.065	0.064	0.064	0.064	0.065	0.065	0.065	0.065	0.064
Rb	4.67	12.60	6.93	5.16	5.88	4.92	8.57	10.24	7.41	4.58	3.91	3.39
Y	0.0008	0.0016	-0.0075	-0.0073	-0.0077	-0.0085	-0.0011	-0.0038	-0.0048	-0.0058	-0.0067	-0.0082
U	0.466	0.189	0.115	0.090	0.080	0.073	0.565	0.276	0.209	0.143	0.126	0.102
Cr	49.399	0.818	0.356	0.329	0.133	0.193	1.661	0.390	0.425	0.459	0.831	0.287
Zr	0.029	0.183	0.019	0.010	0.010	0.009	0.018	0.016	0.013	0.010	0.010	0.052
Nb	0.044	0.038	0.036	0.035	0.036	0.035	0.038	0.037	0.037	0.036	0.038	0.036

APPENDIX B

Comparison of Estimated Ratios of Rock Surface Area to Water Volume in Lab Case and Field Case

Marcellus Formation rock samples were crushed and sieved to 250 μm sized to increase rock surface areas that were exposed water. To identify if the selected rock size is close to field HF case, we compared the estimated rock surface area to water volume ratio in lab conditions with field conditions (Abdulsattar, 2015). First, approximate rock surface to water ratio in lab scale was derived based on two assumptions. Assuming all crushed particles are spheres (radius is 0.0125 cm) and bulk rock density is 2.5 g/cm^3 (Manger, 1963), the surface area for each particle is about $1.96*10^{-3}$ cm^2 and volume is $8.18*10^{-6}$ cm^3. Multiplying particle volume by rock density, the mass of individual particle is $2.045*10^{-5}$ g. Because 10 g and 280 g crushed samples were used in static and dynamic experiments, by dividing the total sample mass by the individual particle mass, the total number of particles in static and dynamic experiments is about $4.89*10^5$ and $1.36*10^7$, respectively. Then multiplying total number of particles by the surface area of individual particle, the total surface areas in static and dynamic experiments are approximately 947 cm^2 and $2.684*10^4$ cm^2. Water used in static and dynamic experiments were 50 mL and 3240mL (18mL/min *180 minutes). Therefore, the rock surface area to the water ratios in static and dynamic experiments are approximately 19.96 cm^2/mL and 8.28 cm^2/mL. Because there are variations in particle shape and size in real case, the actual ratio is

probably higher than this due to non-sphericity and varying sizes of the real particles. In field scale, estimated rock surface area to water ratio ranges in hydraulic fracturing are 2-20 cm^2/mL, based on the assumption the small fracture width ranges are from 0.1-1 cm (Ramurthy et al., 2011; Abdulsattar 2015). Compared the estimated lab and field rock surface to water volume ratios, the size of crushed rock samples and water volume used in static and dynamic experiments are reasonable. While these calculations rely on assumptions that may be in error and there must be variation in fracture widths in the real case. We attempt to make our lab conditions close to field conditions.

Table B-1: The ICP-MS results of the deionized water and flowback water compositions. The negative values are below the detection limit of ICP-MS.

Concentration, ppm		
Element	**Deionized water**	**Filtered flowback water**
Ti	0.0044	0.5161
U	-0.0001	-0.0033
Cr	0.0002	1.4599
Co	0.0000	0.0122
Pb	0.0004	0.0085
Th	0.0000	-0.0005
Rb	-0.0002	0.4121
Y	0.0001	0.0649
Zr	-0.0002	-0.0090
Nb	-0.0001	-0.0055
Mo	-0.0002	-0.0190
Ni	0.0003	0.2136
Cu	0.0150	3.5257
V	0.0001	0.4290
Rh	-0.0002	0.0964
Na	46.9665	84449.2511
Al	0.0108	0.4569
Mg	0.0047	673.8268
Si	2.0118	4.0725
P	0.0009	-0.0124
S	0.1374	1.4691
Ca	0.0286	3903.9911
Mn	0.0003	2.3665
Fe	0.0037	46.2513
As	0.0005	0.2967
Sr	0.0148	7894.4166
Sn	0.0000	0.0015
K	0.0349	113.5039

Table B-2: The ICP-MS results of compositions (ppm) of produced water after dynamic deionized water-rock interaction. The negative values are below the detection limit of ICP-MS.

Dynamic experiment	deionized water-rock interaction					
produced water	1	2	3	4	5	6
Ti	0.0060	0.0061	0.0053	0.0048	0.0046	0.0043
U	0.1778	0.0395	0.0176	0.0108	0.0076	0.0061
Cr	0.0023	0.0007	0.0002	0.0001	0.0003	0.0001
Co	0.0672	0.0096	0.0020	0.0009	0.0003	0.0004
Pb	0.0007	0.0006	0.0004	0.0003	0.0003	0.0002
Th	0.0000	0.0000	0.0000	0.0000	0.0000	0.0000
Rb	0.0580	0.0334	0.0169	0.0116	0.0092	0.0074
Y	0.0003	0.0001	0.0001	0.0001	0.0001	0.0001
Zr	-0.0002	-0.0002	-0.0002	-0.0002	-0.0002	-0.0002
Nb	-0.0001	-0.0001	-0.0001	-0.0001	-0.0001	-0.0001
Mo	36.1271	36.4213	24.3421	14.0459	7.7243	5.0371
Ni	1.5993	0.4775	0.2168	0.1211	0.0657	0.0499
Cu	0.0206	0.0508	0.0213	0.0107	0.0049	0.0031
V	0.0142	0.0197	0.0168	0.0151	0.0126	0.0121
Rh	0.0002	-0.0001	-0.0002	-0.0002	-0.0002	-0.0002
Na	108.6095	55.3854	45.9675	45.2081	47.0870	48.8684
Al	0.0136	0.0519	0.1117	0.1641	0.1996	0.2290
Mg	2.7370	1.2839	0.7230	0.5842	0.5204	0.4750
Si	6.9891	10.1431	7.5687	6.3340	4.9663	4.4430
P	0.0008	0.0006	0.0002	0.0002	0.0003	0.0001
S	388.4728	30.5289	15.1198	11.2941	8.2687	7.1798
Ca	119.3402	36.6021	16.0740	11.0930	8.2334	6.8950
Ti	0.8625	0.2433	0.1215	0.0842	0.0615	0.0527
Mn	0.0996	0.0232	0.0095	0.0060	0.0041	0.0032
Fe	0.0035	0.0038	0.0037	0.0046	0.0068	0.0042
As	0.0218	0.0273	0.0252	0.0252	0.0244	0.0239
Sr	39.0281	12.5556	2.6852	1.7379	1.2090	0.9609
Sn	0.0001	0.0001	0.0002	0.0002	0.0002	0.0002
K	73.7100	12.8370	5.7328	3.7548	2.6524	2.1383

Table B-3: The ICP-MS results of compositions (ppm) of produced water after dynamic flowback water-rock interaction. The negative values are below the detection limit of ICP-MS.

Dynamic experiment	flowback water-rock interaction					
produced water	1	2	3	4	5	6
Ti	0.2356	0.2995	0.3572	0.3661	0.3806	0.4106
U	0.0487	0.0821	0.0624	0.0450	0.0311	0.0202
Cr	1.5384	1.3404	1.4685	1.4395	1.3653	1.4296
Co	0.3345	0.2838	0.1561	0.0897	0.0637	0.0518
Pb	0.0691	0.0533	0.0754	0.0279	0.0193	0.0257
Th	-0.0002	-0.0004	-0.0004	-0.0005	-0.0005	-0.0005
Rb	0.6196	0.5113	0.4826	0.4163	0.3850	0.3955
Y	0.0775	0.0700	0.0698	0.0661	0.0632	0.0639
Zr	-0.0086	-0.0088	-0.0091	-0.0089	-0.0091	-0.0091
Nb	-0.0052	-0.0054	-0.0054	-0.0054	-0.0055	-0.0055
Mo	4.1663	2.9766	2.7174	1.9441	1.5055	1.0748
Ni	10.5375	8.1539	4.8186	3.0491	2.3858	2.2135
Cu	0.9531	1.6681	2.0207	2.1900	2.2675	2.5094
V	0.4642	0.4039	0.4382	0.4263	0.4095	0.4128
Rh	0.0898	0.0911	0.0945	0.0956	0.0922	0.0898
Na	98699.1593	87390.7765	91493.5069	80922.5269	84678.9868	84978.6328
Al	0.7130	0.5044	0.5836	0.4607	0.4527	0.4685
Mg	678.5225	652.0701	671.1166	643.4000	629.8997	668.3804
Si	7.0587	8.6245	8.0393	6.1806	5.4130	5.5669
P	-0.0087	-0.0102	-0.0105	-0.0129	-0.0141	-0.0125
S	13.1819	11.8029	6.5160	3.7127	3.0220	2.6328
Ca	3814.4731	3621.4787	3717.2427	3609.2705	3577.1497	3741.6305
Mn	3.2932	2.8377	2.6248	2.5757	2.5663	2.5479
Fe	0.2904	0.3672	0.6551	1.5938	1.8936	4.2065
As	0.3160	0.2804	0.2578	0.2827	0.2332	0.2537
Sr	8766.1513	8070.8859	7921.9738	7656.6650	7361.2351	7574.9766
Sn	0.0018	0.0017	0.0016	0.0015	0.0016	0.0016
K	152.6234	119.5182	111.7084	105.4240	102.1875	110.1394

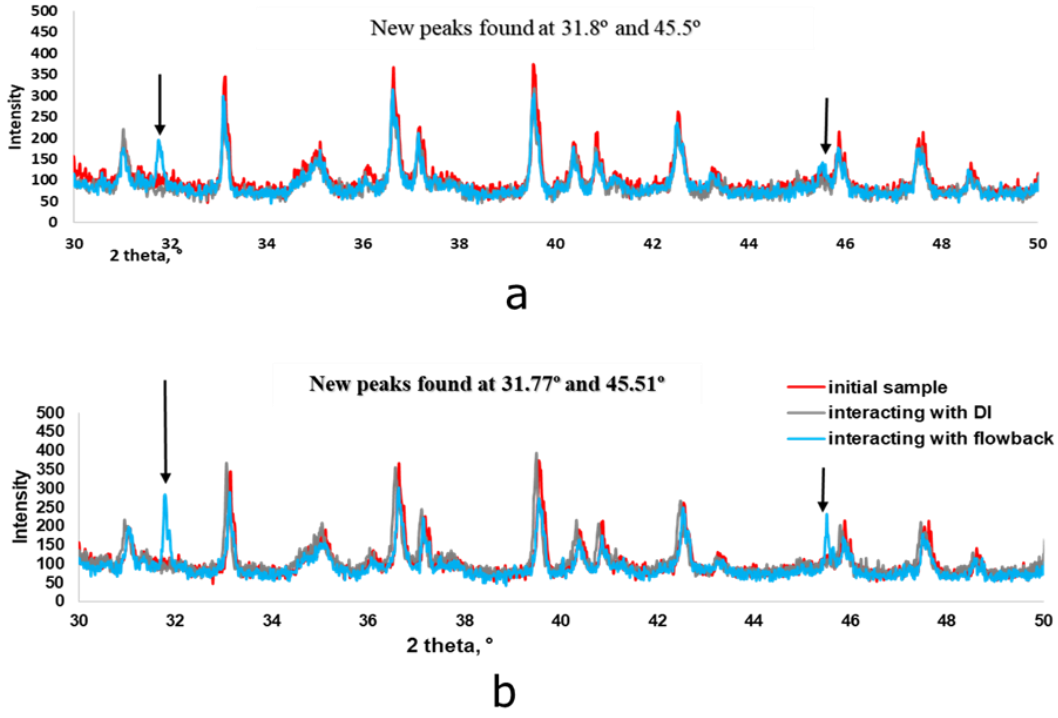

Figure B-1: Overlay XRD diagrams of initial rock sample, sample after deionized water-rock interaction, and sample after flowback water-rock interaction. a) Overlay diagrams after static experiments. b) Overlay diagrams after dynamic experiments. Two new peaks (NaCl) were detected and caused by flowback water contamination.

Table B-4: Characterization of water parameters in produced water samples from dynamic experiment

	Produced Water	TDS, ppm	Particle Size, nm	Absolute Zeta Potential, mv
DI water-rock Interaction	**1**	1630	23318	6.21
	2	545	13739	6.95
	3	332	17933	8.52
	4	269	25503	4.50
	5	221	22424	10.75
	6	206	13245	13.47
	1	168530	14784	1.59
Flowback water-rock Interaction	**2**	113760	28011	0.27
	3	111590	14203	0.46
	4	117310	13892	1.80
	5	116300	19018	2.84
	6	118660	11797	0.50

APPENDIX C

Table C-1: Standard minerals were chosen at four different concentrations to investigate interactions between one single mineral and water.

Concentrations, mg/mL				
Calcite (C)	1	2	3	4
Quartz (Q)	1	2	3	4
Illite (I)	1	2	3	4
Pyrite (P)	1	2	3	4

Table C-2: Standard minerals were chosen at four different concentrations to investigate interactions between two standard minerals and water.

Concentrations, mg/mL							
Calcite + Quartz	Calcite	Quartz	Calcite + Illite	Calcite	Illite	Quartz + Illite	Quartz	Illite
	1	1		1	1		1	1
	1	2		1	2		1	2
	1	3		1	3		1	3
	1	4		1	4		1	4
	2	1		2	1		2	1
	3	1		3	1		3	1
	4	1		4	1		4	1

Table C-3: Standard minerals were chosen at four different concentrations to investigate interactions between three standard minerals and water.

Concentrations, mg/mL															
Calcite + Quartz + Illite	Calcite	Quartz	Illite	Calcite + Quartz + Pyrite	Calcite	Quartz	Pyrite	Calcite + Illite + Pyrite	Calcite	Illite	Pyrite	Quartz + Illite + Pyrite	Quartz	Illite	Pyrite
	1	1	1		1	1	1		1	1	1		1	1	1
	1	1	2		1	1	2		1	1	2		1	1	2
	1	1	3		1	1	3		1	1	3		1	1	3
	1	1	4		1	1	4		1	1	4		1	1	4
	1	2	1		1	2	1		1	2	1		1	2	1
	1	3	1		1	3	1		1	3	1		1	3	1
	1	4	1		1	4	1		1	4	1		1	4	1
	2	1	1		2	1	1		2	1	1		2	1	1
	3	1	1		3	1	1		3	1	1		3	1	1
	4	1	1		4	1	1		4	1	1		4	1	1

Table C-4: Standard minerals were chosen at four different concentrations to investigate interactions between four standard minerals and water.

Concentrations, mg/mL				
	Calcite	Quartz	Illite	Quartz
Calcite + Quartz + Illite + Pyrite	1	1	1	1
	1	1	1	2
	1	1	1	3
	1	1	1	4
	1	1	2	1
	1	1	3	1
	1	1	4	1
	1	2	1	1
	1	3	1	1
	1	4	1	1
	2	1	1	1
	3	1	1	1
	4	1	1	1

Table C-5: Summary of water parameters in produced water after two-component rock and water interactions at room and reservoir temperature.

Calcite + Illite	**Mineral concentration, mg/mL**		**Experiments at room temperature**					**Experiments at reservoir temperature**			
	calcite concentration, mg/mL	illite concentration, mg/mL	pH	TDS, ppm	Particle Size, nm	Zeta Potential, mV		pH	TDS, ppm	Particle Size, nm	Zeta Potential, mV
Calcite 1	1	0	8.99	21.4	568	-12.25		8.73	28.0	890	-13.35
C+I 1	1	1	9.09	23.7	336	-9.93		8.65	35.2	789	-13.33
C+I 2	1	2	9.11	25.2	468	-11.06		8.67	36.1	727	-13.30
C+I 3	1	3	9.12	28.3	323	-12.21		8.66	37.9	770	-13.51
C+I 4	1	4	9.16	30.9	442	-12.59		8.64	43.6	776	-13.72
Illite 1	0	1	7.56	10.1	549	-14.33		8.64	26.7	554	-13.63
C+I 1	1	1	9.09	23.7	336	-9.93		8.65	35.2	789	-13.33
C+I 5	2	1	9.23	23.9	597	-12.13		8.65	35.4	781	-13.34
C+I 6	3	1	9.30	24.3	673	-12.16		8.67	35.8	771	-13.85
C+I 7	4	1	9.32	25.2	821	-12.35		8.72	36.0	818	-13.62
Calcite + Pyrite	calcite concentration, mg/mL	pyrite concentration, mg/mL	**Experiments at room temperature**					**Experiments at reservoir temperature**			
			pH	TDS, ppm	Particle Size, nm	Zeta Potential, mV		pH	TDS, ppm	Particle Size, nm	Zeta Potential, mV
Calcite 1	1	0	8.99	21.4	568	-12.25		8.73	28.0	890	-13.35
C+P 1	1	1	8.44	25.5	14336	-9.60		8.07	70.6	>20000	-10.27
C+P 2	1	2	8.26	28.9	14986	-9.34		7.94	78.4	>20000	-8.78
C+P 3	1	3	7.83	35.2	16600	-9.21		7.92	83.3	>20000	-6.68
C+P 4	1	4	7.53	37.9	>20000	-9.20		7.85	91.3	>20000	-3.39
Pyrite 1	0	1	6.55	7.2	143	-4.38		3.70	65.6	1242	+6.19
C+P 1	1	1	8.44	25.5	14336	-9.60		8.07	70.6	>20000	-10.27
C+P 5	2	1	8.67	25.8	13746	-11.96		8.12	71.6	>20000	-11.01
C+P 6	3	1	8.76	26.3	14321	-12.16		8.20	71.8	>20000	-12.24
C+P 7	4	1	8.89	27.2	13868	-12.62		8.23	72.4	>20000	-12.38
Calcite + Quartz	calcite concentration, mg/mL	quartz concentration, mg/mL	**Experiments at room temperature**					**Experiments at reservoir temperature**			
			pH	TDS, ppm	Particle Size, nm	Zeta Potential, mV		pH	TDS, ppm	Particle Size, nm	Zeta Potential, mV
Calcite 1	1	0	8.99	21.4	568	-12.25		8.73	28.0	890	-13.35
C+Q 1	1	1	8.59	40.1	458	-9.04		8.68	45.4	249	-9.34
C+Q 2	1	2	8.41	47.3	470	-9.29		8.66	45.8	277	-10.86
C+Q 3	1	3	8.23	53.4	476	-9.75		8.66	46.0	385	-11.76
C+Q 4	1	4	7.90	58.9	513	-10.76		8.65	46.1	481	-12.03
Quartz 1	0	1	7.5	6.3	523	-20.91		7.36	7.9	433	-19.82
C+Q 1	1	1	8.59	40.1	458	-9.04		8.68	45.4	249	-9.10
C+Q 5	2	1	8.60	40.2	409	-9.33		8.78	46.1	306	-11.67
C+Q 6	3	1	8.65	40.7	683	-9.35		8.82	46.3	350	-12.24
C+Q 7	4	1	8.68	41.4	463	-9.68		8.82	46.4	355	-14.01

Table C-5 Continued

Quartz + Illite	quartz concentration, mg/mL	illite concentration, mg/mL	**Experiments at room temperature**					**Experiments at reservoir temperature**			
			pH	TDS, ppm	Particle Size, nm	Zeta Potential, mV		pH	TDS, ppm	Particle Size, nm	Zeta Potential, mV
Quartz 1	1	0	7.50	6.3	523	-20.91		7.36	7.9	433	-19.82
Q+I 1	1	1	7.48	8.4	309	-13.77		8.23	25.8	481	-6.72
Q+I 2	1	2	7.43	11.9	241	-13.41		8.38	30.1	222	-6.77
Q+I 3	1	3	7.34	12.5	430	-12.46		8.40	35.6	160	-7.64
Q+I 4	1	4	7.20	14.5	295	-12.02		8.47	43.2	483	-8.25
Illite 1	0	1	7.56	10.1	549	-14.33		8.64	26.7	554	-13.63
Q+I 1	1	1	7.48	8.4	309	-13.77		8.23	25.8	481	-6.72
Q+I 5	2	1	7.08	8.0	438	-13.94		8.05	19.6	369	-9.28
Q+I 6	3	1	7.02	8.6	423	-14.03		8.03	18.2	412	-10.09
Q+I 7	4	1	7.02	9.3	457	-14.68		7.98	18.2	385	-10.64

Quartz + Pyrite	quartz concentration, mg/mL	pyrite concentration, mg/mL	**Experiments at room temperature**					**Experiments at reservoir temperature**			
			pH	TDS, ppm	Particle Size, nm	Zeta Potential, mV		pH	TDS, ppm	Particle Size, nm	Zeta Potential, mV
Quartz 1	1	0	7.50	6.3	523	-20.91		7.36	7.9	433	-19.82
Q+P 1	1	1	6.34	8.0	177	-8.84		3.79	63.8	246	-9.66
Q+P 2	1	2	5.67	11.5	483	-2.02		3.69	73.0	1274	-7.44
Q+P 3	1	3	4.81	17.7	517	+1.71		3.58	84.8	1487	-6.78
Q+P 4	1	4	4.59	19.5	1981	+1.61		3.56	87.2	13969	-3.16
Pyrite 1	0	1	6.55	7.2	143	-4.38		3.70	65.6	1242	+6.19
Q+P 1	1	1	6.34	8.0	177	-8.84		3.79	63.8	246	-9.66
Q+P 5	2	1	6.10	8.1	491	-11.20		3.81	59.3	391	-9.73
Q+P 6	3	1	6.09	8.2	467	-12.72		3.85	57.6	424	-10.13
Q+P 7	4	1	6.09	8.2	478	-13.01		3.91	45.8	415	-10.32

Illite + Pyrite	illite concentration, mg/mL	pyrite concentration, mg/mL	**Experiments at room temperature**					**Experiments at reservoir temperature**			
			pH	TDS, ppm	Particle Size, nm	Zeta Potential, mV		pH	TDS, ppm	Particle Size, nm	Zeta Potential, mV
Illite 1	1	0	7.56	10.1	549	-14.33		8.64	26.7	554	-13.63
I+P 1	1	1	6.78	13.2	506	-9.23		5.70	44.7	1158	-7.31
I+P 2	1	2	6.56	15.5	1451	-8.47		4.87	51.3	3172	+2.68
I+P 3	1	3	6.24	23.0	2147	-8.24		4.85	51.7	4443	+3.36
I+P 4	1	4	6.14	24.2	4592	-7.00		4.84	52.1	5217	+3.90
Pyrite 1	0	1	6.55	7.2	143	-4.38		3.70	65.6	1242	+6.19
I+P 1	1	1	6.78	13.2	506	-9.23		5.70	44.7	1158	-7.31
I+P 5	2	1	6.86	14.5	436	-9.26		7.06	61.4	773	-11.23
I+P 6	3	1	6.94	17.4	336	-9.85		7.51	63.5	549	-11.29
I+P 7	4	1	6.95	19.4	198	-11.39		7.54	64.3	410	-11.51

*Particle sizes of some samples are above detection limit of equipment (20000 nm).

Table C-6: Summary of water parameters in produced water after three-component rock and water experiments at room and reservoir temperature.

Calcite + Quartz + Illite	**Mineral concentration, mg/mL**			**Experiments at room temperature**					**Experiments at reservoir temperature**			
	calcite concentration, mg/mL	quartz concentration, mg/mL	illite concentration, mg/mL	pH	TDS, ppm	Particle Size, nm	Zeta Potential, mV		pH	TDS, ppm	Particle Size, nm	Zeta Potential, mV
C+Q 1	1	1	0	8.59	40.1	458	-9.04		8.68	45.4	249	-9.34
C+Q+I 1	1	1	1	8.62	41.8	369	-7.11		8.85	46.8	530	-10.36
C+Q+I 2	1	1	2	8.60	42.8	277	-9.38		8.83	48.9	546	-10.57
C+Q+I 3	1	1	3	8.58	42.9	352	-9.98		8.73	52.8	571	-12.09
C+Q+I 4	1	1	4	8.57	43.5	283	-10.62		8.70	55.1	655	-12.38
C+I 1	1	0	1	9.09	23.7	336	-9.93		8.65	35.2	789	-13.33
C+Q+I 1	1	1	1	8.62	41.8	369	-7.11		8.85	46.8	530	-10.36
C+Q+I 5	1	2	1	8.46	46.3	428	-8.39		8.84	50.1	522	-11.63
C+Q+I 6	1	3	1	8.33	53.6	303	-8.95		8.81	52.7	511	-12.42
C+Q+I 7	1	4	1	8.17	63.6	393	-12.64		8.71	54.7	370	-12.83
Q+I 1	0	1	1	7.48	8.4	309	-13.77		7.43	25.8	481	-10.17
C+Q+I 1	1	1	1	8.62	41.8	369	-7.11		8.85	46.8	530	-10.36
C+Q+I 8	2	1	1	8.63	43.3	359	-11.42		8.86	50.3	532	-11.33
C+Q+I 9	3	1	1	8.64	43.6	314	-11.70		8.86	51.8	547	-11.57
C+Q+I 10	4	1	1	8.64	43.8	417	-12.48		8.86	54.7	530	-12.05
Calcite + Quartz + Pyrite	calcite concentration, mg/mL	quartz concentration, mg/mL	pyrite concentration, mg/mL	**Experiments at room temperature**					**Experiments at reservoir temperature**			
				pH	TDS, ppm	Particle Size, nm	Zeta Potential, mV		pH	TDS, ppm	Particle Size, nm	Zeta Potential, mV
C+Q 1	1	1	0	8.59	40.1	458	-9.04		8.63	45.4	249	-9.34
C+Q+P 1	1	1	1	8.42	42.1	503	-7.74		8.40	73.1	202	-10.38
C+Q+P 2	1	1	2	8.36	47.8	439	-7.47		8.38	82.2	320	-10.11
C+Q+P 3	1	1	3	8.29	49.8	445	-7.26		8.35	100	281	-10.09
C+Q+P 4	1	1	4	8.16	56.1	437	-6.54		8.34	108	283	-8.96
C+P 1	1	0	1	8.44	25.5	14336	-9.60		8.07	70.6	>20000	-10.27
C+Q+P 1	1	1	1	8.42	42.1	503	-7.74		8.40	73.1	202	-10.38
C+Q+P 5	1	2	1	8.38	48.0	105	-8.09		8.41	73.9	270	-10.73
C+Q+P 6	1	3	1	8.33	53.7	120	-8.42		8.39	76.2	402	-12.40
C+Q+P 7	1	4	1	8.23	59.7	239	-9.01		8.42	76.4	414	-13.44
Q+P 1	0	1	1	6.34	8.0	177	-8.84		3.79	63.8	246	-9.66
C+Q+P 1	1	1	1	8.42	42.1	503	-7.74		8.40	73.1	202	-10.38
C+Q+P 8	2	1	1	8.47	44.4	458	-7.81		8.44	81.2	455	-10.66
C+Q+P 9	3	1	1	8.53	47.1	380	-8.32		8.50	83.2	405	-11.04
C+Q+P 10	4	1	1	8.55	47.8	359	-9.09		8.50	84.4	438	-12.74

Table C-6 Continued

Calcite + Illite + Pyrite	calcite concentration, mg/mL	illite concentration, mg/mL	pyrite concentration, mg/mL	**Experiments at room temperature**					**Experiments at reservoir temperature**			
				pH	TDS, ppm	Particle Size, nm	Zeta Potential, mV		pH	TDS, ppm	Particle Size, nm	Zeta Potential, mV
C+I 1	1	1	0	9.09	23.7	336	-9.93		8.65	35.2	789	-13.33
C+I+P 1	1	1	1	8.54	32.7	9255	-9.87		7.91	66.8	4218	-8.58
C+I+P 2	1	1	2	8.20	46.9	18600	-9.82		7.86	74.9	13673	-7.14
C+I+P 3	1	1	3	8.00	63.0	>20000	-9.51		7.84	93.2	>20000	-6.59
C+I+P 4	1	1	4	7.98	70.5	>20000	-9.44		7.80	104	>20000	-4.34
C+P 1	1	0	1	8.44	25.5	14336	-9.60		8.07	70.6	>20000	-10.27
C+I+P 1	1	1	1	8.54	32.7	9255	-9.87		7.91	66.8	4218	-8.58
C+I+P 5	1	2	1	8.62	33.8	656	-14.53		8.08	70.1	1227	-9.92
C+I+P 6	1	3	1	8.72	36.2	654	-14.48		8.19	71.4	1082	-10.84
C+I+P 7	1	4	1	8.74	37.0	637	-14.55		8.30	74.6	1034	-11.45
I+P 1	0	1	1	6.78	13.2	506	-9.23		5.7	44.7	1158	-7.31
C+I+P 1	1	1	1	8.54	32.7	9255	-9.87		7.91	66.8	4218	-8.58
C+I+P 8	2	1	1	8.59	34.3	10873	-11.75		8.12	67.9	5353	-10.14
C+I+P 9	3	1	1	8.65	43.2	18112	-12.6		8.14	71.0	8992	-10.37
C+I+P 10	4	1	1	8.67	45.7	>20000	-12.71		8.19	71.9	>20000	-11.29
Quartz + Illite + Pyrite	quartz concentration, mg/mL	illite concentration, mg/mL	pyrite concentration, mg/mL	**Experiments at room temperature**					**Experiments at reservoir temperature**			
				pH	TDS, ppm	Particle Size, nm	Zeta Potential, mV		pH	TDS, ppm	Particle Size, nm	Zeta Potential, mV
Q+I 1	1	1	0	7.48	8.4	309	-13.77		7.43	25.8	481	-6.72
Q+I+P 1	1	1	1	6.58	15.7	328	-10.69		5.83	44.1	547	-8.56
Q+I+P 2	1	1	2	6.15	21.3	490	-6.62		5.35	50.9	1027	-8.12
Q+I+P 3	1	1	3	5.78	30.3	1088	-1.63		4.59	61.0	>20000	-6.45
Q+I+P 4	1	1	4	5.37	33.3	2753	+0.90		4.27	68.7	>20000	-1.96
Q+P 1	1	0	1	6.34	8.0	177	-8.84		3.79	63.8	246	-9.66
Q+I+P 1	1	1	1	6.58	15.7	328	-10.69		5.83	44.1	547	-8.56
Q+I+P 5	1	2	1	6.68	19.5	462	-11.33		7.05	48.1	612	-8.82
Q+I+P 6	1	3	1	6.81	22.4	489	-11.86		7.55	52.8	584	-9.19
Q+I+P 7	1	4	1	6.90	31.7	574	-12.16		7.80	60.6	563	-9.80
I+P 1	0	1	1	6.78	13.2	506	-9.23		5.7	44.7	1158	-7.31
Q+I+P 1	1	1	1	6.58	15.7	328	-10.69		5.83	44.1	547	-8.56
Q+I+P 8	2	1	1	6.55	16.0	305	-10.37		6.02	41.3	557	-8.82
Q+I+P 9	3	1	1	6.53	16.4	271	-11.75		6.12	41.1	573	-9.19
Q+I+P 10	4	1	1	6.53	16.8	277	-12.31		6.39	40.9	520	-9.98

*Particle sizes of some samples are above detection limit of equipment (20000 nm).

Table C-7: Summary of water parameters in produced water after four-component rock and water experiments at room and reservoir temperature.

Calcite + Quartz + Illite + Pyrite	**Mineral concentration, mg/mL**				**Experiments at room temperature**					**Experiments at reservoir temperature**			
	C	Q	I	P	pH	TDS, ppm	Particle Size, nm	Zeta Potential, mV		pH	TDS, ppm	Particle Size, nm	Zeta Potential, mV
C+Q+I 1	1	1	1	0	8.62	41.8	369	-7.11		8.85	46.8	530	-10.36
C+Q+I+P 1	1	1	1	1	8.46	48.8	103	-8.63		8.46	75.1	511	-10.63
C+Q+I+P 2	1	1	1	2	8.41	59.0	202	-8.23		8.40	84.2	597	-9.69
C+Q+I+P 3	1	1	1	3	8.28	62.8	435	-6.04		8.36	104	539	-9.33
C+Q+I+P 4	1	1	1	4	8.21	70.3	524	-5.72		8.31	108	614	-8.16
C+Q+P 1	1	1	0	1	8.42	42.1	503	-7.74		8.40	73.1	202	-10.38
C+Q+I+P 1	1	1	1	1	8.46	48.8	103	-8.63		8.46	75.1	511	-10.63
C+Q+I+P 5	1	1	2	1	8.46	50.3	314	-9.64		8.47	77.9	584	-11.42
C+Q+I+P 6	1	1	3	1	8.47	50.9	451	-10.41		8.45	87.3	591	-12.55
C+Q+I+P 7	1	1	4	1	8.47	52.5	458	-11.59		8.47	89.6	637	-13.41
C+I+P 1	1	0	1	1	8.54	32.7	9255	-9.87		7.91	66.8	4218	-8.58
C+Q+I+P 1	1	1	1	1	8.46	48.8	103	-8.63		8.46	75.1	511	-10.63
C+Q+I+P 8	1	2	1	1	8.30	56.6	104	-10.76		8.43	78.7	512	-11.92
C+Q+I+P 9	1	3	1	1	8.28	63.8	289	-11.11		8.43	80.6	522	-12.16
C+Q+I+P 10	1	4	1	1	8.28	71.0	407	-11.15		8.43	81.8	446	-12.42
Q+I+P 1	0	1	1	1	6.58	15.7	328	-10.69		5.83	44.1	547	-8.56
C+Q+I+P 1	1	1	1	1	8.46	48.8	103	-8.63		8.43	75.1	511	-10.63
C+Q+I+P 11	2	1	1	1	8.57	50.7	284	-11.14		8.47	81.6	536	-11.92
C+Q+I+P 12	3	1	1	1	8.59	51.9	406	-11.89		8.48	84.7	631	-11.55
C+Q+I+P 13	4	1	1	1	8.62	55.6	420	-12.56		8.50	85.0	638	-12.43